CRANFIELD UNIVERSITY

Damien Paul Thibaut Lancereau

Experimental Investigation of the Nonlinear Dynamic Behaviour of Bolted Lap Joints

CRANFIELD DEFENCE AND SECURITY
Centre for Defence Engineering

Ph.D.
Academic Year: 2015 - 2019

Supervisor: Hugh Goyder
Associate Supervisor: David Purdy
April 2019

CRANFIELD UNIVERSITY

CRANFIELD DEFENCE AND SECURITY
Centre for Defence Engineering

Ph.D.

Academic Year 2015 - 2019

Damien Paul Thibaut Lancereau

Experimental Investigation of the Nonlinear Dynamic Behaviour of Bolted Lap Joints

Supervisor: Hugh Goyder
Associate Supervisor: David Purdy
April 2019

This thesis is submitted in partial fulfilment of the requirements for the degree of Ph.D.

ABSTRACT

The physics behind the vibration of joints is currently unknown and therefore unpredictable. Consequently in sensitive structures, like aircraft or turbines, prototype testing is necessary to evaluate the dynamic behaviour and avoid catastrophic failures. The thesis objective is to reduce the unpredictability by identifying the dominant parameters linked to bolted lap joint nonlinear behaviour. This study has found that the size of the interface had the most impact. A large interface creates a receding contact which created an amplitude dependent damping and stiffness. In contrast, a small interface creates a complete contact, with limited nonlinear behaviour. In-between interface sizes involved a lock-up which was interpreted as amplitude dependent slip or bound regions in the lap joint interface. Accordingly, the bending moment dynamic loading at the joint location is correlated to the nonlinear behaviour, only if there is a receding contact. This correlation between bending and damping was interpreted as a rolling effect with a changing contact patch during a cycle of vibration, which creates a specific behaviour in different regions of the lap joint interface. An experimental approach was used to reach these conclusions. The use of shims allowed the comparison of seven sizes of interfaces on the same structure. Then, a novel method was developed to measure the effect of a receding contact at 18 joint locations, by placing or removing washer-size-shims in a beam with 18 identical lap joints. Hammer impact excitation allowed the 12 first bending modes to be measured with minimum interference. The decaying vibration time histories were filtered and fitted in the time domain, using novel signal processing methods, to extract the amplitude dependant damping ratio and natural frequencies. Also, a finite element simulation enabled the natural frequency to be predicted, using an approximated contact patch.

Keywords:

Contact-patch, Bolt, Micro-friction, Interface, Damping, Vibration, Bending Moment, Shear Force, Slip, Rolling, Contact, Receding Contact, Complete Contact, Contact Mechanics, Tribomechadynamics, Dynamic Contact Patch

ACKNOWLEDGEMENTS

I would like to express my complete appreciation to my supervisor Hugh Goyder. Without you, Hugh, I would not be writing those lines today. You raised the standard of what it means to be a great supervisor. Thank you as well to David Purdy for being a fantastic second supervisor. Also, I would like to offer my special thanks to Cranfield, EPSRC and AWE for sponsoring this Ph.D.

I wish to acknowledge the support provided by my family and my friends, especially to my mother and my sister. Some of my best ideas, like the shim length experiment, came from our conversations. Special thanks to my brother for helping me restructure my plan and help me choose this path four years ago. Thanks to my Father and Danielle. I would like to show my infinite gratitude to Robert, my prized English teacher, for cheering me up, sometimes just listening to me and correcting all my writing. Robert, if I would have not met you, this document would have been ludicrously different. My gratitude to Sylvia's yoga lessons, Sue's English lessons and Ciara's conversations classes. I am grateful to Shabarish and Fergie for their reviewing. Thank you to Jim, Rob, the DA workshop, the design centre and the librarians for their assistance.

My expressed thanks also goes to my fellow colleagues and friends: Alejandro, Axel, Maud, Encina, Ozgun, Luc, Eddie, Ray, Tania, Michelle, Shan, Antonia, Amelie, Jiacopo, Carole and Hugo, Akhil, Asha, Tatjana, Monica, Marco, Mel, Antonio, Lucia, Gonzalo, Ana, Krasin, Efi, Alexandra, Peter, Dean, Leon, Seb, Vic, Rich, Duarte, Dami, Alan, Ayush, Emma, Jayne, Nasyitah, Eric, Louis-Pierre, Tobi, Stefano, David, Matt, Jughead, Sabrina and many others like Alice, Brice, Julia and Daphné. Many thanks to all the defence academy players for letting me embark on three and an half pantomimes and also to the CSA, the DA, the RSC gym, B gym and the DAMC for all your events.

I would like to say *merci* to the emission "Par Jupiter", on France Inter radio, for making me laugh when I was performing the 1040 hammer hits necessary for this thesis. Thanks to France Culture, Reporterre and The Guardian for opening up my mind. Similarly, my gratitude to Pablo Servigne for making me believe in

the concept of the *collapse* of our thermo-industrial human civilisation (that includes you, so, you should look it up). Moreover, thank you to the Framalang community for welcoming my help in the translation of free and open source software (FOSS) articles published on “Framablog.org” website. Finally, my regards to all the employees of my “second office”, the Brunel Swindon’s Coffee One, where I am writing these lines.

TABLE OF CONTENTS

LIST OF FIGURES

LIST OF TABLES

LIST OF EQUATIONS

LIST OF ABBREVIATIONS

FRF	Frequency Respond Function
ZEFFT	Zeroed early-time fast Fourier transforms
BEND	Backwards extrapolation for nonlinearity detection
DFT	Discrete Fourier Transform
SDOF	Single degree of freedom model composed of a mass, a spring and a dashpot
N.A.	Not Applicable
BRB	Nominal Brake and Reuss Beam Source: Cooper et al. (2017)
SBRB	Stiffness Modified Brake and Reuss Beam (SBRB). Source: Cooper et al. (2017)

NOMENCLATURE

Variable	Definition	Unit
A_{ref}	Reference amplitude (value = $1\mathrm{ms}^{-2}$)	$[\mathrm{ms}^{-2}]$
A_{start}	Estimated envelope amplitude at the start of the interval	$[m\ s^{-2}]$
B	Amplitude variable for the direct fitting model	$[m\ s^{-2}]$
$B(\lambda, x_b)$	unscaled-absolute-bending-moment function	$[Nm]$
C	Amplitude variable for the direct fitting model	$[m\ s^{-2}]$
E	Young Modulus	$[ms^{-2}]$
$F_{viscous\ damping}$	Friction force of viscous damping	$[N]$
$FitScalDampTwo$	Fitted variable P from the data set of the scaled damping ratio with two receding contact	$[no\ unit]$
$FitScalDampOne$	Fitted variable P from the data set of the scaled damping ratio with one receding contact	$[no\ unit]$
$FitScalFreqTwo$	Fitted variable P from the data set of the scaled natural frequency with two receding contact	$[no\ unit]$
$FitScalFreqOne$	Fitted variable P from the data set of the scaled natural frequency with one receding contact	$[no\ unit]$
$H(w)$	Frequency Respond Function (FRF)	$[no\ unit]$
I	Second moment of area	$[m^4]$
L_c	Unknown length of the contact patch	$[\mathrm{mm}]$
L_s	Length of the shim(s)	$[\mathrm{mm}]$
M	In chapter 2: Bending moment	$[Nm]$
M	In chapter 7: First fitting variable for data display using the damping ratio or the natural frequency	$[no\ unit]$ $or\ [Hz]$
N	In chapter 4: Number of points in the interval	$[point]$
N	In chapter 7: Second fitting variable for data display using the damping ratio or the natural frequency	$[no\ unit]$ $or\ [Hz]$
P	Third fitting variable used to scale the absolute bending moment model based on the scaled data set	$[no\ unit]$
Q	Q factor (damping)	$[no\ unit]$
V	Shear force (Q also used)	$[N]$
X	Relative Displacement	$[m]$
a	Frequency of vibration in hertz	$[\mathrm{Hz}]$
b	Sum of the thickness of multiple shims	$[\mathrm{mm}]$
c	Modal / effective viscous damping or also proportional damping	$[Nm^{-1}s]$
err	Total error of the fitting for the interval	$[m^2\ s^{-4}]$
f	Estimated natural frequency of the direct fitting model	$[Hz]$
Variable	**Definition**	**Unit**

f(A)	Instantaneous frequency at an amplitude A	[Hz]
i	'i' defined as $i = \sqrt{-1}$	$[no\ unit]$
k	Curvature of plane curves	$[m^{-1}]$
k	Rigidity	$[N\ m^{-1}]$
l	Length of beam	$[m]$
m	Mass	[Kg]
n	Data point number from the start of the interval	$[point]$
q	Distributed Loading	$[Nm^{-1}]$
t	Time	$[s]$
t_{middle}	Time at the middle of the interval	$[s]$
t_{start}	Time at the start of the interval	$[s]$
x	Relative Displacement	$[m]$
x_b	Position on the beam	$[m]$
y	Deflection (w also used)	$[m]$
$y_{fit}(t)$	Value of the model used for fitting at a time t	$[m\ s^{-2}]$
$y_{md}(n)$	Measured data for point n	$[m\ s^{-2}]$
$*$	Pattern symbol use to represent any other variable	$[no\ unit]$
$*_j$	Subscript for the recording point j	$[no\ unit]$
$*_r$	Subscript for the mode of vibration r	$[no\ unit]$
$*_k$	Subscript for the excitation point k	$[no\ unit]$
$[*]$	Matrix form	$[no\ unit]$
$[\alpha(\omega)]$	FRF receptance matrix	$[mN^{-1}]$
α	Abstract variable for the direct fitting	$[Rad\ point^{-1}]$
$\alpha_{\mathrm{jk}}(\omega)$	FRF receptance for a recording point j and an excitation point k	$[mN^{-1}]$
β	Abstract variable for the direct fitting	$[Rad\ point^{-1}]$
$\epsilon(n)$	Residual error between the measured data and the fitting model for point n	$[m\ s^{-2}]$
ζ	For chapter 2: Damping ratio	$[no\ unit]$
ζ	Anywhere else: Estimated damping ratio of the direct fitting model	$[no\ unit]$
θ	In Subsection 2.1.5: Slope	$[rad]$
θ	Anywhere else: phase	$[rad]$
$\Delta f(A,A_{ref})$	:= f(A) - f(A_{ref})	[Hz]
λ	Solutions of Equation (7-2)	$[m^{-1}]$
ρ	Radius of the curvature	$[m]$
ω	Frequency of vibration	$[\mathrm{rad}\ s^{-1}]$
ω_0	Natural frequency	$[\mathrm{rad}\ s^{-1}]$
$\overline{\omega}_r$	Natural frequency for the mode r	$[\mathrm{rad}\ s^{-1}]$

1 INTRODUCTION

The mechanical behaviour of a joint submitted to vibration is unpredictable, (Matthew R W Brake 2017). When manufacturing a product, numerous parameters can be quantified or estimated during the design phase, but not the dynamic behaviour of joints which is directly linked to a possible structural failure. This thesis tries to challenge this situation by reducing the uncertainty around the nonlinear dynamic behaviour of joints by identifying which parameters are dominant.

Currently in the industry, the workflow used to validate the design of a product submitted to severe vibration requires the fabrication and testing of one or multiple prototypes, source: (Ewins 2016). These products include aircrafts, turbines, machines, vehicles or satellites. This validation procedure is expensive, time-consuming and limits the innovation.

To improve this workflow, a reliable predictive model of the dynamics of joints is needed. This model needs to be simple enough to be useful and precise enough to represent the different physical phenomenena in the joints. However, the limited understanding of the inner physics of joints forbids the creation of such predictive models.

Structures are assemblies of components. An individual component, for example a shaped piece of metal, can be perfectly modelled in a computer simulation. A component behaves as a linear structure. A linear structure has natural frequencies and damping ratios independent of the amplitude of vibration.

However, the joints between components are poorly understood, which means that a joint is difficult to simulate especially in a dynamic environment. One of the most important aspects of a dynamic behaviour of joint is its ability to dissipate energy. Joints dissipate energy by friction which introduces non-linearity. This nonlinearity complicates the understanding of the dynamic behaviour of joints. Therefore, joints requirements dedicated model and signal processing.

The main objective of this thesis is to investigate the nonlinear dynamic behaviour of joints.

As there is multiple designs, material and fastener to make a joint, this thesis focused on a common design which is bolted lap joint. A bolted lap joint is composed of two overlapping components fastened together by a bolt.

In a bolted joint there is a contact patch at each interface between components. These contact patches have an impact on the dynamic properties of the structure. The position, the behaviour of the regions in the contact patch and the size of these contact patches could be the key to the understanding of the nonlinear dynamic behaviour of joint and are investigated in this thesis.

2 LITERATURE REVIEW

This Chapter presents the literature review related to this thesis.

The first section of this chapter, Section 2.1 , will present the technical background linked to the experimental investigation of vibration. The second section, Section 2.2, will examine the modelling of joints. The third section, Section 2.3, will review in detail the experimental methods adopted for the investigation of the dynamics of joints. The fourth section, Section 2.4, will present the different signal processing methods used to analyse the vibration of built-up structures.

2.1 Technical Background

This section will introduce the theoretical and technical background around the experimental testing of bolted joints. The first section, Section 2.1, introduces the linear theory of vibration which is the foundation of this thesis.

Most of the theory presented in this section, if not referenced, is from two books: (Ewins 2000) and (Maia and Silva 1997).

Table 1 Nomenclature of Section 2.1

Variable	Definition	Unit
x	Relative Displacement	$[m]$
k	Rigidity	$[N\ m^{-1}]$
m	Mass	[Kg]
X	Relative Displacement	$[m]$
ω_0	Natural frequency	$[\text{rad}\ s^{-1}]$
i	i defined as $i = \sqrt{-1}$	$[no\ unit]$
$H(w)$	Frequency Respond Function (FRF)	$[no\ unit]$
$F_{viscous\ damping}$	Friction force of viscous damping	$[N]$
A	Instantaneous amplitude in the middle of the interval fitted	$[ms^{-2}]$
c	Modal / effective viscous damping or also proportional damping	$[Nm^{-1}s]$
ω	Frequency of vibration	$[\text{rad}\ s^{-1}]$
a	Frequency of vibration in hertz	[Hz]
Q	Q factor (damping)	$[no\ unit]$
ζ	Damping ratio	$[no\ unit]$
$*$	Pattern symbol use to represent any other variable	$[no\ unit]$
$*_j$	Subscript for the recording point j	$[no\ unit]$
$*_r$	Subscript for the mode of vibration r	$[no\ unit]$
$*_k$	Subscript for the excitation point k	$[no\ unit]$
$[*]$	Matrix form	$[no\ unit]$
$\alpha_{\text{jk}}(\omega)$	FRF receptance for a recording point j and an excitation point k	$[mN^{-1}]$
$[\alpha(\omega)]$	FRF receptance matrix	$[mN^{-1}]$
$\bar{\omega}_r$	Natural frequency for the mode r	$[\text{rad}\ s^{-1}]$
k	Curvature of plane curves	$[m^{-1}]$
ρ	Radius of curvature	$[m]$
y	Deflection (w also used)	$[m]$
θ	Slope	[rad]
E	Young Modulus	$[ms^{-2}]$
I	Second moment of area	$[m^4]$
ρ	Radius of the curvature	$[m]$
M	Bending moment	$[Nm]$
V	Shear force (Q also used)	$[N]$
q	Distributed Loading	$[Nm^{-1}]$

2.1.1 Linear Theory 1D

This subsection presents briefly the one-dimensional spring-mass model. This model is one of the foundations of modal analysis. Some equations, developed in this subsection, are used as reference later on in this document to interpret experimental results.

The simplest vibration model consists of a mass ‘m’ and a spring with a rigidity ’k’. When this mass is isolated, the second principal of Newton can be used: the sum of the forces is equal to mass times acceleration. The only force connected is the spring. Therefore, this system is defined by the equation (2-1), with x as defined in Figure 1:

$$m\ddot{x}(t) + kx = 0 \qquad \textbf{(2-1)}$$

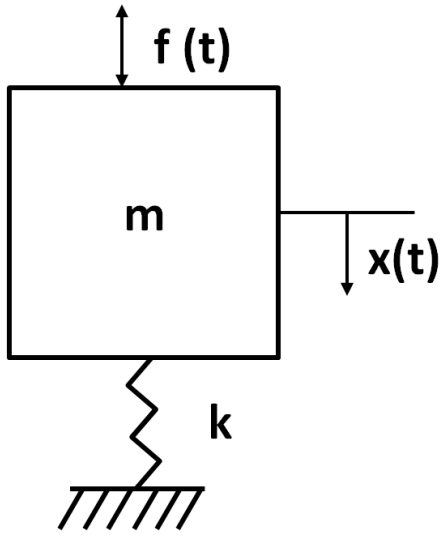

Figure 1 Single-degree-of-freedom (SDOF) system mass-spring

A trivial solution to this second order differential equation is (2-2) with a variable ‘X’ complex.

$$\mathrm{Re}(x(t)) = Re(Xe^{\mathrm{i}\omega\mathrm{t}}) \qquad \textbf{(2-2)}$$

Afterward, the Real function will be omitted which gives:

$$x(t) = Xe^{\mathrm{i}\omega\mathrm{t}} \qquad \textbf{(2-3)}$$

If the solution is inserted in (2-1) the equation can be rewritten as in (2-4) and (2-5).

$$mw^2Xe^{\mathrm{i}\omega t} + kXe^{\mathrm{i}\omega t} = 0 \quad \textbf{(2-4)}$$

$$(m\omega^2 + k)\, Xe^{\mathrm{i}\omega t} = 0 \quad \textbf{(2-5)}$$

If Xe^{iwt} is different to 0 then:

$$k - \omega^2 m = 0 \quad \textbf{(2-6)}$$

The equation (2-6) leads to the equation of natural frequency linked to the mass and rigidity, (2-7):

$$w_0 = \sqrt{\frac{k}{m}} \quad \textbf{(2-7)}$$

The equation (2-7) is important, as it allows for the interpretation of the evolution of natural frequency due to an evolution of stiffness. Indeed, if the rigidity increases the natural frequency will increase. Also if the mass increases, the natural frequency will decrease.

If we assume a sinusoidal excitation as written in (2-8) and described in Figure 1.

$$f(t) = Fe^{\mathrm{i}\omega t} \quad \textbf{(2-8)}$$

Then, if the force is added in (2-5) we obtain (2-9) with ‘F’ a complex variable.

$$(m\omega^2 + k)Xe^{\mathrm{i}\omega t} = Fe^{\mathrm{i}\omega t} \quad \textbf{(2-9)}$$

We can extract the Frequency Respond Function (FRF) from (2-9) defined as $H(w)$ as in (2-10).

$$H(w) = \frac{X}{F} = \frac{1}{k - \omega^2 m} \quad \textbf{(2-10)}$$

Using the equation of natural frequency (2-7), we can rewrite (2-10) as in (2-11).

$$H(w) = \frac{1/k}{1 - (\frac{\omega}{\omega_0})^2} \quad \textbf{(2-11)}$$

The Magnitude of the FRF is as in (2-12).

$$|H(w)| = \left| \frac{1/k}{1 - (\frac{\omega}{\omega_0})^2} \right| \quad \textbf{(2-12)}$$

With $\omega_0 = 1\ \mathrm{rad} s^{-1}$ and $\mathrm{k} = 1\ \mathrm{N}\, m^{-1}$, we can plot the value of the magnitude of the FRF in function of the frequency w, see Figure 2. The shape obtained is typical of a resonance peak.

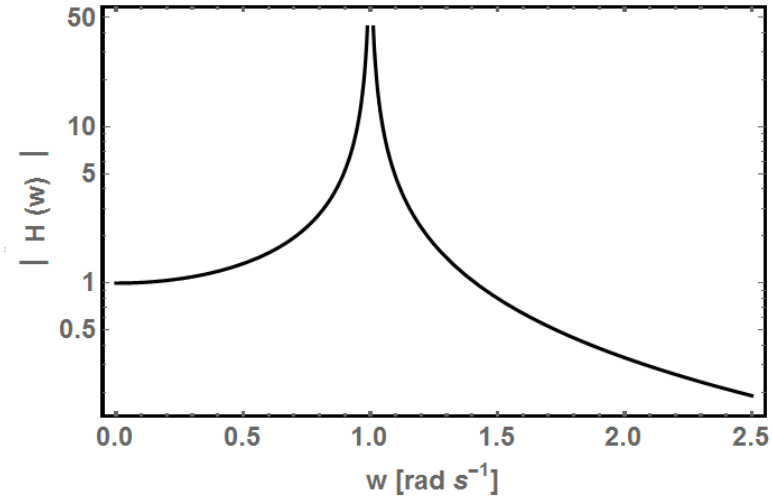

Figure 2 Magnitude of the FRF of an SDOF with a natural frequency at 1rads^{-1}. Without damping, the response is infinite at the natural frequency.

Even the simplest model of vibration can resonate at his natural frequency. If the model doesn't have damping, the response of the system from any continuous input is an infinity output at the natural frequency.

Another approach is to consider the energy input and output of this model. At the resonance the energy increases because the input excitation is in phase with the velocity of the mass. Therefore at the natural frequency, the energy becomes infinite with time, which is completely unrealistic. Adding some dissipation of energy or damping in this model makes it more realistic.

2.1.2 Damping

Damping is a concept which contains all the phenomena linked to the dissipation of energy inside a vibrating system.

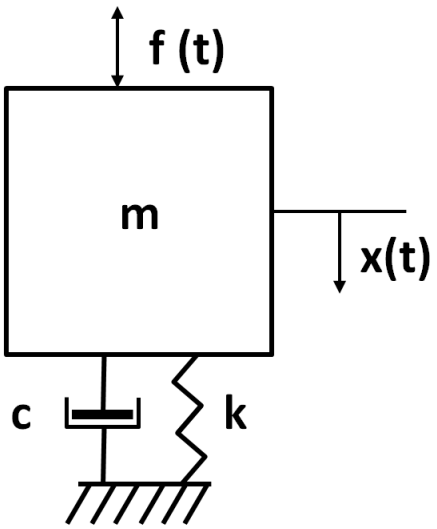

Figure 3 Single-degree-of-freedom (SDOF) system: mass-spring-dashpot from (Ewins 2000, p28)

There are multiple ways to introduce damping in an SDOF, for example by using coulomb friction, a linear or quadratic dashpot. This subsection only develops the simplest and most used version which is linear viscous damping.

Moving one step closer to reality consists of adding viscous damping to include the dissipation of energy in the SDOF. This viscous damping is defined as a proportional resistance to the velocity ($\dot{x}$).

$$F_{viscous\ damping} = c\,\dot{x} \qquad \textbf{(2-13)}$$

This viscous damping is represented by a dashpot. This dashpot introduces some damping inside the SDOF model. The equation of motion obtained turns into the (2-14) with this dashpot.

$$m\ddot{x}(t) + c\,\dot{x} + kx = Fe^{\mathrm{i}\omega\mathrm{t}} \qquad \textbf{(2-14)}$$

The same trial solution as in (2-3) is used but with a variable‘s’ imaginary ‘s’ instead of “$i\omega$” in (2-15).

$$x(t) = Xe^{\mathrm{st}} \qquad \textbf{(2-15)}$$

A solution exists if and only if the condition defined in (2-16) is verified. Which gives two conditions (2-17) and (2-18) only if $c^2 > 4\mathrm{km}$. The condition "$c^2 > 4\mathrm{km}$" is verified for all the systems studied in this thesis.

$$\mathrm{ms}^2 + \mathrm{cs} + k = 0 \quad \textbf{(2-16)}$$

$$s_1 = -\frac{c}{2m} + \frac{\sqrt{c^2 - 4\mathrm{km}}}{2m} \quad \textbf{(2-17)}$$

$$s_2 = -\frac{c}{2m} - \frac{\sqrt{c^2 - 4\mathrm{km}}}{2m} \quad \textbf{(2-18)}$$

The damping ratio 'ζ' and the constant 'c_0' are, then, introduced. The Greek letter 'ζ' is pronounced "zeta". These changes of variable allow a simplification of the equation.

$$c_0 = 2\sqrt{km} \quad \textbf{(2-19)}$$

$$\zeta = \frac{c}{c_0} = \frac{c}{2\sqrt{km}} \quad \textbf{(2-20)}$$

The solutions (2-17) and (2-18) turn as (2-21) and (2-22).

$$s_1 = -\zeta \mathrm{w}_0 + i\,\omega_0\sqrt{1-\zeta^2} \quad \textbf{(2-21)}$$

$$s_1 = -\zeta \mathrm{w}_0 - i\,\omega_0\sqrt{1-\zeta^2} \quad \textbf{(2-22)}$$

The modal solution to the equation of motion is as in:

$$x(t) = Xe^{-\omega_0 \zeta \mathrm{t}} e^{i(\omega_0\sqrt{1-\zeta^2})t} \quad \textbf{(2-23)}$$

The real part of the previous equation is:

$$x(t) = \quad Xe^{-\omega_0 \zeta \mathrm{t}} \quad \mathrm{Sin}[\left(\omega_0\sqrt{1-\zeta^2}\right)t + \phi] \quad \textbf{(2-24)}$$

This can be separated into two parts: the envelope decay and the sinusoid. Using $w = 50rad\ s^{-1}, \zeta = 0.05(no\ unit), \phi = 0rad\ , and\ X = 10m,$ an example of sinusoidal decay is plotted in Figure 4.

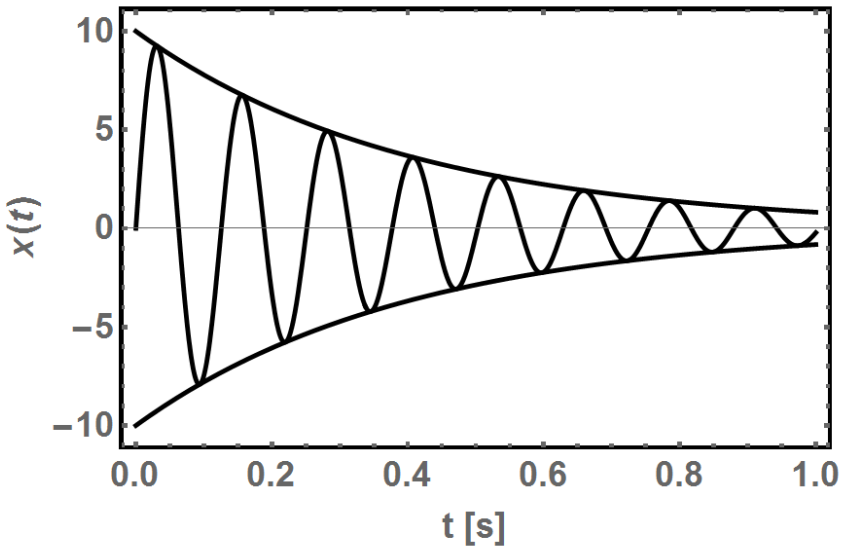

Figure 4 Example of sinusoidal decay with the positive and negative decay envelopes

The instantaneous amplitude of vibration, which corresponds to the value of the envelope at an instant t is defined as:

$$A(t) = \quad Xe^{-\omega_0 \zeta t} \tag{2-25}$$

Considering the same force as before, the equation (2-14) can be rewritten as in (2-26).

$$(-\omega^2 m + i\,\omega\, c\ + k)e^{i\omega t} = \ Fe^{i\omega t} \tag{2-26}$$

The FRF is as in (2-27).

$$H(\omega) = \frac{X}{F} = \frac{1}{(k - \omega^2 m) + i(\omega c)} \tag{2-27}$$

Using the change of variable defined in (2-19), (2-20) the FRF is as in (2-28).

$$H(\omega) = \frac{X}{F} = \frac{1/k}{1 - \left(\frac{\omega}{\omega_0}\right)^2 + 2i\zeta\frac{\omega}{\omega_0}} \tag{2-28}$$

Therefore, $|H(w)|$ is as in:

$$|H(w)| = \frac{1/k}{\sqrt{(1-\left(\frac{\omega}{\omega_0}\right)^2)^2 + (2\zeta\frac{\omega}{\omega_0})^2}} \quad \textbf{(2-29)}$$

The effect of the introduction of damping in the SDOF FRF is plotted in Figure 5. The value of rigidity and natural frequency are respectively: $k = 1\ N\ m^{-1}$ and $\mathrm{w}_0 = 1\ rad$.

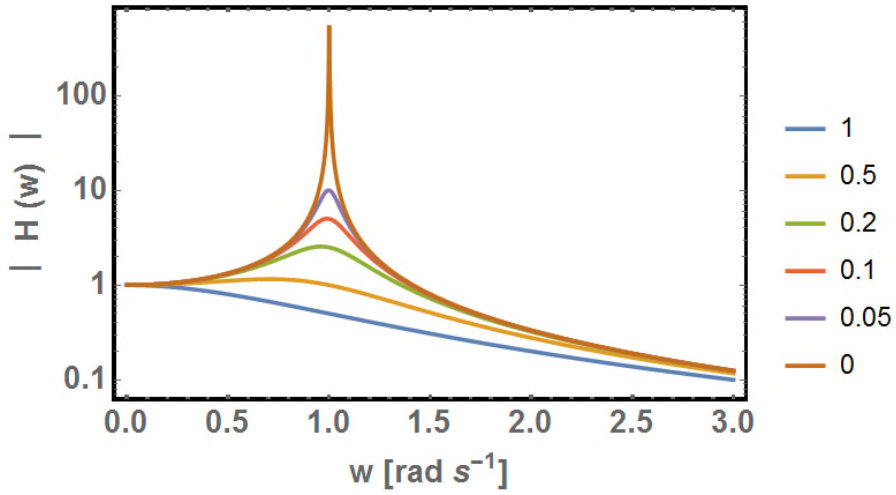

Figure 5 Evolution of the FRF as a function of the damping ratio. The higher the damping ratio, the broader the resonance peaks. The different values of damping ratio are displayed on the right side.

Another way to write the equation (2-28) is to use the Q factor, short for Quality factor, to obtain the equation (2-30). The Q factor is linked to the damping ratio by equation (2-31).

$$H(\omega) = \frac{X}{F} = \frac{1/k}{1-\left(\frac{\omega}{\omega_0}\right)^2 + i\frac{\omega}{\omega_0 \mathrm{Q}}} \quad \textbf{(2-30)}$$

$$Q = \frac{1}{2\zeta}\ or\ \zeta = \frac{1}{2Q} \quad \textbf{(2-31)}$$

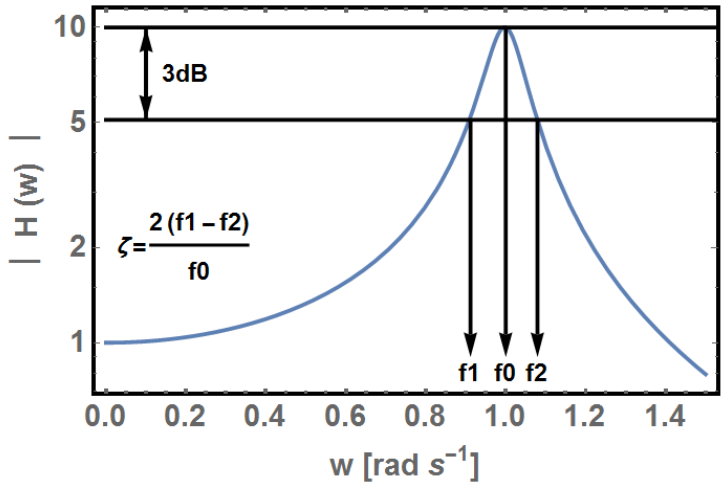

Figure 6 Illustration of the 3db method. This method allows an estimation of the damping ratio from an FRF

The damping ratio can be estimated from the FRF using the so-called “3dB method”, illustrated in Figure 6. First, take the peak value of the amplitude modulus (or $|H(w)|$). Then, remove 3 decibel (divide the value by the square root of two) from the peak value giving the value “m3”. After, measure the two frequencies, f1 and f2, of the FRF which have an amplitude modulus of m3. Then, the equation (2-40) is used to calculate an estimation of the damping ratio. Once again we see that the broader the peak, the larger is the damping.

$$\zeta = \frac{2(\mathrm{f1} - \mathrm{f2})}{\mathrm{f0}} \qquad \textbf{(2-32)}$$

However, the 3dB method is imprecise. It uses only 3 points of the FRF to estimate the damping ratio. Indeed, the FRF plots are composed of many data points, and if the frequency resolution is small, large errors can be expected. Another example, if the FRF is noisy the calculated value can be far from the true value. Furthermore, the results of the 3dB method can be completely absurd if multiples of the natural frequencies of modes are close to each other, as in Figure 7. Nevertheless, this technique is widely used due to its simplicity and its satisfactory precision.

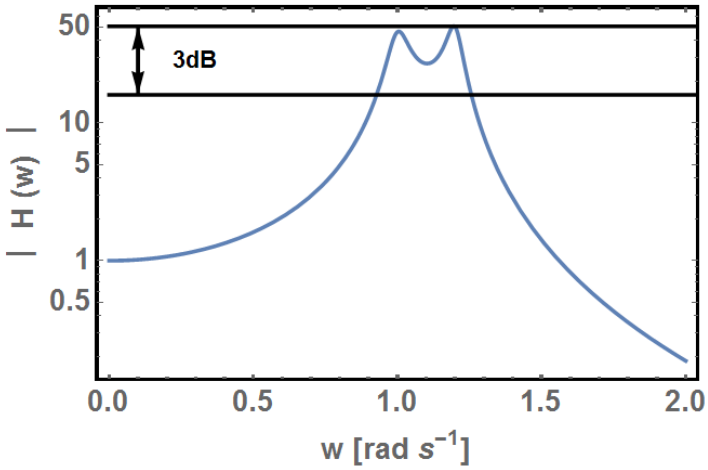

Figure 7 The 3dB method cannot be used when multiples modes are too close to each other

Friction is supposed to be the main source of damping in a joint. Friction is mostly associated with large relative displacement, and there is no macroscopic displacement in joint. Therefore the term “microfriction” is used to speak about the damping of a joint.

Due to the friction inside the joint multiple failure mechanisms may occur. Fretting (wear or corrosion of asperity) may happen to the surfaces in contact inside a joint and create the start of a crack. Fatigue (weakening caused by repeated loading) may also happen. When a different type of material is in contact, there is a risk of chemical reaction happening at the interface due to the presence of heat and broken asperities.

Material damping consists of the energy dissipation inside a monolithic isotropic piece of material. This material damping is very small in general. Lazan (1968) lists a very large number of values of material damping for different materials and different types of loading. Maloney and Peairs (2000) measured the material damping of a steel beam to be around 2x10^-3, whatever the amplitude, expressed as a damping ratio, whereas the comparable beam with a bolted joint had a damping ratio two to five times bigger depending on the amplitude of vibration.

2.1.3 Linear Theory 3D

Linear theory has been further developed to consider systems with multiple degrees of freedom. When there are two degrees of freedom, two resonances are measured. In the real world, any component has an infinite number of degrees of freedom and therefore an infinite number of resonances.

The finite element method allows the calculation of the natural frequencies of a component, based only on the distribution of mass and the rigidity. The rigidity connects the elements of masses together. A matrix of mass and rigidity is used to quantify these two components. The equation (2-14) can be rewritten into matrix form:

$$[M]\{\ddot{x}\} + [K]\{x\} = \{f\} \quad \textbf{(2-33)}$$

The Matrix of mass is $[M]$ and the Matrix of rigidity is $[K]$, $\{\ddot{x}\}$ is the acceleration vector and $\{x\}$ is the displacement vector which regroups all the degrees of freedom of the finite element model.

The system of differential equation (2-33) can be solved in the same way as an SDOF system, following the same method as in (Ewins 2000).

Let us assume that the system can vibrate at a single frequency ω using a simple harmonic motion. The vector of displacement can be written as in (2-34) and the force as in (2-35). Let's consider that the system studied has N degrees of freedom. Then, the vector $\{X\}$ and $\{F\}$ are Nx1 time independent complex amplitudes.

$$\{x(t)\} = \{X\}e^{\mathrm{i}\omega\mathrm{t}} \quad \textbf{(2-34)}$$

$$\{F(t)\} = \{F\}e^{\mathrm{i}\omega\mathrm{t}} \quad \textbf{(2-35)}$$

This results in the following equation:

$$([K] - \omega^2[M])\{X\}e^{\mathrm{i}\omega\mathrm{t}} = \{0\} \quad \textbf{(2-36)}$$

The non-trivial solution which satisfies equation (2-36) is equation (2-37):

$$\det|K] - \omega^2[M]| = 0 \quad \textbf{(2-37)}$$

This equation can be solved using linear algebra. The complete solutions of this linear system are the eigenvalues and eigenvectors. The eigenvalues are the natural frequencies of the system, and the eigenvectors are the mode shapes of the structure.

The mode shapes are represented by the matrix $[\Psi]$. In $[\Psi]$, each column of imaginary numbers represents one mode shape.

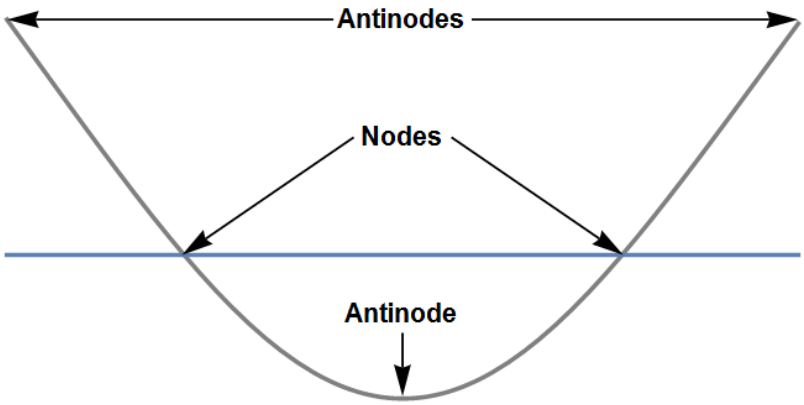

Figure 8 First mode shape of a Free-Free beam is grey; the blue line represents the beam without motion

An illustration of the concept of mode shape, node and antinode are plotted in Figure 8. A mode shape represents the shape the component takes when it is excited at a natural frequency. The nodes of the mode shape are the point locations where the amplitude of displacement is null. The nodes do not move whatever the phase of the mode shape. The antinode(s) of a mode shape is the point which always maintains the maximum amplitude of displacement. The word “mode” is a synonym of the word “resonance”.

The subscript $*_r$ will describe an element for a specific mode. The natural frequency will be named $\bar{\omega}_r$. The mode shape of one mode will be written $[\Psi]_r$.

The respond model can be rewritten as the receptance FRF matrix $[\alpha(\omega)]$. This matrix is of size NxN. Please refer to (Ewins 2000), p 41, for more details about the concept of receptance. The subscript $*_j$ refers to the position where the movement is observed, and the subscript $*_k$ refers to the position where the force is applied. One element of the $[\alpha_{\mathrm{jk}}(\omega)]$ matrix is defined as in (2-38).

$$\alpha_{\mathrm{jk}}(\omega) = \frac{X_j}{F_k} \quad \textbf{(2-38)}$$

The variable X_j stands for the displacement at the position j, whereas the variable F_k stand for the force input at a position k. Therefore, the matrix $[\alpha_{\mathrm{jk}}(\omega)]$ allows a prediction of the vibration response of a linear structure whatever the position of the excitation or the measured motion.

It is also possible to compute an FRF based only on a sum of mode shapes, the modal mass (see (Ewins 2000), p 54) and the natural frequencies as shown in equation (2-39). The concept of modal mass is given by Ewins (2000) in his book at page 54. The demonstration to obtain this equation can be found in (Ewins 2000), p 60.

$$\alpha_{\mathrm{jk}}(\omega) = \Sigma_{r=1}^{N} \frac{(\Psi_{\mathrm{jr}})(\Psi_{\mathrm{kr}})}{m_r(\bar{\omega}_r{}^2 - \omega^2)} \quad \textbf{(2-39)}$$

The term Ψ_{jr} corresponds to the complex amplitude at a point of interest j for the mode of vibration r. The term Ψ_{kr} corresponds to the complex amplitude of a point of excitation k for the mode r. For a mode r, the modal mass is expressed as m_r, the natural frequency $\bar{\omega}_r$.

From equation (2-39), we can see that the position at which the vibration is measured and where the excitation is applied is important. For example, if the accelerometer is at a node of a mode, then no vibration will be recorded for that mode. Also, the location and orientation of the excitation have a direct impact on which mode will be exercised and which one will not.

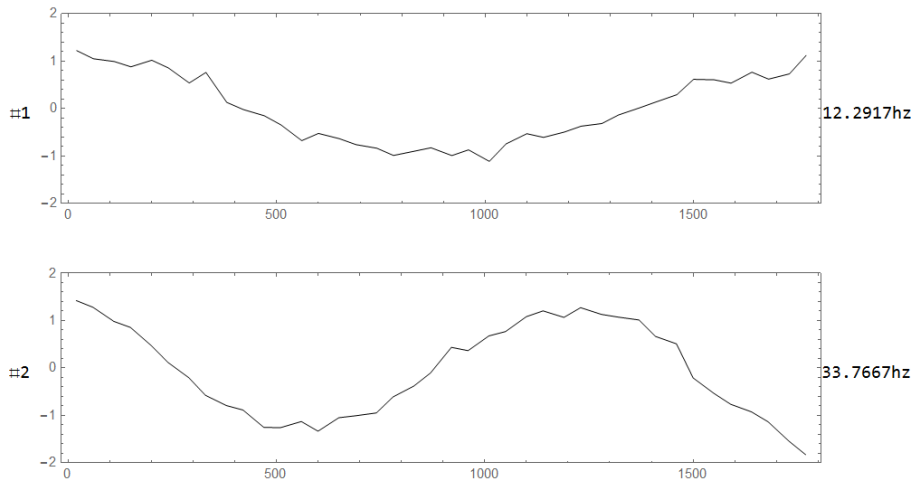

Figure 9 Experimental mode shapes made by hitting a structure at multiple locations with a hammer. This figure is in three parts: on the left, the mode number, in the middle, the measured mode shapes, and on the right, the measured natural frequencies.

Also, one important result from equation (2-39) is that it is possible to extract the mode shape of a structure using experiments with either multiple input forces or multiple recording places. Indeed, if the recording point or the force position is modified, only the terms Ψ_{jr} and respectively Ψ_{kr} will modified, as the modal mass and the natural frequencies are constant in theory. It is therefore possible to measure the mode shape of a structure by either changing the excitation location or by changing the recording location or even by recording the vibration at multiple locations for each recording.

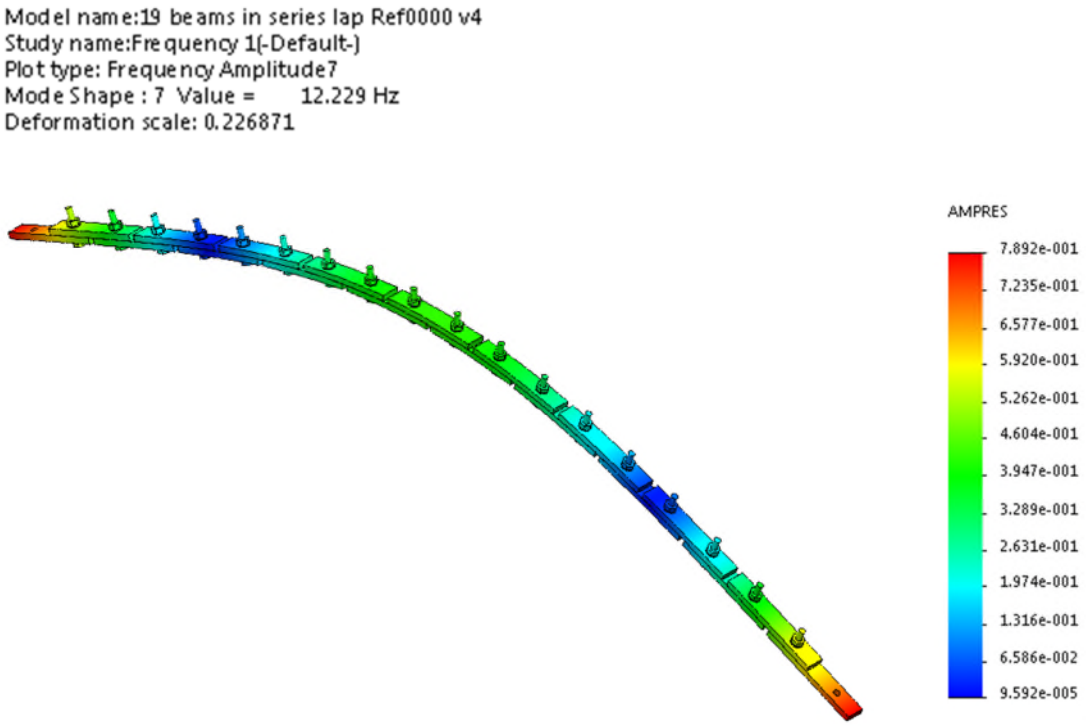

Figure 10 Example of a mode shape calculated using the software SOLIDWORKS of a free-free beam. The associated natural frequency is 12.229Hz as written above. The colours are linked to the unscaled amplitude of displacement.

A modern finite element modal analysis software can calculate mode shapes and natural frequency, see Figure 10. The software requires three elements to solve the frequency analysis: the geometry, the Young's modulus and the density of the component. The geometry is defined by the user of the software. The Young's modulus provides the link between stress and strain (in other words the stiffness) of the component. And the density allows the distribution of mass to be quantified.

2.1.4 Static Beam theory

One of the most used models in mechanics is beam theory. For this subsection, the notation used follows Shigley's notation (Budynas and Nisbett 2015). This one-dimensional model is extremely useful, even though current computers allow detailed finite element analysis.

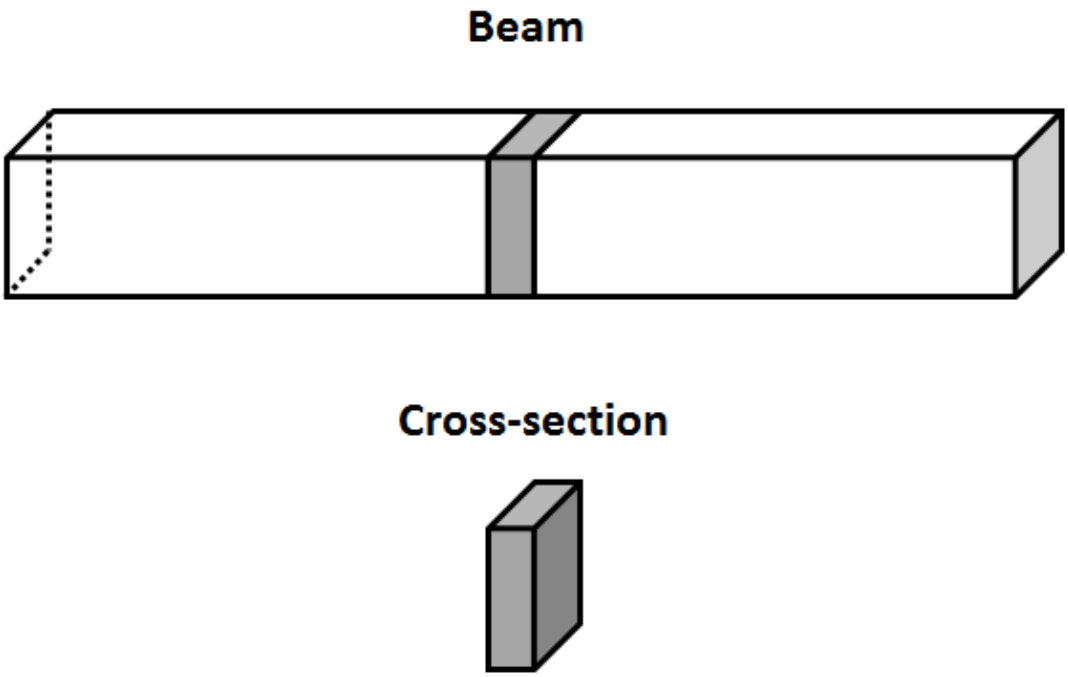

Figure 11 Illustration of the fundamental element of the beam theory.

The element of this model is a cross-section of a beam as in Figure 11. The cross-section is then isolated. The bending moment of the section can be calculated because the sum of the moments acting on the cross-section must be equal to zero. Moreover, the shear force is obtained the same way, this time using the sum of the external forces acting on the cross-section. The external forces are due to the way the beam is loaded. An example of a load is gravity which consists of a distributed force in the beam. Another classic loading is a point force located at an extremity of the beam.

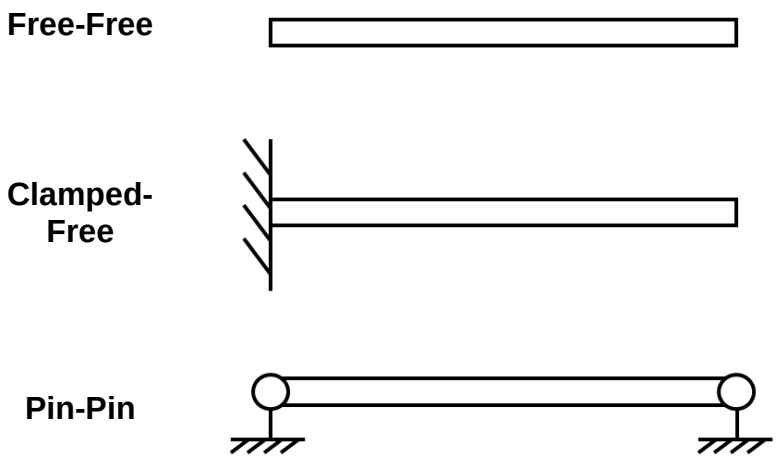

Figure 12 Tree types of model for the boundary condition to a beam. “Free” means no constraint, “Pin” blocks the displacement, and “Clamped” which blocks displacements and rotations

The connection the beam has with its environment can also generate an external force. These connections can block one or multiple degrees of freedom as shown in Figure 59. By doing so, external forces are introduced into the beam.

The relation between the load (q), the shear force (V) and the bending moment (M) is as in (2-40). The variable ‘x’ defines the position inside the beam. It is necessary that the multiple identical cross-sections stay perpendicular to the centroid of the section. Another assumption is that the cross-section stays flat for this relation to be true.

$$q = \frac{\mathrm{dV}}{\mathrm{dx}} = \frac{d^2M}{\mathrm{dx}^2} \qquad \textbf{(2-40)}$$

The equation (2-40) allows the calculation of the shear and the bending of a beam from the load as illustrated in Figure 13.

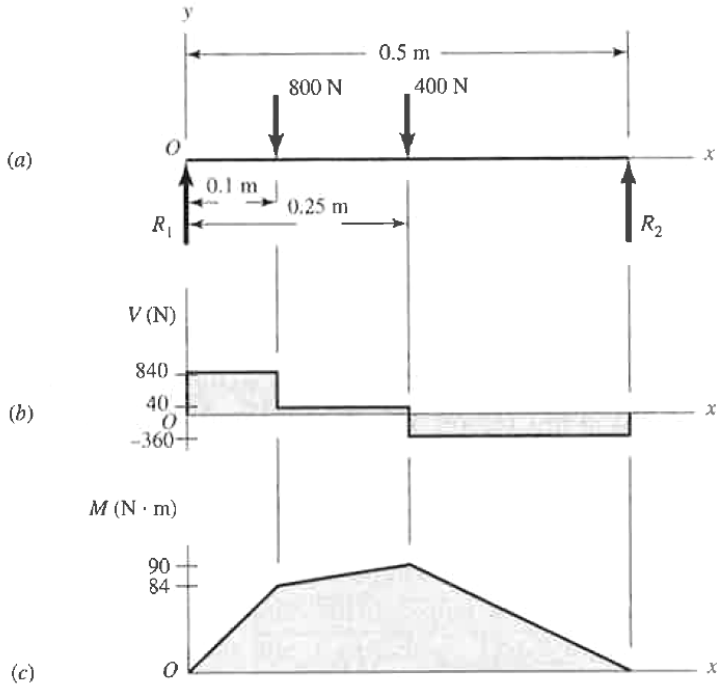

Figure 13 Example of the diagram of loading (a), Shear force (b) and bending-moment (c) from (Budynas and Nisbett 2015, p91). The diagrams (b) and (c) can be calculated from the diagram (a) and equation (2-40).

2.1.5 Relation between deflection and the bending moment

Budynas and Nisbett (2015, p164-165) compile the different equations which link the deflection of a beam with the bending moment. This subsection enumerates the different equations which relate the two concepts.

The deflection is a function of the position on the beam:

$$y = f(x) \tag{2-41}$$

The slope is defined as follow:

$$\theta = \frac{\mathrm{dy}}{\mathrm{dx}} \tag{2-42}$$

The curvature (k), the radius of curvature (ρ) and the bending moment (M) are related to the deflection (y) as follow, assuming that the slope is very small ($\mathrm{dy}/\mathrm{dx} \approx 0$):

$$k = \frac{1}{\rho} = \frac{d^2\,y/\mathrm{dx}^2}{(1 + (\mathrm{dy}/\mathrm{dx})^2)^{3/2}} = \frac{M}{\mathrm{EI}} \approx \frac{d^2y}{\mathrm{dx}^2} \quad \textbf{(2-43)}$$

The shear force can be calculated with this equation:

$$\frac{V}{\mathrm{EI}} \approx \frac{d^3y}{\mathrm{dx}^3} \quad \textbf{(2-44)}$$

Morover, the distributed load is related to the deflection this way:

$$\frac{q}{\mathrm{EI}} \approx \frac{d^4y}{\mathrm{dx}^4} \quad \textbf{(2-45)}$$

2.1.6 Relation between displacement and acceleration

The fundamental relation between acceleration, velocity and displacement is:

$$a(t) = \frac{\mathrm{dv}(t)}{\mathrm{dt}} = \frac{d^2y(t)}{\mathrm{dt}^2} \quad \textbf{(2-46)}$$

If the acceleration signal is a sinusoid, if the integral variables are equal to zero and if the phase is neglected the following relation can be applied:

$$v(t) = \frac{a(t)}{2\pi\mathrm{f}} \quad \textbf{(2-47)}$$

$$y(t) = \frac{a(t)}{4\pi^2 f^2} \quad \textbf{(2-48)}$$

2.1.7 Introduction to modal analysis

Table 2. The four classic steps of a modal analysis

1 - Preliminary analysis
2 – Experimental investigation
3 – Signal processing
4 – Model fitting

The following subsections are a brief description of the field modal analysis. This description is following the different steps listed in Table 2. The order of the steps

may vary according to the goal of the study. Also, an iterative process is often used to refine the results.

2.1.7.1 Preliminary analysis

The first step is to create a “test strategy”. This strategy should define the objectives of the analysis and how they will be reached. For example, the aim could be to obtain a precise digital model to understand the run time behaviour of a pump.

During the second step, the preliminary mode shapes are used to create a “test plan”. This test plan will detail which modes should be investigated, where the structure should be excited, how and where the vibration will be recorded. The structure is modelled using a “Computer-Aided Engineering” (CAE) software to obtain the natural frequencies and the associated mode shapes. Figure 14 is an illustration of the test plan step.

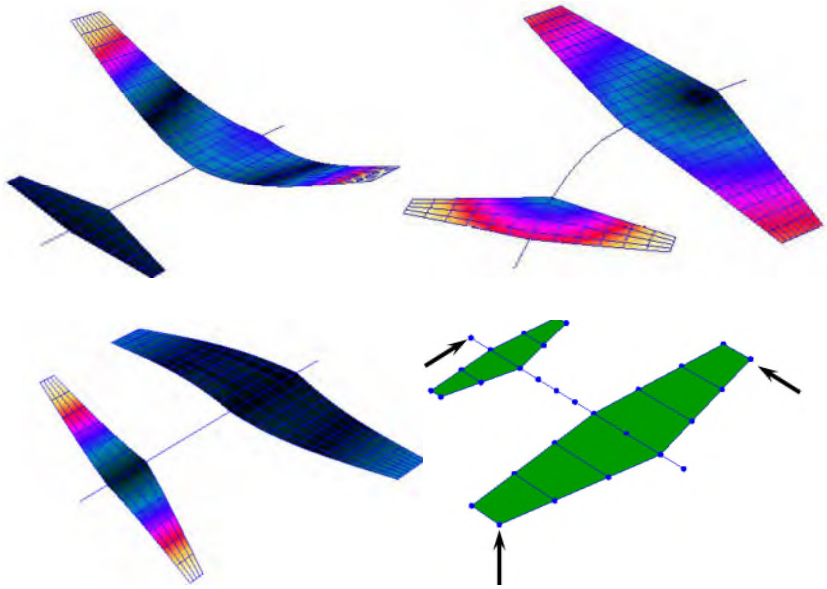

Figure 14 Example of mode shapes from a numerical model and on the bottom right example the excitation locations which could be part of a experimental planning, from (Mains 2015)

This preliminary model will include four different inputs from the structure analysed:

1. The shape
2. The mass distribution
3. The rigidity

4. The damping

Each input has uncertainty associated with it, which will have an impact on the quality of the simulation. These inputs could be updated later using measurements from the experimental stage.

2.1.7.2 Modal analysis: Experimental investigation

During this stage, the structure to be investigated is excited and the resulting vibration is recorded, see Figure 15. The investigated structure could be a simple beam, a bridge, a satellite, a building or even a planet. The boundary of the structure needs to be selected carefully, and, often, the structure is suspended to simplify the testing. The excitation is often performed using either a hammer or a shaker, but other ways exist. For example with the planet earth, earthquakes and nuclear explosions are strong enough to allow a study of the inner core. Finally, the vibration is, in most cases, recorded using an accelerometer or a laser. Then an acquisition computer samples the analogue signal to create time histories, which will be treated in the signal processing stage.

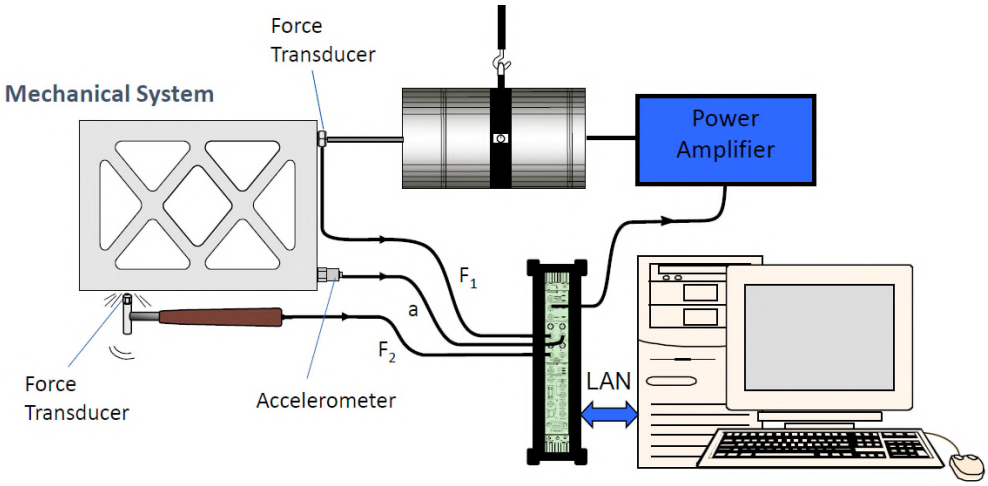

Figure 15 Illustration of an experimental investigation. The cylinder shape on top is a shaker. Source: (Mains 2015)

In addition to vibration testing, precise measurement of the mass distribution and the shape of the real structure could be done. For example the real thickness of a cast. part or the real length of a part would help the model to be as precise as possible.

2.1.7.3 Modal analysis: Signal processing

The raw measurement signal needs to be post-processed. This signal is in the time domain, and most often the goal is to create a modal model. There are multiple methods which have been developed over the years to create a modal model of a structure. The most simple is to use the Fourier transform to display the experimental data in the Frequency domain under the form of an FRF (also called Bode Plot) or a Nyquist plot. Then, the data is fitted to extract the modal parameters. These modal parameters are the natural frequencies, damping and the mode shape of each mode.

2.1.7.4 Modal analysis: Finite element updating

Using the modal parameters extracted, a finite element model is “updated” to be more realistic. This step uses the experimental data as the objective. The parameters of the model are modified like the mass distribution, the rigidity or the damping. The value of the natural frequencies and the damping can be directly compared. Another way is to use a MAC matrix (for “Modal Assurance Criterion”). A MAC matrix allows a correlation between the experimentally-measured mode shapes and the theoretically predicted ones. This MAC matrix allows a visual inspection of the quality of the modal for the rigidity and the mass distribution. For example in Figure 16, The mode 4, 5, 6, 7, 8, 9 and 11 are well modelled as there is a high MAC value on the diagonal, whereas the modes 1, 2, 3, 10, 12, 13 are correlated with others modes.

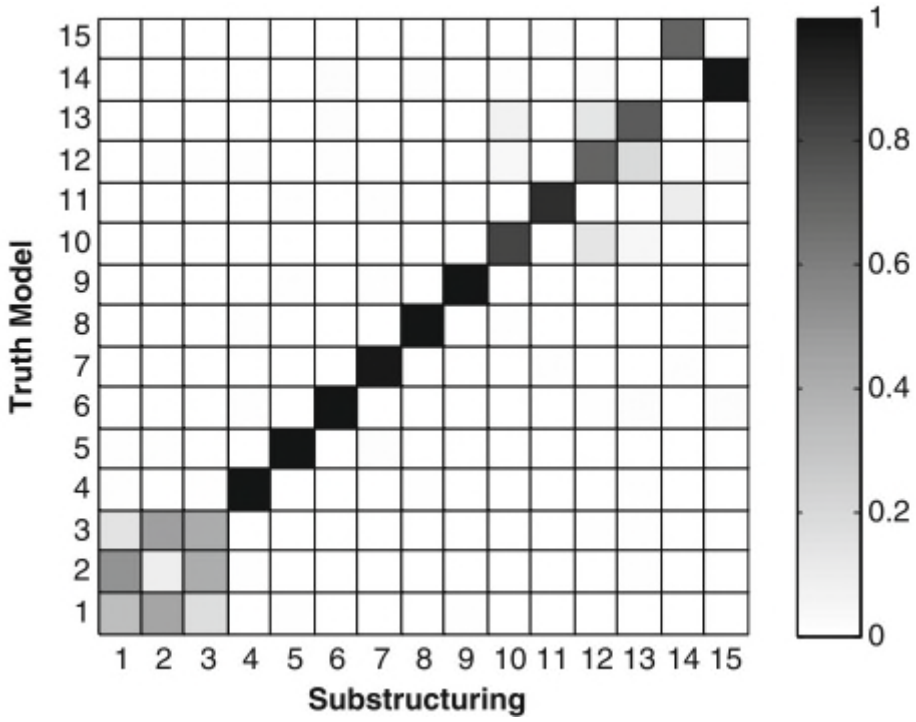

Figure 16 Example of MAC matrix plot

2.1.7.5 Summary

Table 3 and Figure 17 give a summary of what a linear modal analysis is about.

Table 3 Summary of the different vocabulary associated with the field of modal analysis

	Concepts	Visualisation tools	Damping concept	Illustration
Reality	Structure, Component, Vibration, Bolt, Failure	Pictures, Videos, Movement	Energy Dissipation	
Time Domain	Time, Acceleration, Speed, Position	Time History, Speed Against Position	Damping Ratio (ζ)	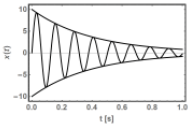
Frequency Domain	Frequency, Phase, Imaginary Part, Real Part	FRF, Nyquist Plot	Sharpness of Peak	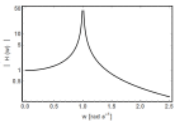
Modal Analysis	Mode, Natural Frequency, MAC	Mode shape, Table of Mode	Viscous Damping (c)	
Finite Element Analysis	Young Modulus, Volume Mass	Mesh	Viscous Damping (c)	
Mathematical Equations	Mass (m), Rigidity (k), Dash Pot(c), Second Order Differential Equation	Symbols, Equations	$F_{viscous\ damping} = c\,\dot{x}$	$m\ddot{x}(t) + c\,\dot{x} + kx = Fe^{i\omega t}$

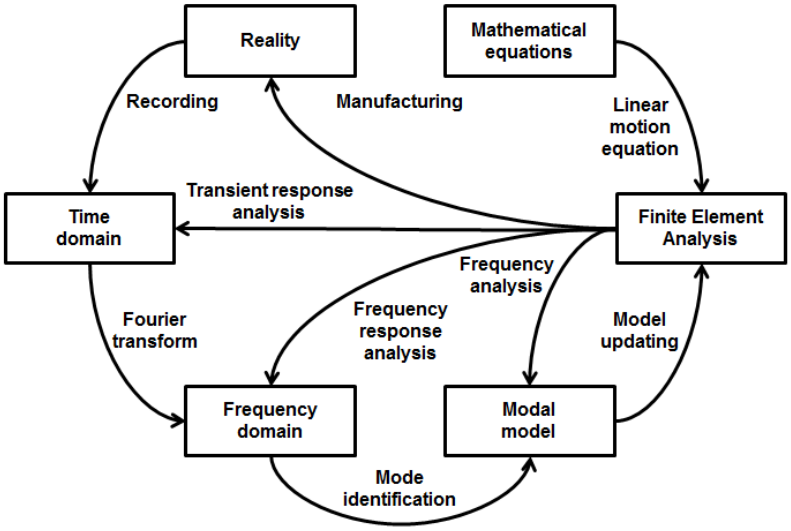

Figure 17 Illustration of some actions under taken during a modal analysis

2.1.8 Introduction to nonlinear models

This subsection will introduce the main types of nonlinearity which are associated with the vibration of real structures.

The linearity of a differential equation is defined as followed: if two functions ‘g’ and ‘j’ are solutions of a differential equation. If the differential equation is linear, then, any linear combination ag + bj is a solution of the differential equation too, with ‘a’ and ‘b’ real numbers.

The linear model states that there is a linear relation between the input force and the displacement output. This rigidity relation is often not realistic in real structure. The rigidity of real structures is often nonlinear. The rigidity could either increase or decrease when the vibration amplitude of the excitation increases. If the rigidity increases, there is what it is called a hardening effect. Conversely, if the rigidity decrease then there is a loosening effect. To model this nonlinear phenomenon a cubic stiffness is often used. Table 4 gives a comparison of the linear stiffness and the nonlinear stiffness depending on the point of view.

The damping of real structure is also commonly nonlinear. In a linear model the damping is directly linked to the velocity of the structure. The damping, like the rigidity, could vary as a function of the excitation input. However, it could be more

realistic to model it as a coulomb friction or a quadratic damping, see Table 4 for the definitions. These two models of nonlinear damping are the most common in the literature. Other types of nonlinear behaviour are observed, which leads to creation of more elaborated nonlinear models, but they are out of the scope of this introduction.

Table 4 Summary of the different representation of nonlinear rigidity and nonlinear damping

	Linear behaviour	Loosening / Hardening effect	Coulomb friction / quadratic damping
Reality	Vibration of an isolated component: the natural frequency and the damping ratio are constant	A loosening effect is often observed in lap joint, but a hardening effect can also happen on real structure with joints.	Most structure with joint seems to experiences a nonlinear damping with an intensity correlated to the amplitude excitation.
Time Domain	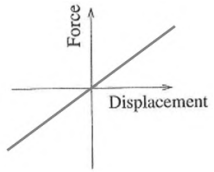	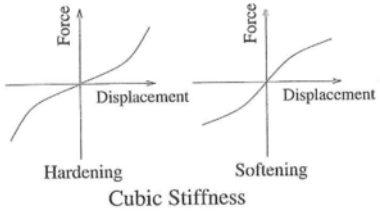	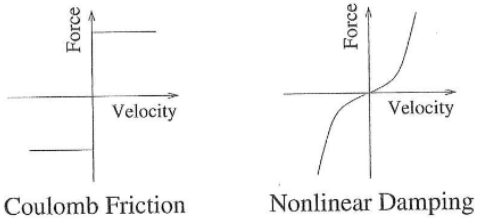
Frequency Domain	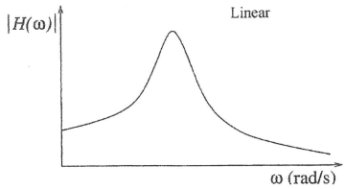	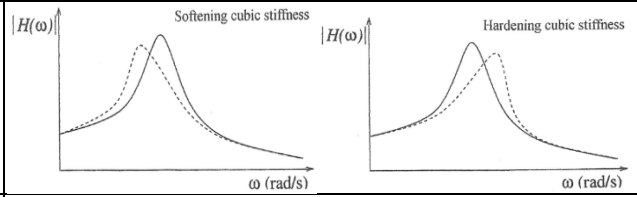	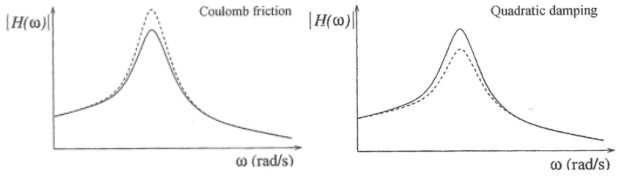
Modal Analysis	Each mode have a single natural frequency, damping and one mode shape whatever the amplitude of excitation	The natural frequency at each resonance depends of the amplitude of the input.	The damping depend on the amplitude of the input
Finite Element Analysis	Linear finite element	Nonlinear spring element	Nonlinear dashpot elements
Mathematical Equations	$m\ddot{y} + c\dot{y} + ky = x(t)$	$m\ddot{y} + c\dot{y} + ky + k_3 y^3 = x(t)$ Softening cubic stiffness: k3 < 0 Hardening cubic stiffness: k3 >0	$m\ddot{y} + f_d(\dot{y}) + ky = x(t)$ Coulomb friction: $f_d(\dot{y}) = c_F \mathrm{Sign}(\dot{y})$ Quadratic damping: $f_d(\dot{y}) = c_2\, \dot{y}\, \lvert\dot{y}\rvert$

2.2 Modelling of joints

In this section, a literature review of the modelling of joints submitted to vibration is presented.

2.2.1 Modelling of joints: Introduction

Segalman (2009) reviews the experimental investigation of the dynamics of joints in the introductory chapter of the "Handbook on Dynamics of Jointed Structures",(Daniel J Segalman et al. 2009). Even though the focus is on the work conducted by the Sandia National Laboratories (later called only Sandia in this document), this review is the closest to the work presented in this thesis. The work carried out at Sandia is focused on the investigation of bolted lap joints with a longitudinal excitation with the final aim of creating a predictive model and conducting intensive research in that direction.

The domain of the model is a classic way to categorise models depending on which parameters are fitted. Three categories have been found as described in (Ewins 2000, page 27) along with the type of parameters:

- Spatial (mass, damping, stiffness)
- Modal (natural frequencies, mode shape)
- Response (Frequency responses, impulses response)

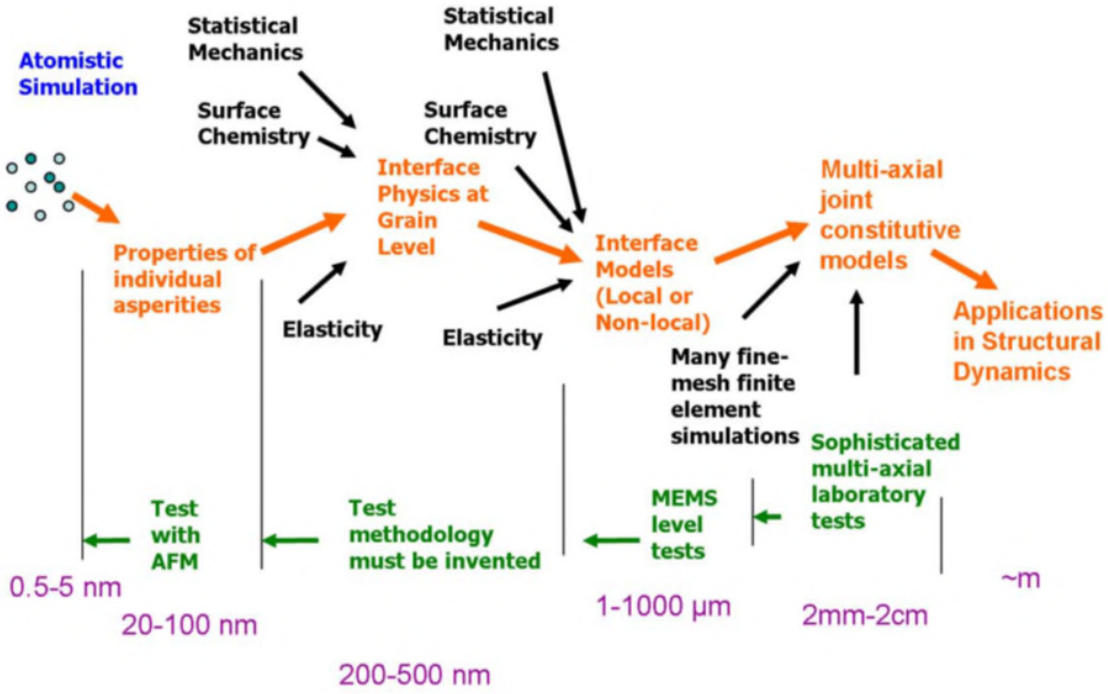

Figure 18 Experimental road map from (Daniel J Segalman and Gregory 2009)

The following subsections are inspired by the scale classification of an experiment made by Daniel J Segalman and Gregory (2009) as shown in Figure 18. The next subsection, Subsection 2.2.2, will focus on microscopic (<2mm) models. Subsection 2.2.3 will present mesoscopic scale models which have the size of a joint. Subsection 2.2.4 reviews the models which take a macroscopic approach to the nonlinear behaviour of joints. The last subsection, Subsection 2.2.5, gives a synthesis of the different models used.

2.2.2 Microscopic scale

Various reviews show that there is great uncertainty surrounding the friction model. Berger (2002) reviews different models of friction and their implementation to predict experimental results. His main conclusion is that “the system model and friction model are fundamentally coupled,” which means there is no general friction model which will work in every case. He also lists many parameters which have been shown to influence friction: “sliding speed, acceleration, critical sliding distance, temperature, normal load, humidity, surface preparation, and, of course, the material combination.”

An overview of the research in tribology has been made by Vakis et al. (2018). An illustration of all the parameters which may have an impact on friction can be seen in Figure 19.

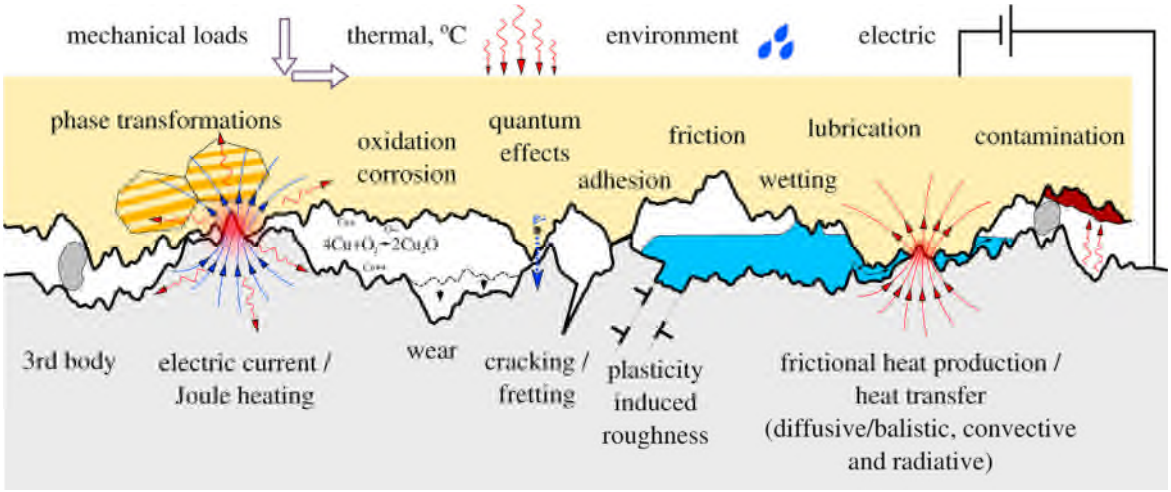

Figure 19 The complexity and multi-physics illustration of the phenomenon of friction from (Vakis et al. 2018) p177.

No predictive models of friction currently exist; therefore “calibrated models” are commonly used. As friction is claimed to be the main mechanism of damping in joints, there is no good foundation on which to build a predictive model of the dynamic behaviour of joints. Therefore, a bottom-up development, which starts from a microscopic model and explains macroscopic phenomenon, is unlikely to succeed.

Brake (2017, chapter 14) reviews the calibrated model of friction used to model joints. These friction models are typically tuned and fitted using friction experiments. They are then applied in advanced nonlinear analysis of the vibration of a structure. Because the work presented here is more focused on experiments and simpler linear finite element models without friction, no comparison of friction models is presented in this document.

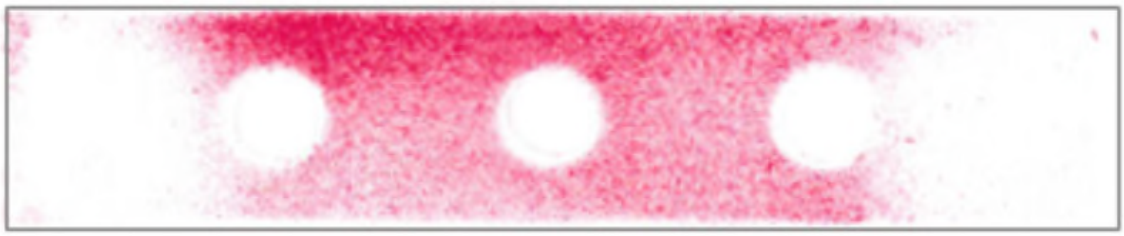

Figure 20 Pressure film of the interface of a bolted lap joint, from (Brake 2017, p210) . The surfaces in contact are in red. The white parts demonstrate a gap either due to a bolt hole or due to a receding contact (see subpart 2.2.3).

One approximation used to model joints is the fact that all interfaces are in contact, as in (Jewell, Allen, and Lacayo 2017) and that each part of the surface is either sliding or stuck, but, as rightly pointed out by Brake (2017), p210, some part of the surface is not even in contact in a static case, see Figure 20. Therefore, placing a friction contact at every possible coupled node could artificially rigidify the surface. Also, this approximation makes possible the dissipation of energy at locations where, in reality, there is no possible contact, which can lead to unrealistic numerical results.

2.2.3 Mesoscopic scale: models of joints

This subsection will describe the effort to model joints at the scale of the size of a joint. Most of the models which follow use a microscopic model of friction. If a joint model takes into account more than one bolt, it is described in the next subsection focused on the macroscopic model of joints.

The word microfriction is often used in the literature, (Groper 1985), to mention the friction which occurs in joints. This word is used because there is no macro displacement inside joints, only the microscopic phenomenon. Segalman (2001) makes a clear distinction between partial slip and microfriction. Partial slip involves a relative displacement of the whole interface between components.

The classic way to model the contact between two components in a joint is to consider that each surface can be modelled as a sphere and, consequently, a Herzian contact can be used.

Segalman (2001) described two regions, see Figure 22. The slip region where friction can happen far from the bolt and stick region where there is no relative

displacement close to the bolt. Goyder (2015) extended the concept by considering that slip may happen close to the bolt, see Figure 24. Then later, the third type of region has been defined by Lancereau et al. (2017), the alternating region, which considers the surface which enters in contact due to the deformation of the interface by vibration. This concept of regions does not have a consistent name in the literature.

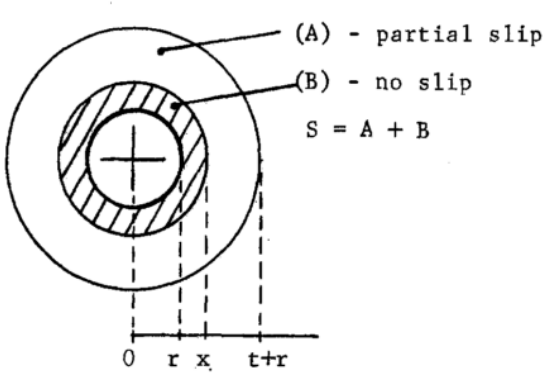

Figure 21 Interpretation of the region where the slip may or may not occur from (Groper 1985)

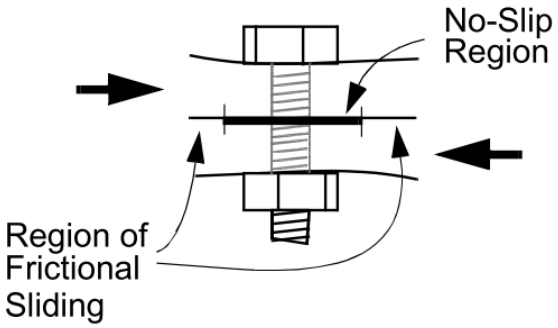

Figure 22 Interpretation of the region where microfriction occurs in joints from (Daniel J Segalman 2001)**, with apparently longitudinal shear loading as the main excitation of the joint.**

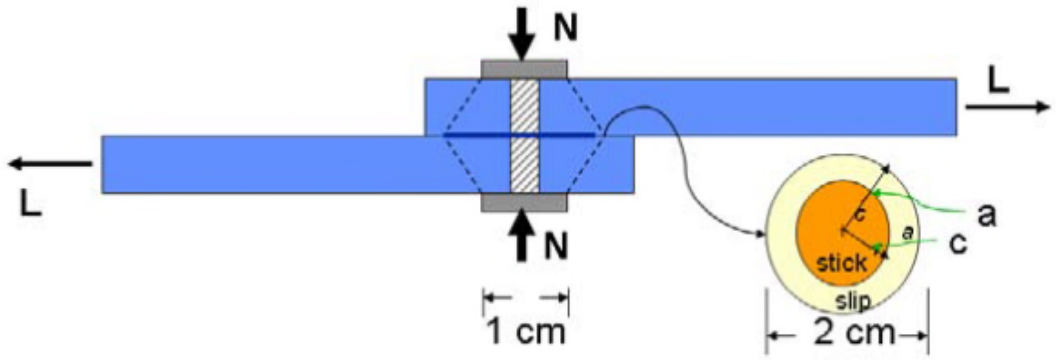

Figure 23 (Daniel J Segalman et al. 2009)**, p31, representation of the possible contact patches inside bolted lap joints.**

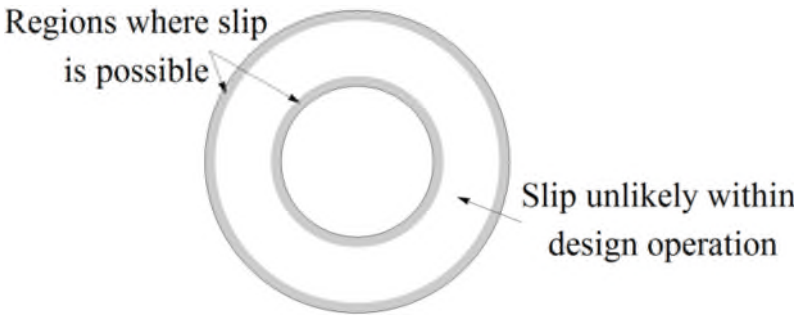

Figure 24 Interpretation of the location the slip and stick region in a bolted joint from (H. Goyder 2015a)

One other way to represent the slip-stick region is to use a spatially discretized model as in Figure 25. Figure 25a) displays a lap joint. Figure 25b) is the spatially discretized model using mass-spring, forces, and some surface region. Due to P, a longitudinal force pulls the lap joint apart, and micro-friction occurs in the joint. The mass C and D have a relative motion which represents the slip region. This motion is possible because of a weak normal constraint at the interface due to the distance to the bolt. The mass A and B are stuck due to a larger constraint at the interface generated by the bolt. The stuck region is therefore between A and B.

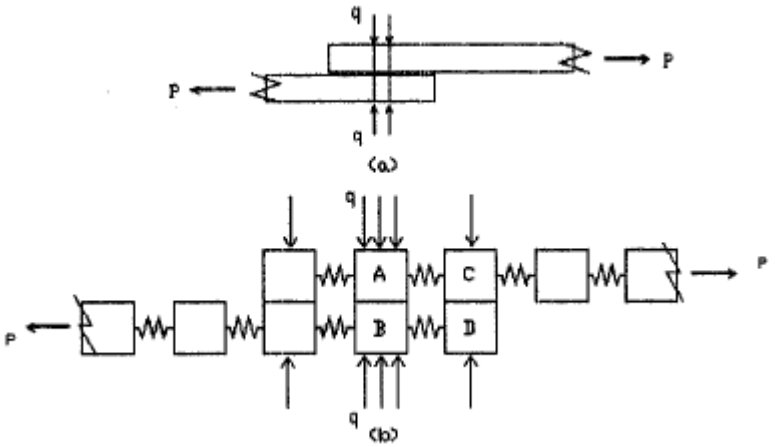

Figure 25 Spatially discretized model of lap joint by Kess, Rosnow, and Sidle (2002).

Other methods have been used to model joints which consist of modelling the joint as only one element. This one element model takes two different forms: either a modified beam element or it can be a nonlinear finite element connected to a linear element using a web.

A different approach has been investigated in (Song et al. 2004). It models the whole lap joint using a custom beam element (“adjusted Iwan beam model”, see Figure 26).

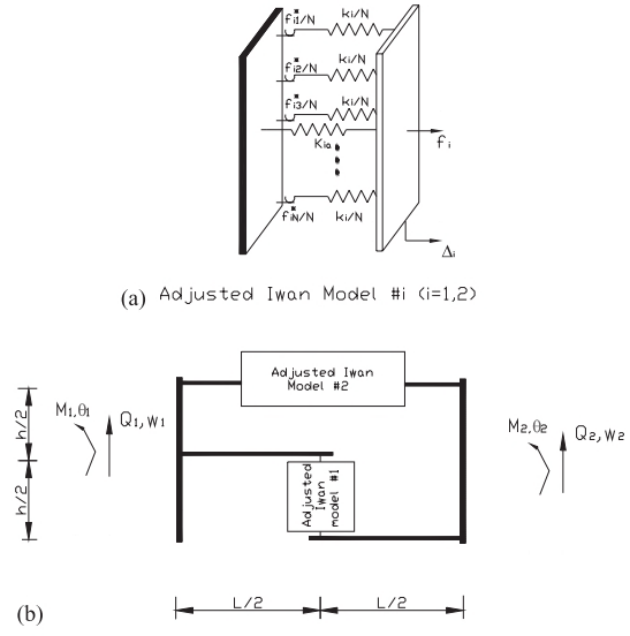

Figure 26 The architecture of the adjusted Iwan beam model used in (Song et al. 2004)

Meyer and Adams (2015) developed a nonlinear element to model a bolted lap joint to achieve a qualitative analysis of the effect of high-frequency probe signals through a bolt. The model has two possible directions: along the longitudinal axis of the beam or rotation at each node. Figure 27 shows the location of the nonlinear bolt element. A spring, a dashpot and a quadratic stiffness spring were used to model the influence of the bolt on the beam.

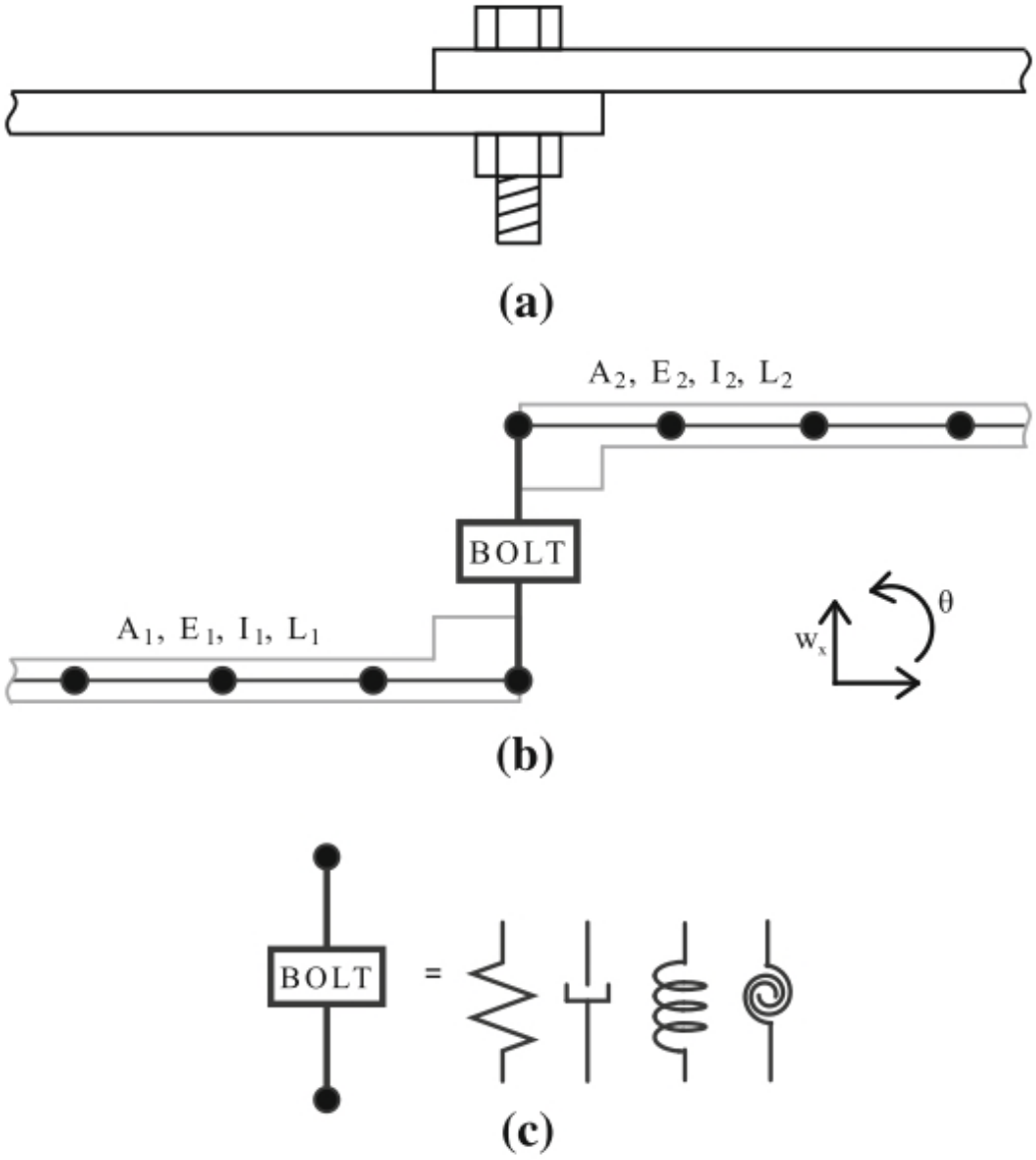

Figure 27 a) lap joint investigated by Meyer and Adams (2015) b) Custom beam theory model of the bolted lap joint c) illustration of the element inside the bolt element, which is a classic Euler–Bernoulli element with a quadratic stiffness and two

dashpots: one for the shear force, one for the bending moment. The thickness of the bolt element is twice the thickness of the other beam element.

Goyder and Lancereau (2016) observed that the frequency of vibration is correlated to the size of the contact patch. The smaller the contact patch, the lower is the frequency. This is a very simple explanation for the softening effect commonly measured in bolted lap joints. Dossogne, Jerome, Lancereau, and Smith (2017) show that the geometry of the interface has a large impact on the vibration behaviour of the structure.

In Figure 28, Hills, Nowell, and Sackfield (1993, p40) have characterized three types of static behaviour of contact patches:

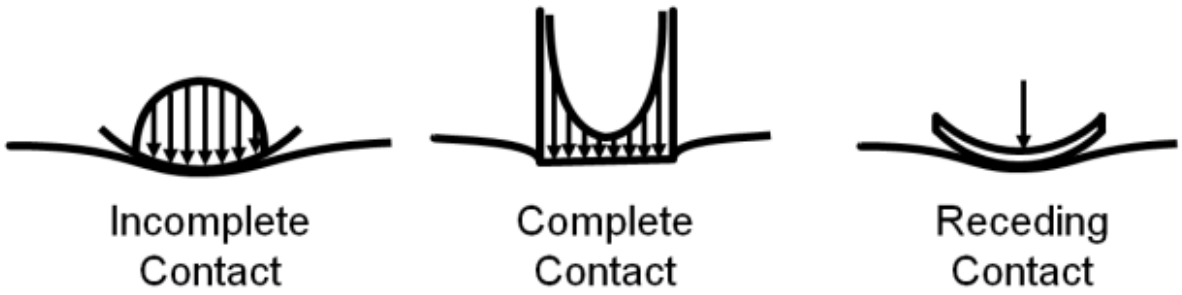

Figure 28 Three types of contact identified by Hills, Nowell, and Sackfield (1993, p40)

- The **incomplete contact** (sphere and plane) can be modeled by the Hertz model. Incomplete contacts create a distribution of the pressure with the highest pressure in the middle. The pressure drops to zero at the limit of the contact. A circular area around the edge is prone to slipping because the normal stress is low.
- The **complete contact** (small pad and plane) has a concentration of stress close to the edge. This concentration of stress avoids any slipping of the interface.
- The **receding contact** (large pad, concentrated force and plane) happens when two large flat surfaces are pressed together at one place, by a bolt, for example. The receding contact still needs to be investigated to understand the stress distribution at the edges.

Hills et al. (2017) have updated the 1993 categorisation of contacts, see Figure 29. Hills et al. (2017) also claim, without published evidence, that receding and “incomplete contacts and non-conformal contact” behave the same way when submitted to vibration.

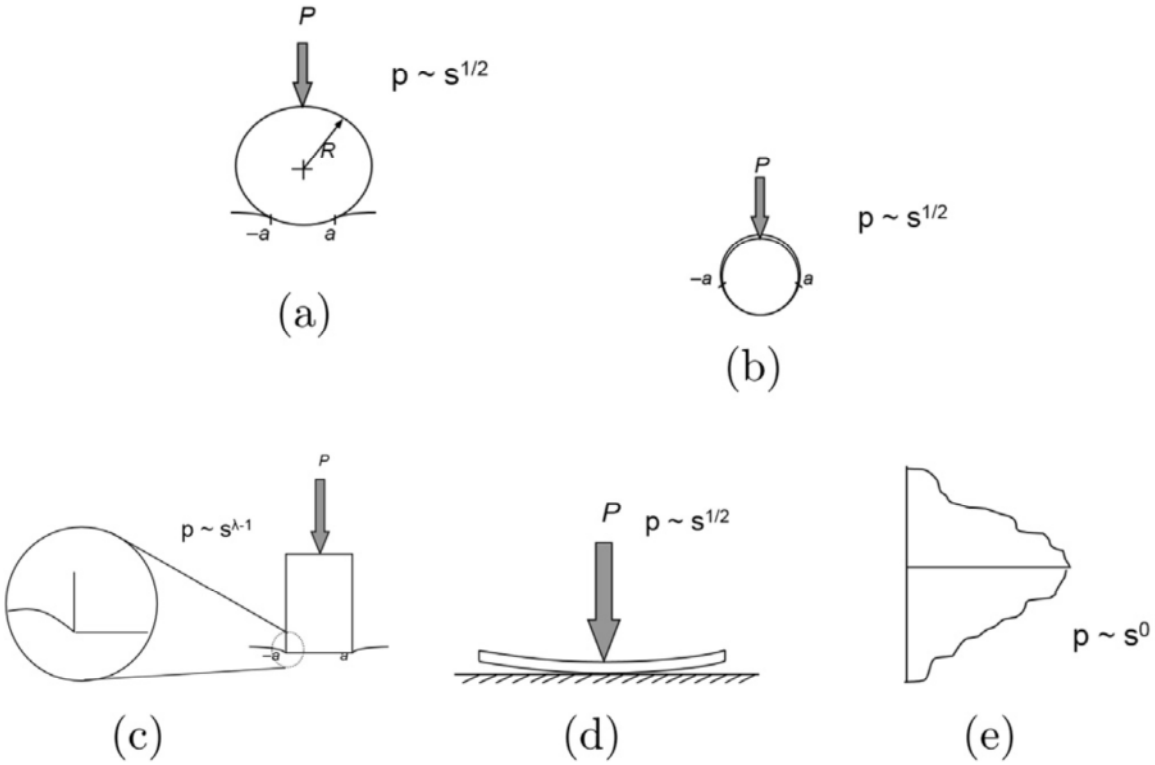

Legend:

(a) incomplete and non-conformal contact

(b) incomplete and conformal contact

(c) complete contact

(d) receding contact

(e) common edge contact

Figure 29 Taxonomy of five different types of contact proposed by Hills et al. (2017).

In his bolt design book, Bickford (2007) categorise mechanical joints depending of two characteristics. The first criterion is the presence of a gasket to seal the joint or not. Indeed, special precautions have to be taken to seal a joint properly. The second criterion is the direction of the load compared to the axis of the joint. He defined two types of joint, "tensile joint or shear joint", with a different procedure to design each. A "tensile joint" (or tension joint) has a load or a force applied

approximatively parallel to the axes of the bolts, see Figure 30. A "shear joint" has the vector of the force almost perpendicular to the axes of the bolts, see Figure 31. He claims that shear joints are more resistant than tensile joints by design, therefore shear joints are used in priority in the construction industry.

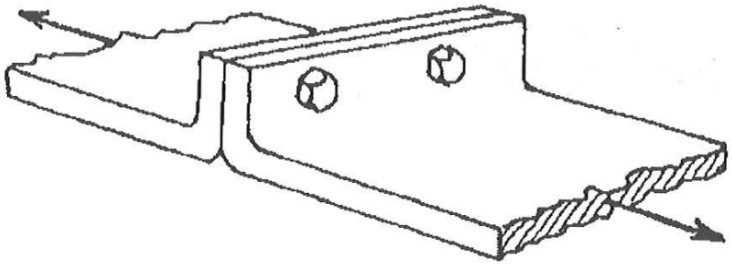

Figure 30 Illustration of a typical “tensile joint” from (Bickford 2007) p2.

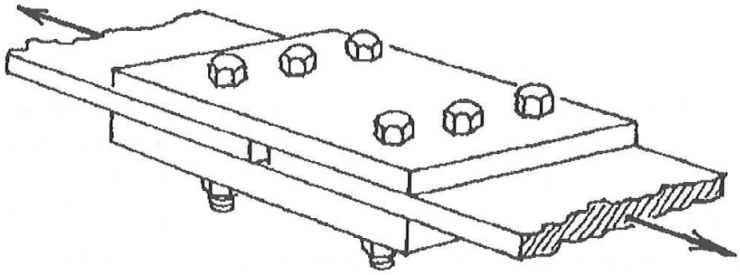

Figure 31 Illustration of a typical “shear joint” from (Bickford 2007) p2.

Also, Bickford (2007) reviews a model with springs to model a bolted joint, which was not reused in the joint dynamic literature, in the knowledge of the author. He represents the bolts as springs and the components locked together as a large spring, as show in Figure 32. This simple representation allows a better understanding of the way the energy is stored inside a bolted.

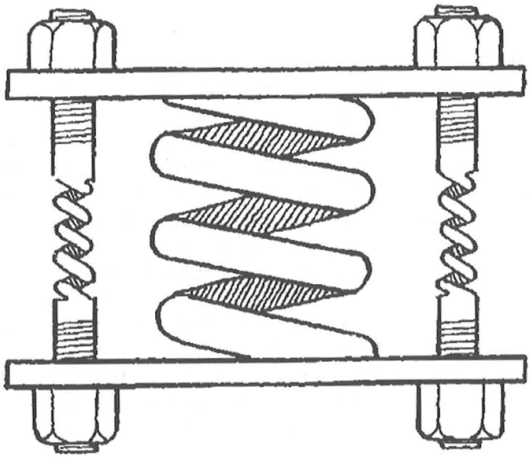

Figure 32 Bolted joints model where each component is assimilated as a spring. Source: (Bickford 2007) p2. This model illustrate that energy is stored in the bolts and the components when the bolts are tight up.

Bickford (2007) presents different procedures to design bolted joints, however very limited consideration are accorded to vibration. The vibration is only consider as an added dynamic loading which needs to be calculated or estimated to avoid a failure of the joint.

Finally, Bickford (2007), p146, gives a formula, (2-49), based on empirical results to relate the bolt preload and the torque applied. This preload corresponds to the real static load applied by the bolt after taking into account the bolt relaxation and friction lost. The relationship between the preload and a bolt torque:

$$T = F_p \, K \, D \qquad \textbf{(2-49)}$$

With :

T	Input Torque	[Nm]	Example: 54.2 Nm
F_p	Archived Preload	[N]	Ex.: 27100 N
D	Diameter of the bolt	[m]	Ex.: (M17 bolt) 0.01 m
K	Nut factor	[Dimensionless]	Ex.: (Stainless steel/ steel) 0.2

The nut factor is an empirical constant which depends on the materials, lubricants and other parameters like the surface treatments of the bolt. Bickford (2007), p146, provides a table of nut factor values.

2.2.4 Macroscopic model of multiple joints

One of the most efficient ways to fit the nonlinear data from a joint vibration experiment is to fit each mode individually. Using a custom single degree of freedom mass-spring system, a calibrated model can be easily reached. The original idea was published by D J Segalman (2010) where an Iwan model was added to a SDOF to introduce friction nonlinearity.

The idea was further developed by Mayes, Pacini, and Roettgen (2014), where, in addition to a Segalman/Iwan model, two other models were fitted: a FREEVIB element using cubic stiffness and damping and an RFS (Restoring Force Surface). The conclusion of this work is that the three models successfully fitted the experimental data; however, the cubic stiffness and damping were easier to interpret because of the similarity with the linear model.

2.2.5 Synthesis

Globally, most of the models of joints found in the literature use a fitted model except the power law model from Sandia and the work on contact patches by Hills. Fitted models, as opposed to predictive models, need experimental data for the vibration of the joint to be accurate.

In these calibrated models, the size of the models allows a classification. A generalisation can be made from this classification. The larger the scale of the model, the faster the model can be computed. Mesoscopic reduced order models of bolted joints are faster to compute than the high fidelity microscopic finite element analysis model. The reduction of computer power necessary can be dramatic, for example (M. R. Brake et al. 2014) found a reduction of 3 orders of magnitude. Also, the microscopic model seems promising, but due to the high computational cost of processing and the risk of divergence, experimental validation does not seem to have been achieved yet. The most promising result of the microscopic model can be

seen in (Jewell, Allen, and Lacayo 2017), where a prediction of damping ratio has been done in a quasistatic analysis, but no experiment has been associated to confirm those results.

Even if a mesoscopic calibrated model has a limited number of parameters, after calibration they efficiently capture the nonlinear behaviour of the structure.

This situation has been effectively summarised by (Meyer and Adams 2015): “As was demonstrated in (Hartwigsen et al. 2004) and (Ahmadian and Jalali 2007), low-order, lumped-parameter models are capable of producing nonlinear phenomena associated with bolted joints.” In other words, those low order models, after they have been fitted with experimental data, can generate numerical signals comparable with the experiment ones. One application of these fitted models is the prediction of the system behaviour at a higher load, but if the design parameters are modified, these fitted models will not predict the new behaviour.

No clear definition of a predictive model has been found in the literature. Brake (2017) explains that the lack of a predictive dynamic joint model is problematic. However, he does not go into details about what a predictive model would look like, how it would be applied and what the expected input and output would be.

For the rest of this document, the following definition will be used for a predictive model. The ideal predictive model of a dynamic joint will, from the design parameters of the structure, predict the nonlinear behaviour of the structure. The design inputs are: geometry, material, type of fastener, torque, excitation (type, location and amplitude), lubrication, surface roughness and life cycle of the product. The ideal core component of the model would need to be comprehensible for any mechanical engineer and easy to use. The ideal outputs are: nonlinear damping, nonlinear stiffness, instantaneous natural frequency, nonlinear mode shape response to any excitations, and the evolution in time due to wear.

2.3 Experimental method

2.3.1 Experimental method: Introduction

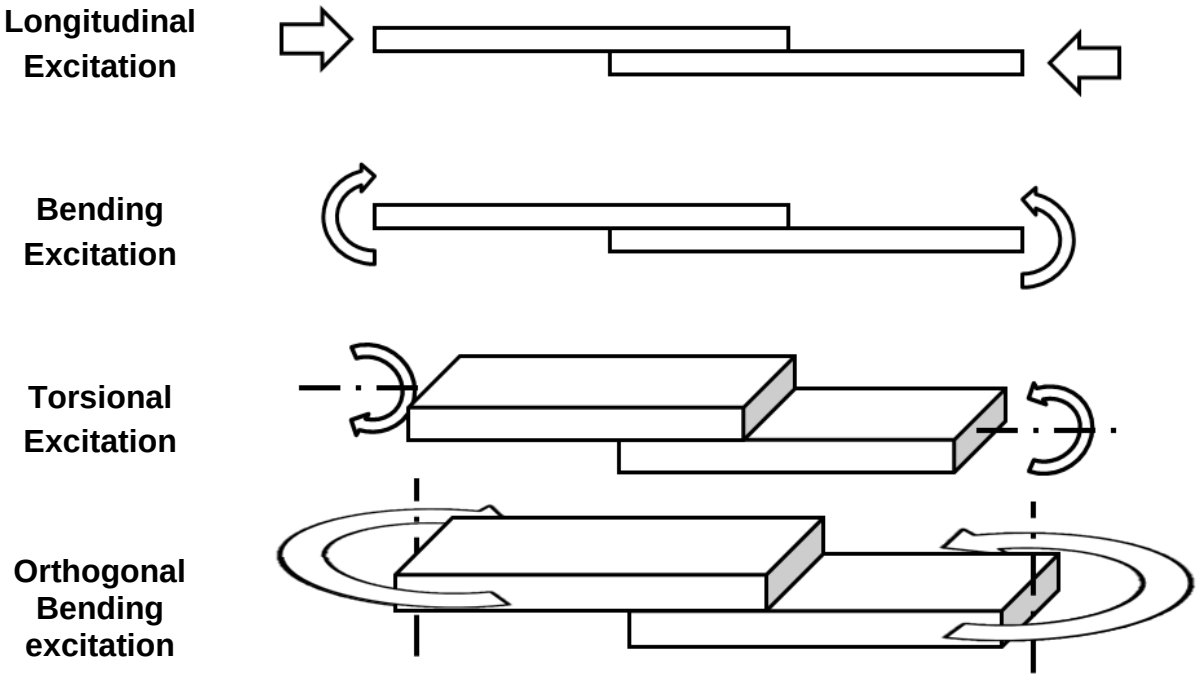

Figure 33 Four types of possible loading of a lap joint

This section on experimental methods is subdivided depending on the loading applied to the lap joint. The author has found that are four ways to exercise lap joints either by longitudinal excitation, by bending, or by torsion or orthogonal bending of the joint as illustrated in Figure 33. Subsection 2.3.2 analyses the experiments with longitudinal loading. A more recent focus has been on bending moment loading. The experiments using bending moment are reviewed in Subsection 2.3.3. Subsection 2.3.4 reviews experiments with torsional loading. No experiments were found in the literature using orthogonal bending excitation. Subsection 2.3.5 will review new experimental tools available to investigate the dynamic of joints. Finally, Subsection 2.3.6 concludes this section on experiments and explains why bending loading is the focus of this thesis. No experiments were found using orthogonal bending excitation.

2.3.2 Longitudinal loading

Extensive work has been carried out on a longitudinal loading. Gregory and Resor (2009) review, in the second chapter of (Daniel J Segalman et al. 2009), the different experimental designs in the literature which are linked to the work made at the Sandia National Laboratory. This laboratory is intensively investigating the dynamic behaviour of bolted lap joints. Most of the experiments before 2009 made at Sandia where with lap joints exercised longitudinally.

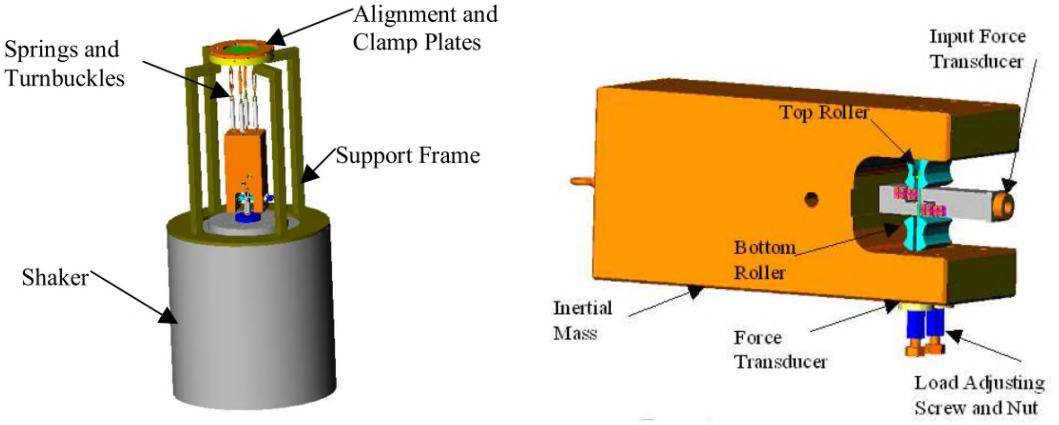

Figure 34 Big Mass experimental set up from (Gregory and Resor 2009b). The bolted lap joint is exercised in longitudinal excitation using the inertia of a suspension mass. The bolts have been replaced by rollers to obtain a precise load of the interface.

Daniel J Segalman et al. (2009) points out the difficulty of measureing the behaviour inside the interface. As a result, indirect measurements of the inner physics are produced. An interpretation of the way lap joints with a longitudinal shear have microslip during a cycle is given. Segalman claims that the slip process is the origin of the nonlinear stiffness and damping in the joint.

One major Sandia experiment is the one conducted by Gregory and Resor (2009b): the big mass device. It proves that the dissipation of energy in a lap joint can be modelled by a power law for a flat lap joint. This same study also investigated three different types of interfaces, multiple pressures at the interfaces and different roughness. The power law will be examined first; the other conclusions will be reviewed subsequently.

$$D = kF^n \quad \textbf{(2-50)}$$

A very simple power law between the force and the damping has been proposed by Gregory and Resor (2009b). The dissipation of energy is given by D; the Force is in F, k is an empirical constant and n is an empirical slope coefficient. N=2 for a linear case where the damping is proportional to the velocity. If the damping coefficient is higher than 2, more energy is dissipated per cycle than the linear case.

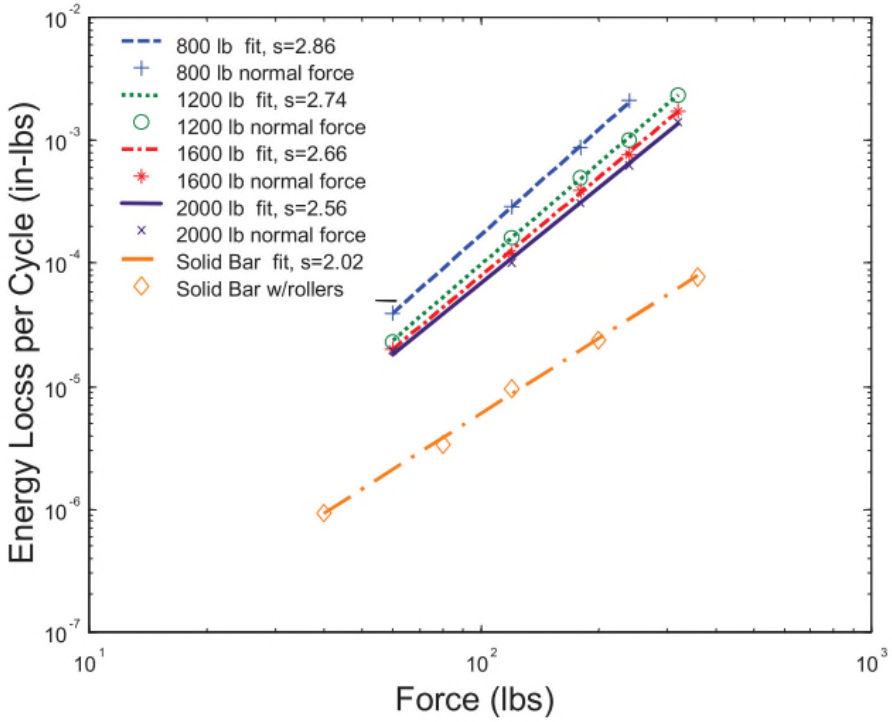

Figure 35 Equivalent viscous damping ratio compare to the force for four different normal interface loads and one solid bar (source: Gregory and Resor (2009b)). This dataset has been measured using the flat lap joint design. The variable 's' is identical to the slope coefficient n of equation (2-50).

The solid block has a measured slope coefficient of 2.02 which is almost linear; this signifies that the energy lost by cycle is proportional to the velocity. With a bolted joint, the slope coefficients are 2.56 to 2.86 for all configurations tested with a good fit each time.

The Gaul and Lenz resonator, (Gaul and Lenz 1997), is composed of two masses, a spring and a joint. One limitation is that the experiment is limited to the resonance of

one mode, (Matthew R W Brake 2017) (Chapter 6 p59). Only the third mode, at 339.7Hz, allows the investigation of the joint. Either a shaker or a hammer could be used to excite it. Segalman et al. (2009) consider that the Gaul and Lenz resonator is the most accurate way to test a joint.

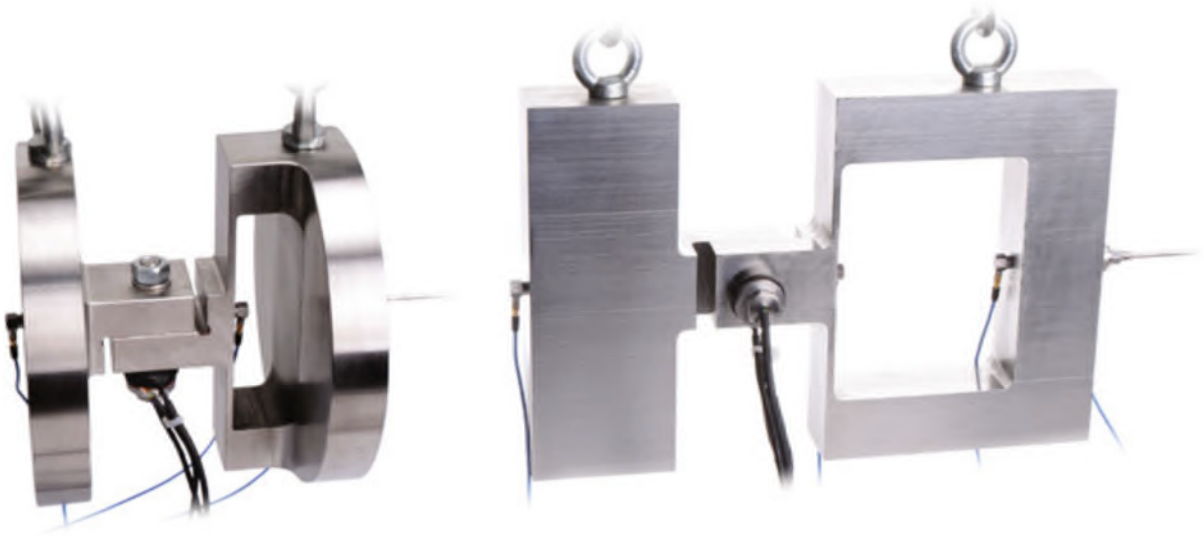

Figure 36 Image from (Matthew R W Brake 2017) (chap 6, p61). Gaul and Bohlen (1987) first generation of Gaul and Bohlen resonator on the left. The second generation, on the right, was designed by Lenz and Gaul (1995)

Also, this system has the advantage of being isolated from the ground. This isolation allows a clean signal recording because the environment does not absorb the energy of the structure. If the structure were connected, an external resonance could corrupt the recording.

For the same reason, it is recommended that a hammer is used instead of a shaker. In fact, the stinger, which connects the structure and the shaker, and the shaker itself have their own resonances. The interaction between the shaker and the structure may corrupt the data.

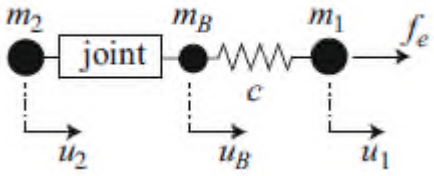

Figure 37 (Matthew R W Brake 2017) (chap 6, p60) Idealisation of the Lenz and Gaul resonator. The 'u' describes displacement, the 'm' stands for mass, the 'c' refers to the stiffness of the spring and the 'fe' describes the force of the excitation.

The main advantage of this structure is that the force and displacement inside the joint can be precisely measured. This is possible because each part of the structure can be modelled as either a mass or a spring. Thus, simple mechanical equations can be used to extract useful basic information. The variables of the two equations below are defined in Figure 37:

$$fjoint = m_2.\ddot{u}_2 \qquad \textbf{(2-51)}$$

Where, $fjoint$ is the force inside of the joint, m_2 the mass directly connected to the joint and $\ddot{u}_2$ the acceleration of this mass.

$$u_{joint} = u_2 - u_b \qquad \textbf{(2-52)}$$

Where u_{joint} is the relative displacement inside the joint, u_2 is the relative displacement of the mass directly connected to the joint and u_b the relative displacement of the point between the joint and the mass.

By extracting precisely the relative displacement and the force, interesting results, like Figure 38 can be plotted. From the information inside of this diagram, a theoretical model of an entire joint interface can be established. Figure 38, (Brake 2017, p66), shows some results from the Lenz and Gaul Resonator. Hysteresis plots display relative displacement against joint force for four different frequencies. As can be seen, the nonlinear behaviour changes at different frequencies. This clearly shows the level of complexity of a simple bolted lap joint.

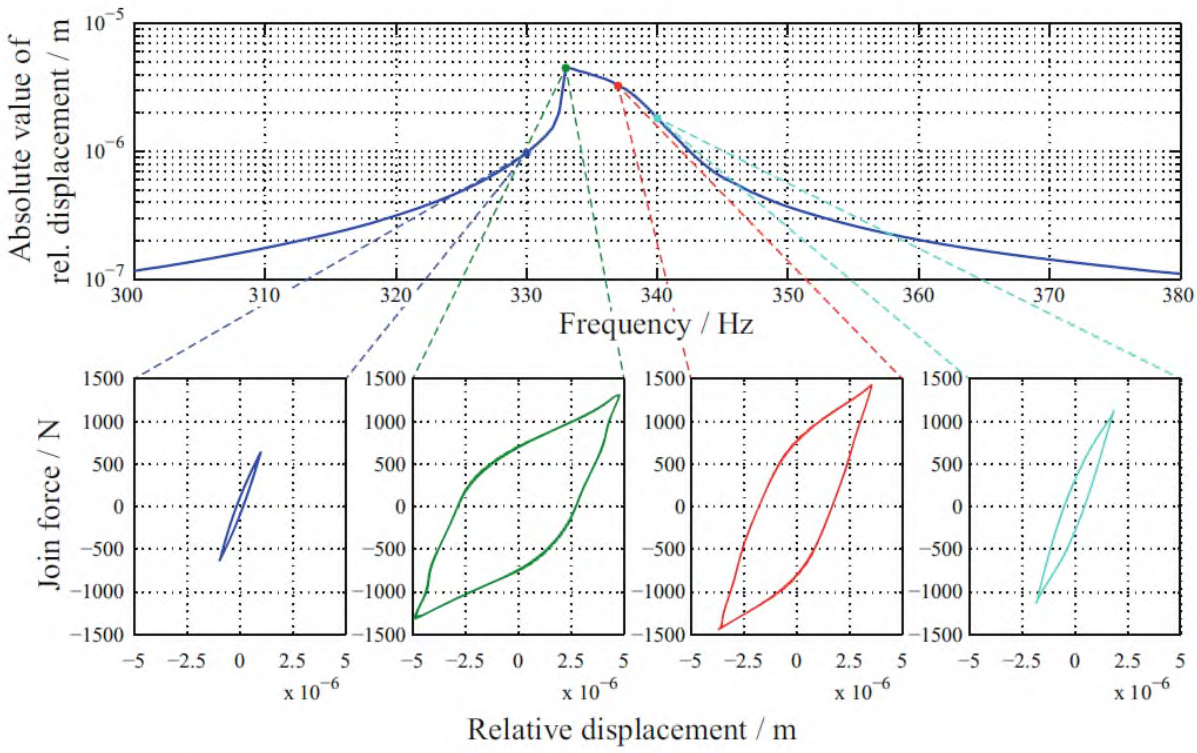

Figure 38 (Brake 2017, p66) four hysteresis cycle of the Lenz and Gaul Resonator at different frequencies

The type of results shown in Figure 38 could be used to create an interpretation of when the friction can happen during one cycle of vibration. For example, hypothetically if an interface locks during one part of a cycle and starts sliding during a second part, this type of diagrams should reveal this type of behaviour.

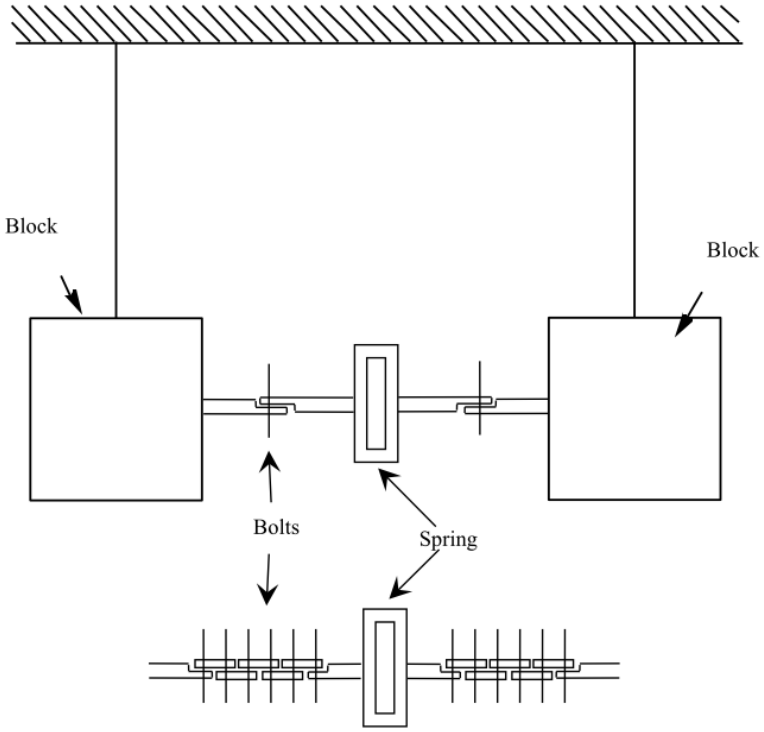

Figure 39 experimental layout investigated by H. Goyder, Ind, and Brown (2013). The design, inspired by the Gaul Resonator, used 1 to 10 bolted lap joints in series surrounded by heavy blocks of metals and a spring in the middle.

H. Goyder, Ind, and Brown (2013) investigated a more modular version of the Gaul resonator. They came to the strange conclusion that the damping is not related to the number of joint in series. The test structure was exercised longitudinally using a shaker and an electromagnet to create a sin-stop input. Multiple configurations of joints in series were tested as shown in Figure 39. The absence of correlation between the number of joints and the measured damping can be very easily explained because the interface had a complete contact as shown in Figure 40.

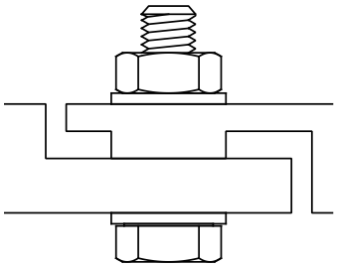

Figure 40 interface design investigated by H. Goyder, Ind, and Brown (2013) which limit the surface of contact below the washer. This interface has, without doubt, a complete contact at the interface.

Figure 41 Interpretation of the deformation link to static longitudinal loading by Heinstein and Segalman (2002). The top image loading is a longitudinal compression. The bottom image loading is longitudinal traction. This type of excitation is named longitudinal loading in this document.

Heinstein and Segalman (2002) concluded that the energy dissipation in a longitudinal loading is not linked to a simple sliding at the interface as previously thought, but linked to a bending of the surrounding beams which lead to shear force at the edge contact. It is often assumed that the surfaces in contact should stay parallel although the loading is longitudinal. This simplification is commonly used when modelling the damping of joint in. This hypothesis leads to neglect of the opening and closing phenomenon pointed out by Heinstein and Segalman. They proposed a new interpretation which is that longitudinal excitation is, in fact, bending the interface, and this bending is the cause of the damping. Am illustration of this possible bending is displayed in Figure 41.

2.3.3 Bending loading

Another way to exercise a bolted lap joint is in bending. The bending loading experiments are simpler compared to the longitudinal loading experiments. Indeed,

bending loading can be easily achieved using a beam shape and using the natural tendency of a beam to bend. This subsection will present the major experiments using bending to exercise lap joints.

A 2004 study of lap joints submitted to bending moments were done by (Hartwigsen et al. 2004). In this publication, a complete state of the art experimental analysis was performed. In a second publication, Song et al. (2004) fitted a model of one joint and a good prediction of a more complex rectangular shape structure with multiple identical joints was achieved. This publication shows the limitation in the field of joint dynamics, where no predictive model can be achieved without fitting experimental data to a completely identical joint.

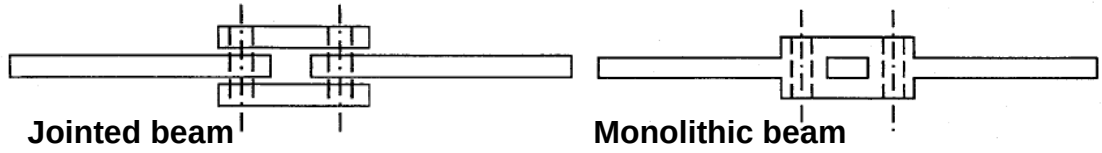

Figure 42 The two joint designs investigated by Maloney and Peairs (2000)

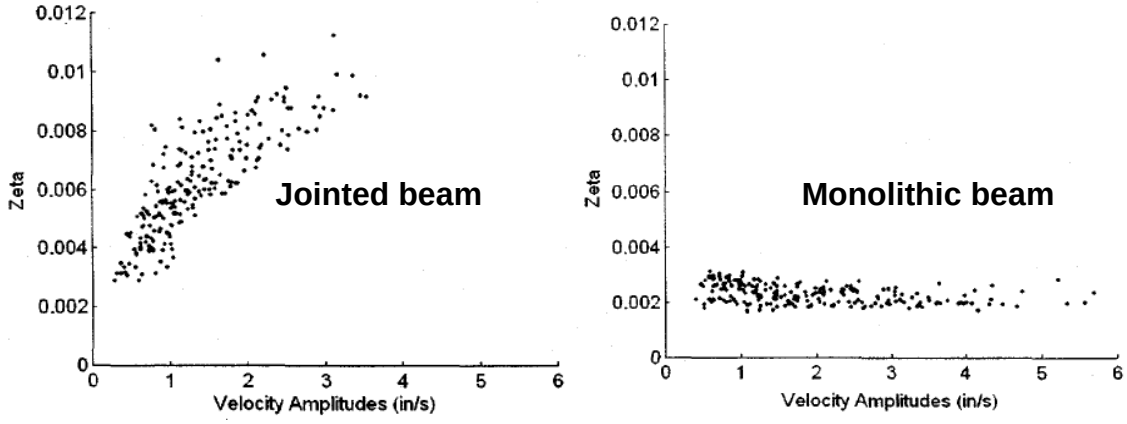

Figure 43 Damping ratio compare to velocity from (Maloney and Peairs 2000)

Maloney and Peairs (2000) made the first comparison between a monolithic and a jointed beam, see Figure 42. The damping measured is 2 to 5 time more important for the jointed beam than the monolithic beam, see Figure 43.

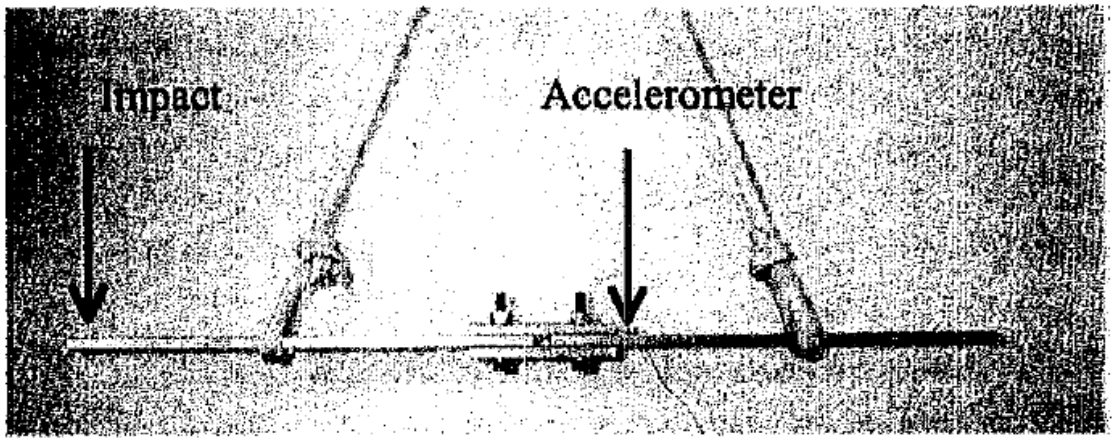

Figure 44 beam-like-structure investigated by Kess, Rosnow, and Sidle (2002)

Another experiment using the same design of joint was carried out by Kess, Rosnow, and Sidle (2002). They identified that the size of the washer seems to be the most a dominant parameter linked to the damping. Kess, Rosnow, and Sidle (2002) identified that the damping of his beam is strongly correlated to the size of the washers used to tighten the bolts: The larger the size of the washer the larger the damping measured.

M. R. Brake et al. (2014) simplified the design and the manufacturing of beam-like-structures with a lap joint. They designed the Brake and Reuss Beam as presented in Figure 45. This lap joint geometry has been used in multiple publications, (Cooper et al. 2017), (Kuether and Brake 2016), (Schwingshackl 2017), (Matthew R W Brake 2017), (Smith, Brake, and Reuß 2015).

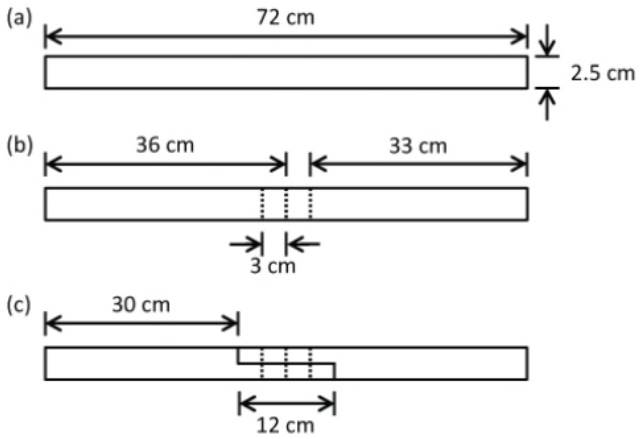

Figure 45 The original design of the three Brake and Reuss Beams presented in (M. R. Brake et al. 2014). The beam (a) is monolithic, (b) have three holes in the middle and (c) have the holes and a lap joint.

In a recent investigation of different design interfaces on customised Brake and Reuss beams, Dossogne, Jerome, Lancereau and Smith in [8], established that the design of the interface influences the dynamic behaviour of the structure. Also, that interfaces with a fading static pressure distribution (receding contact) have a non-linear behaviour. They show that interfaces with high pressure at the edge (complete contacts) do not add significant damping beyond material damping. These experiments have been performed on five customised Brake-Reuß beams by shaping the interface.

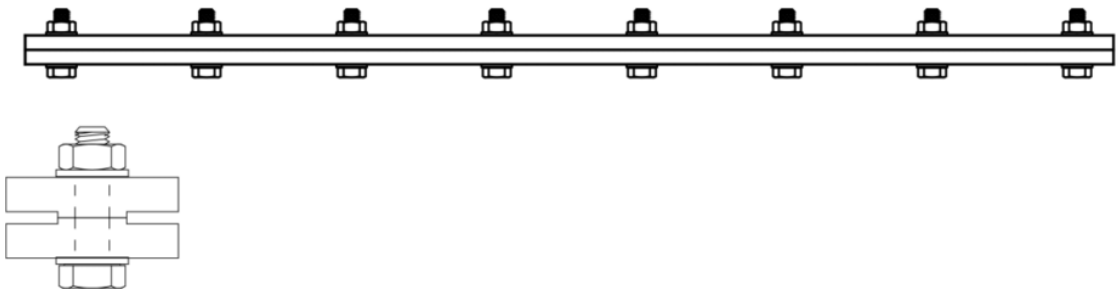

The 29-holes-beam are two modular beams designed by H. Goyder, Ind, and Brown (2013) who describe initial experimental investigations. The-29-holes beam has shown to have extremely different behaviour depending on the number of bolts placed on the structure. The more bolts placed on the structure, the less damping is measured. This unexplained observation had been the starting point of this thesis. The 29-holes-beam was renamed the sandwich beam.

2.3.4 Torsional loading

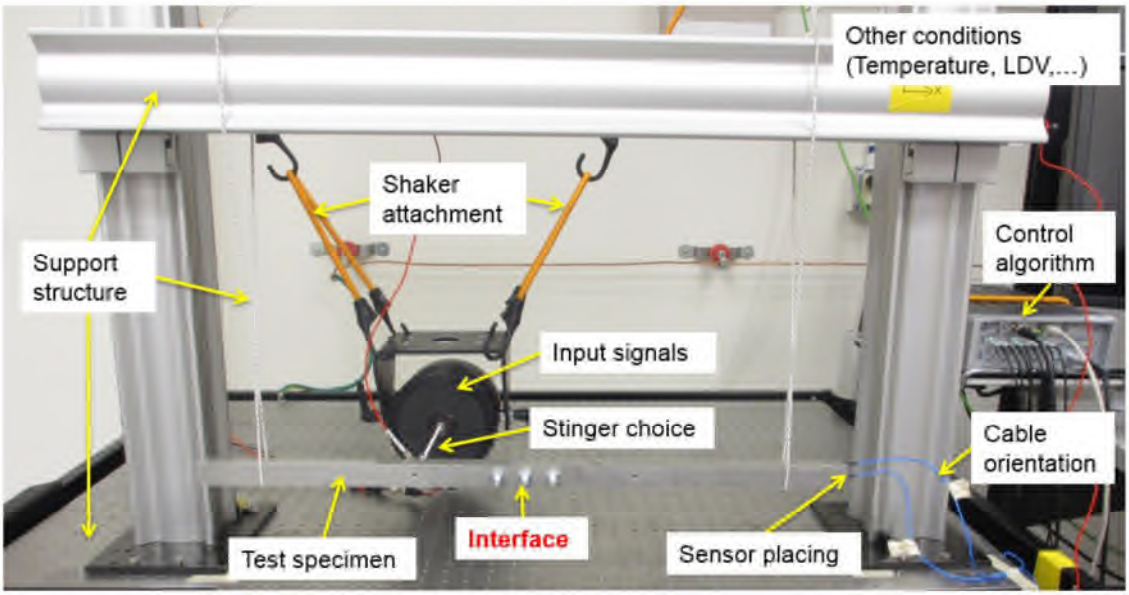

Figure 46 Layout for the testing of the Brake Reuss beam using a shaker, investigated by Smith, Brake, and Reuß (2015)

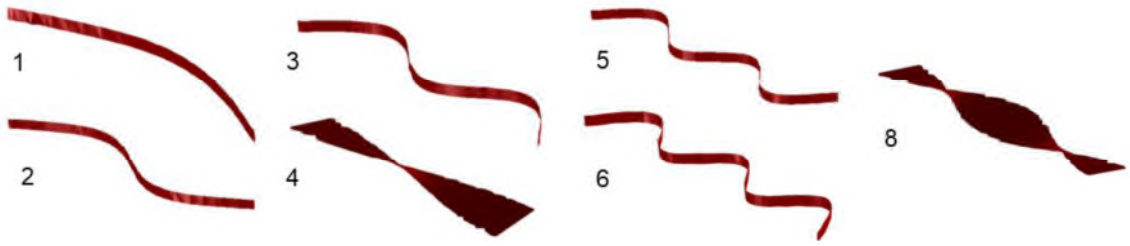

Figure 47 Mode shape of the beam structure investigated by Smith, Brake, and Reuß (2015). Mode 4 and 8 create a torsional loading to the lap joint in the centre of the beam, see Figure 46.

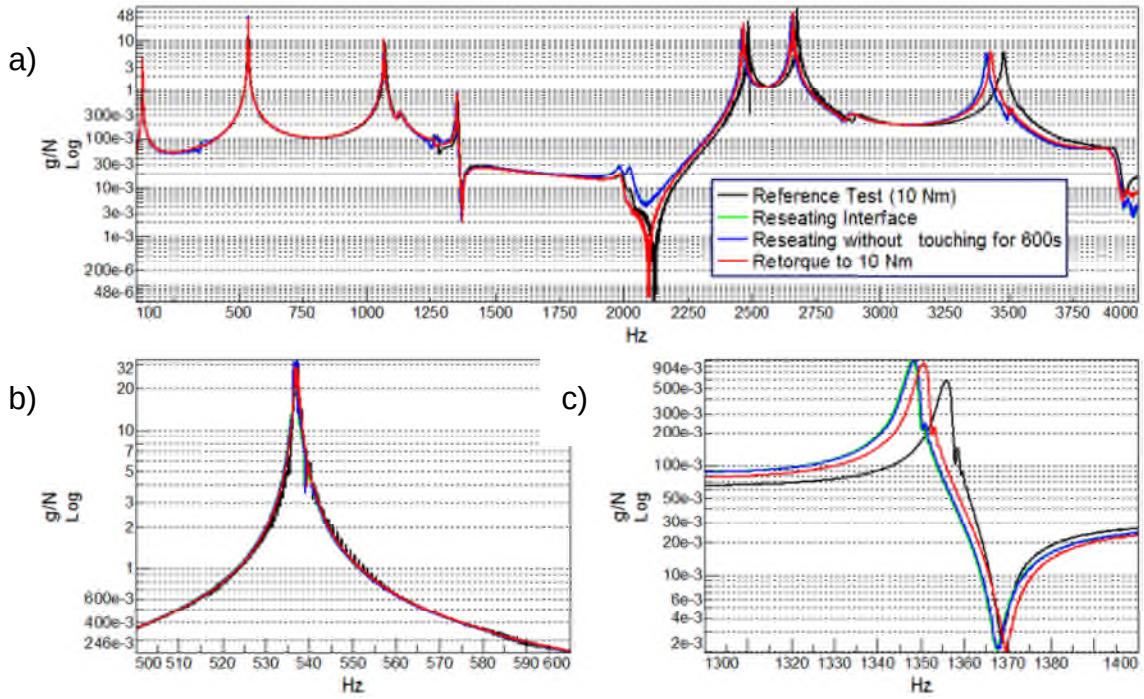

Figure 48 FRF from the repeatability test conducted by Smith, Brake, and Reuß (2015): a) entire range of frequency investigated, b) zoom in on the second mode (bending), c) zoom in on the forth mode (torsional). See Figure 47 for the mode number.

Smith, Brake, and Reuß (2015) revealed that a torsional mode had been found to be more difficult to analysis due to high variability for each disassembly. The brake Reuss Beam investigated displayed in Figure 46, seems to have a repeatable behaviour for the bending modes displayed in Figure 47 but not for the torsional mode. One illustration of the repeatability is the difference between the plot c) and plot b) of Figure 48: The FRF of plot b) overlay on top of each other and the sharpness of the peaks are similar. However, the FRF of plot c) has resonance peaks at different frequencies and different heights. Those differences mean that the frequencies and the damping vary for each disassembly. This variation makes the investigation of torsional modes more difficult than bending modes.

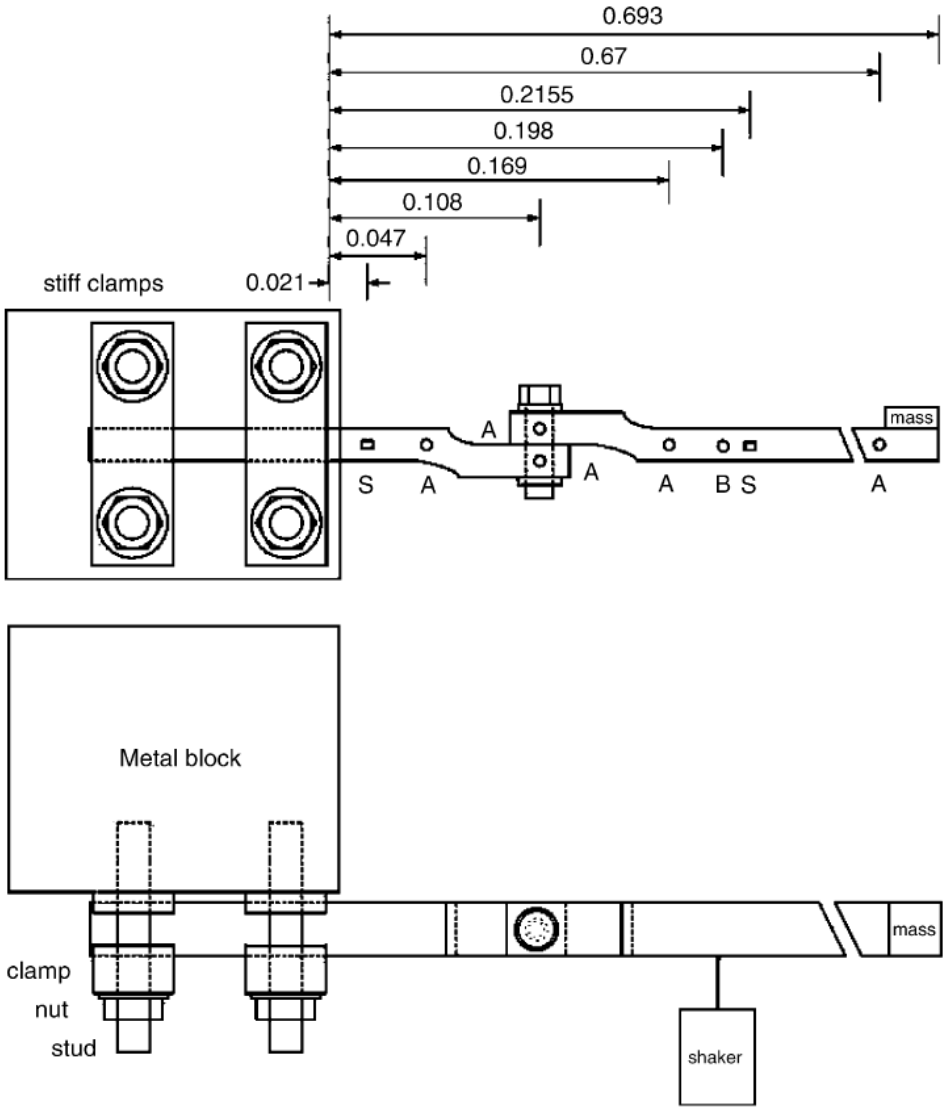

Figure 49 Two views of a bolted lap joint experimental layout exercise in torsion loading from (Ouyang, Oldfield, and Mottershead 2006)

Ouyang, Oldfield, and Mottershead (2006) investigated the effect of a torsional loading on a specifically designed structure. Even though this paper does not precisely describe the set-up used, the parameters investigated nor the excitation method, the observation of harmonics is rare enough to be detailed here.

The type of isolation is not clearly stated in the description of the experimental setup section. The section does not show precisely how the structure is suspended. It seems that the entire structure is in a free-free configuration with a shaker (also suspended) providing excitation in the middle.

Also the presence of multiple additional joints could be problematic as the structure investigated (see Figure 49) has 5 bolts and multiple lap joint interfaces with relatively similar contact patches as the bolted lap joint investigated. Those additional interfaces could have dissipated energy. Ideally ,this experiment should have been composed of only two components and one lap joints. However, those additional interfaces do not create any micro-friction when the main bolted lap joint is highly torqued, see left image in Figure 50. Therefore the results at low torque could be interpreted as only the effect of the main bolted lap joint.

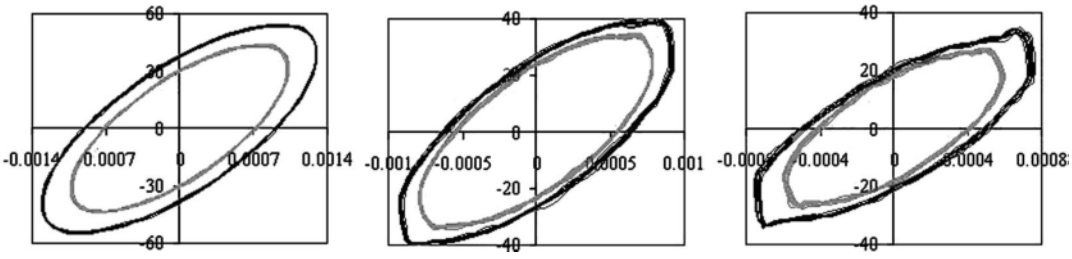

Figure 50 Bending loading (vertical axis of the graphs in Nm) against the angular displacement (horizontal axis in Rad) at the main bolted lap joint. From left to right, the level of bolt torque is “low”, “intermediary” and “high” (exact value not given). The grey and black lines represent two level of excitation amplitude (again exact value not given). Source: (Ouyang, Oldfield, and Mottershead 2006)

This torsional loading investigation shows that the torque of the main bolt lap joint has an impact on the behaviour of the structure. The weaker the torque the more micro-friction is observed, as show in Figure 50.

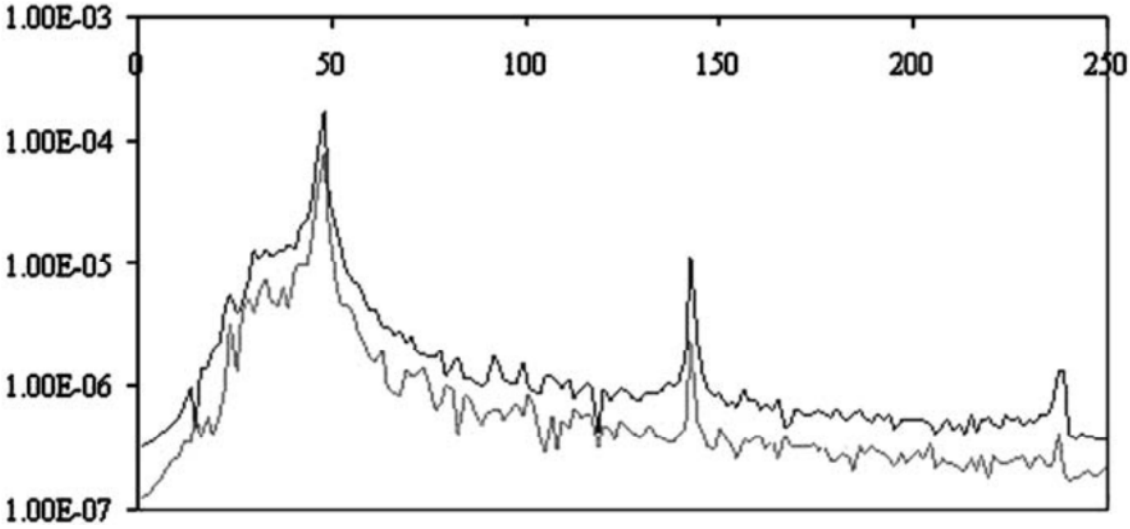

Figure 51 Frequency spectrum of the "low" bolt torque from (Ouyang, Oldfield, and Mottershead 2006). The pick at 48 Hz is the frequency of excitation. The two picks on the right are odd harmonics. The grey and black lines represent two amplitude levels (exact value not given). The x-axis is assumed to be the frequency in Hz. The type of vertical axis (acceleration, velocity or position) is not precise in the article.

The most interesting result of this investigation is that odd harmonics (at three and five times the exercised natural resonance frequency) were measured as shown in Figure 51. Those harmonics were interpreted by Ouyang, Oldfield, and Mottershead (2006) as a cubic stiffness effect.

From an outside point of view, another possible interpretation is an evolution of the stiffness during a part of the cycle, which would lead to an asymmetric sinusoidal signal and therefore odd harmonics. This stiffness evolution could be due to a change in the contact patch due to an opening of the interface, during part of the cycle.

In summary, Ouyang, Oldfield, and Mottershead (2006) show that odd harmonics could appear due to a weakly torque bolted lap joint submitted to torsional loading. It also shows that the behaviour of the same lap joint dramatically changes with different value of the torque.

2.3.5 New experimental tools

Static and dynamic pressure films are two methods which give additional information concerning the stress within a joint.

Static pressure films are a thin piece of plastic that changes colour depending on the pressure. They are composed of multiple spheres of ink which colour the paper as a function of the pressure. Static pressure films are currently being used to measure the pressure distribution inside the interface of a Brake Reuss beam (Catalfamo et al. 2016). The use of pressure film allows the authors to confirm that the order in which the bolts are tightened up is not relevant if the surface is smooth enough, see Figure 52 (Smith, Brake, and Reuß 2015).

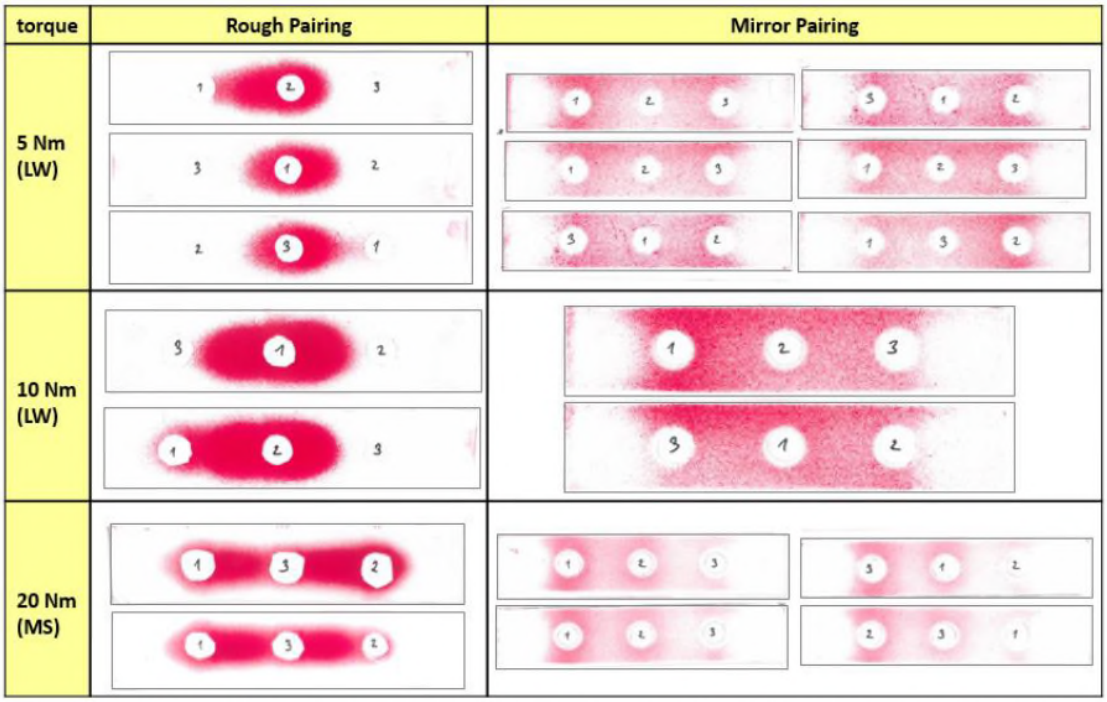

Figure 13 Pressure distributions of the specimens with bolt tightening order indicated on each pressure distribution

Figure 52 (Smith, Brake, and Reuß 2015), measurement of the static contact patch of a Brake and Reuss Beam depending on the bolt torque and the roughness of the surfaces. A pressure film was inserted between the two components; the film turned red due to the static constraint in the interface.

A project in which dynamic pressure film will be used to measure normal pressure during a vibration test is currently in progress led by Matt Brake at Rice University.

Even if this pressure film is unable to measure the shear force (and so the friction), this new piece of equipment will definitely revolutionize understanding of the behaviour inside a bolted lap joint. M. R. W. Brake et al. (2017) show the feasibility of using this dynamic pressure film to study lap joints.

2.3.6 Conclusion experimental method

Longitudinal excitation has been deeply investigated or more than 30 years, whereas bending and torsion are less explored. The set-up to investigate longitudinal excitation of lap joint is more complex than bending excitation. Moreover, a study seems to indicate that the damping of longitudinal excitation is in fact due to the bending of the interface. In addition, a predictive model of the damping as a function of the loading under the form of a power law exists for the longitudinal excitation, whereas no predictive models were found for bending or torsion. The torsional mode has been found to be more difficult to analyse due to the high variability for each disassembly. Also torsional loading could lead to odd harmonics, something not measured for bending excitation.

In conclusion, bending seems to be the most promising excitation method. Therefore, this thesis focused on the effect of a bending excitation on a lap joint. Pressure films were also used, as they give great insight into the pressure at the interface.

2.4 Signal Processing

This section will review the signal processing methods used in experiments on the vibration of joints. The First subsection, Subsection 2.4.1, will describe the main signal processing method used to analyse the nonlinear vibration of joints. The second subsection, Subsection 2.4.2, will make a synthesis of the signal processing methods.

2.4.1 Description of signal processing used in joint dynamics experiments

In Figure 53**,** Ewins (2016) describes a future workflow to incorporate nonlinear behaviour into a modal analysis. The different steps to investigate nonlinearity are

“Detection, Characterisation, Localisation, and Quantification.” Some of these steps can be achieved using the methods described below. The updating of the linear or nonlinear model and the validation are not reviewed here. Ewins’ work assumes that an appropriate nonlinear model of a joint is available. However, no general purpose models for joints are applicable. Consequently, novel signal processing methods are needed to understand the joint behaviour.

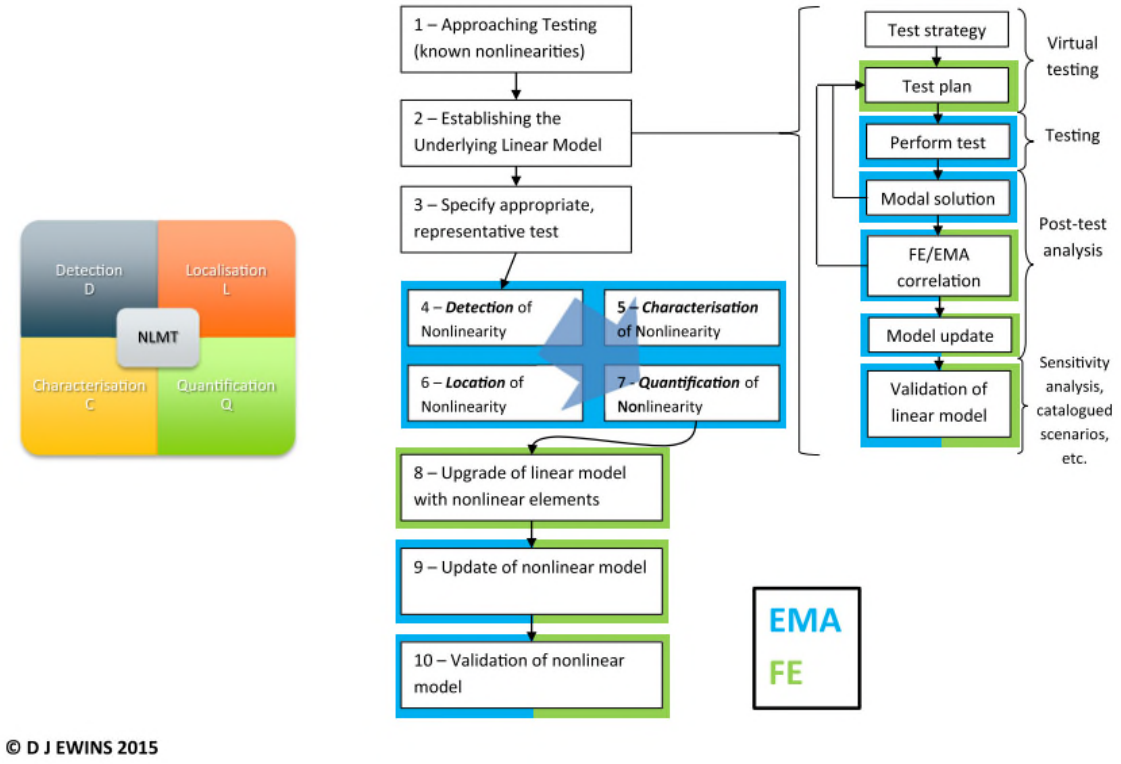

Figure 53 (Ewins 2016) categorization of the different steps necessary to include nonlinear behaviour inside a linear modal analysis.

The acceleration signal generated by a bolted joint is nonlinear. The natural frequency and damping ratio change in relation to the instantaneous amplitude. To capture the variation of those parameters during a vibration decay, it is necessary to use a nonlinear signal processing methods. Nonlinear signal processing methods can be traced back to (Feeny and Liang 1996). Feeny and Liang used the values of each peak and valley of a transient decay time-history to estimate the instantaneous amplitude and the damping ratio. (Maloney and Peairs 2000), used a low pass filter, then a Hilbert transform and finally a log decrement to extract the same parameters.

Currently, there are two dominant methods to extract the nonlinear parameter: using the Hilbert transform or using the Fourier transform. Both allow the extraction of the damping ratio, natural frequency, and instantaneous amplitude of a nonlinear transient decay.

The Hilbert transform signal processing method is defined by Sracic, Allen, and Sumali (2012). The technique starts by filtering the time history with a standard bandpass filter to isolate one mode. The Hilbert transform can, in principle, extract the envelope of a decay signal. From that information, the natural frequency and the damping ratio is also extracted.

The extraction of the amplitude is the most original step. The Hilbert transform can create a version of the signal with a phase shift of $\pi/2$. A complex signal is created, the real part is the original signal and the imaginary part is the phased shifted signal. The modulus of this complex signal gives the envelope depending on the time. From the envelope, a polyline is fitted and the damping ratio and the instantaneous amplitude are extracted.

The Hilbert transform is subject to Gibbs oscillations, which can corrupt the start of the signal when the nonlinear vibration is dominant.

The second technique is the Short Time Fourier Transform (STFT) presented in (Kuether and Brake 2014). It can also extract natural frequency, damping ratio and instantaneous amplitude from vibration decay. It uses different custom windows to segment the time history. A discrete Fourier transform is used in each section. The result is often a peak from which the instantaneous frequency (frequency of the peak) and damping ratio (-3dB formula) can be extracted. This technique can be applied to multi-harmonic signals, and therefore it does not require any pre-processing such as band-pass filtering. This approach is relatively straightforward, but the necessity of tuning the windows to compromise between resolutions and averaging may create some difficulty. Indeed, this method is limited in resolution by the time windows.

A new technique has been introduced in (Peyret, Dion, and Chevallier 2016) using Kalman filtering. Other techniques which are worth mentioning because of their

simplicity are the Zeroed early-time fast Fourier transforms (ZEFFT) and the Backwards extrapolation for nonlinearity detection (BEND) presented in (Allen and Mayes 2010). These two techniques use simple discrete Fourier transform (DFT) to generate clear graphics which allows identification of the non-linearity of the system.

Key questions which have not been addressed in the literature are as follows:

- What is the influence of the bandpass filter on the nonlinear vibration?
- Is it possible to extract the damping ratio in the time domain?
- How is it possible to generate an artificial nonlinear signal?

2.4.2 Synthesis of the signal processing methods

There is a rise of new signal processing methods which tend to be oriented for time domain application rather than to the more common frequency domain methods for the study of joints.

This is probably due to the desire to extract more meaningful information from experimental signals. The investigated structures tend to have their behaviour corrupted by any attachment to other structure. Therefore, shakers tend to be used less often than hammers. This shift directly limits the possible signal processing methods. Indeed, the signal measured from a hammer lasts for a short duration compare with a shaker, but, the frequency resolution is inversely proportional to the duration of the signal. A low resolution means a reduced number of points useful for a signal processing method in the frequency domain. On the other hand, time domain method tends to work well with the signal from hammer hits. That is probably why there two new signal processing methods in the time domain developed during the last 10 years.

This thesis used a new method developed by Goyder and Lancereau (2017) which will be presented in the signal processing section (chapter 4).

2.5 Publications linked to this thesis

Table 5 Publications linked to this thesis

Authors	Paper Titles	Contribution of DPT Lancereau
Goyder, Ind, Brown, Lancereau DPT (2016)	Friction and Damping Associated with Bolted Joints: Results and Signal Processing	Co-creation of experimental data set. 25% of the work.
Goyder HGD , Lancereau DPT (2017)	Methods for the Measurement Of Non-Linear Damping and Frequency in Built-Up Structures	Active secondary author: co-designer of the experiments and the model. Main contributor to the experimental data set. Reviewer of the writing and plotting. 50% of the work.
Dossogne T, Jerome T, Lancereau DPT, Smith SA (2017)	Experimental Assessment of The Influence of Interface Geometries on Structural Response	Work in collaboration with three other PhD students. 25% of the work.
Brake MRW, Stark JG, Smith SA, Lancereau DPT, Jerome TW, Dossogne T (2017)	In Situ Measurements of Contact Pressure for Jointed Interfaces During Dynamic Loading Experiments	Participation in the creation of the experimental data set and the reviewing of the final article draft. 3% of the work.
Lancereau DPT, Goyder, Ind, Brown (2017)	Some Dynamic Properties of Contact Patches in Bolted Joints	Main contributor in term of conception of the experiment, creation of the experiment data set, signal processing, plotting, analysis and writing. 80% of the work.
Goyder H G D, Lancereau DPT (2018)	Extracting natural frequency and damping from time histories. Better than the frequency domain?	Participation in the thinking process, creation of experimental data set and reviewing of the writing. 10% of the work.
Goyder H G D, Lancereau DPT, Ind P, Brown D. (2018)	Two types of dynamic joint behaviour: theoretical and experimental analysis	Active secondary author: co-designer of the experiments and the model. Main contributor to the experimental data set. Reviewer of the writing and plotting. 45% of the work.

2.6 Conclusion of the literature review

There is a lack of predictive models for bolted lap joints. Most of the models in the literature that explain the behaviour of bolted lap joints are fitted model. Those fitted models have a range of application limited in interactive design processes. Whereas an ideal predictive model would predict the behaviour of the joint without testing, using only design parameters. This thesis was not oriented to the fitting of another abstract mathematical model from experimental data. Instead, an experimental approach was favoured to obtain a better understanding. A better understanding should lead to the creation of predictive models.

The best conceptual interpretation of the origin of the dissipation of energy inside a lap joint is as follows. The main mechanism causing damping is thought to be micro-friction in the joint. This micro-friction is claimed to happen in a “slip region” far from the bolt, where a “stuck region” close to the bolt locks the interface in place. The concept of micro-friction and regions seems coherent, but there is room for improvement.

Many experimental results lack a clear and simple explanation. So far, the most intriguing results are as follow. Some experimental results show that the design of the interface and the size of the washer have a large impact on the nonlinear vibration behaviour of joint. In addition no precise explanation exists for the causes of this behaviour. Therefore, these results show that there is still a large uncertainty linked to the nonlinear behaviour of bolted lap joints. For this thesis, some results are replicated. In addition, the role of the interface design on the behaviour of bolted joint was investigated in more details.

This thesis aims to reduce the uncertainty linked to the nonlinear behaviour of joints. To tackle this challenge, multiple experiments were performed to have a better understanding of what is happening at the interface of a bolted lap joint. These experiments identified some of the key parameters linked to the nonlinear behaviour of joints. The results for this thesis should help researchers to create more realistic models of the behaviour of bolted lap joints.

2.7 Objectives of this thesis

The main objective of this thesis is to investigate the nonlinear dynamic behaviour of joints.

The detailed objectives are as follows:

Objective 1: Identify the dominant parameters which affect the nonlinear behaviour of bolted lap joints

Objective 2: Investigate the damping and stiffness properties of bolted lap joints

Objective 3: Reduce the uncertainty linked to the dynamics of joints

Objective 4: Improve the experimental method and signal processing workflow applicable to nonlinear dynamic structures

3 EXPERIMENTAL METHOD

This thesis investigates the behaviour of steel bolted lap joints. This chapter details the choices made in order to identify the experimental method used across this thesis.

3.1 Definitions of key concepts

In this section, the key concepts elaborated in this thesis are defined and illustrated.

Joint Physical connection between two components. A joint can have multiple contact patches.	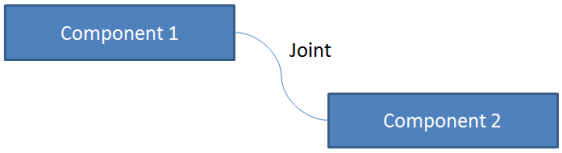
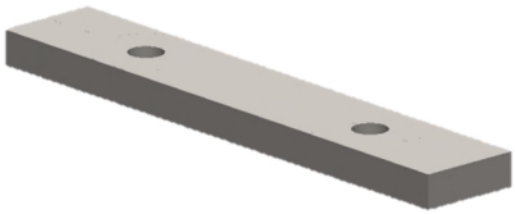	***Component*** Manufactured item with no joints.
Bolted Lap Joint A bolted lap joint is created when two overlying components are fastened together with a bolt.	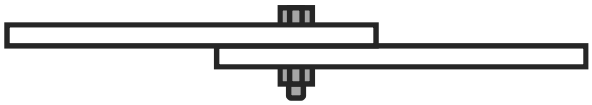

Components inside a bolted lap joint

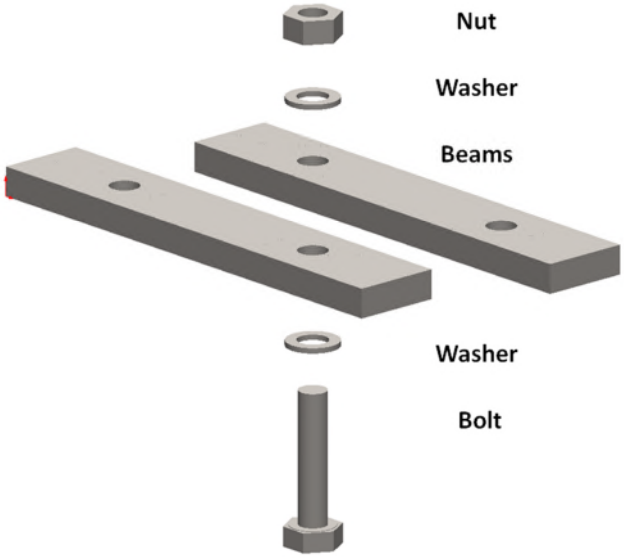

Interface

Area where two components *may* enter in contact. In the image, the contact patch is in red, the gap between the components is in blue, and the interface limit is in black.

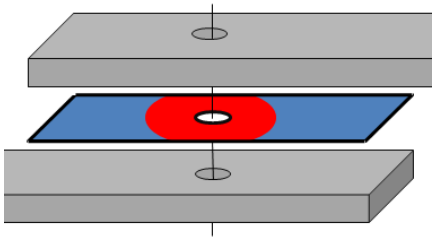

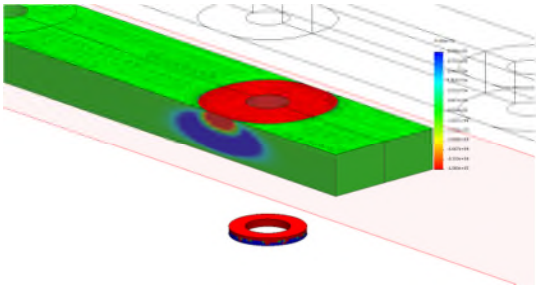

Contact Patch

Actual surface in contact at the interface of a joint. In the image, the two contact patches are in red.

Interface limit

Edge of the area where component *may* enter in contact in a joint.

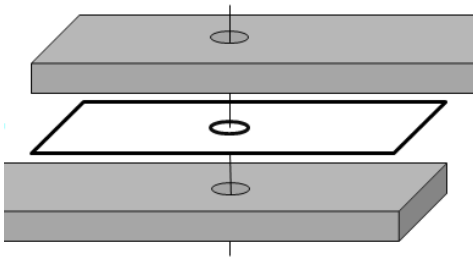

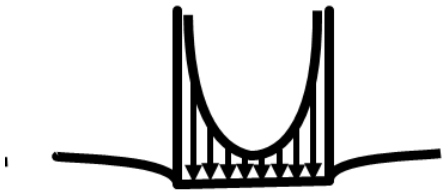	***Complete contact*** Type of contact where the edge of the contact patch has high normal stress. Diagram made by Hills, Nowell, and Sackfield (1993).
Receding contact Type of contact where the normal stress at the edge of the contact patch is null. Diagram made by Hills, Nowell, and Sackfield (1993).	
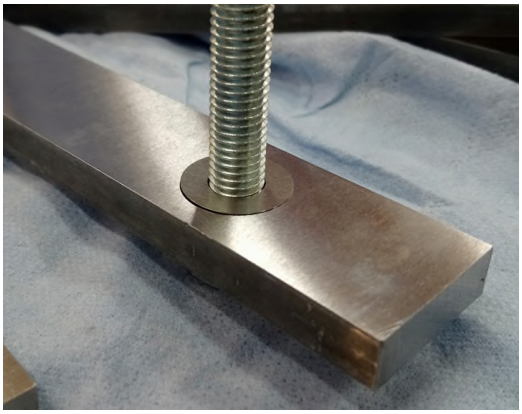	***Shim*** Thin sheet of metal. Shims can be placed in lap joints to change the interface limit, which modified the size of the contact patch. The washer size shim, see left, transforms a receding contact into a complete contact.

3.2 Investigation of the bending of lap joints in beams

Many research publications investigate the vibration of real manufactured structures like car parts, a missile attachment or an entire satellite. This thesis is more focussed on simple structures, because the analysis of the vibration behaviour is straightforward.

Lap joints were selected for investigation. Lap joints are commonly used in all industries. They are a simple way to join components together, as illustrated in Figure 54. lap joints are also a simplified version of other joints, so the results of experiments on lap joints should be easy to generalise.

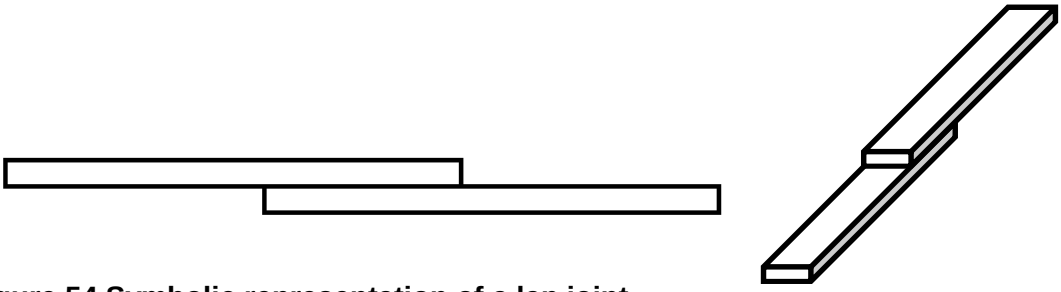

Figure 54 Symbolic representation of a lap joint

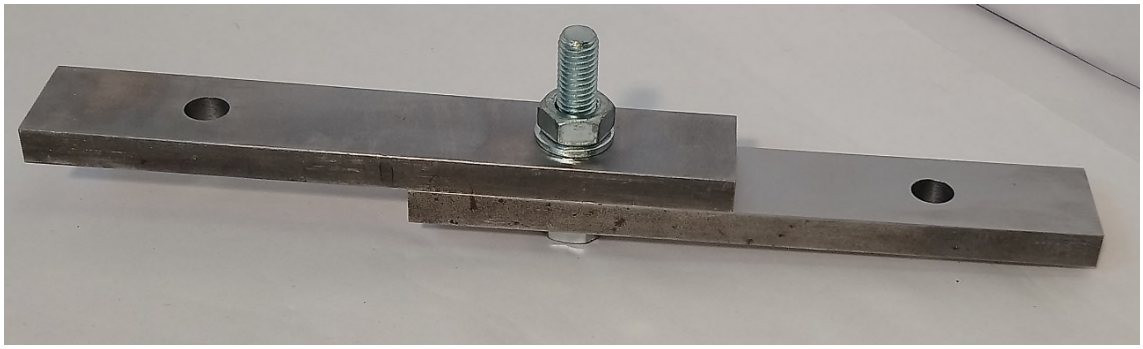

Figure 55 Photo of a bolted lap joint

Lap joints in a beam configuration were selected for the study. As discussed in the conclusion of the experiments literature review, 2.3.6, a bending excitation is the most promising to investigate, and a beam shape has multiple bending modes.

A beam configuration was set because the vibration of the beam is simple and understood. Beam vibration allows a controlled bending excitation of one or multiple lap joints. A one dimensional beam model can be used to predict the vibration behaviour of a beam. From this model, the bending moment and shear force are known at every point of the beam, as show in Figure 56. Therefore by using a test structure in a beam configuration, an overall understanding of the linear behaviour is available.

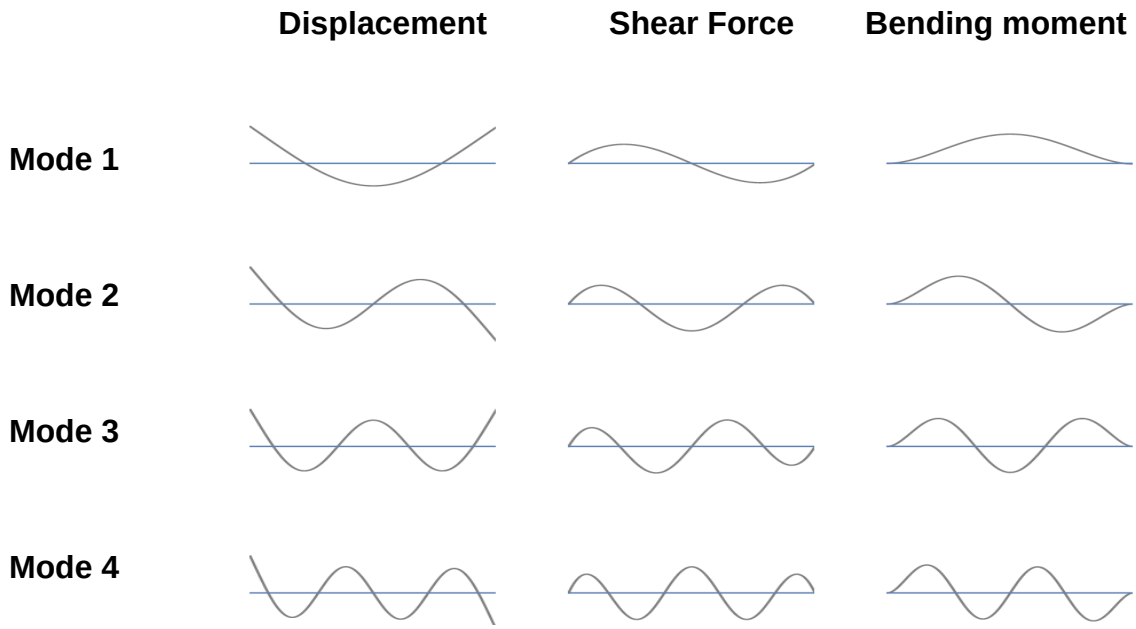

Figure 56 Theoretical mode shape, shear force and bending moment of the first four bending modes of a free-free beam

The literature review identified nonlinear dynamic behaviour in a lap joint: the loosening effect and the nonlinear damping when submitted to bending excitation.

The loosening effect is the decrease of the natural frequency when the amplitude of vibration increases. The structure is *looser* due to the vibration.

The nonlinear damping is defined here as an increase of damping ratio when the amplitude of vibration increases. Microfriction is claimed to be the source of the nonlinear damping.

The main output of the literature review is that the current lack of a predictive model of the dynamics of lap joints is due to the limited understanding of the inner mechanism at the interface of the joint. No explanation has been found in the literature of the origin of the loosening effect measured in a lap joint submitted to bending moment, nor a method to predict the presence of micro-friction in a lap joint.

The aim of this thesis was to identify precisely the dominant parameters which affect the loosening effect and the nonlinear damping.

The following sections present the minor but still necessary choices which were made in order to further narrow down the research topic and improve the quality of measurements.

3.3 Bolts with high torque within steel lap joints

The focus is on the behaviour of a lap joint submitted to bending inside beam-like structures. The selection of the material of the test structure and the fastener method is described here.

This thesis focusses exclusively on joints made out of steel because steel joints are common. Steel is an isotropic material. Also, steel is well represented in the literature. New composite materials could have been chosen but they are not isotropic, in other words, the orientation of the material has an impact on their mechanical properties. Another type of isotropic metal could have been picked, like aluminium, but steel joints are so inexpensive and are more extensively used than any other isotropic metal. Therefore steel is the only material investigated in the thesis. Mild steel was selected. It is expected that other isotropic metals behave similarly.

Bolted joints were the only type of fastener to be investigated. Bolted joints seem to be a good choice because they can be easily disassembled, unlike riveted joints. Also, the widespread utilisation, the low manufacturing cost, and their relative simplicity were influencing factors in the decision to use bolted joints. It is expected that a rivet or bolt, as they have the same function, should behave the same.

An high torque of 54.2N.m with an M10 bolt was selected for the study. High torque, until 50% yield, is generally used in the oil and gas industries to limit possible leaks in pipe flanges (source: Hugh G D Goyder 2017). The M10 size was picked because it is a standard size. An example of three bolts used is displayed in Figure 57. It is expected that the result from this bolt size can be scaled up or down.

Figure 57 Three M10 bolts with nuts and washers

A polished surface finish inside the interface of the bolted lap joint was chosen, as a rough surface finished is expected to increase the variability of the experimental results.

However, the geometry of the joint, the interface, the number of bolts and their location varied in the different experiments made. These parameters were thought to be the key parameters to investigate. Therefore, these parameters are detailed for each experiment in the following sections.

3.4 Impulse excitation

To investigate the vibration of bolted lap joints, an excitation method and a vibration recording method are necessary. The thinking process behind the choice of a hammer hit and an accelerometer at each extremity of the beam is developed in this section.

Impulse excitation using a hammer was selected as an excitation method. The alternative of using a shaker was rejected because, the attachment method of a

shaker can affect the resonance natural frequency of the test structure as concluded in (Smith, Brake, and Reuß 2015). The use of a shaker plus a separation device could have been used, but previous attempts show the complexity of this system. The use of a piezoelectric actuator as an excitation method seems promising, see (Peyret, Dion, and Chevallier 2016), but more complex than a hammer excitation. Using a hammer as an excitation method is well-established. The main advantage of the hammer is that it stays in contact with the structure for only a few microseconds, so the measured vibration decay is not corrupted by the excitation device. Figure 58 is a picture of the instrumented hammer used.

Figure 58 Instrumented hammer used to excite the structure

The advantage of the hammer overcame the drawbacks. The consequence of using a hammer is that multiple modes of vibration are excited at the same time. A complex signal processing methods is necessary to extract meaningful results from the recording. Also, impulse excitation may have unknown effects, like mode interferences. However, the absence of corruption overcomes these drawbacks. In addition, the hammer has another advantage: as multiple modes are recorded, the time necessary to perform a test is reduced. After considerations of the alternatives, only hammer hits were used as an excitation method in this work.

3.5 Selection of a free-free configuration and the suspension

A free-free configuration for the test structure was used to simplify the experimental method. A free-free configuration was selected because it minimises the interaction with the environment. Other configurations are possible by “locking” or “pinning” one

or multiple extremities as illustrated in Figure 59. Those fixations points are never infinitely rigid in practice. In reality, external modes can be measured with a pin or clamped extremity. Thus those constrained extremities corrupt the measured signal and so make the interpretation of the results more complex. The free-free configuration implies the use of an isolation device to counter the gravitational force.

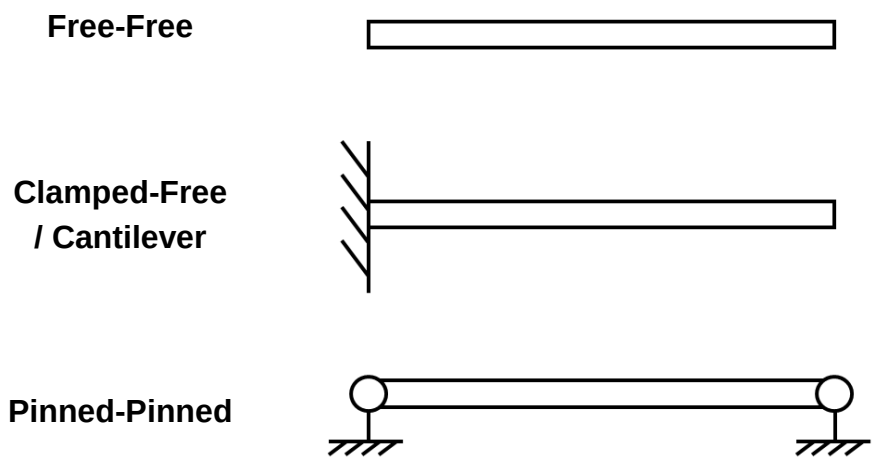

Figure 59 Three types of model for the boundary condition of a beam. “Free” means no constrain, “Pinned” blocks the displacements but not the rotations, and “Clamped” blocks displacements and rotations

The best isolation found used a long static string attached to a frame on top of a heavy test bed. A large frame was used to allow long strings. Different types of isolation were tested to select the isolation which corrupts the signal the least. Three lengths, three strings materials, two locations and two types of string were compared. A monolithic beam was exercised, and the average damping was extracted. The configuration with the least damping ratio for the three first bending modes was considered the best. The least damping ratio means that less energy is sent to the supporting structure. Use of this simple comparison method excluded the use of bungee material, a short suspension string, string at the extremity and a u-shape loop. This test allowed the validation of the use of long stiff ropes, like fishing wire or static rope, with a loop at each extremity positioned at the node of the first bending mode. A static rope is recommended because is it easier to work with and safer than fishing wire, as shown in Figure 60.

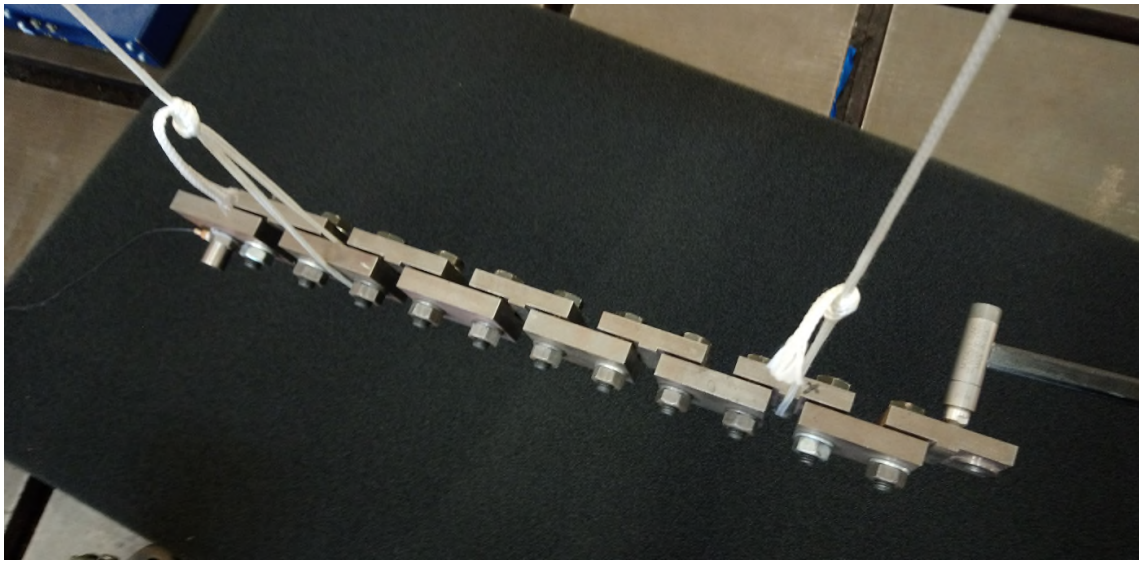

Figure 60 Top view of a structure suspended by the static rope suspension.

Also, vibration in the horizontal direction was chosen as it showed less corruption than a vertical direction. It is thought that the pendulum created by the horizontal direction helps the isolation of the structure. Indeed, the force excitation received by the suspension frame is weaker with the horizontal motion than with vertical motion.

3.6 Location of impact and accelerometer

A single accelerometer was used to record the vibration. Multiple accelerometers could have been used to obtain an experimental mode shape, but it would have increased the number of cables attached to the structure and may have corrupted the signal. Also, experimental mode shapes tend to be noisy in a structure with nonlinear dynamic behaviour, which is the main subject of research. In addition, experimental mode shapes did not seem to show any special usefulness according to the publications read. A laser-vibrometry method could have been used, but this type of facility was not available. The use of a laser also forces the structure to face the same direction, therefore limits the experimental design. A single uniaxial accelerometer was selected.

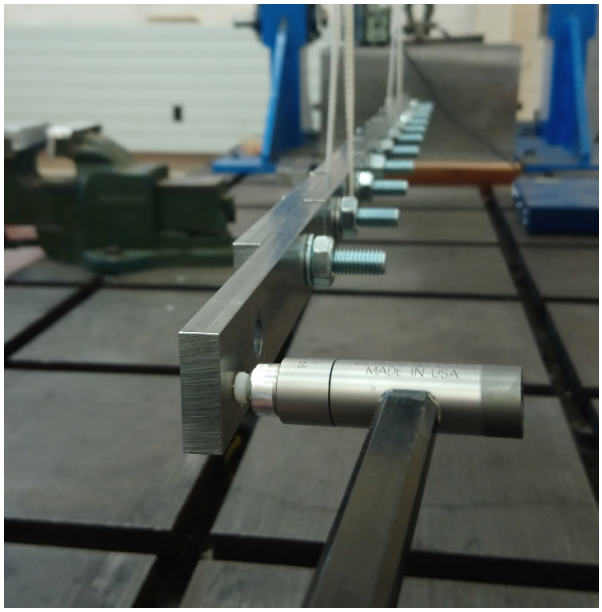

Figure 61 Hammer hit location at one extremity using in this work

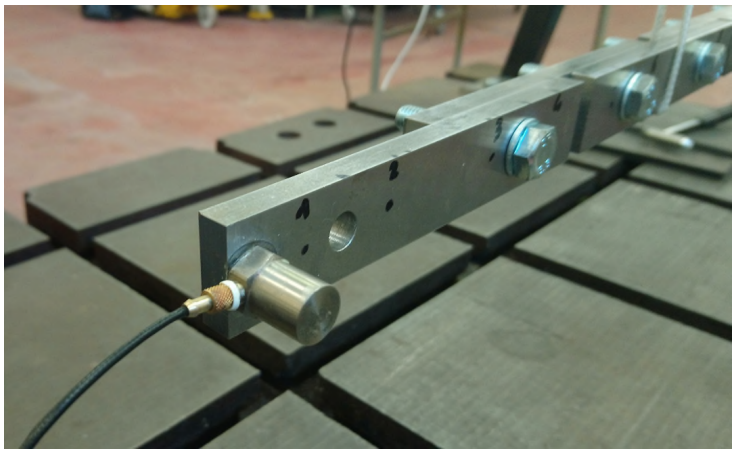

Figure 62 Typical accelerometer location at one extremity: centred vertically on the main face of a beam

The location of the hammer hit and the accelerometer were chosen to be the extremities of the beam, as in Figure 61 and Figure 62, because the amplitude of the mode shapes is large for all bending modes, as previously shown in Figure 56. Furthermore, as the displacement is directly linked to the acceleration, the acceleration measured will be high for all bending modes.

Finally, the hammer hit and the accelerometer were placed on the centre line of the beam to avoid excitation and the recording of the torsional modes.

This chapter has explained how the experimental methods of this thesis were decided. The choice of using impulses as excitation device had consequences on the signal processing workflow which is presented in the next chapter.

4 SIGNAL PROCESSING

This chapter describes how the signal processing is performed. To treat the signal, two nonlinear signal processing methods developed by Goyder and Lancereau (2017) were implemented and used. First, the signal processing workflow is described. Then, Section 4.2 describes how “reverse filtering” allowed the isolation of vibration decay. The third section explains the way in which “direct fitting” extracts the instantaneous frequency, damping, and amplitude from different parts of the decay time history.

4.1 Signal processing workflow

The workflow is in two steps as shown in Figure 63.

The use of impulse excitation allows the recording of acceleration time history. The choice of impulse excitation is explained in the experimental method Chapter 3. This time history is a superposition of multiple nonlinear decaying sinusoidal signals. These decaying sinusoidal signals are nonlinear because the natural frequencies and the damping ratios change depending of the amplitude. Assuming there is no mode interaction, each mode may be analysed independently. Therefore, a method that separates each mode was developed. Then due to the nonlinearity, a new fitting method was necessary to determine the instantaneous natural frequency and damping ratio.

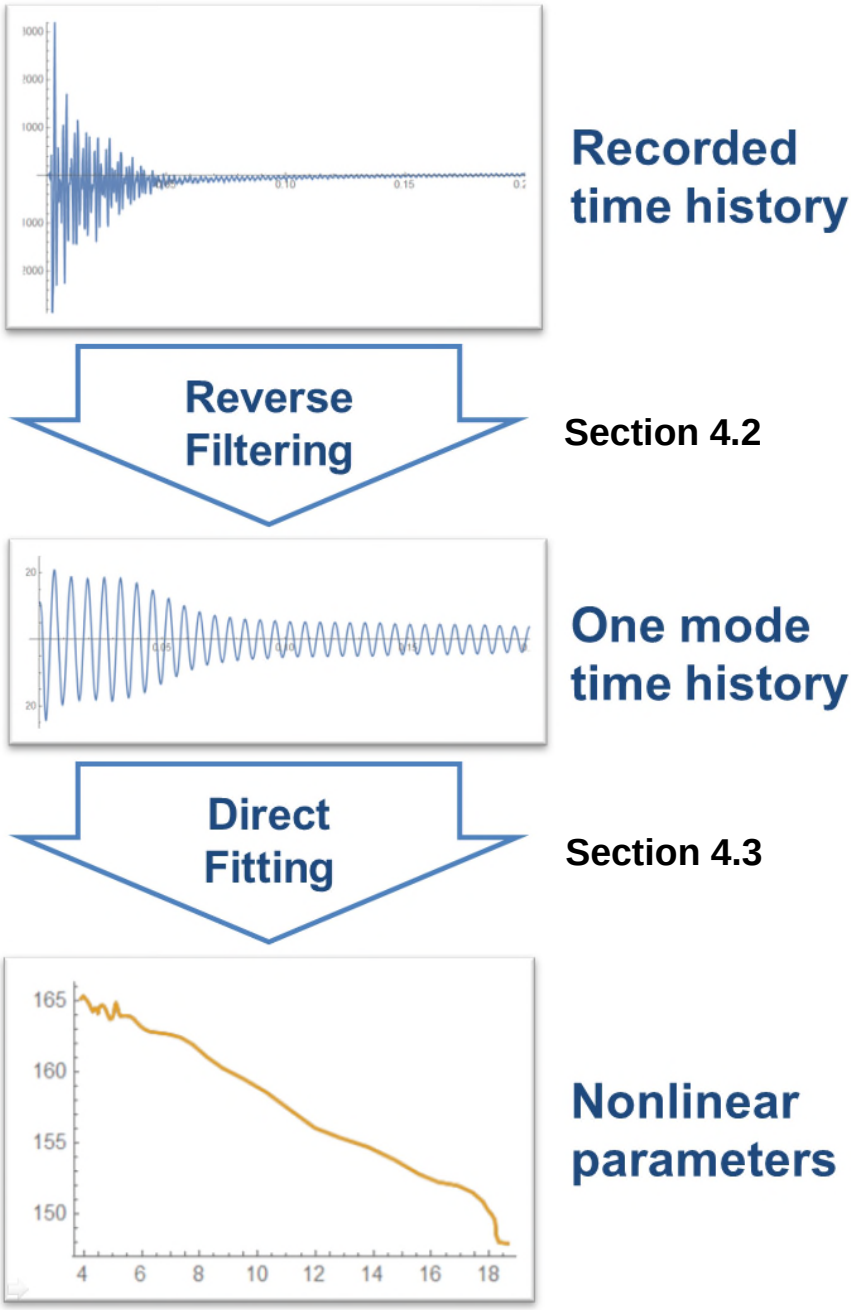

Figure 63 Illustration of the workflow used to extract nonlinear parameters from the recorded time history.

4.2 Reverse Filtering

In this section, the reverse filtering method is described. The reverse filtering method allows the isolation of individual decay time histories from the recorded signal.

The reverse filtering method used narrow band Butterworth filters. This filter has the advantage of having a limited effect on the signal between the pass frequency and the stop frequency as show in Figure 64.

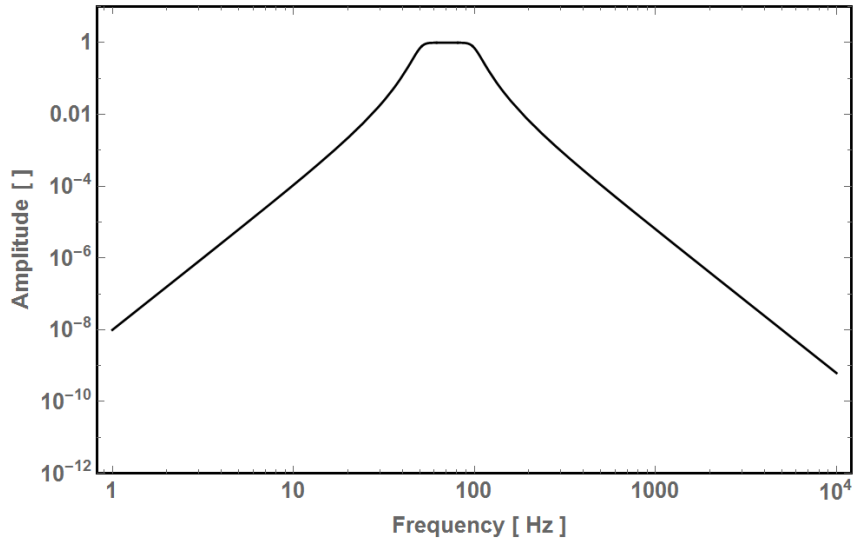

Figure 64 Butterworth filter spectrum (order four) with a bandwidth of 50Hz to 100Hz

The band pass filtering fails if the natural frequencies which need to be separated are too close to each other. Investigations not included in this document point out that if the natural frequency is less than 12 Hz apart, then the separation between two modes using a Butterworth filter does not work. Therefore, all the structures tested in this document were designed to have well separated natural frequencies to allow the filtering step to work.

One of the side effects of the band pass is the ringing generated. This ringing is generated by the filtering of the discontinuity at the sudden start of the time history. Before the hammer hit, there is no vibration. After the hammer hit, multiple modes are superimposed. The filtering of this discontinuity creates ringing which corrupts the signal at the beginning of the time history. A theoretical decaying time history was generated using Equation (2-24). The theoretical data is defined in Equation (4-1), with $Acc(t)$ (the acceleration, at a time t, in ms^{-2}), $A = 15\ ms^{-2}$ (the envelope start amplitude), $\omega_0 = 10 * 2\ \pi\ rad$ (the natural frequency), $\zeta = 0.04$ (the damping ratio), t (the time in second) and $\phi = 0\ rad$ (the phase).

$$\text{If } t < 0: A(t) = \quad 0 \qquad \textbf{(4-1)}$$

$$\text{If } t > 0\text{: } Acc(t) = A\, e^{-\omega_0 \zeta t}\ \text{Sin}\left(\omega_0\sqrt{1-\zeta^2}\, t + \phi\right)$$

This theoretical signal was filtered once using a Butterworth filter order 3 (pass frequency: 7Hz; stop frequency: 13Hz). The ringing generated by the filter is shown in Figure 65.

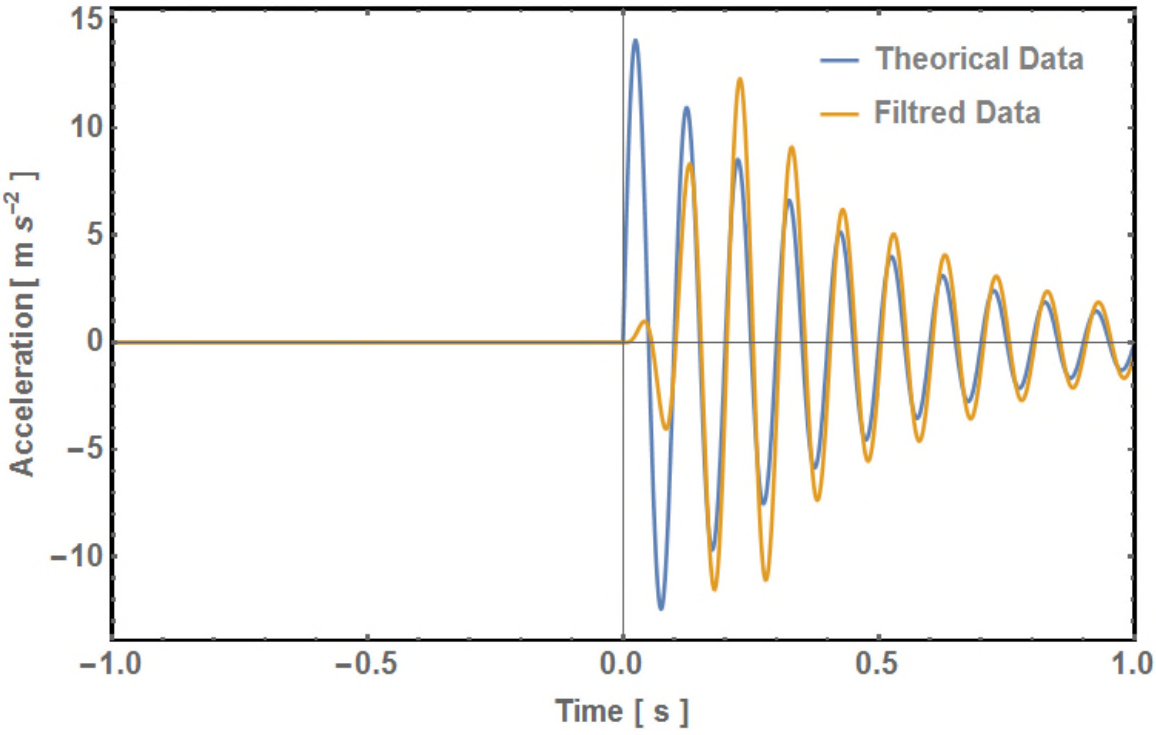

Figure 65 Ringing generate by a basic Butterworth filter (forward filtering)

Indeed this ringing is problematic as it corrupts the data where the structure tested is the most non-linear. The reverse filtering method avoids this problematic ringing. The solution found by Goyder (2015b) was to reverse the signal in time before passing it through the filter, and then reverse it back again, as shown in Figure 66. The advantage of this method is that there are no starting transients and the early part of the signal is uncorrupted.

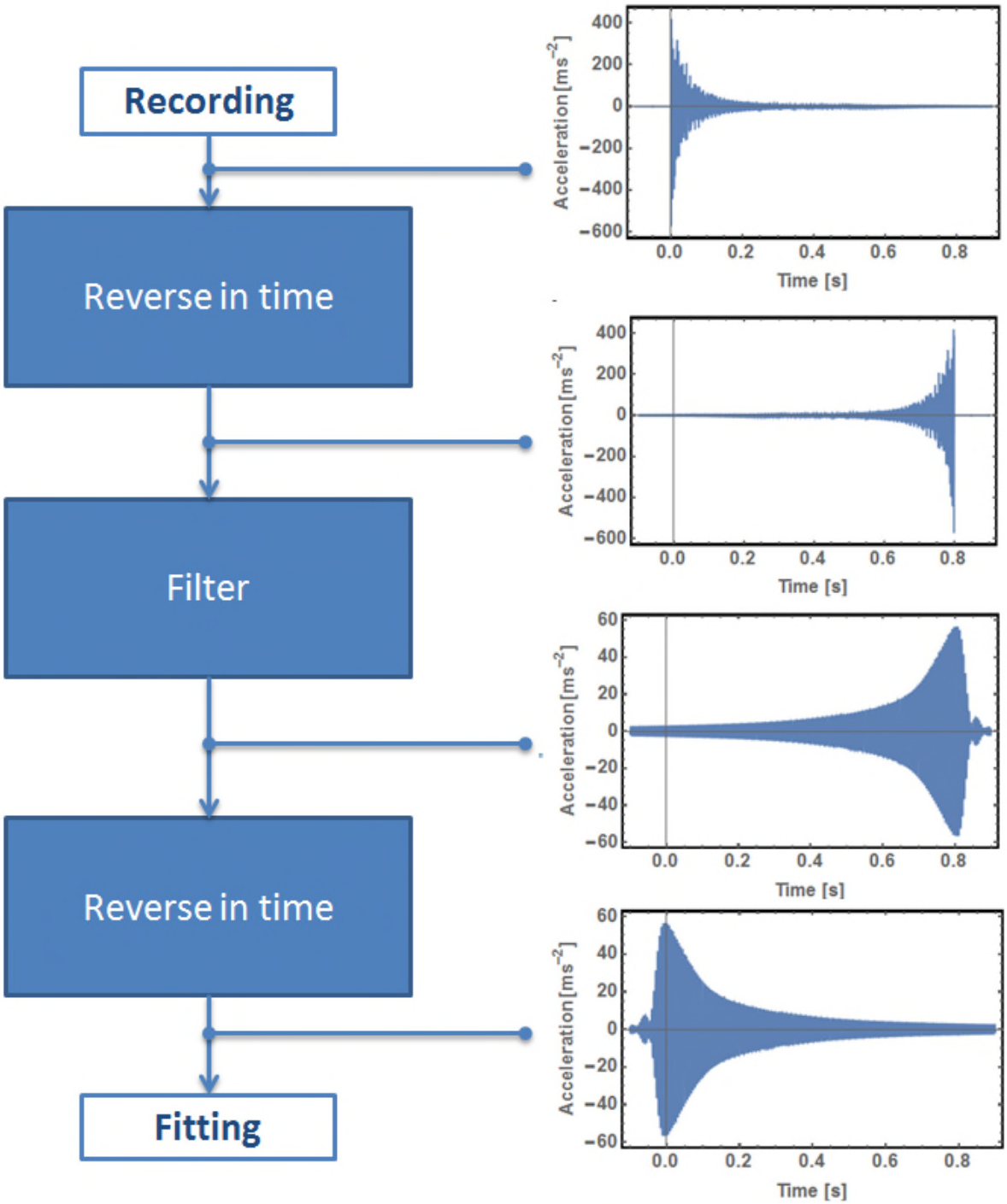

Figure 66 Illustration of the steps of the reverse filtering method

Although the ringing is removed, the reverse filtering has some side effects. The reverse filtering method changes the phase and reduces the amplitude of the signal. To illustrate these side effects, the same theoretical decaying time history was reverse filtered. The difference between the reverse filtered and the unfiltered signal

are shown in Figure 67. As desired the shape of the signal stays the same after the hammer hit (t=0s). However, the filtered signal has a phase shift of around $\pi/10$ compared to the original signal. In addition, the filtered signal has an amplitude drop of around 30%.

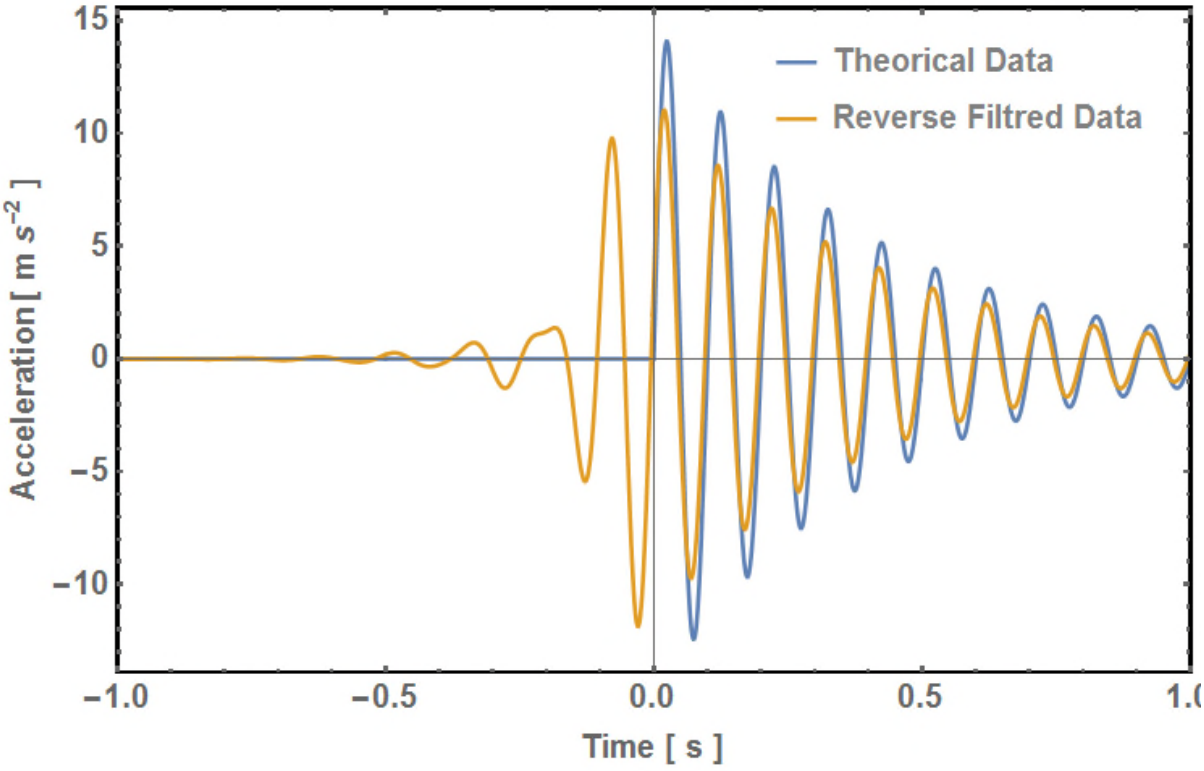

Figure 67 Illustration of the side effects of the reverse filtering method.

This reduction of amplitude and the phase shift has a small effect on the two estimators of interest. The two estimators of interest are damping ratio and natural frequency. In addition, as all the signals are filtered the same way, the filtered amplitude values are comparable.

The implementation of the reverse filtering used is this thesis has the following specific setting:

- The centre frequency of the filter
- The bandwidth
- The order of the filter
- How many time the filter is applied

The centre frequency of the filter was selected using the peak frequency of the spectrum of the signal.

The bandwidth was selected by trial and error at six hertz on both sides of the peak frequency. The bandwidth needed to be small enough to isolate one mode only, but large enough to include the nonlinear frequencies investigated.

A typical a third order filter was used. Higher order filters often lead to numerical errors, which crash the program, especially at small frequencies.

The filtering was applied two times, successively increasing the order of the filter.

An optimal solution is validated each time, for each mode, by comparing the spectrum before and after filtering of the experimental data sets, as shown in Figure 68: The filter is validated if the entire resonance peak filtered is the same as the unfiltered one. Also the other resonances peaks are reduced, as in this example. If necessary, the bandwidth was adjusted or the experimental signal was reverse filtered three times.

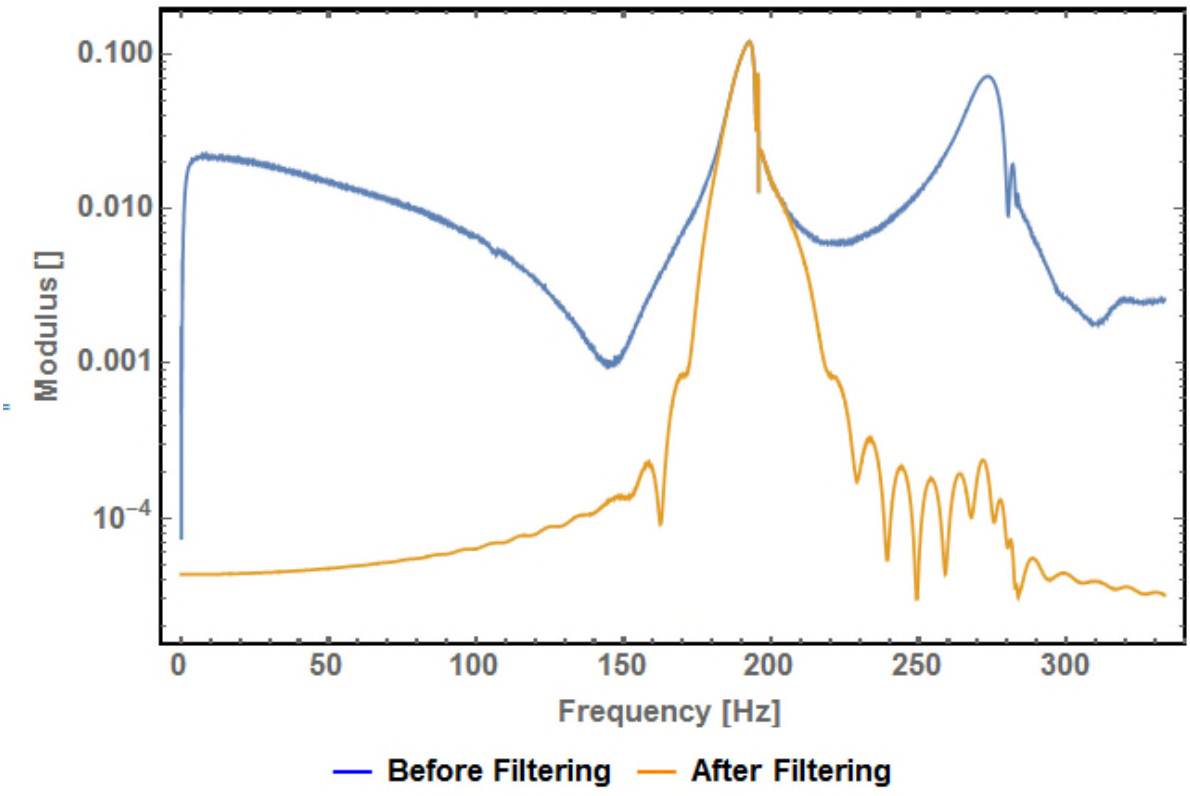

Figure 68 Spectrum of an experimental signal before and after filtering

4.3 Direct fitting

The previous section explained how each resonance has been isolated. This section presents the direct fitting method and how it was applied to extract parameters from the filtered time histories.

The method was named direct fitting because, compared to other comparable signal processing methods, it does not require any extra transformation before fitting a model. It fits a model directly to the filtered signal in the time domain.

To extract meaningful parameters, the approach was to linearize multiple short intervals of the signal. The variation of linear parameters is easier to interpret than nonlinear parameters. The signal is cut into intervals, see 4.3.1, and then each interval is fitted with a linear exponential decay, see 4.3.2.

4.3.1 Dividing the signal into multiple intervals

To select the intervals, two steps are needed. First, the number of cycles per interval is selected, then the number of points in the interval is deduced from the sample rate and the estimated frequency from the spectrum.

An example of the division of the signal in multiple intervals of 5 periods is given in Figure 69. The signal before t equal zero is neglected, as it is before the hammer hit.

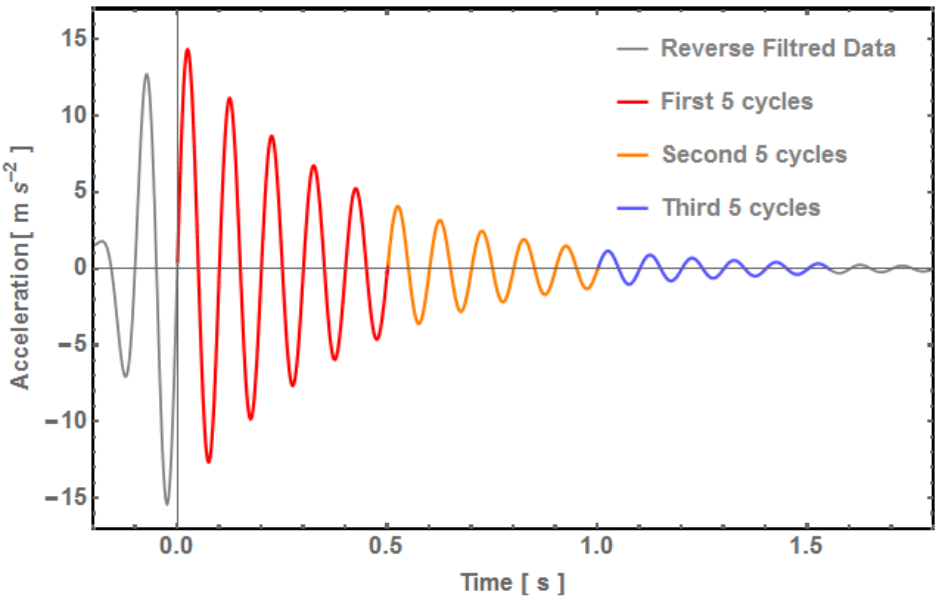

Figure 69 Example of the division of the signal in multiple intervals of 5 cycles each.

a)

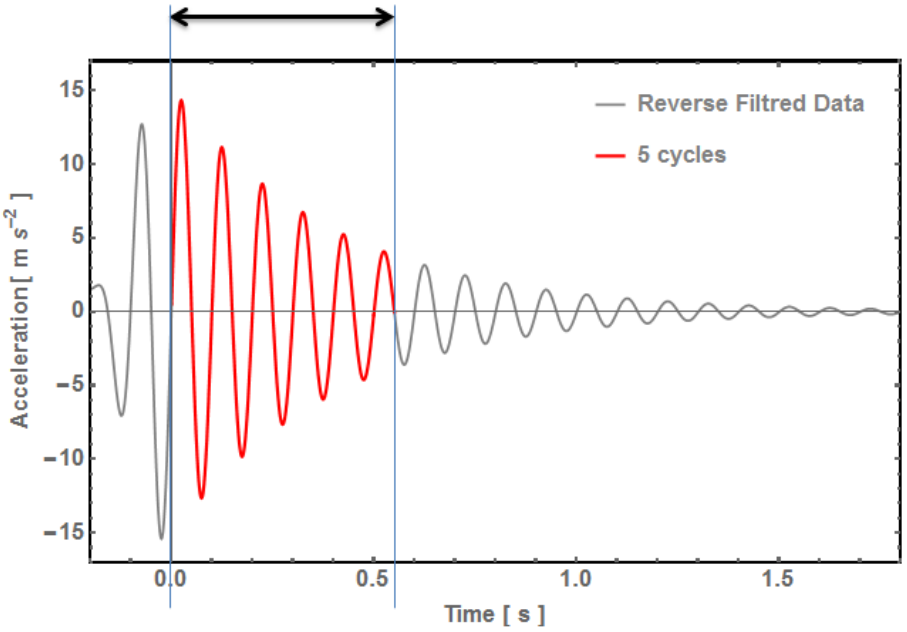

b)

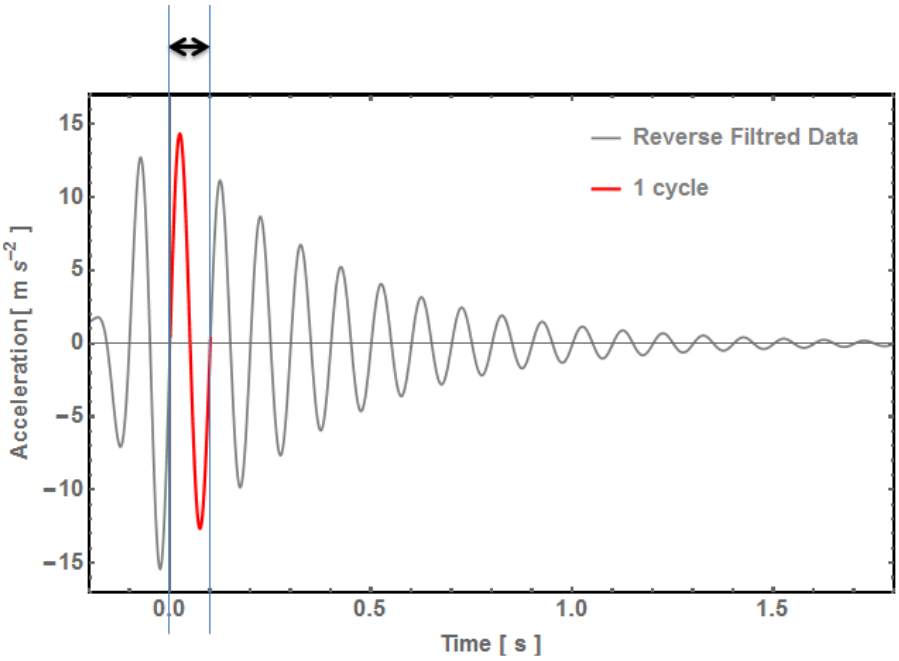

Figure 70 Division of the signal in a) five cycles or b) 1 cycle

The multiple lengths of the interval can be used as input the fitting method. Figure 70 gives two examples of the interval which can be used as input to the direct fitting method. The effect of the number of cycles per interval was investigated.

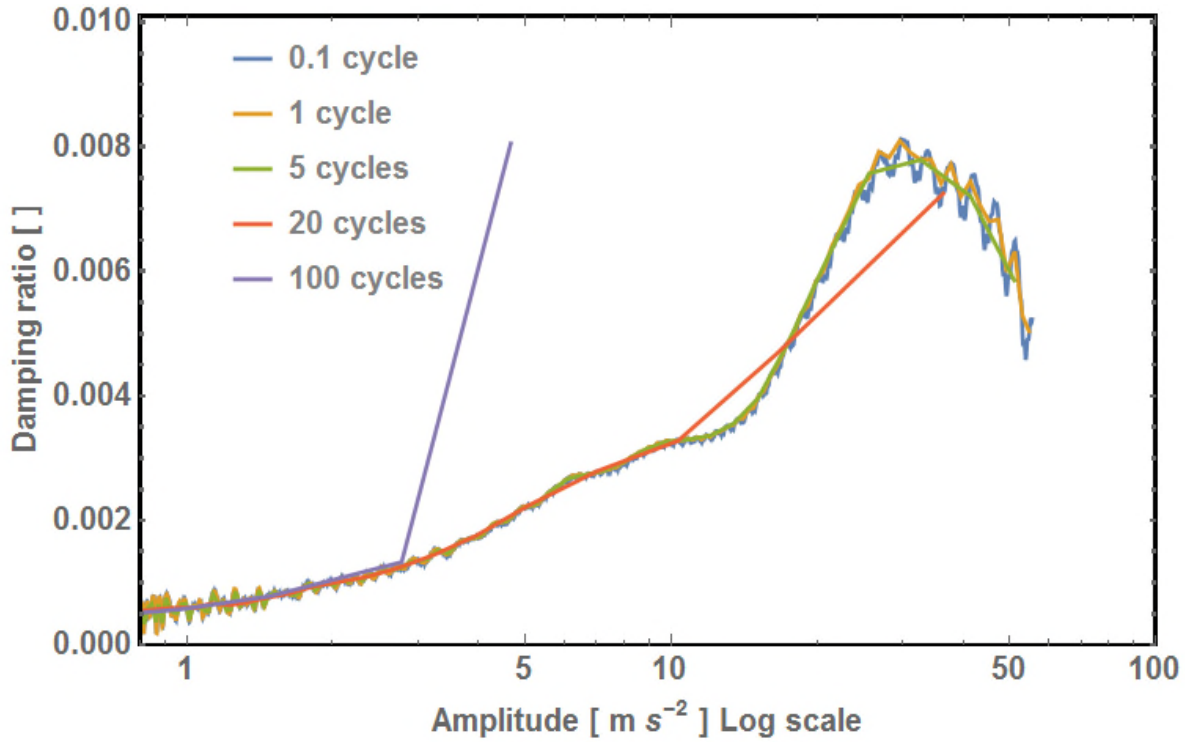

Figure 71 Damping ratio against amplitude in log scale with a different number of cycles par interval. A typical experimental data from the first mode of the sandwich beam was reverse filtered and direct fitted. The data points are joined by lines.

The choice of the number of cycle per interval has a dramatic effect on the estimation of the damping ratio as a function of the amplitude, see Figure 71. If the interval is large, then a small number of fitted parameters average the behaviour. This averaging reduces, for example, the effect of the noise at low amplitudes. Conversely, if the intervals are small, then there are a large number of fitted parameters, therefore more detail in the behaviour, but also the noise is more visible, especially at low amplitude.

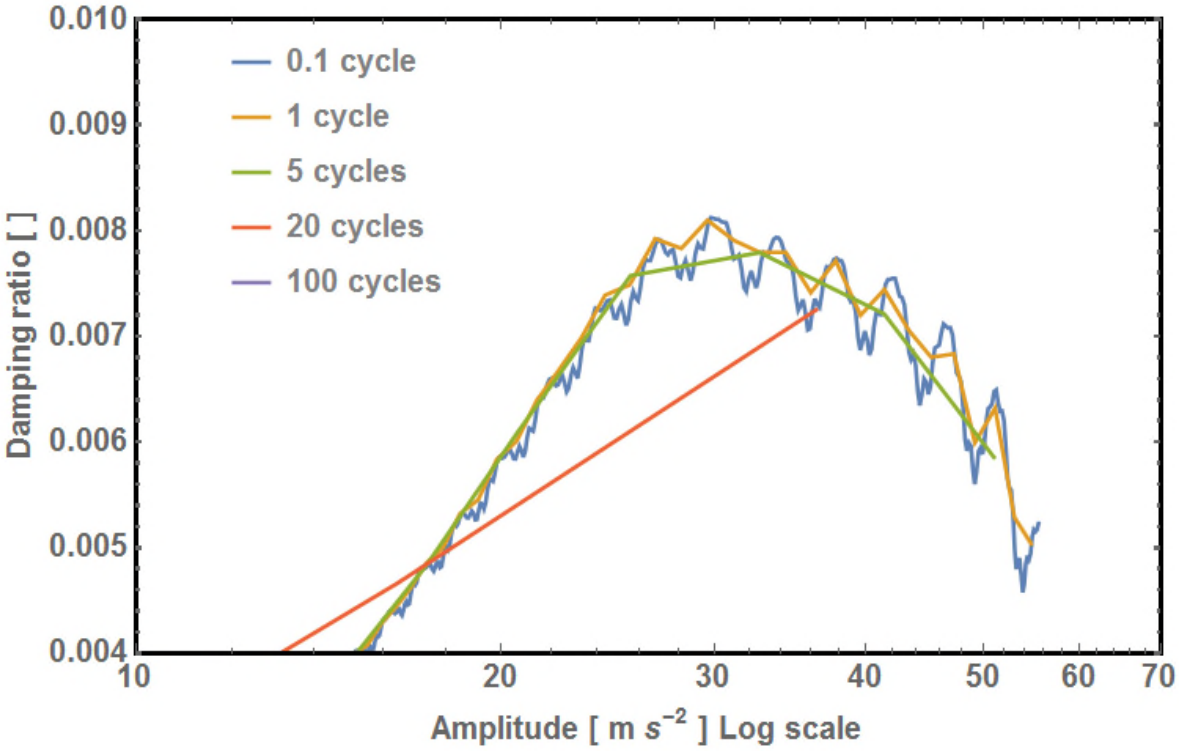

Figure 72 Zoom on the large amplitude of Figure 71, which represents the damping ratio against amplitude in log scale with a different number of cycles per interval

A compromise is needed between precision and noise. A practical value of five periods per interval was typically selected, as it captures the main trend as shown in Figure 72. This choice means that all departure from linear behaviour inside the five periods was neglected. This choice means that fast-changing phenomena, faster than five cycles, were ignored. In Figure 72, the fast-changing damping ratio, extracted by a direct fitting with 1 or 0.1 cycle per interval, are believed to be side-effects of the signal processing workflow.

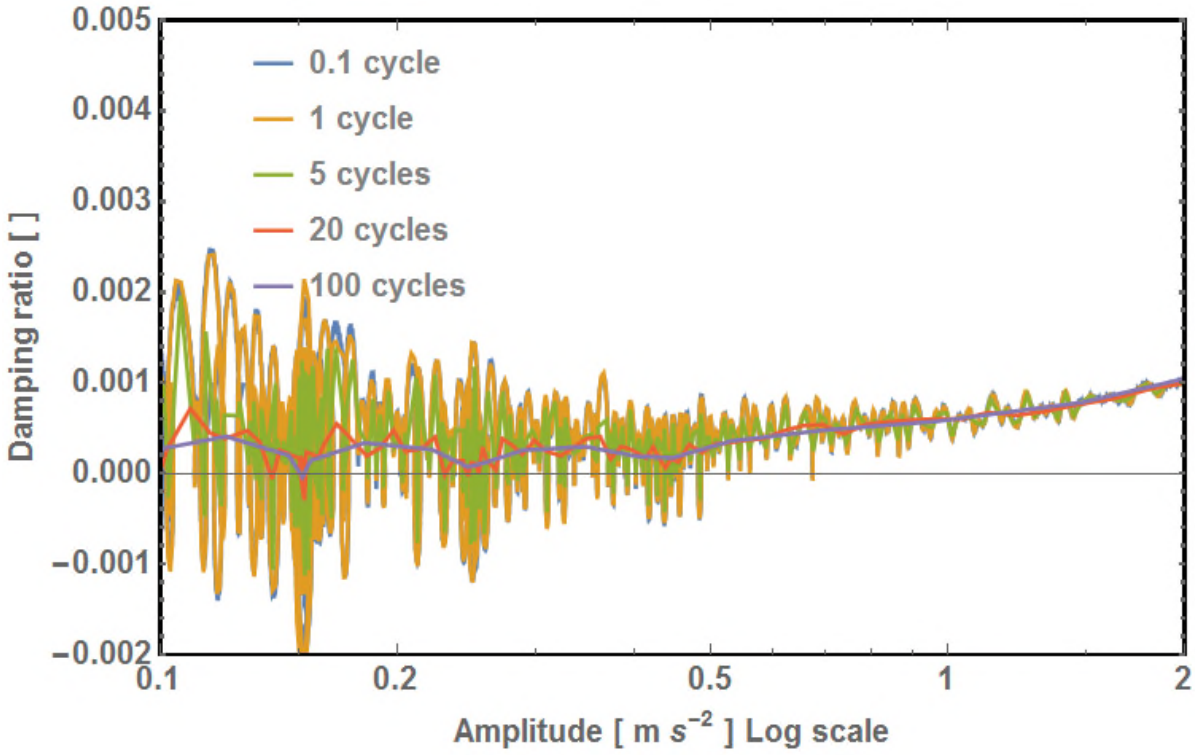

Figure 73 Zoom on the low amplitude of Figure 71, which represents the damping ratio against amplitude in log scale with different numbers of cycles per interval

Five cycles per interval were chosen, however, more work could be done on optimising this choice.

Future work could be carried out around the size of the interval used for fitting. Also, it was noted that the amount of damping may be a variable to consider when defining the number of periods in the interval. It is thought that a highly damped signal needs smaller intervals compared to lightly damped one which is more sensitive to noise. A large interval allows an averaging of the noise captured at low amplitude as shown in Figure 73. As this question of the size of the intervals seems to be a minor detail for this work, no further investigation was carried out.

4.3.2 Fit each Interval

Table 6 Nomenclature for this subsection in the order of definition:

Variable	Definition	Unit
$y_{fit}(t)$	Value of the model used for fitting at a time t	$[m\ s^{-2}]$
A_{start}	Estimated envelope amplitude at the start of the interval	$[m\ s^{-2}]$
f	Estimated natural frequency of the model	$[Hz]$
ζ	Estimated damping ratio of the model	$[no\ unit]$
θ	Estimated phase of the interval	$[rad]$
t	Time	$[s]$
B	Amplitude variable for the direct fitting model	$[m\ s^{-2}]$
C	Amplitude variable for the direct fitting model	$[m\ s^{-2}]$
α	Abstract variable for the direct fitting	$[Rad\ point^{-1}]$
β	Abstract variable for the direct fitting	$[Rad\ point^{-1}]$
n	Data point number from the start of the interval	$[point]$
t_{start}	Time at the start of the interval	$[s]$
$y_{md}(n)$	Measured data for point n	$[m\ s^{-2}]$
$\epsilon(n)$	Residual error between the measured data and the fitting model for point n	$[m\ s^{-2}]$
err	Total error of the fitting for the interval	$[m^2\ s^{-4}]$
N	Number of points in the interval	$[point]$
A	Instantaneous amplitude in the middle of the interval fitted	$[m\ s^{-2}]$
t_{start}	Time at the start of the interval	$[s]$
t_{middle}	Time at the middle of the interval	$[s]$

The method of fitting named Direct Fitting was developed by Goyder (2015b). This subsection explains this method. This subsection is in two parts: First, the refinement of the model equation, 4.3.2.1, then, the custom fitting procedure, 4.3.2.2.

4.3.2.1 Refinement of the model equation

The goal of the refinement of the model equation is to make the equation as easy to compute as possible for the fitting procedure.

The origin of the equation of motion used is developed in Subsection 2.1.2. The version of the equation used in this section is:

$$y_{fit}(t) = A_{start}\ e^{-\zeta 2\pi f t}\ cos[\sqrt{1-\zeta^2}2\pi f t + \theta] \quad \textbf{(4-2)}$$

This classic model, (4-2), used for data fitting has three nonlinear parameters (ζ, f and θ) and one linear one (A_{start}). The variables ζ, f and θ represent respectively the damping ratio, the natural frequency and the phase. The variable A_{start} is defined in Equation (2-1), with $y_{fit}(t_{start})$ the value of the fitting model at the starting time of the interval.

$$A_{start} = y_{fit}(t_{start}) \quad \textbf{(4-3)}$$

The first refinement of Equation (4-2) uses the trigonometric identity:

$$cos[a+b] = cos[a]\,cos[b] - sin[a]\,sin[b] \quad \textbf{(4-4)}$$

to change (4-2) into (4-5):

$$y_{fit}(t) = A_{start}\ \ e^{-\zeta 2\pi f t}\ \ (\,cos[\theta] cos\left[\sqrt{1-\zeta^2}2\pi f t\right] - \ sin[\theta] sin\left[\sqrt{1-\zeta^2}2\pi f t\right]\,) \quad \textbf{(4-5)}$$

Then, a change of variable, defined in (4-6) and (4-7), is used. This operation merges the starting amplitude A_{start} and the phase θ into two linear parameters B and C. Having two linear parameters simplify the fitting. This change of variable transforms Equation (4-5) into Equation (4-8).

$$B = A_{start}\ cos[\theta] \quad \textbf{(4-6)}$$

$$C = A_{start}\ \ sin[\theta] \quad \textbf{(4-7)}$$

$$y_{fit}(t) = e^{-\zeta 2\pi f t}(\ B\ cos\left[\sqrt{1-\zeta^2}2\pi f t\right] -\ C\ sin\left[\sqrt{1-\zeta^2}2\pi f t\right]) \quad \textbf{(4-8)}$$

The square root function leads to complex value if $\zeta > 1$ and is best avoided. The damping ratio, ζ, is always less than 1 in the signals investigated and cannot be negative. Therefore ζ and f are replaced by the variables β and α using the change of variables defined in Equation (4-9) and Equation (4-10). The variable s_r is the sample rate of the interval fitted. This second change of variable transforms Equation (4-8) into Equation (4-11).

$$\alpha = \frac{2\,\pi\sqrt{1-\zeta^2}\,f}{s_r} \quad \textbf{(4-9)}$$

$$\beta = \frac{2\,\pi\,\zeta\;f}{s_r} \quad \textbf{(4-10)}$$

$$y_{fit}(t) = e^{-\beta\,t\,s_r}(B\,cos[\alpha\,s_r\,t] - C\,sin[\alpha\,s_r\,t]) \quad \textbf{(4-11)}$$

Finally, as the last transformation, Equation (4-12), replaces the real variable t with an integer n using the sample rate (s_r) to reach Equation (4-13). Therefore the first point of the interval has a value of one.

$$n = (t - t_{start})\,s_r + 1 \quad \textbf{(4-12)}$$

$$y_{fit}(n) = e^{-\beta\,(n-1)}(B\,Cos[\alpha\,(n-1)] - C\,Sin[\alpha\,(n-1)]) \quad \textbf{(4-13)}$$

The Equation (4-13) is simpler to fit compared to the equation of motion (4-2), because (4-13) has two linear variables (B and C) instead of one (A_{start}), no square root functions are inside the trigonometric function and there is one integer variable (n) instead of the real variable (t).

With this optimised formulation of the equation, a classic least square formulation was used. The residual at a point n, $\epsilon(n)$, is calculated by subtracting the measured data, $y_{md}(n)$, from the fitted model at point n, $y_{fit}(n)$:

$$\epsilon(n) = y_{md}(n) - y_{fit}(n) \quad \textbf{(4-14)}$$

The residual is then squared and summed to obtain the total error (err), see Equation (4-15) and (4-16). The variable N represents the number of points in the interval.

$$\mathrm{err} = \sum_{n=1}^{N} \epsilon(n)^2 \quad \textbf{(4-15)}$$

$$\mathrm{err} = \sum_{n=1}^{N} \{y_{md}(n) - e^{-\beta(n-1)}(B\,cos[\alpha\,(n-1)] - C\,sin[\alpha(n-1)])\}^2 \quad \textbf{(4-16)}$$

The total error, err, is small when the fitting is precise; therefore the goal now is to minimize this error. In Equation (4-16), the term $y_{md}(n)$ is the amplitude of the measured data at a point n.

4.3.2.2 Fitting procedure

To minimise the total error and therefore fit the data with the model, a custom procedure was implemented. Taking into consideration the presence of two linear terms in the model equation, the procedure was segmented into two minimisation steps. One step fits only the linear parameters B and C. Then, in another step, the two nonlinear parameters α and β are fitted. This separation into two steps allows a faster fitting as it reduces the number of variables treated with the nonlinear minimisation. The procedure is detailed in Figure 74.

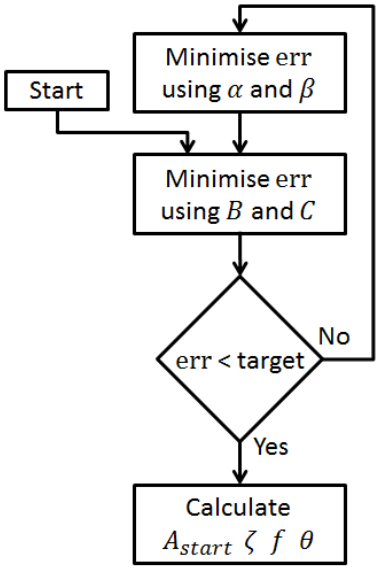

Figure 74 Custom procedure used to fit the data of one interval

The minimisation procedure was implemented using a standard minimisation function. The last step consists of calculating the nonlinear parameter as defined in the first version of the model, equation (4-2). Indeed, the original formulation of the estimator in (4-2) should lead to estimators which are independent of each other and easier to interpret than the abstract estimators α and β. The equations (4-17), (4-18), (4-19), (4-20) and (4-21) are based on the previous change of variable.

$$t = \frac{(n-1)}{s_r} + t_{start} \quad \textbf{(4-17)}$$

$$A_{start} = \sqrt{B^2 + C^2} \quad \textbf{(4-18)}$$

$$f = \frac{\sqrt{\alpha^2 + \beta^2}}{2\pi} \quad \textbf{(4-19)}$$

$$\zeta = \frac{\beta}{\sqrt{\alpha^2 + \beta^2}} \quad \textbf{(4-20)}$$

$$\theta = \arccos\left(\frac{A}{C}\right) \quad \textbf{(4-21)}$$

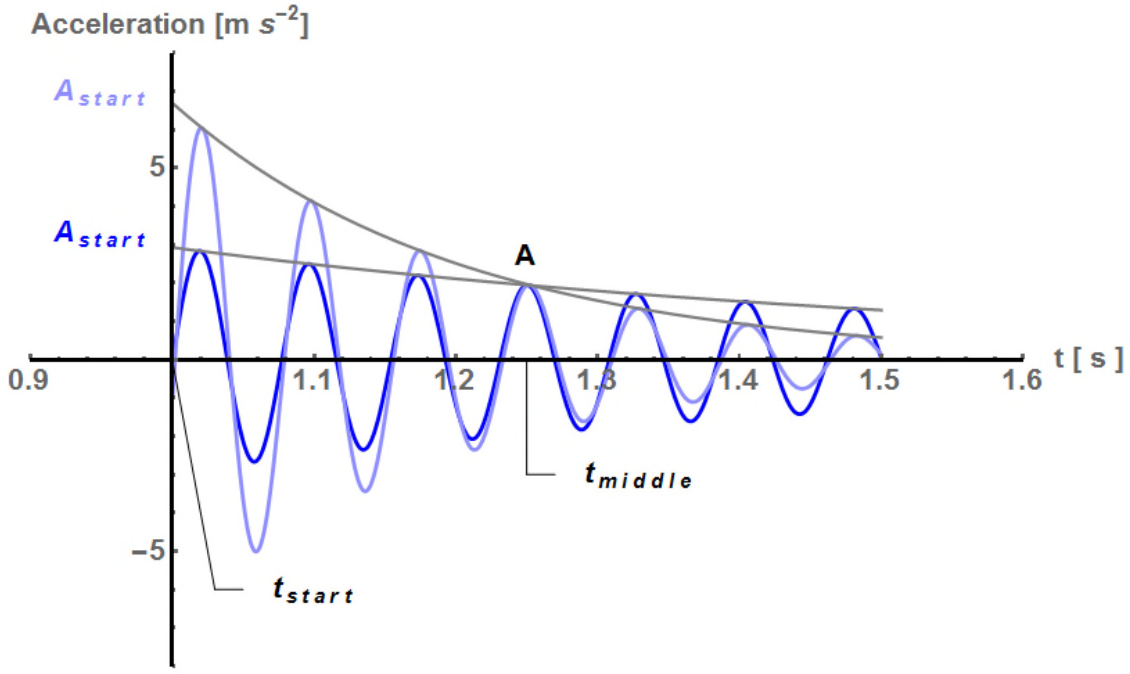

Figure 75 The difference between A and A_{start}

The estimator A_{start} is less representative than the estimator A, the instantaneous amplitude in the middle of the interval fitted; see Equation (4-22) and Figure 75. Also, A is independent of the damping ratio ζ. The variable t_{start} and t_{middle} are respectively the time at the start and in the middle of the interval. The estimated envelope amplitude in the middle of the interval fitted, A, is calculated with:

$$A = A_{start} e^{-\zeta 2\pi f (t_{middle} - t_{start})} \quad \textbf{(4-22)}$$

The estimator A is important for the rest of this document. The meaning of 'A' is illustrated in Figure 75. Note that A will be referred to only as "envelope amplitude", "instantaneous amplitude" or just "amplitude" for the rest of this document.

This subsection on direct fitting concludes the chapter on signal processing. The workflow presented in this chapter is used on multiple occasions in the next chapter which will present the experimental results.

5 EXPERIMENTS ON THE INTERFACE GEOMETRY

The chapter investigates the effect of the interface geometry on the nonlinear behaviour of a bolted lap joint. The use of shims of different size exposes the strong correlation between the length of the contact patch and the nonlinear behaviour of a bolted joint. These experiments were performed on the sandwich beam with two bolted lap joints.

5.1 Nomenclature

Table 7 Nomenclature of Chapter 3

Variable	Definition	Unit
L_c	Unknown length of the contact patch	$[\mathrm{mm}]$
L_s	Length of the shim(s)	$[\mathrm{mm}]$
b	Sum of the thickness of multiple shims	$[\mathrm{mm}]$
A	Instantaneous amplitude	$[\mathrm{ms}^2]$
A_{ref}	Reference amplitude (value = $1\mathrm{ms}^{-2}$)	$[\mathrm{ms}^2]$
f(A)	Instantaneous frequency at an amplitude A	$[\mathrm{Hz}]$
$\Delta f(A,A_{ref})$	:= f(A) - $f(A_{ref})$	$[\mathrm{Hz}]$
$\zeta(A)$	Instantaneous damping ratio at an amplitude A	$[\mathrm{no\ units}]$

5.2 Introduction sandwich beam shim experiments

This section describes the experimental results associated with the sandwich beam.

5.2.1 Experimental design

The author participated in the NOMAD Research Institute (2016) at Albuquerque in New Mexico, USA during which multiple experiments designed by M. R. Brake (2019) were tested. In one experiment, five custom beams where machined and tested, see Figure 76. The geometry of the interface had a strong correlation with the dynamic behaviour of the bolted lap joint.

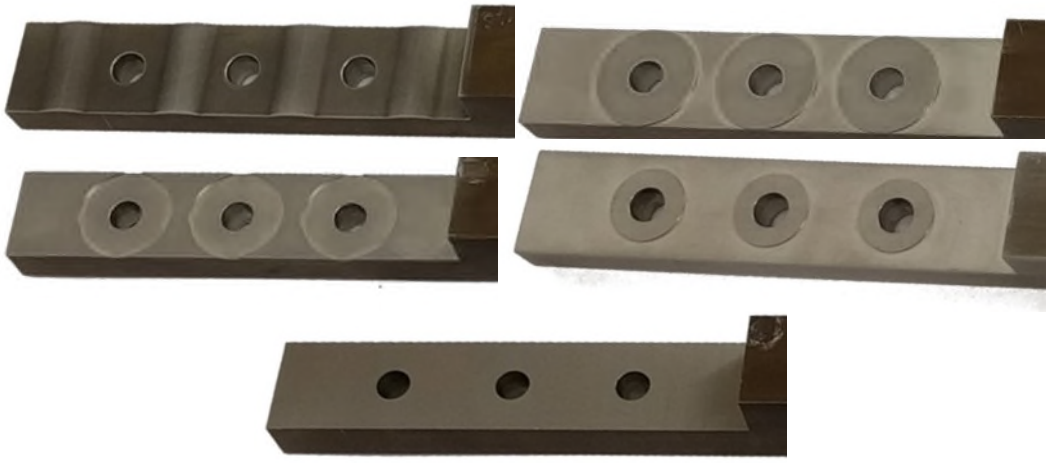

Figure 76 The five custom interfaces tested during the NOMAD Research Institute (2016)designed by M. R. Brake (2019)

The main goal was to replicate experiments performed by Dossogne et al. (2017) in which the author of this document participated during the 2016 NOMAD institute. The main drawback of the 2016 NOMAD institute experiment was that five different beams were manufactured. Manufacturing five beams create variation in the surface finish, mass and stiffness distribution of each beam. The variations of physical properties make the experimental results difficult to compare.

Therefore, an alternative experimental method was needed. A new experimental method is presented in the sections below which combine the sandwich beam, described in Subsection 5.2.2 and a novel way to modify the interface geometry described in Subsection 5.2.3.

5.2.2 The sandwich beams experiment layout

A description of the sandwich beam's experiment layout is presented in this section.

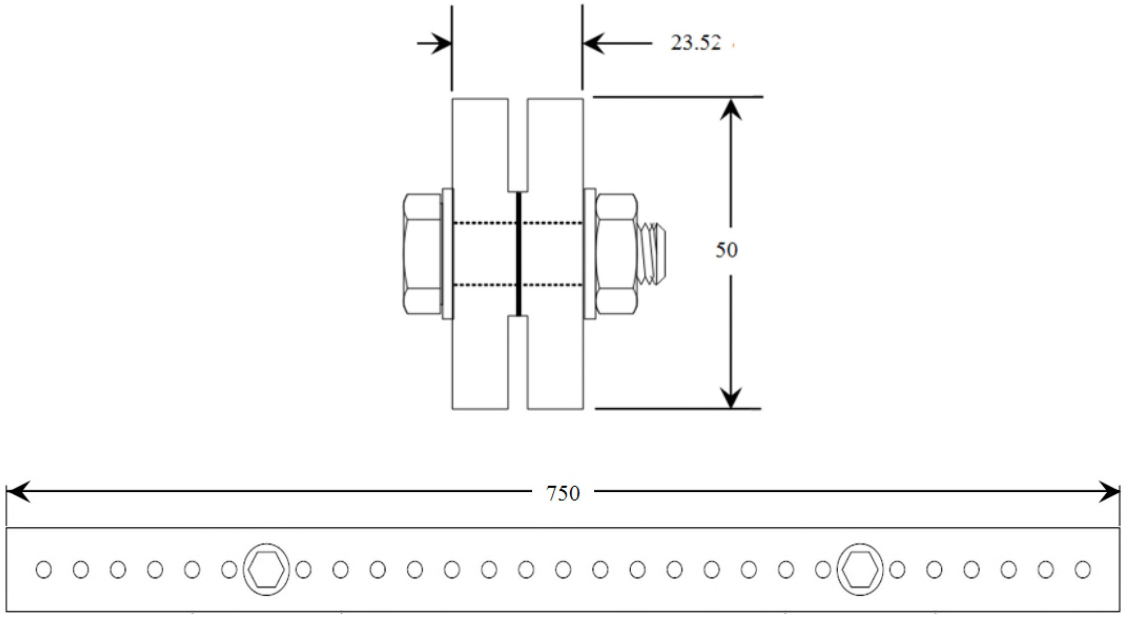

Figure 77 Dimensions of the sandwich beams with two bolts at hole locations 7 and 23 with a general tolerance of 10 microns

The dimensions of the sandwich beams are given in Figure 77. The experimental layout for excitation and vibration measurement is presented in Figure 78. The structure is excited with a hammer. The vibration of the structure is recorded by an accelerometer. This built-up structure had previously been investigated in (H G D Goyder et al. 2016; H. Goyder and Ind 2013). It consists of two beams in a sandwich configuration jointed by two M10x52 bolts with washers. The interfaces were ground to achieve a polished surface finish. The structure is suspended using two strings with loops at the extremities of fishing-wire placed next to the bolts as presented in Figure 78.

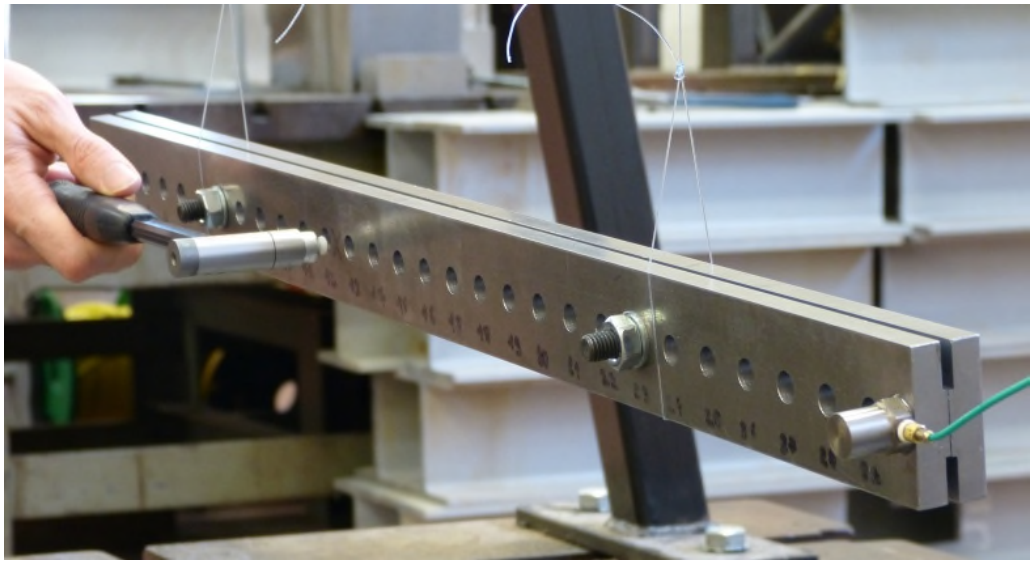

Figure 78 Sandwich beam suspended by 0.6mm fishing wires

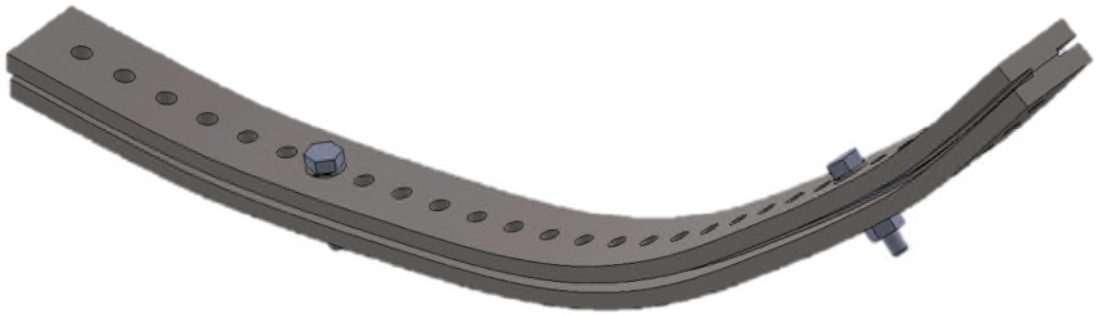

Figure 79 First bending mode of the sandwich beam from a finite element model analysis. The simulated structure is in a Free-Free configuration as described in Section 3.5.

Two bolts were placed at the 7th and 23rd holes which coincide with the nodes of the first bending mode, see Figure 79. This configuration of bolt positions was selected because the preliminary test shows that this position of bolts had the highest damping ratio compare to other positions of bolts with symmetrical placement on the beam.

The bolt torque was 54.2 Nm as previously used in (H G D Goyder et al. 2016; H. Goyder and Ind 2013). A vice was used to hold the structure during assembly to improve the repeatability, see Figure 80 a).

a) **b)**

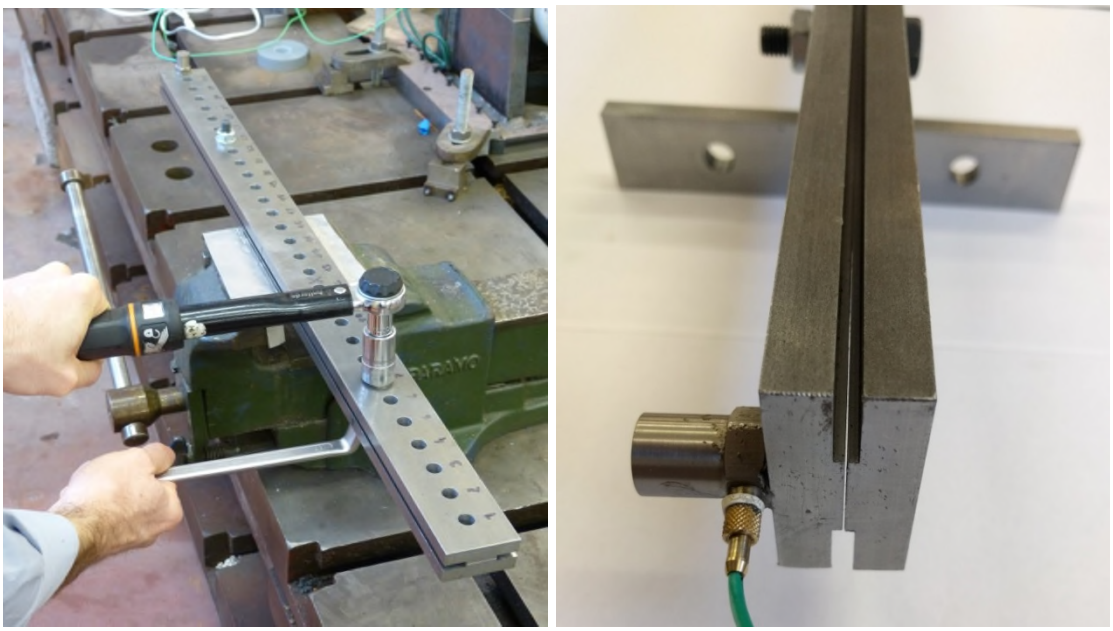

Figure 80 a) Vice used for the assembly of the sandwich beam. b) View of the sandwich beam edge without shims. The gap, between the two beams, appears when the bolts are tightened.

The beams spring apart leaving a gap between the beams, at the middle and at the extremities, see Figure 80 b). From this observation, it was assume that a receding contact exists, between the two beams close to each bolt location, as a result of bolt tightening as shown in Figure 81. All the experiments describe below have been performed with this set up.

Figure 81 Receding contact: Type of contact where the normal constraint at the edge of the contact patch is null. Diagram made by Hills, Nowell, and Sackfield (1993)

This concludes the presentation of the set up.

5.2.3 Modification the interface geometry using shims

This subsection, Subsection 5.2.3, presents how the geometry of the interface was modified using shims.

a) **b)**

Figure 82 a) Typical shims used to investigate the impact of the geometry of the interface on the dynamic behaviour of bolted lap joint. b) Sandwich beam opened-up

Adding a shim between the two surfaces of a bolted lap joint was proposed. A shim is a thin piece of metal of any shape. Examples of shims manufactured for the experiments presented in this chapter can be seen in Figure 82 a). The long interface of the sandwich beam is displayed in Figure 82 b). No previous record of the use of shims to investigate the nonlinear dynamic behaviour of joint was found.

The shims allow multiple interface geometries to be investigated with limited impact on the structure. Indeed, the mass of the shims is negligible compare to the mass of the beam. The heaviest shim weighted 0.7g plus or minus 0.1g whereas the sandwich beam all assembled weighted 5941g plus or minus 1g. Also because the two beams are separated by shims, the two beams can only enter in contact in the interface delimited by the shims geometry. Therefore, the shims allow precise control of the interface limit without noticeable impact on the mass distribution. In addiction the use of shim allows a modular approach very inexpensive and easy to

manufacture. The shims were manufactured by pressing a metal sheet between two parts of the desired shape and removed the excess material.

However, introducing shims could have an impact on the dynamic behaviour due to the increase of the surfaces in contacts in the lap joint. Indeed, without shims, a lap joint has two main surfaces in contact, but with a shim, there are four surfaces in contact. Therefore a test was necessary to measure the impact of having multiple surfaces in contact inside a lap joint.

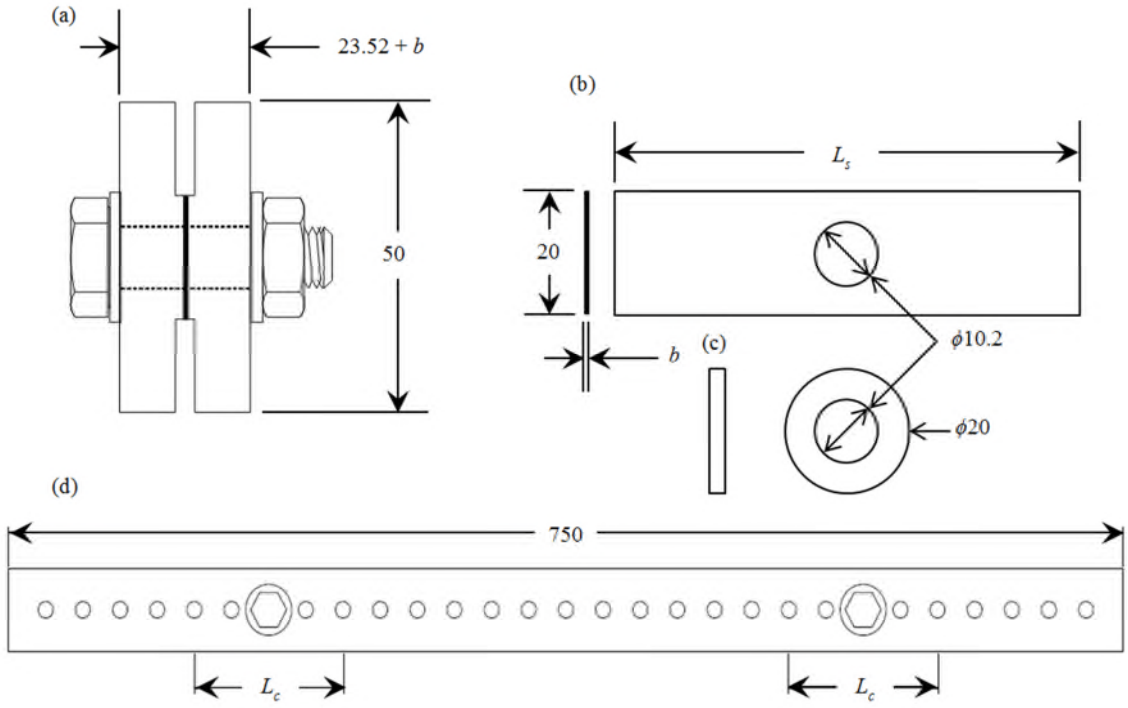

Figure 83 Sandwich Beams with shims (a) cross-section (b) plan views of a shim placed between the two beams. L_S is the length of the shim, *b* is the sum of the thickness of one or multiple shims. (c) Plan views of the 3.2mm thick washer (d) plan view of the structure. L_C is the unknown length of the bound region. Dimensions in mm.

To simplify the description of the experiments configuration described after three variables were defined: L_S, L_C and b as defined in Figure 83.

5.3 Filtering of the first bending mode

Each hammer hit was filtered to isolate the first bending mode. As an illustration, Figure 84 and Figure 85 show the time history of one of the vibration decays before and after the filtering. Also, Figure 86 shows the spectrum of the same decay before and after the filtering step.

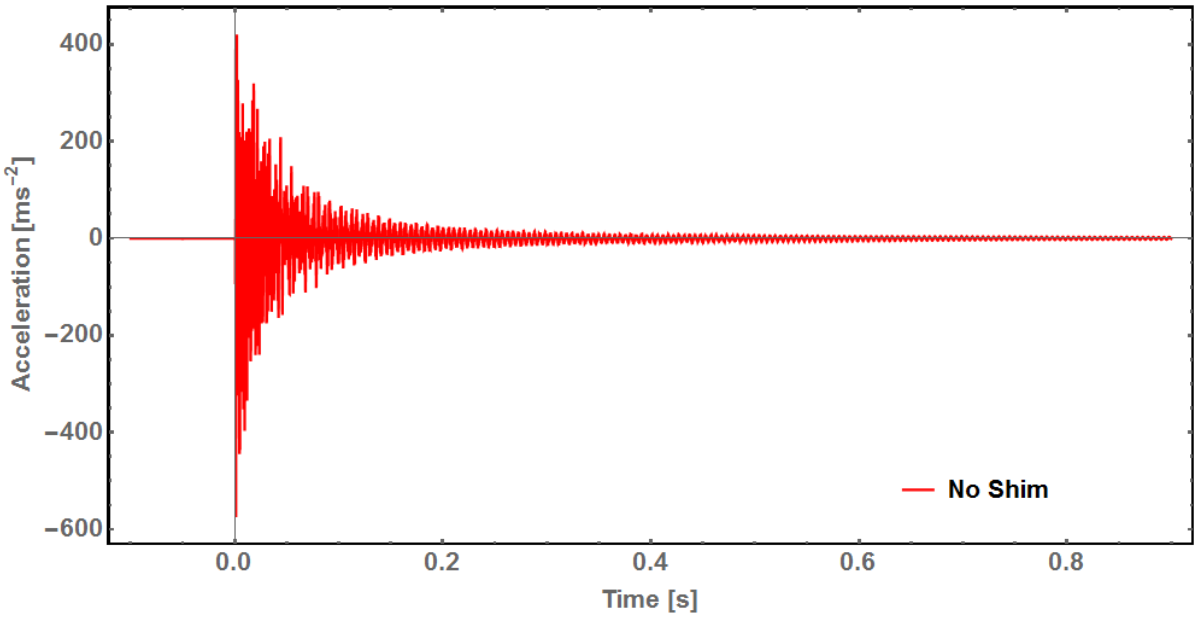

Figure 84 Time history before filtering from the no shim case

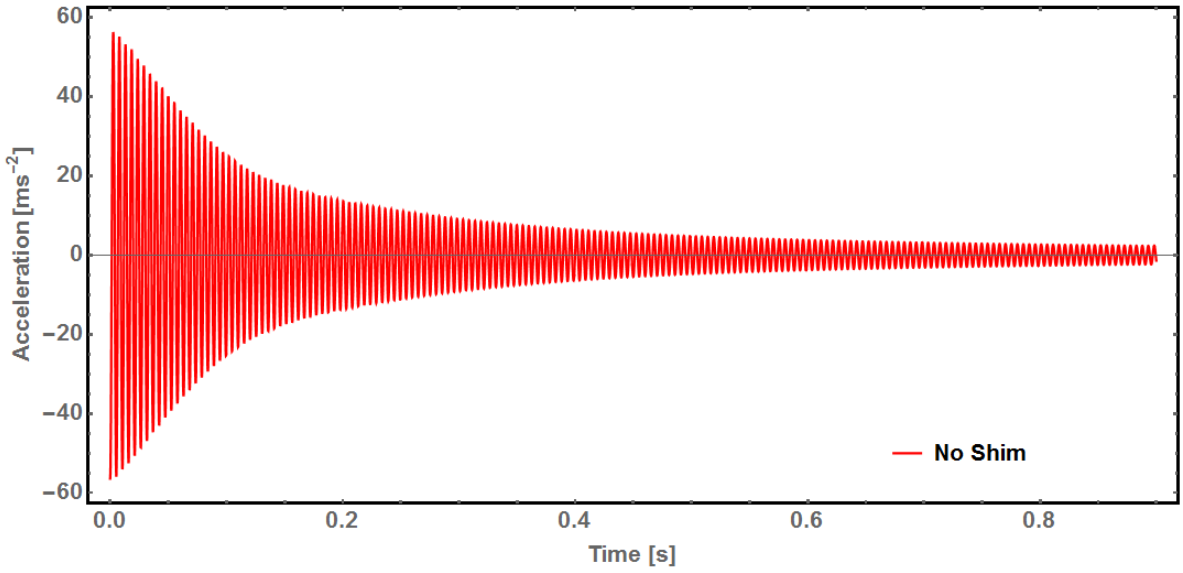

Figure 85 Time history after filtering of the first bending mode of the data in Figure 84

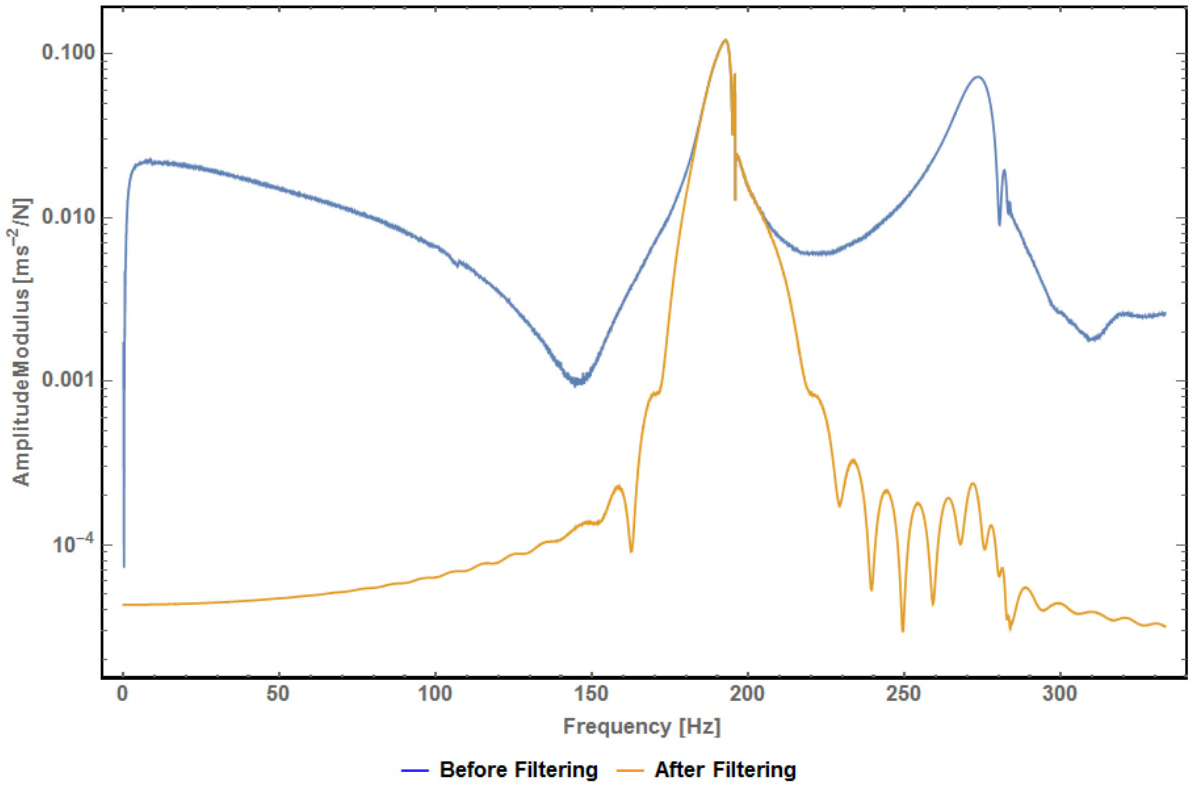

Figure 86 Spectrum of the no shim test vibration decay before and after filtering

5.3.1 Preliminary investigation

The following hypotheses were investigated:

Hypothesis 1. The damping ratio is linked to the number of surfaces in contact in a lap joint. Thus, stacking several shims should multiply the numbers of interfaces in a lap joint and the damping ratio measured should increase with the number of interfaces.

Hypothesis 2. The thickness of the shim has an impact on the nonlinear dynamic behaviour of the bolted lap joint.

To investigate Hypothesis 1 and Hypothesis 2, the 16 tests detailed in Table 8 were performed.

Table 8 Shim thickness and stacking experiment on long shim

Shims length	Number of shim	Shim thickness
No shim	0 shim	N.A.
100mm	1 shims	0.5 or 0.2 or 0.1 mm for each case
	2 shims	
	3 shims	
	4 shims	
	5 shims	

The shim thickness and stacking experiment was performed following the test detail in Table 8. Identical shim thicknesses and identical number of shims were used for the two bolts at each test. The result of the thickness and stacking experiment are presented in Section 5.

5.3.2 Results preliminary investigations on shim thickness

This section presents and interprets the experimental results of the thickness and stacking of multiple shim experiments. Multiple shims of 100 mm length were stacked on top of each other at both bolt locations. Also, three thicknesses of shim were tested: 0.1, 0.2 and 0.5mm.

The results from the thickness and multiple shims test are shown in Figure 87, Figure 88 and Figure 89. The figures correspond to damping ratio, change in frequency and natural frequency all as a function of amplitude, respectively.

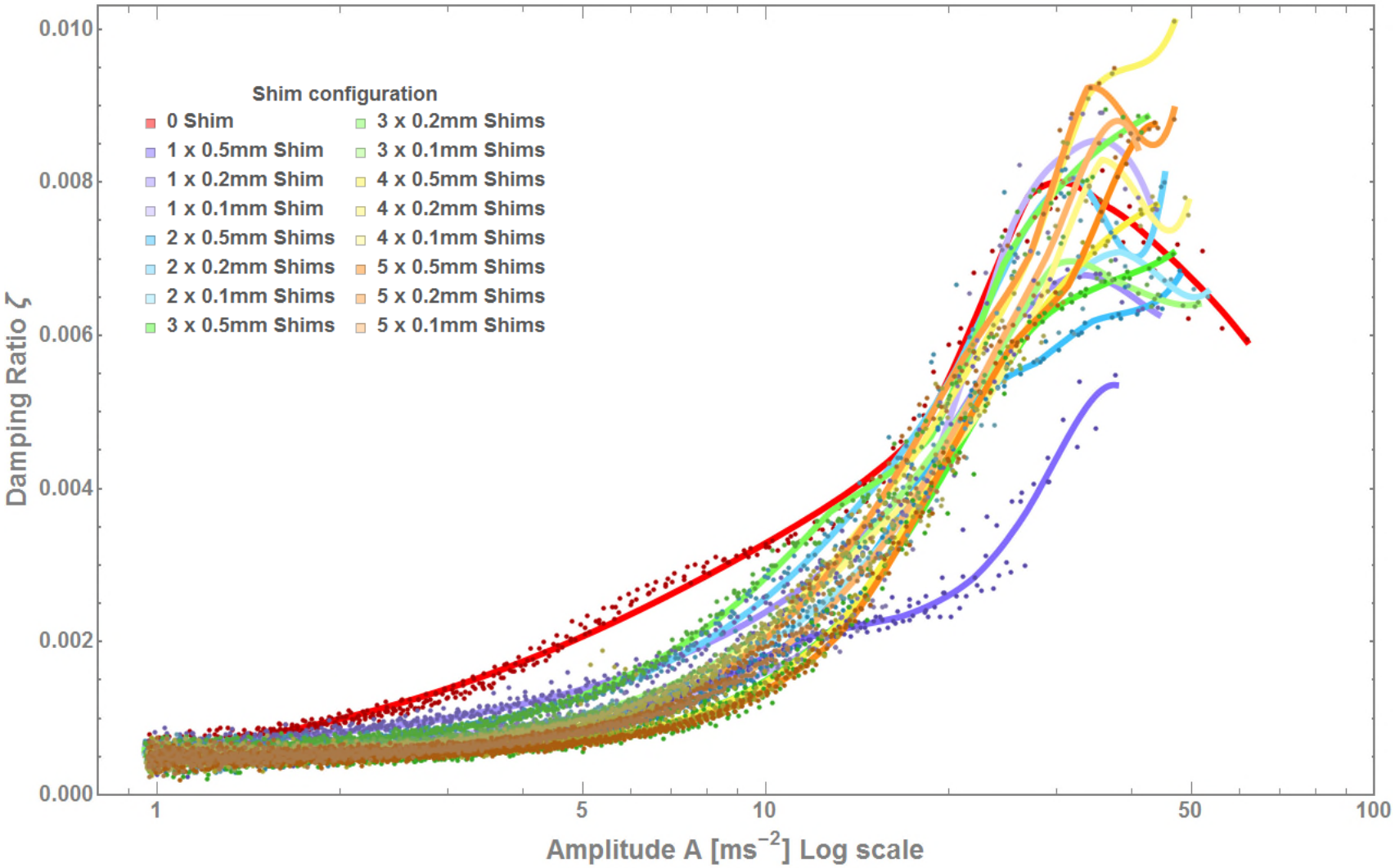

Figure 87 Thickness and multiple shim experiment: Semi-log plot of the damping ratio against the amplitude

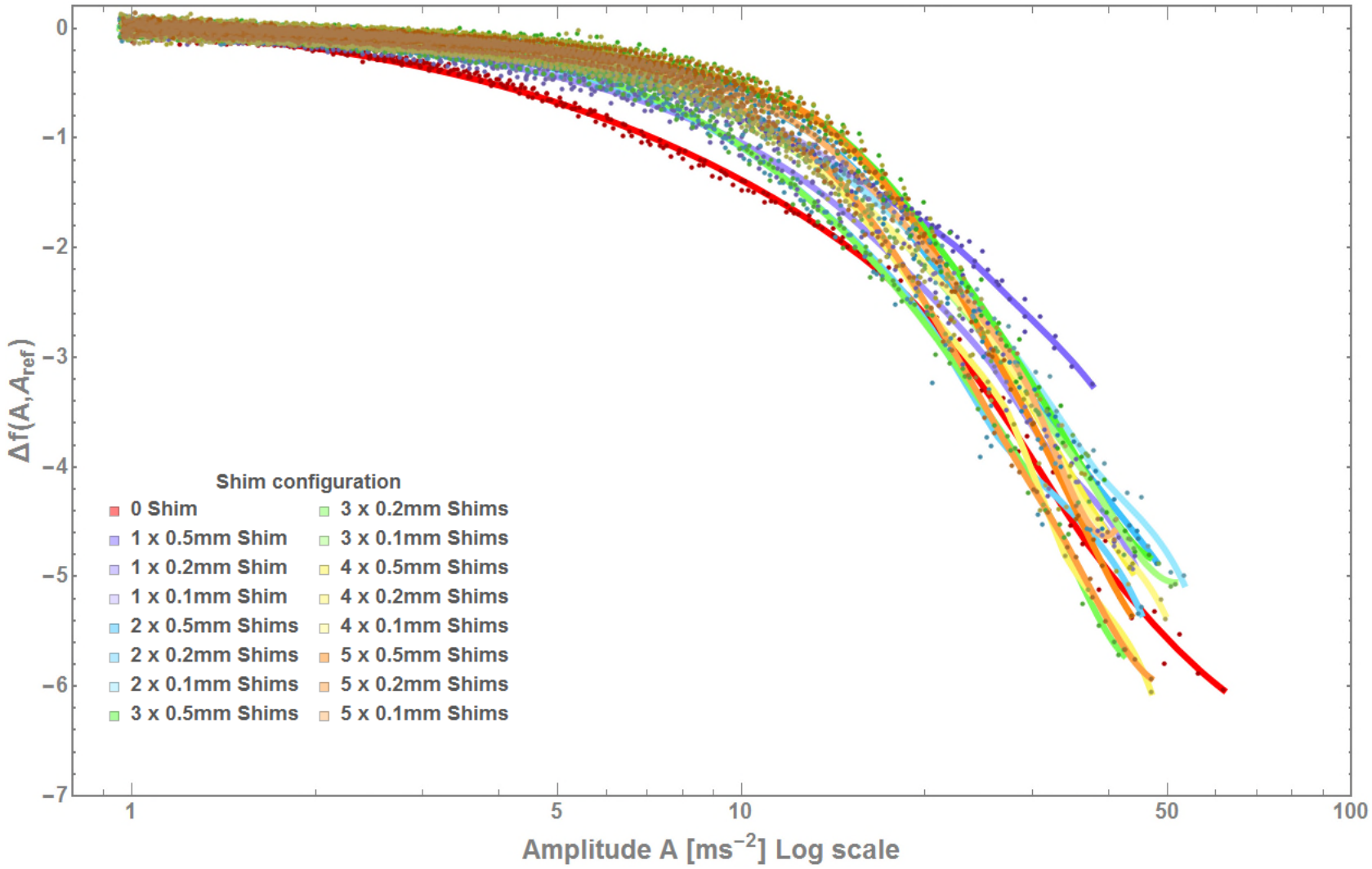

Figure 88 Thickness and multiple shim experiment: Semi-log plot of the Change in frequency ($\Delta f(A, A_{ref})$) against the amplitude.

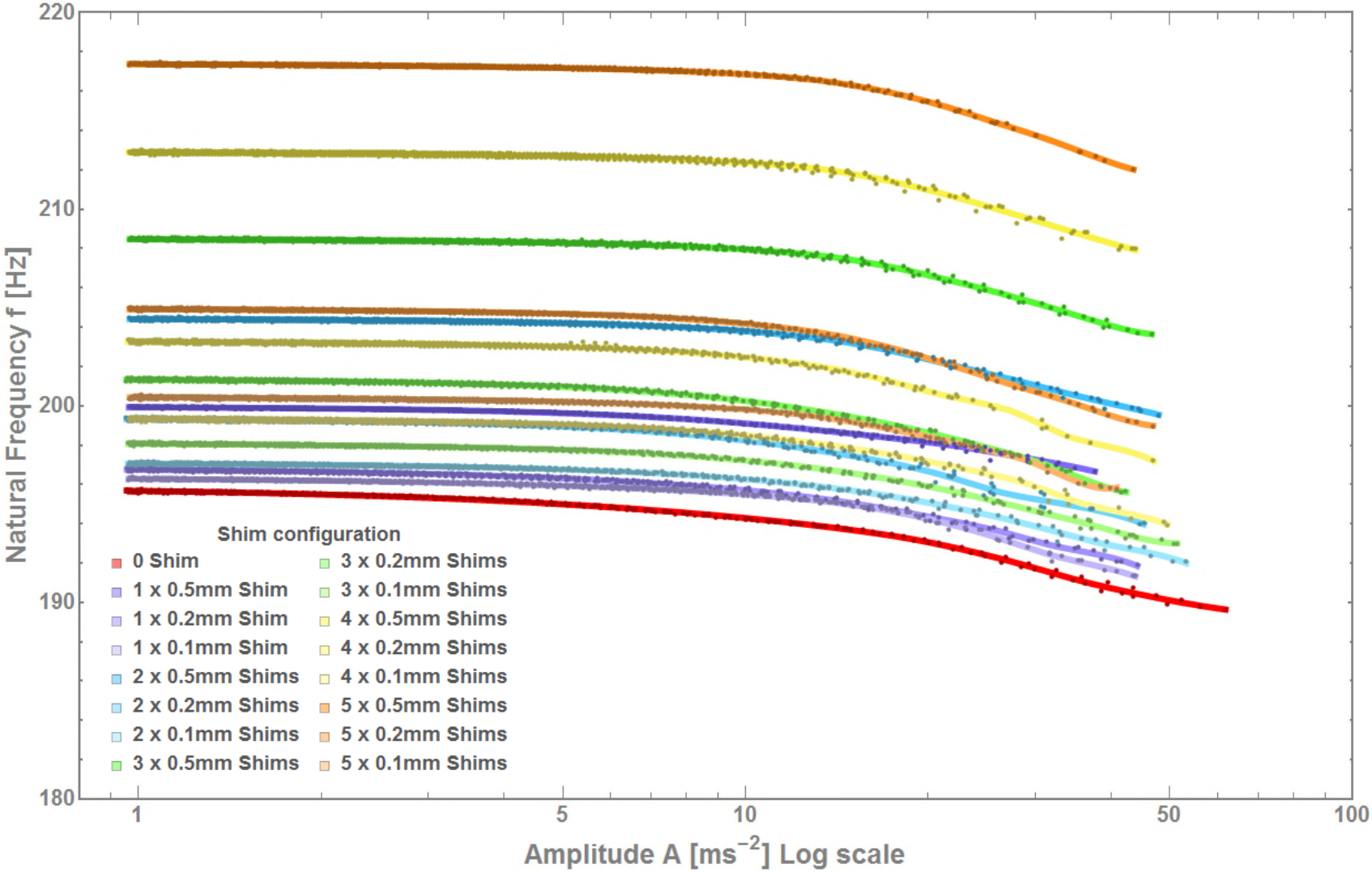

Figure 89. Thickness and multiple shim experiment: Semi-log plot of the natural frequency against the amplitude.

The results for zero or up to five shims are remarkably similar, for both natural frequency, Figure 87, and damping ratio, Figure 88. Furthermore, there is no difference between the results for different shim thicknesses. This is surprising as there are up to six individual contact patches between all the different shims.

In Table 9 and Figure 90, there is a clear linear trend between the frequency at low amplitude, $f(A_{ref})$ with $A_{ref}=1ms^{--2}$, and the sum of the thickness of the shims stacked in the joint. This trend in interpreted as follows: The introduction of the different number of shims separating the two beams increases the second moment of area of the sandwich beam and hence increases the observed natural frequencies at low amplitude.

Table 9 Natural frequency in Hz of each trend line at 1.0 ms^{-2} of amplitude from Figure 89

Shim\Thickness	0.5mm:	0.2mm:	0.1mm:
No shim:	195.67 Hz		
1 shim:	199.92 Hz	196.75 Hz	196.28 Hz
2 shims:	204.41 Hz	199.32 Hz	197.06 Hz
3 shims:	208.47 Hz	201.32 Hz	198.06 Hz
4 shims:	212.89 Hz	203.25 Hz	199.32 Hz
5 shims:	217.37 Hz	204.91 Hz	200.42 Hz

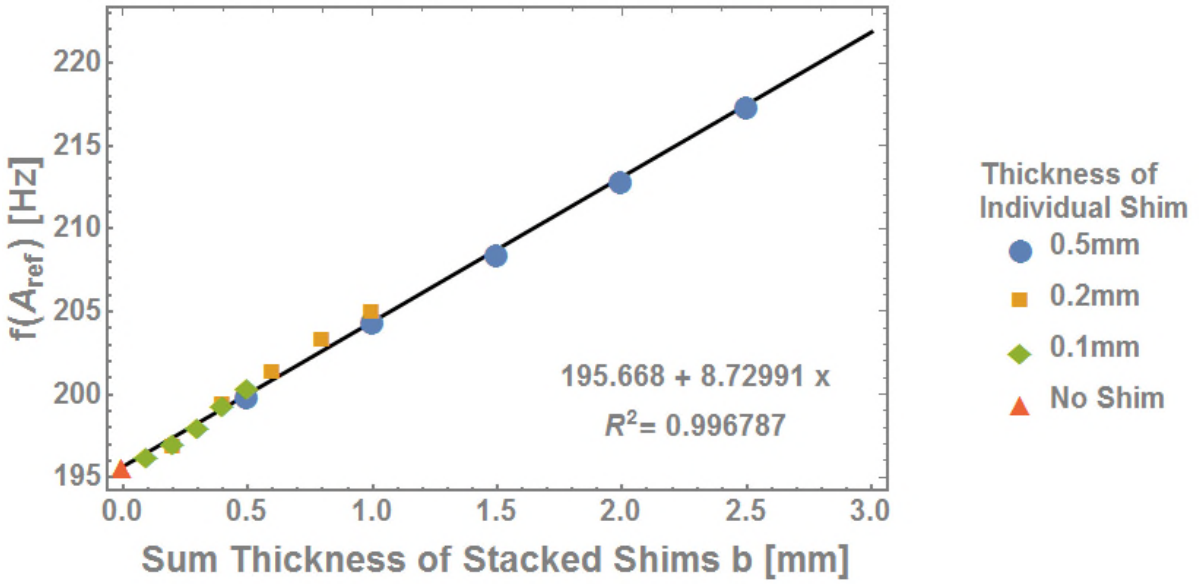

Figure 90 Natural Frequency as a function of the thickness of the shims stacked together

The multiple curves superposed in Figure 90 are the reason that the useful technique of using the natural frequency difference, $\Delta f(A, A_{ref})$, was developed. The variable $\Delta f(A, A_{ref})$ is defined in Equation (5-1). The natural frequency difference allows the separation of the amplitude dependent natural frequency shift, $\Delta f(A, A_{ref})$, and the absolute natural frequency shift., The value $f(A_{ref})$ is the reference natural frequency for each configuration.

The amplitude dependant natural frequency shift is assumed to be caused by the changing bound region, as explained in the following Section 5.7, whereas the absolute natural frequency shift is due to the evolution of second moment of area of the structure.

$$\Delta f(A, Aref) := f(A) - f(Aref) \quad \textbf{(5-1)}$$

It had been hoped that, in the experiment with multiple shims, there would be a significant increase in damping, due to a multiplicity of contact patches. Clearly, the presence of the multiple shims does not increase the damping ratio. This is disappointing since a method for increasing damping is always desirable.

However, the results presented in this section show that the sandwich beams with a shim of 100mm long are behaving almost the same way, as the sandwich beam without shims.

If this experiment was performed again, another set of shims with the size of a washer would have been included in the tests. Indeed in the next section, Section 5.4, the size of the shim is correlated to the nonlinear behaviour of the joints. This section only tests 100mm long shims. An investigation of the thickness with washer size shims could give completely different results than the results presented in this section.

5.4 Shim lengths experiment

In this section, the tests performed for the shim lengths experiments are detailed:

The following hypothesis is investigated in this section:

Hypothesis 3. The geometry of a joint interface has an impact on its nonlinear dynamic behaviour.

To investigate Hypothesis 3, ten 100mm long shims were cut to different lengths. The ten 0.2mm thick shims were cut to length using metal shears, cutting two at the same time to obtain the same length. A nylon hammer was used to flatten the edges. The length was measured after cutting. Figure 91 shows the different shims used.

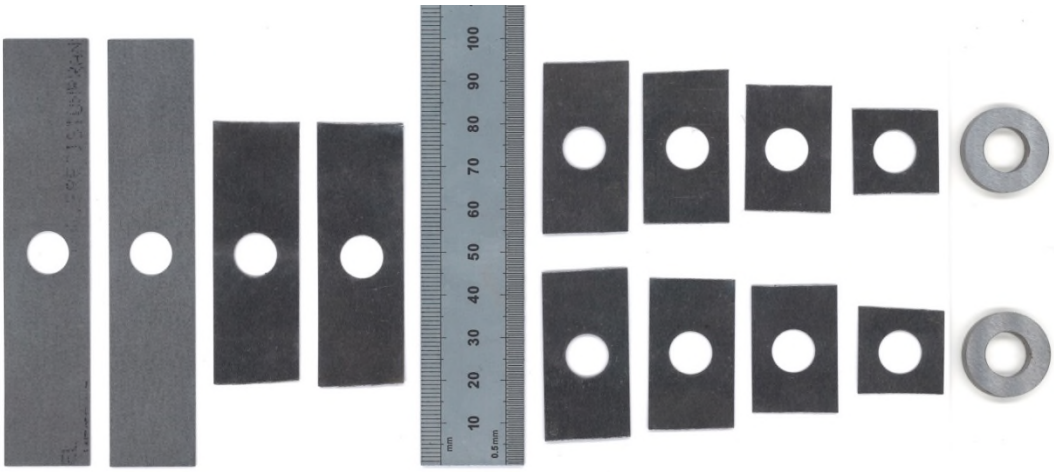

Figure 91 Scan of the stainless-steel shims and the stainless-steel washers used for the shim length experiment, ruler for scale. All the ten 100 x 20 x 0.2mm shims have

been cut to perform the shim length experiment. The shims on the left are 0.5mm thick, but are the same size as the 100 mm long shim with 0.2mm thickness.

Table 10 present the different shim lengths tested for the shim length experiment.

Table 10. Shim lengths experiment

Shims length (L_s)	**Number of shim**	**Shim thickness**	**Lubricant**
No shim	0 shim	Not Applicable	Dry contact
100 mm	1 shim	0.2mm	
61.9mm	1 shim		
40.2mm	1 shim		
36.0mm	1 shim		
29.9mm	1 shim		
20.3mm	1 shim		
20 mm diameter Washer	1 washer	3.2mm	

The results of the shim length experiment are presented in Section 5.5 and discussed in Section 5.7.

5.5 Results of the shim lengths experiment

The results from the shim lengths experiment are shown in Figure 92, Figure 93 and Figure 94 which are respectively the damping ratio, the natural natural frequency change and the natural natural frequency. All three plots have the same layout with the amplitude axis in logarithmic scale to improve the readability at small amplitudes. A six order polynomial trend line was fitted to the data to improve the readability.

In Figure 92, the damping ratio decreased with decreasing amplitude. The damping is large for long shims or no shim. The damping curve is shifted to the right when the length of the shim decreases.

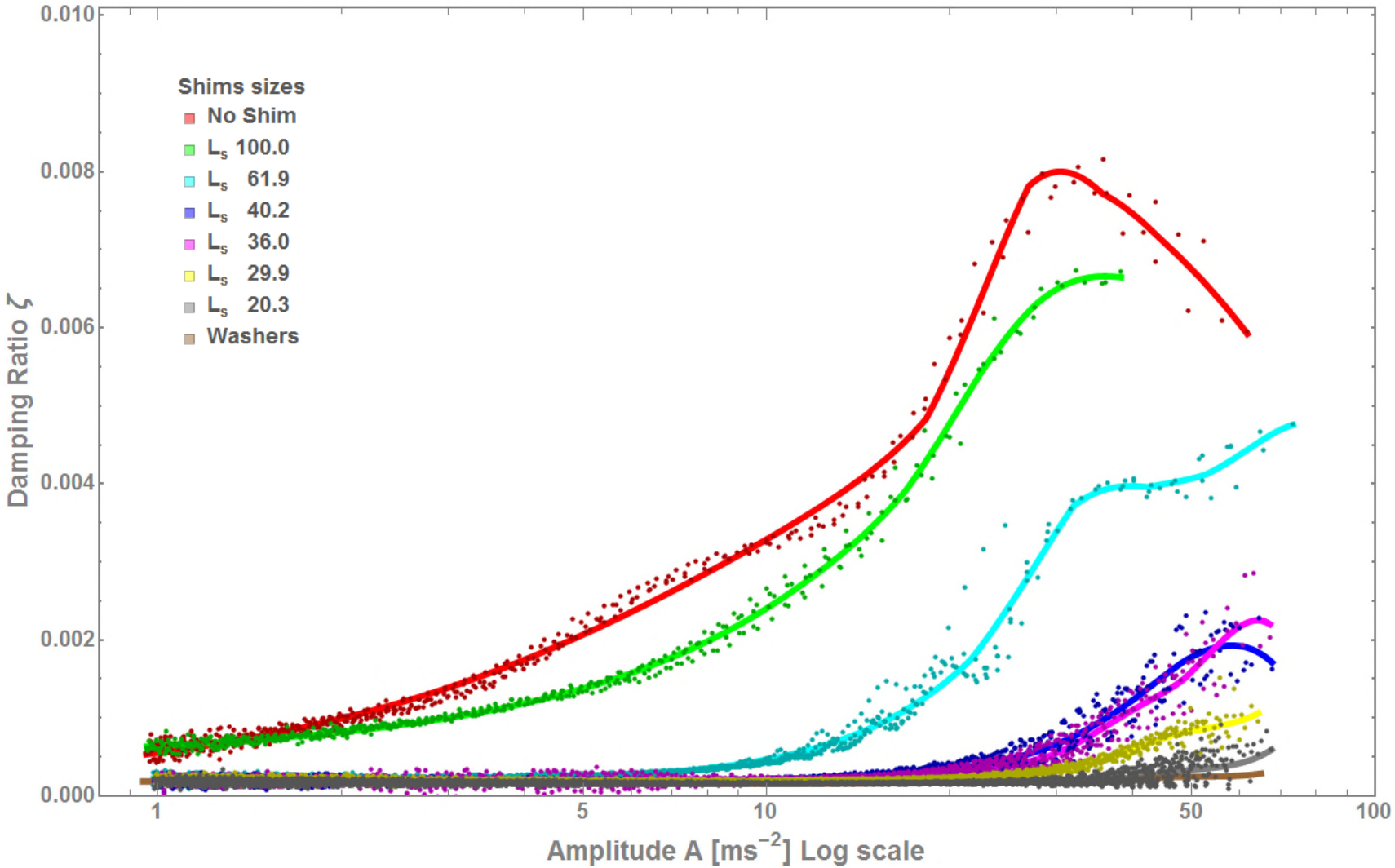

Figure 92 Semi-log plot of the damping ratio against the amplitude for multiple shim lengths (L_s) with trend lines

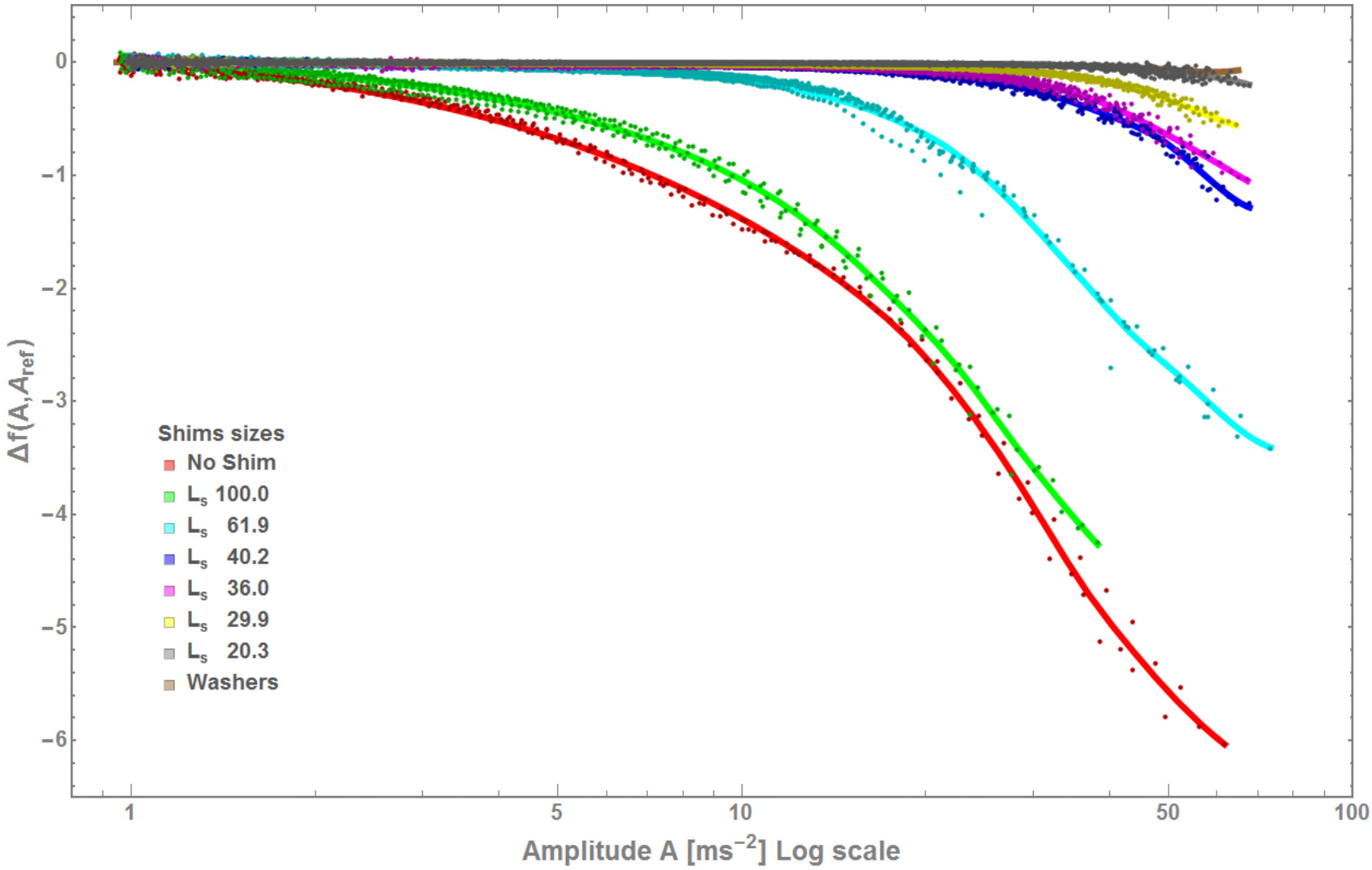

Figure 93 Test with multiple shim lengths: Semi-log plot of the change of natural frequency ($\Delta f(A, A_{ref})$) against the amplitude.

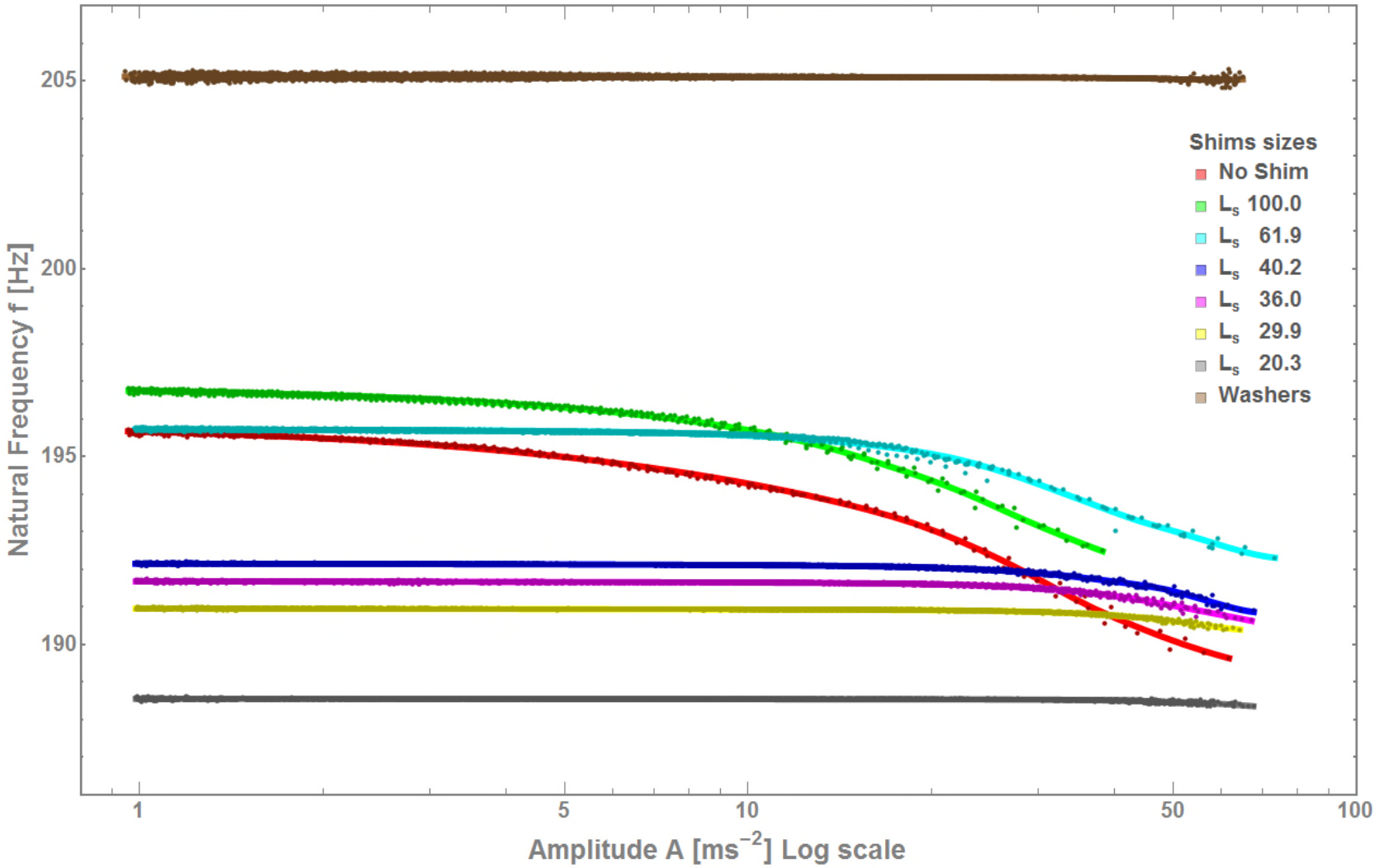

Figure 94 Test with different shim lengths: Semi-log plot of the natural frequency against the amplitude.

Similarly, the natural frequency shift, plotted in Figure 93, has the same trend as the damping ratio. The natural frequency shift increased with decreasing amplitude. The natural frequency shift is weaker the smaller the shim length, in the same way as in Figure 92.

Finally, in Figure 94, the natural frequencies do not show a clear trend. However, examining the value of the natural frequency at small amplitude, f(A_{ref}), gives the trend plotted in Table 11 and Figure 95. The natural frequency increases with the length of the shim almost in an linear manner.

Table 11 Natural frequency in Hz of each trend line at 1.0 ms^{-2} of amplitude, f(A_{ref}), from Figure 94.

Shim sizes:	f(A_{ref}):
No Shim	195.674 Hz
L_s 100.0 mm	196.754 Hz
L_s 61.9 mm	195.719 Hz
L_s 40.2 mm	192.152 Hz
L_s 36.0 mm	191.681 Hz
L_s 29.9 mm	190.954 Hz
L_s 20.3 mm	188.557 Hz
Washers	205.121 Hz

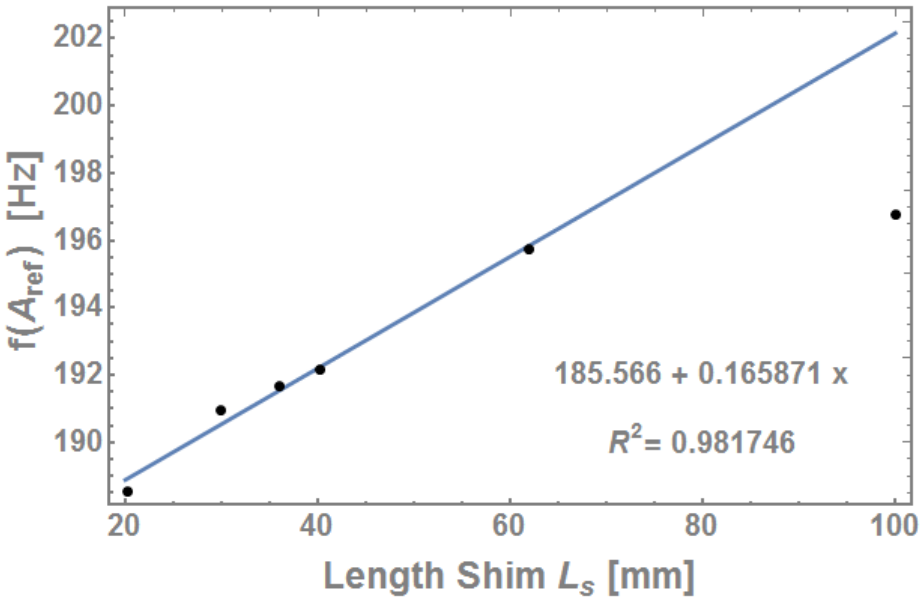

Figure 95 Natural frequencies of the trend lines at 1.0 ms^{-2} of amplitude compare to the length of the shim. L_s. The test with no shim and with the thick washers were

removed because they were not comparable. The point with a 100mm long shim was not fitted in the linear trend line displayed in this plot because the 100mml long shim is expected to exceed the size of the contact patch.

It is clear that there a good correlation between shim length, damping, and change in natural frequency. The longer the shim length the higher the damping. Similarly, the longer the shim length; the higher the change in natural frequency. Note also, that the damping curves and the change in natural frequency curves are similar in shape. Besides as typically observed in the literature, the larger the amplitude of vibration, the higher the damping ratio.

In conclusion, the length of the interface is a dominant parameter in the nonlinear dynamic behaviour of bolted joint

5.6 Higher modes of the shim length experiment

This subsection explains why the higher modes were not analysed in details. Indeed, only the first bending mode was analysed for the shim size experiment. The spectrum of the first bending mode is displayed in Figure 96.

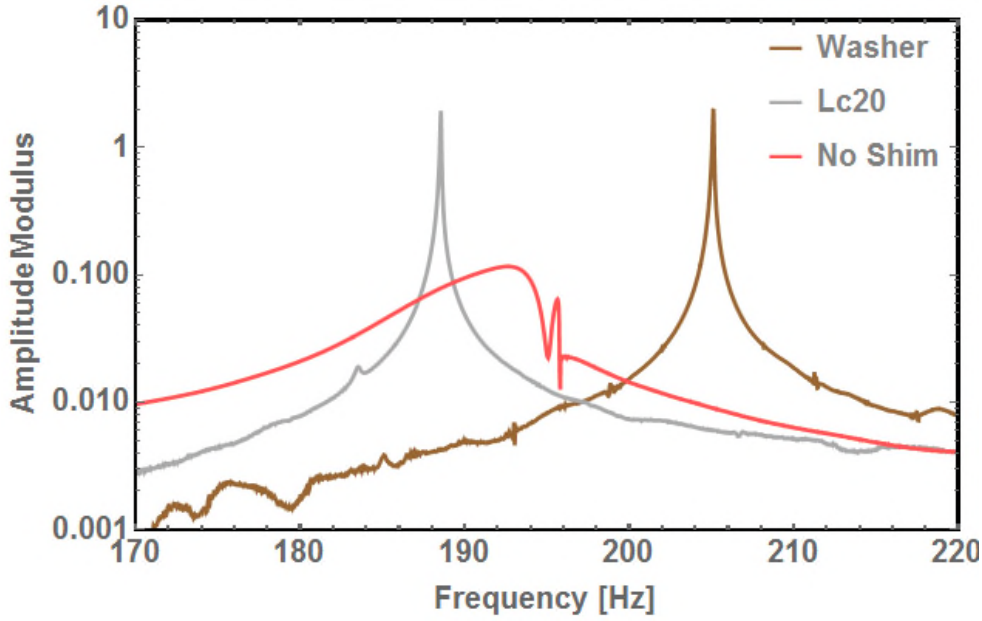

Figure 96 First bending mode

The average spectrum of the five hammer hits of the washer, Lc20 and no shim are displayed in Figure 97. A finite element analysis of the configuration with washers

was conducted using SOLIDWORKS. The simulated mode shapes are overlaid on top of the graphs in Figure 97. The simulated natural frequencies are displayed in Table 12.

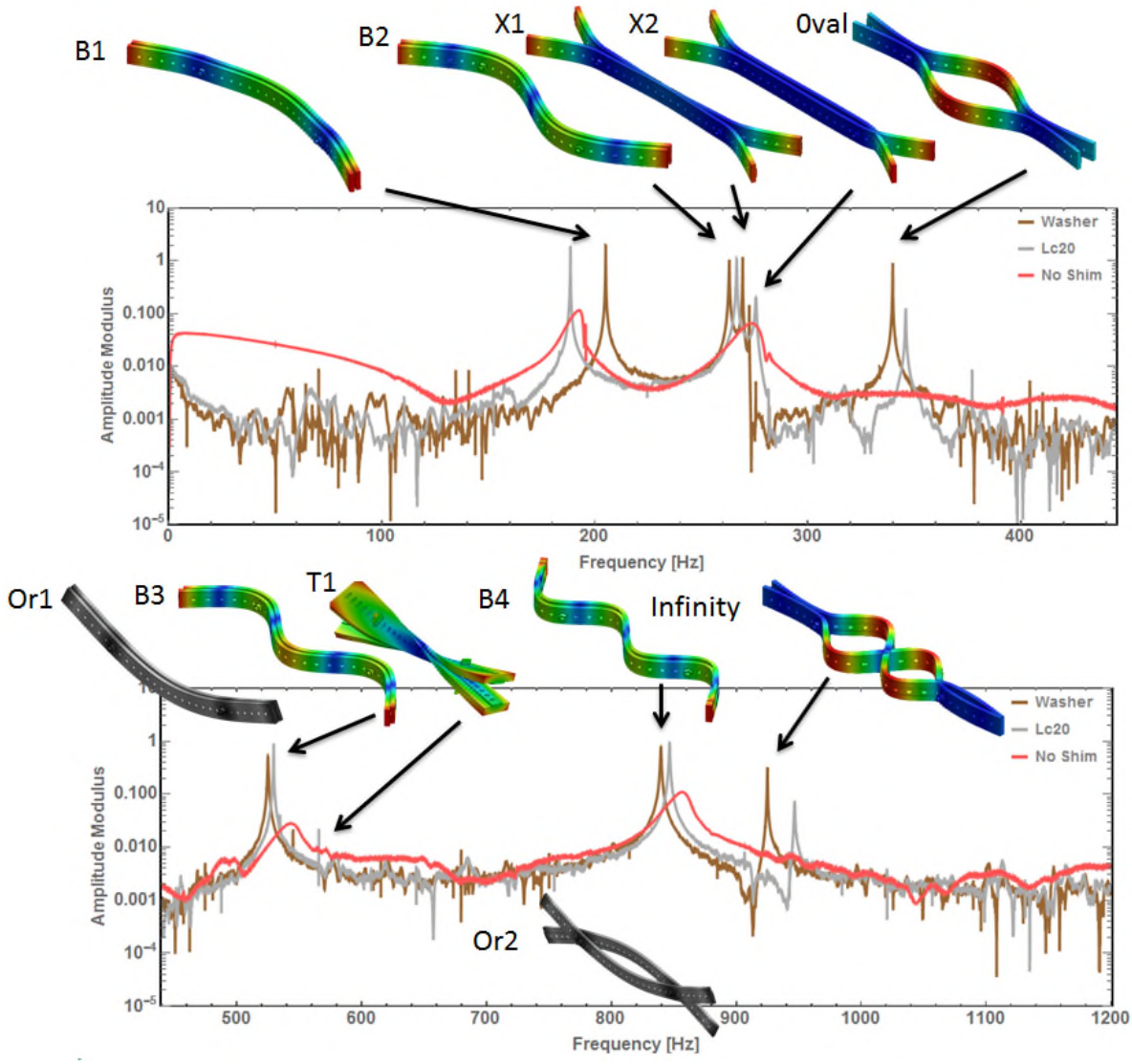

Figure 97 Spectrum with corresponding mode shapes. The mode shapes in grey were not measured due to the placement of the accelerometer and the impact position.

Table 12 Mode shape names, measured natural frequency and simulated natural frequency for the sandwich beam with washer

Name	Mode description	Measured natural frequency from spectrum peak	Simulated natural frequency
B1	Bending 1	205.100 Hz	210.637 Hz
B2	Bending 2	263.100 Hz	270.784 Hz
X1	Cross shape 1	269.417 Hz	279.24 Hz
X2	Cross shape 2	272.483 Hz	280.674 Hz
Oval	Oval shape	339.867 Hz	346.16 Hz
Or1	Orthogonal bending 1	No peak	467.378 Hz
B3	Bending 3	524.883 Hz	534.198 Hz
T1	Torsional 1	No peak	663.38 Hz
Or2	Orthogonal bending 2	No peak	752.371 Hz
B4	Bending 4	839.617 Hz	854.777 Hz
Infinity	Infinity shape	925.000 Hz	943.16 Hz

The filtering of the second bending mode was impossible due to the proximity, in terms of natural frequency, of two other modes. The proximity between the second mode bending mode (B2) and the two extremity bending modes (X1 and X2) makes the isolation of the second bending mode impossible. The oval mode shape was very different from the beam theory. Therefore, no meaningful information could be interpreted from it.

Because of the difficulty encounter during the filtering of the second bending mode, no further investigation was carried out on higher frequency modes.

5.7 Discussion of shim lengths experiment

The change of natural frequency and damping ratio is interpreted as a change of the contact patch inside the interface of the bolted joint. Three types of regions have been defined to illustrate this interpretation: the bound region, the slip region and the alternating region.

The evolution of the natural frequency has been interpreted as follows: The instantaneous natural frequency increase as the amplitude decays. This increase in natural frequency is due to an increase of the rigidity of the structure. Indeed the natural frequency is directly linked to the rigidity of a structure in a single degree of

freedom system, as described in equation (2-7). This change of rigidity is interpreted as a changing connection between the two beams at the bolt locations. This change is due to the presence of microslip at the edge of the contact patch. When microslip exists the connection is less rigid compared to when there is no slip. The region where the micro slip is located changes as the amplitude decreases.

The first assumption is that the bolted joint has receding contacts at both bolt locations. This implies that there is only contact between the beams around the bolt location and there is a gap between the beams everywhere else in the interface. The situation at a bolt should look like the exaggerated case of Figure 98. Therefore, only a limited area of the interface actually enters into contact during the vibration: this is the contact patch. The interface refers to the entire surfaces which may enter in contact.

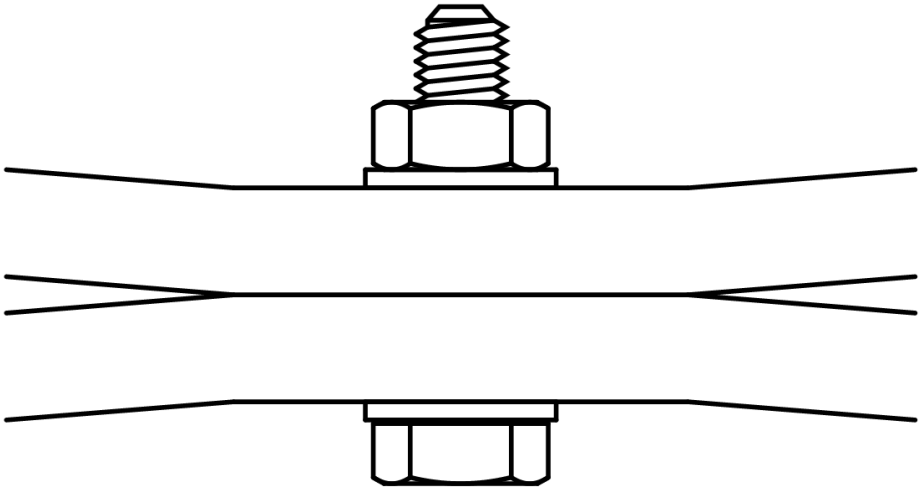

Figure 98 Interpretation of the effect of the receding contact on the contact patch at a bolt location of the sandwich beam

It is suggested that the contact patch has three regions with different behaviours. The boundaries of those regions change as the vibration decays. One region, around the bolt, covers the surfaces which remain bound to each other during the test; this is the bound region. The bound region has no microslip. The second region, outside the bound region, has sliding surfaces; this is the sliding region. Beyond this region, the contact patch is opening and closing during the vibration; this is the alternating region. These regions are illustrated in Figure 99. The definition of these three

regions was created for this thesis. These definitions are inspired by other region definitions found in the literature listed in Subsection 2.2.3.

The alternating region is the surfaces which are not in contact when there is no vibration but where sliding happens with vibration. The sliding and alternating regions are the locations where slip happens in the interface. The sliding and alternating regions explain the dissipation of energy due to vibration in a joint. For example, if there is no sliding or alternating region then no slip happens in the joint, therefore only material damping is recorded. In the opposite case, if there is a sliding region and/or an alternating region, a large damping due to microslip is measured.

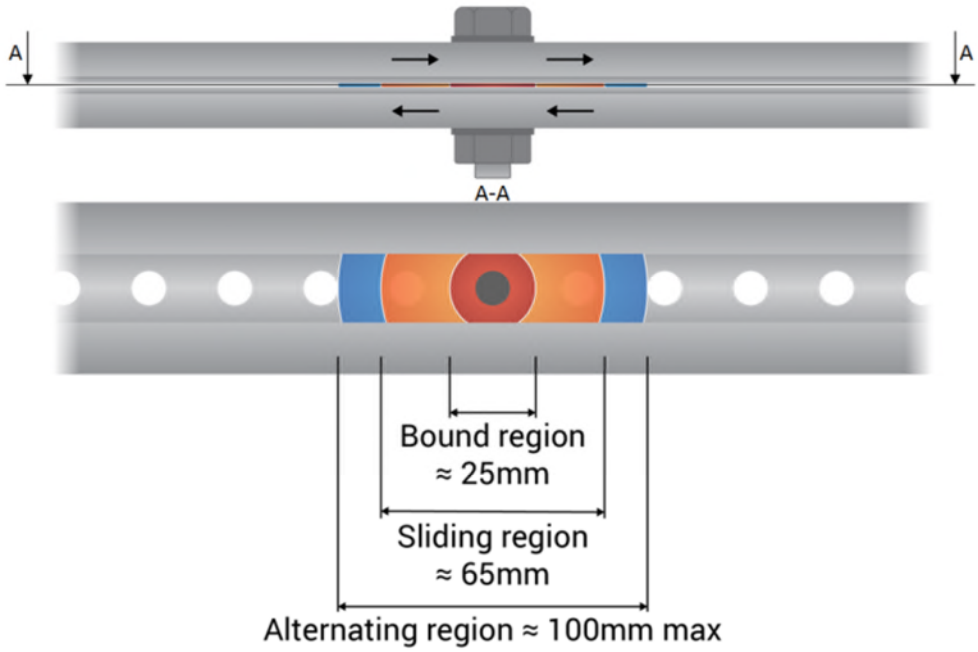

Figure 99. Side view and section view of the sandwich beam around one bolt. The length of the bound region, sliding region and alternating regions are estimated at high amplitude. The arrows (upper illustration) represent the relative microscopic motion between the two surfaces. This motion creates micro-friction.

The nonlinear behaviour (damping and loosening effect) measured is almost identical between the 100mm shim and the no shim configuration. Therefore, the size of the contact patch at the bolt is expected to measure around 100mm, see Figure 100. As the 60mm shim reduces the amount of damping measured it is expected that the contact patch is larger than 60mm.

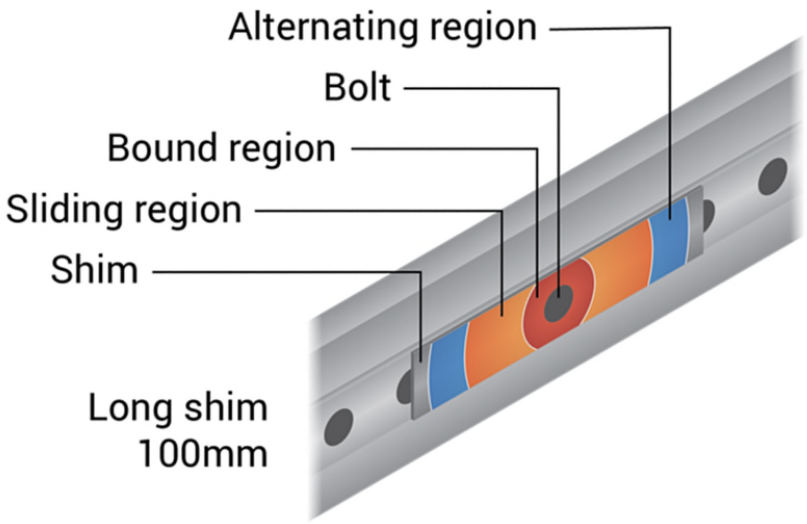

Figure 100 The three regions at high amplitude (50 ms^{-2}) with a 100mm shim

The increase of the area of the bound region, as the vibration decays, has consequences for the natural frequency of vibration as shown in Figure 102. The beams are more constrained for small amplitudes than for large amplitudes, causing an increase of natural frequency as the amplitude decays. This explains the evolution of the natural frequency measured.

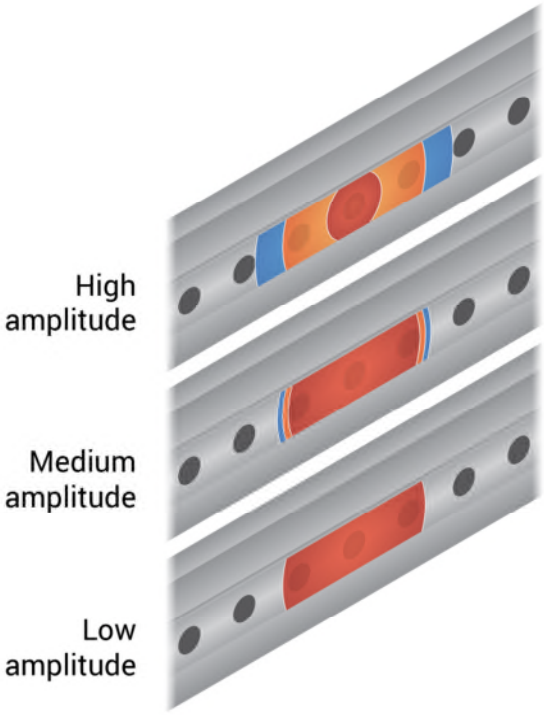

Figure 101 Interpretation of the evolution of the three regions depending on the amplitude. High amplitude = 50 ms^{-2}. Medium amplitude = 5 ms^{-2}. Low amplitude = 1 ms^{-2}.

The size of the bound region can be deduced from the experiment with the different shim lengths. Figure 95 presents the reference natural frequency, $f(A_{ref})$ which is the natural frequency at low amplitude, as a function of shim length. There is a clear correlation between shim length and the natural frequency at small amplitudes. At small amplitudes of vibration, the natural frequencies are fixed, which is interpreted as the bound region expanded to the full length of the shim.

In Figure 93, the natural frequency of the 60mm long shim is fixed at low amplitude, but the natural frequency of the 100mm long shim keeps changing at low amplitude. These two curves suggests that the length of the bound region, at small amplitudes, when there is no shim, is more than 60mm and less than 100mm. This interpretation explains also why the separation between the sliding and alternating region is estimated at 65mm in Figure 99.

Also in Figure 93, the natural frequency of the 20mm long shim does not change whatever the amplitude. This observation suggests that the bound region for no shim at large amplitudes is more than 25mm as shown in Figure 99.

The effect of the different shim lengths can be interpreted as follows. For the small shims, the bound region grows to equal the shim length. The interface length is then fixed. From this amplitude onwards, the natural frequency remains constant. This fixed natural frequency phenomena can be seen in Figure 93. When the bound region is equal to the length of the shim, the interface is no longer a receding contact but becomes effectively a complete contact. This proposition is illustrated in Figure 102.

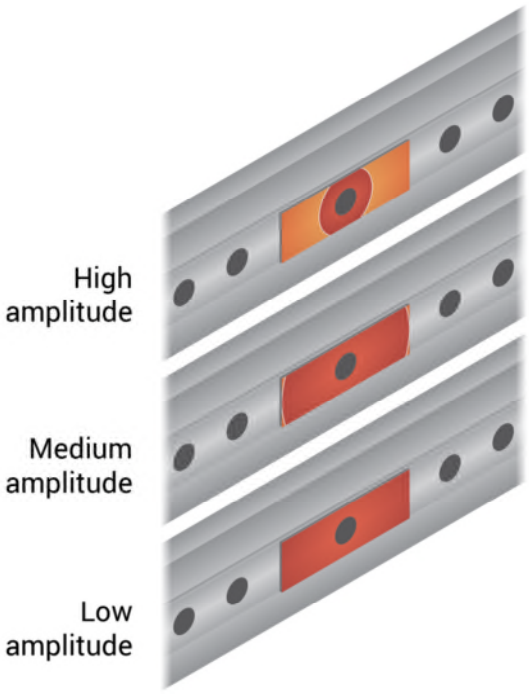

Figure 102. Illustration of the bound region in red depending on the amplitude for a 60 mm long shim. High amplitude = 50 ms^{-2}. Medium amplitude = 5 ms^{-2}. Low amplitude = 1 ms^{-2}.

This interpretation also describes the damping behaviour. Within the sliding region, the surfaces have relative motion. This relative motion, which involves friction, will cause energy dissipation and hence damping. For large amplitudes, the slipping region is large and the relative displacement is large. This gives rise to large damping. This is observed in all the experiments except when there is a complete contact, for example with the 20mm long shim. At small amplitudes, the damping is comparable to the material damping for all the shims bellow 60mm long. This suggests that the slipping region completely disappears in those cases.

In a previous paper (Goyder et al. 2016), a finite element model satisfactorily correlated the length the contact patch and the natural frequency. This further corroborates the above interpretation.

As the sliding region and the alternating region are where slip happens, this three-region model could be simplified by merging those two regions into one region where microfriction happens.

A summary illustrating the three-region model is given in Figure 103:

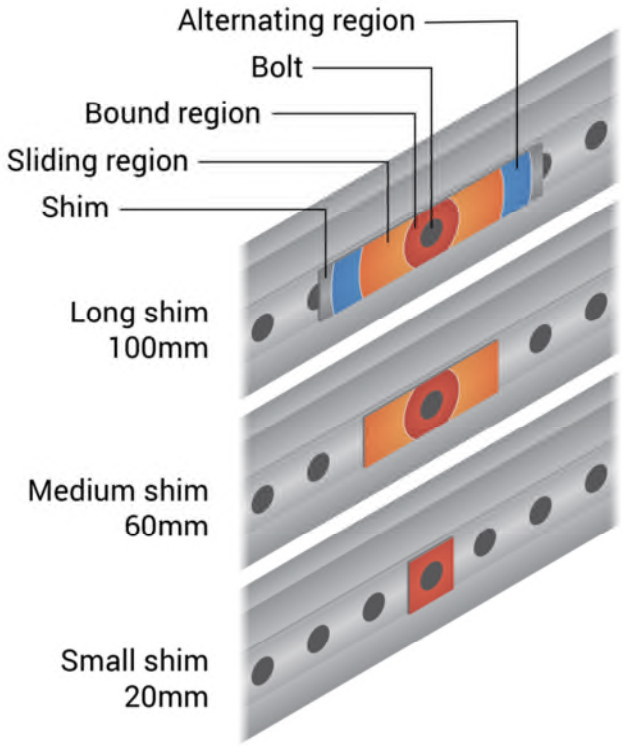

Figure 103 Interpretation of the behaviour inside the interface at high amplitude (50 ms^{-2}) for three lengths of shims. The long shim is longer than the contact patch. The 60mm shim reduces the length of the sliding region. The 20mm shim does not allow sliding.

5.8 Lubrication experiment

This subsection presents and interprets the experimental result of the lubrication experiment. Grease and oil were applied to all lengths of the sandwich beams. The result of the lubrication test is shown in Figure 104, Figure 105 and Figure 106.

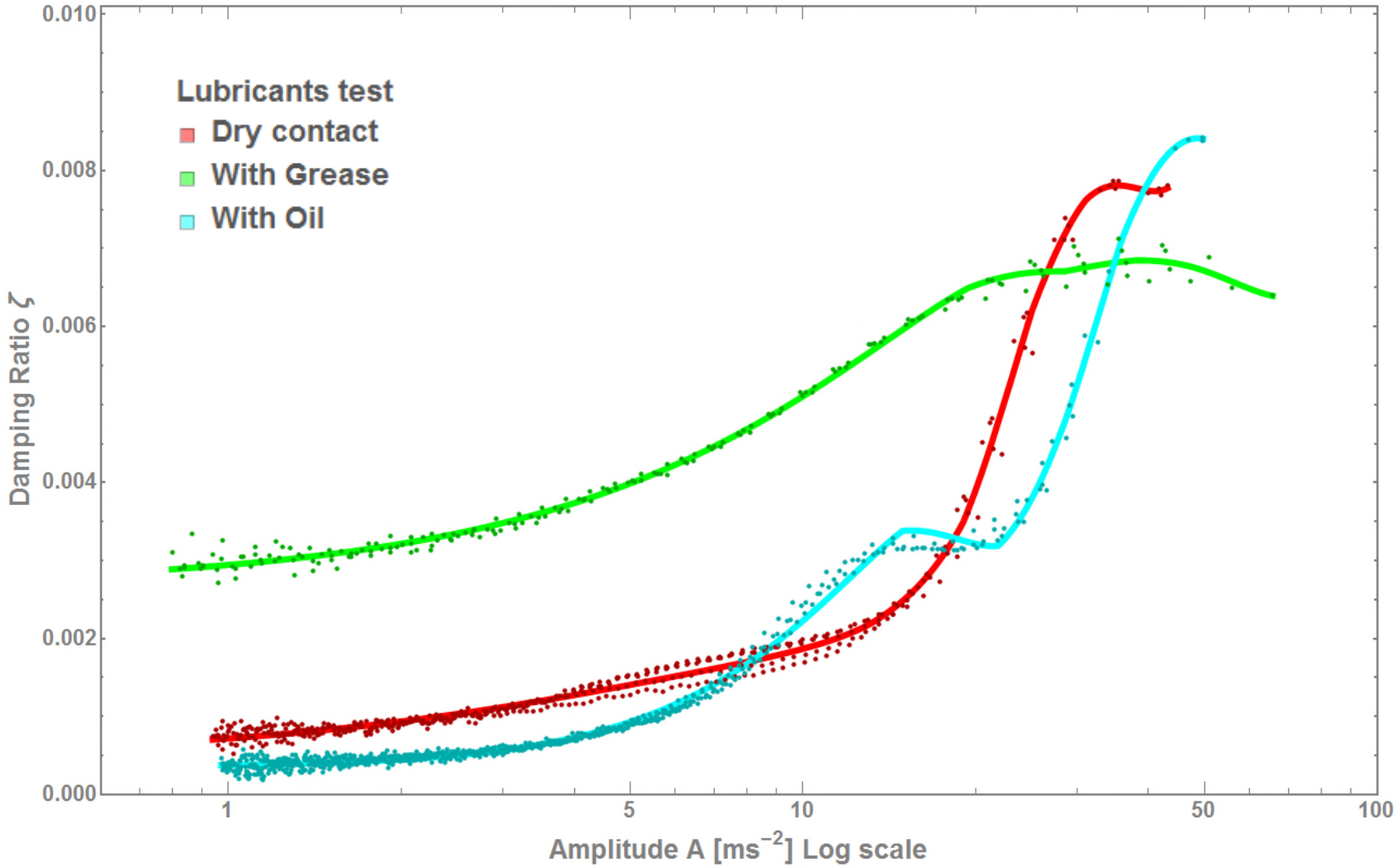

Figure 104 Lubrication experiment: Semi-log plot of the damping ratio against the amplitude

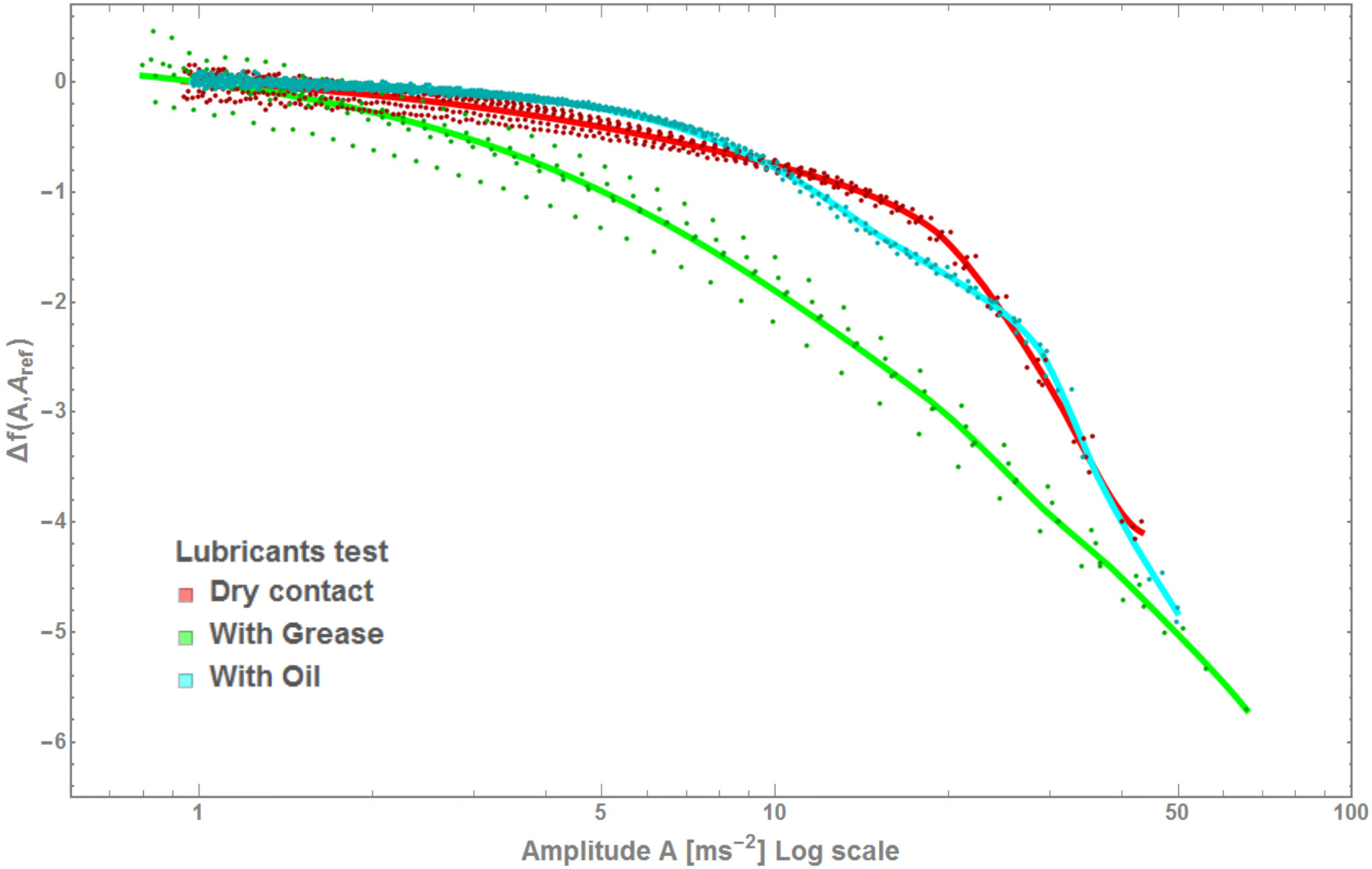

Figure 105 Lubrication experiment: Semi-log plot of the change of natural frequency against the amplitude.

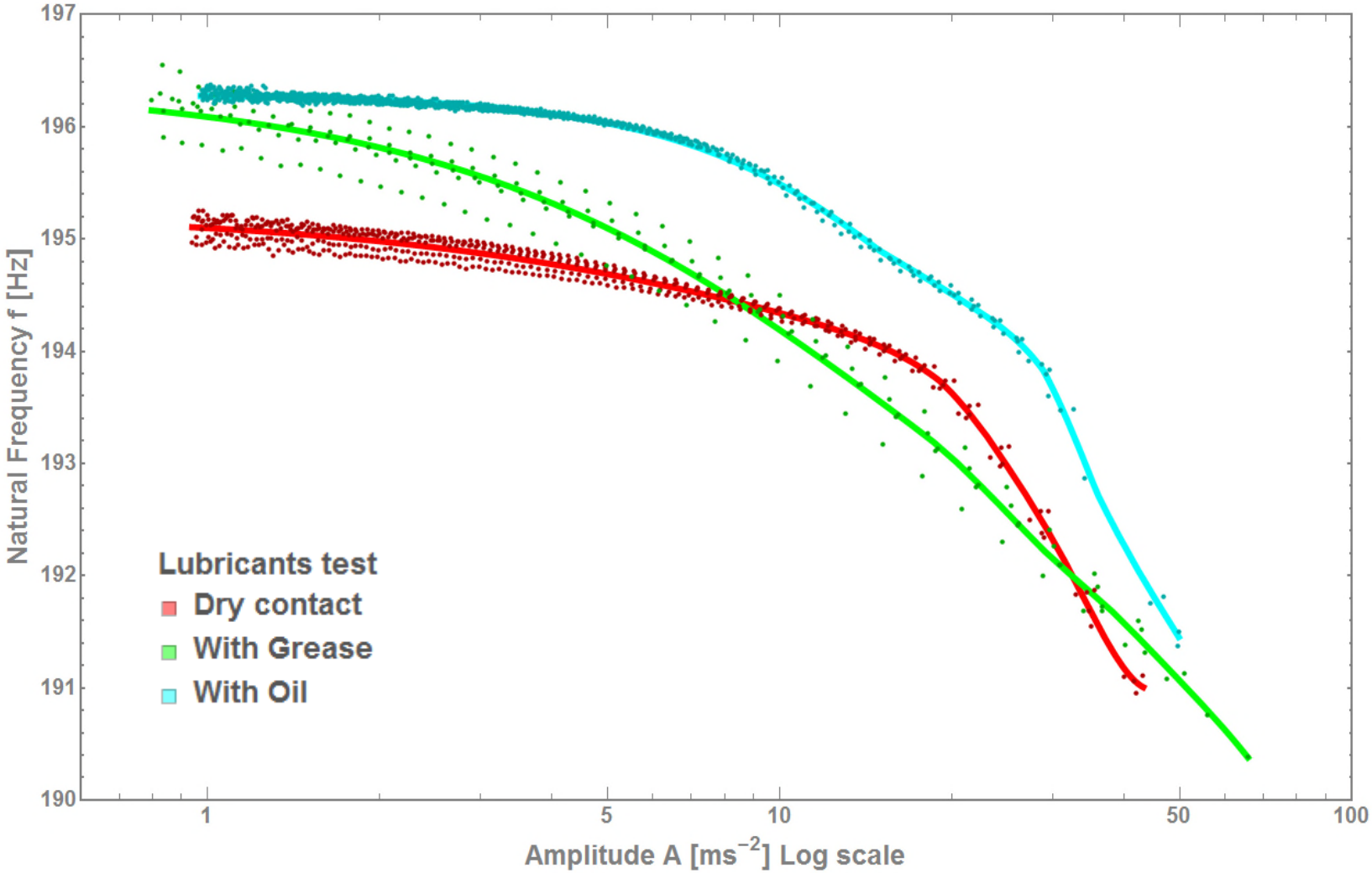

Figure 106 Lubrication experiment: Semi-log plot of the natural frequency against the amplitude.

For the oil, there is little difference between the dry dynamic behaviour and lubricated dynamic behaviour, except a global increase of 1Hz show in Figure 106. This 1Hz increase of natural frequency could be due to the added mass of the oil.

Also, the vertical spread of the data points for the natural frequency for different tests is large with grease, medium for the dry contact and small with oil. This evolution of the variability between tests is noticeable.

For the grease, there is a substantial difference, particularly at small amplitudes ($1ms^{-2}$). At $A=1ms^{-2}$, note that the damping ratio is 30 times greater with grease than the dry contact. Also, the natural frequencies difference curve with grease has a significant bigger gradient even at small amplitudes compared to the dry contact case.

There is a very clear difference between the behaviour of oil and grease when applied to the contact patch. One possible interpretation could be a pumping action, thus viscous damping may occur with grease but not oil. The effect of lubricant on the nonlinear dynamic behaviour of joints needs further investigation.

5.9 Conclusions of Chapter 3

The following conclusion may be drawn from the experimental results of this chapter:

The experiments suggest that the contact patch plays a key role in the dynamics of a bolted joint. Furthermore, the contact patch size evolves during vibration giving rise to a large variation in the amplitude dependent natural frequency and damping ratio.

The experiments suggest that there are three different regions in the contact patch that change their sizes depending on the vibration amplitude. These regions involve a bound region, a slipping region and an alternating region. The bound region controls the instantaneous natural frequency of the vibration. The relative displacement inside the slipping regions and the alternating regions is controlled by the damping.

Experiments with shims of different length, which change the area of the possible contact patch, support the interpretation of a bound and slipping region. The contact patch gets fixed depending on the amplitude of vibration and the length of the shims.

It was found that experiments with multiple shims did not increase the damping. The thickness of the shims had no impact on the dynamic behaviour. Therefore, experiments with long shims are equivalent to the case without shims. Also, it was found that grease, but not oil, inserted in the interface increases the damping.

6 JOINT LOCATION EXPERIMENTS

6.1 Introduction

The aim of this chapter is to investigate the effect of the position of bolted lap joints on the nonlinear dynamic behaviour of a structure. A new experimental method was designed which used washer sized shims. This method led to the testing of a built-up beam with 18 bolted joints in series. This chapter concludes that the dynamic behaviour of lap joints is correlated to the position of the joints.

6.1.1 Method used to investigate the effect of the position of a joint

This section explains the method used to investigate the impact of the position on the nonlinear behaviour of a bolted lap joint.

The author concluded that using experiments was currently the only way to investigate the impact of the position of a joint. Modelling is not an option as there is currently no predictable way to compute friction in a joint, as explained in the literature review in Section 2.6. The only way to model vibration of a joint is to fit experimental data into a model, but there is currently no experimental data available, to the knowledge of this author which measures the impact of the position of a joint. Thus a new experiment was necessary. Firstly, an experiment allows the investigation of the impact of the position of a joint on the structure. Secondly, an experiment creates data which can be fitted to a model to obtain a better understanding of the experimental data.

The experimental method developed in Chapter 3, which allowed the investigation of nonlinear behaviour of a structure with bolted lap joints, is still relevant for the objective of this chapter. Here is a summary of the experimental method of Chapter 3: the investigation conducted in this document focused only on the bending modes in the same plain as the bolt axis. Only bolted lap joints made out of steel with high torque are investigated. The choice of using a hammer hit and recording the whole body vibration using an accelerometer was made because this excitation and measurement method allows the precise recording of the dynamic behaviour. The structure needs to be suspended, and a free-free configuration created, to isolate the structure and avoid any interference. Lastly, the hammer hit and accelerometer need

to be placed in the right position to match the modes which need to be investigated. All the choices made in Chapter 3 are aligned with the objectives of this chapter. Therefore, those choices will not be reconsidered here. The only exception is the choice of the positions of the accelerometer and the impact force which will be described later.

Additionally, the signal processing workflow detailed in Chapter 4 will fit for the purposes of the objectives of this chapter. Briefly, as a reminder, the reverse filtering method and the direct fitting method were developed in Chapter 4. Those two methods allow the extraction of the instantaneous amplitude, damping ratio and natural frequency of each mode directly from the time history. This time history comes from the experimental method described in the previous paragraph. This signal processing workflow only requires that the natural frequencies of the tested structure are more than 12 Hz apart to allow the filtering of each mode.

To reach the objective of investigating experimentally the impact of the joint position, the experimental tests need to be comparable. Which leads to the question: How to vary the position of a joint in a structure in a comparable way?

Manufacturing multiple structures with different joint positions for each structure will not work. Indeed, the simplest solution seems to be to have multiple comparable test structures with different joint positions. However, manufacturing multiple structures may be counterproductive, as the process may lead to variability in the geometry, the mass, the rigidity and the surface finish. The manufacturing variability will make the different tests incomparable as more than one parameter changes between each test.

The solution found was to vary the position of one or multiple receding contacts, instead of varying the position of the joint. One of the main results of chapter 3 is that there are two extreme behaviours linked to bolted lap joints with either a complete contact or a receding contact.

The concept of complete contact and receding contact are defined in subsection 2.2.3. A receding contact has a natural frequency and a damping ratio which is significantly correlated to the amplitude of vibration. However, for a complete

contact, the natural frequency and damping ratio have almost no correlation to the amplitude.

Another main result of chapter 3 is that placing a washer in the interface of a receding contact turns it into a complete contact. Therefore, placing washer size shims in the interface should allow the nonlinear behaviour of a bolted lap joint to be turned on and off.

Instead of changing the position of the joint, it was decided to study the position of a receding contact, by placing and removing washer size shims. Comparing the behaviour between a test with only complete contacts and a test with one or multiple receding contacts should give clear information of the impact of the position of the receding contacts. By extension, the impact of the position of a joint will be investigated.

Investigating the position of the receding contacts assumes that a complete contact has a negligible impact on the nonlinear dynamic behaviour of the structure. It was demonstrated in Chapter 3, that a structure with a complete contact has a small damping ratio and a limited amplitude dependent shift of natural frequency. It is therefore assumed that the behaviour of a complete contact is almost the same as if there were no joints. Thus, a complete contact could be placed everywhere except where receding contacts are desired, and the impact of the joints with complete contacts could be neglected. Therefore, only the impact of the receding contact will be measured as complete contact behaviour is negligible.

The effect of the position of the joint will be investigated by measuring the effect of the position of a receding contact compared to a test where there is only complete contacts everywhere.

Now that the general method used in this chapter is explained, the following section describes the practical detail, for example, the physical shape of the structure, the design of the lap joint and the washer size shim dimensions.

6.1.2 Geometry of the structure tested

This section explains how the geometry of the structure tested was chosen. Also, the geometries of the main components are detailed.

A beam shape was selected because beam shaped structures have well separated modes, which is a requirement of the signal processing workflow. As explained before, the reverse filtering method can work only if the natural frequencies are well spaced, see detail in 4.2. Then, the shape of the structure should be chosen to facilitate the signal processing. A beam shape is adequate as the natural frequencies of a beam are well separated.

The design of the lap joint used was inspired by the one used by Esteban and Rogers (2000), see Figure 107. This design seems to be most simple as it requires the smallest number of components. The length of the interface was chosen to be 100mm long as the shim. The 100mm long shim was a promising design for a receding contact, see Section 5.7. A symmetrical “lap joint” would be possible with a “double lap joint”, see Figure 107. However, a double joint would have doubled the number of parts and therefore the overall complexity. No other considerations, like the number of bolts, were taken into account, as the literature did not give any recommendation on which design of bolted lap joint should be used.

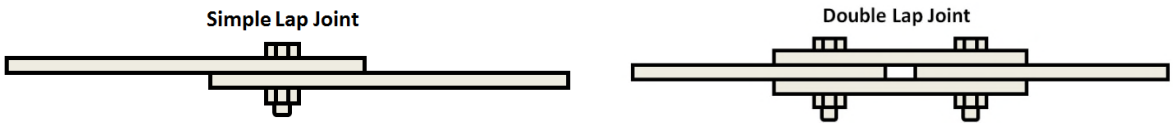

Figure 107 Comparison between a “simple lap joint” used by Esteban and Rogers (2000) and a “double lap joint” as tested by Song et al. (2004)

The final design used of the lap joint is displayed in Figure 108.

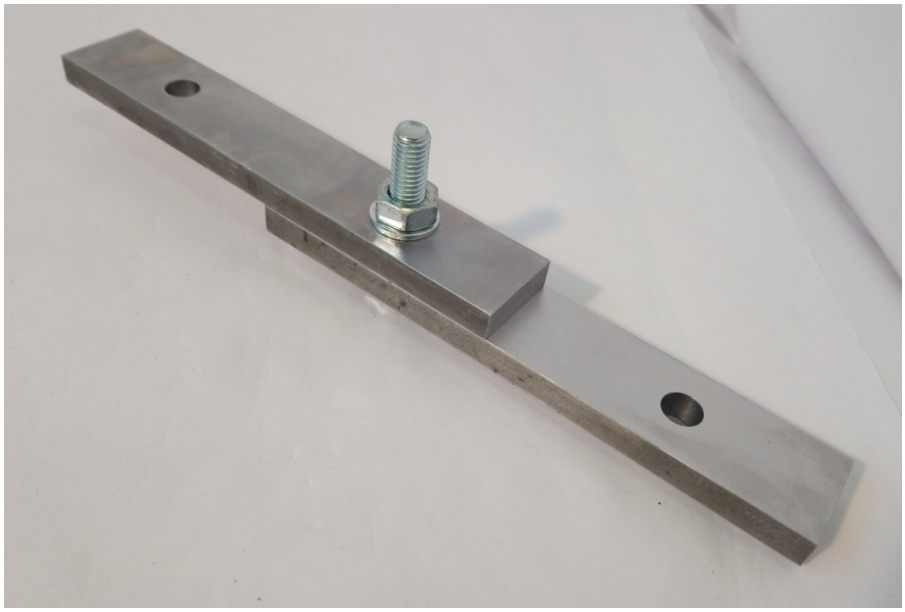

Figure 108 Bolted lap joint made out of two small beams with an interface which is exactly 100mm long.

The dimensions of each component beam are displayed in Figure 109.

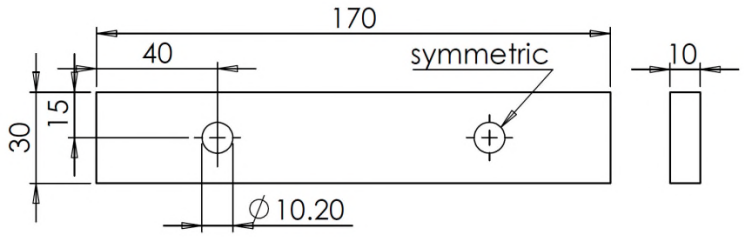

Figure 109 On the left, two views of one component beam.

To transform the receding contact created by the lap joint, washer size shims were designed as shown in Figure 110.

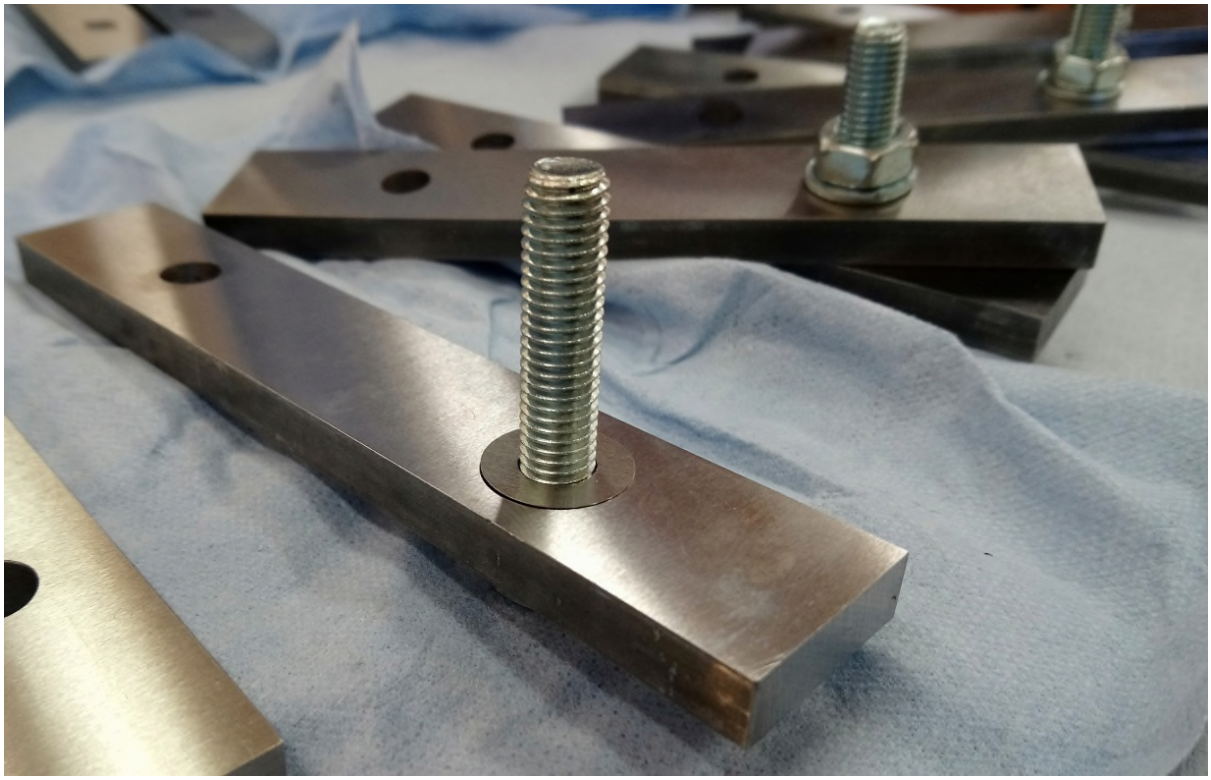

Figure 110 Picture of one of the shims placed in the interface of a bolted lap joint during the clean-up and assembly process.

The dimensions of the washer size shims are given in Figure 111. One conclusion of Chapter 3 is that the thickness of the shim does not have an impact, thus the thickness was picked at 0.05 mm to minimize the shim mass. Indeed, the shim mass could alter the dynamic behaviour of the structure. The exterior diameter of the shim, which is critical to make a complete contact, was selected based on the standard size of washer of an M10 bolt, source: Organisation Internationale de Normalisation (ISO 7089:2000). A smaller exterior diameter could have been selected, but, the author wanted to protect the surface from excessive constraint which could plastically deform the surfaces. A smaller exterior diameter should reduce even more the joint damping.

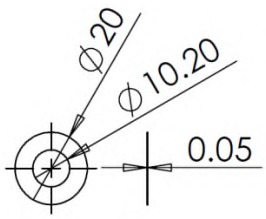

Figure 111 two views of one of the washer size shims inserted between the beams to create a complete contact.

All the hardware used in the experiments are presented in Figure 112

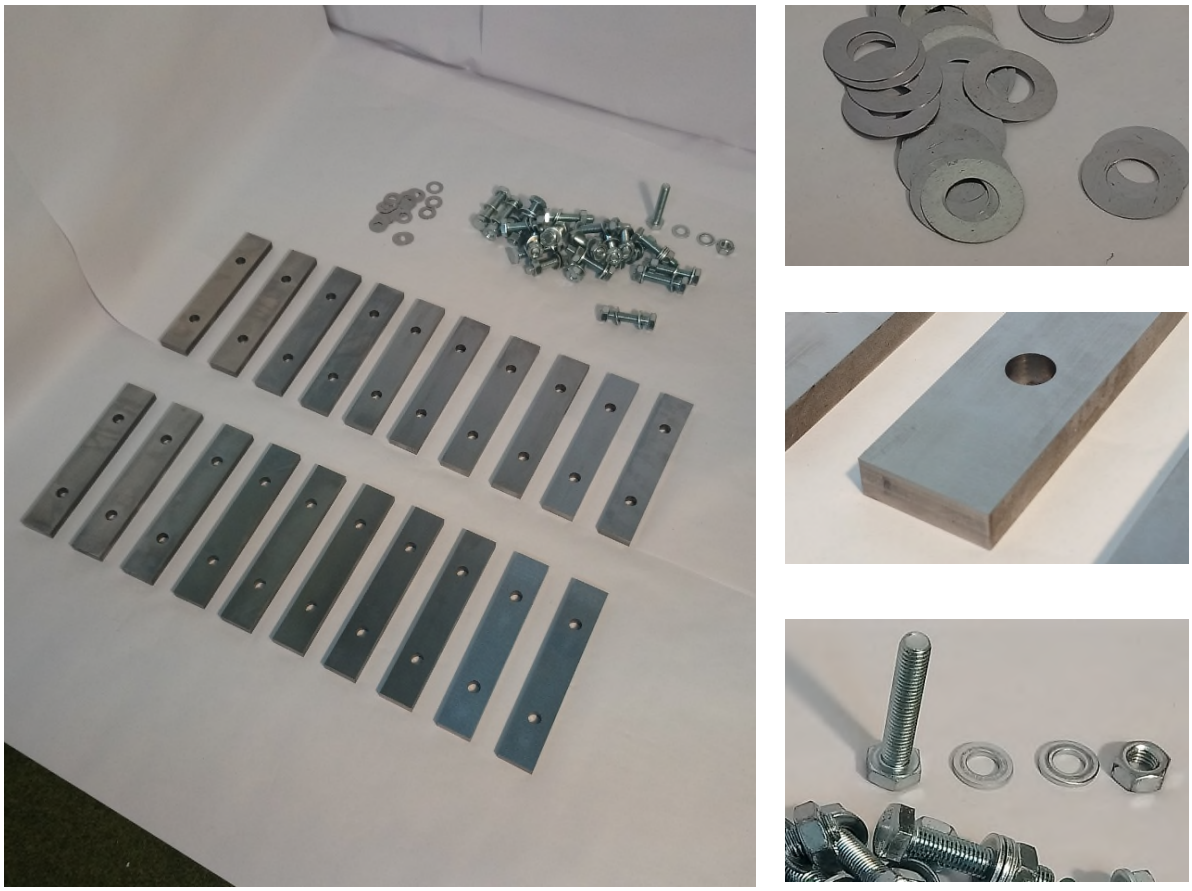

Figure 112 Hardware used in the joint position experiment. Of the 20 component beams manufactured, only 19 were used.

As the test with different positions of receding contact needed to be comparable, 18 identical lap joints were placed in series. The result of the design process is the built-

up beam displayed Figure 113. Having 18 positions for the receding contact was thought to be enough to provide a clear picture of the behaviour.

Figure 113 Photograph of the beam in position. Two static ropes have beams placed at the node of the first bending mode to isolate the structure from the ground.

The structure tested is composed of 19 identical component beams. A component beam is defined in this document as a subsidiary element of the structure shape as a beam and without any joint inside. These component beams, when assembled together, created a built-up beam of 1790mm (+/– 1mm) long. The built-up beam weighed 8.753Kg (+/– 1g). The 18 bolts are M10x45 with a 54.2Nm torque (+/– 1Nm). Inside the built-up beam, there are 18 identical bolted lap joints as displayed in Figure 108.

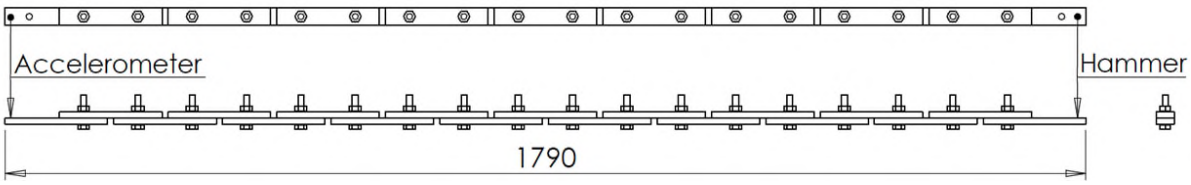

Figure 114 Top view and side view of the built-up beam with 19 component beams, and 18 bolts, one accelerometer at one extremity and the hammer hit location at the other extremity. The arrows indicate the direction of the excitation and recording device.

The suspension makes a pendulum of 1.35m (plus or minus 1mm). The longest possible pendulum was used. The steel frame, to which the suspension is bolted, is attached to a cast iron bed, see Figure 115. The cast iron bed should reduce environmental noise.

Figure 115 Photo of the experimental set-up used for the joint position experiment. The built-up beam was suspended from a steel frame. This frame is bolted to a cast iron bed resting on a second cast iron bed. A stiffer frame would have been better.

As explained in Section 3.2, the focus of this work is only on the bending mode in the same plain as the bolt axis. The author wanted to investigate the maximum number of bending modes for each hammer impact, so, the impact location and the accelerometer location were selected to be at each extremity of the beams. Indeed, for all bending modes, the extremities always have a high displacement, and so acceleration. As a result of this choice, the 12 first bending modes were excited, measured, filtered, fitted, plotted and analysed.

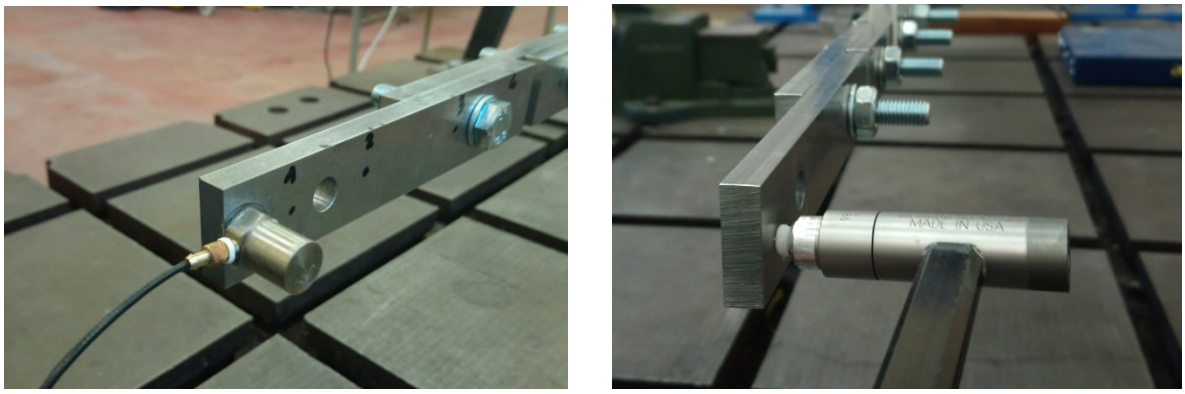

Figure 116 Position of the unidirectional accelerometer and the hammer hit at each extremity

Only one accelerometer was used to minimise damping from the cable. One end of the beam has been chosen for excitation and the other end for the accelerometer, see Figure 116. The position of the unidirectional accelerometer, far away from the hammer impulse site, allows a more sensitive setting for the accelerometer. Indeed, the shockwave is dampened by the structure before it reaches the accelerometer. Also, because the position of the hammer impact site and the accelerometer is in the same plain as the bolt axis, twisting and longitudinal compression modes were not measured. However, this position has the drawback of generating “double hits”.

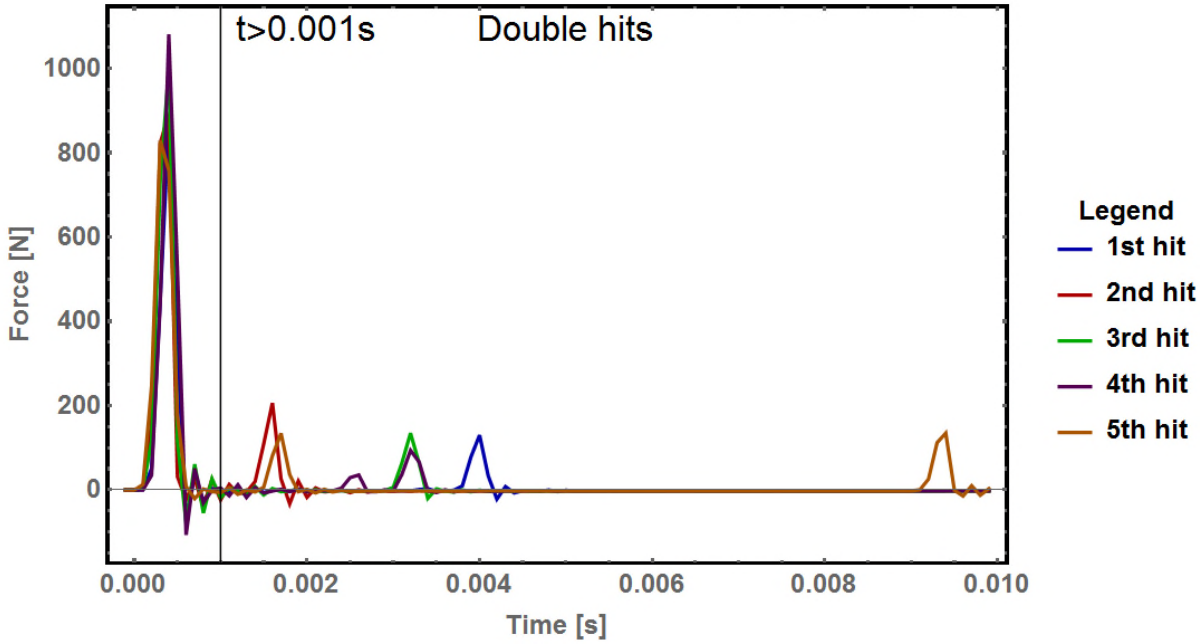

Figure 117 Impact force time-history of five hammer hits

Double hits happen when the hammer twice touches the structure tested. In this document, a double hit is defined as an impact after 1ms. The impact before 1ms will be named the main impact and the impact after 1ms will be called secondary impact. Figure 117 gives some examples of impact force time histories with double hits.

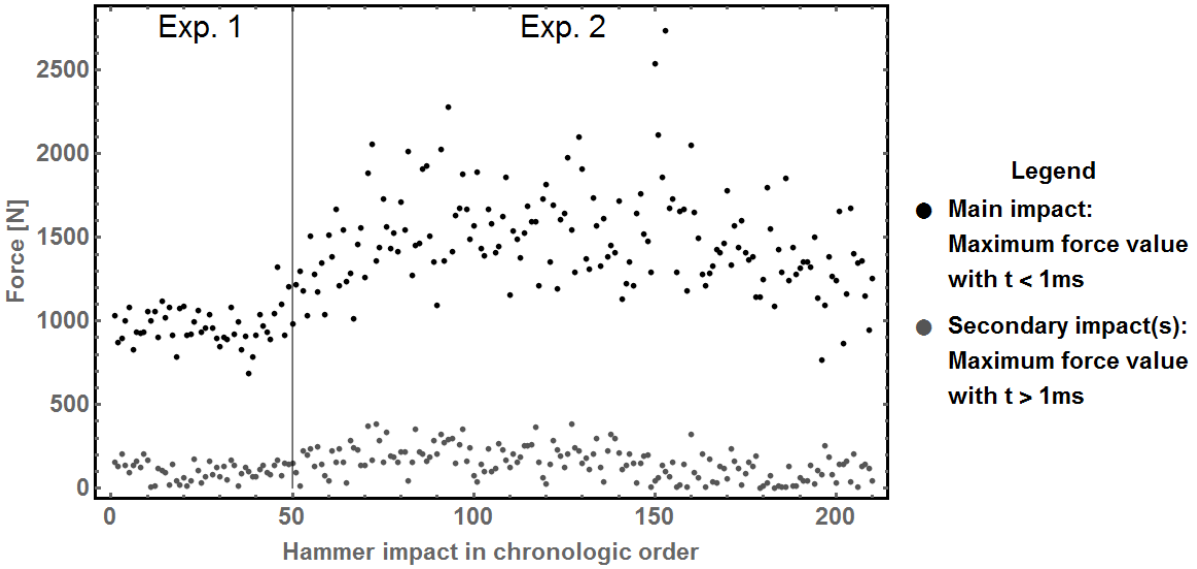

Figure 118 Impact force of the entire hammer hits conducted during Experiment 1 (Exp.1) and Experiment 2 (Exp.2). Exp.1 and Exp.2 are defined in Subsection 6.1.3. The points in black are the force of the main impact. The point in grey gives the force of the secondary impact(s). If the value of the grey dot is zero then there is no secondary impact.

This position of hammer hits creates a high chance of double hits. As displayed in Figure 118, double hits are more the norm than the exception. It was assumed that double hits did not have an impact on the nonlinear behaviour of bolted lap joints. More work is necessary to verify this claim.

Hammer impacts were used to excite the structure, not only because it is straight forward to use; but also because the hammer stays in contact with the structure for less than one millisecond if there is no double hit. If there is a double hits, the interaction last around 50 milliseconds. When the hammer stops touching the structure, the structure vibrates without any interference. The absence of interference is an advantage in favour of using a hammer and not a shaker. Indeed,

the interferences generated by the constant attachment of a shaker are not negligible.

A standard hammer has been used with a hard plastic tip (cut-off frequency of 4000 Hz). If the author could have repeated the experiment, a metal tip could have been used to obtain a higher cut-off frequency, thus, a better excitation of the higher modes. If the experiment were performed again, the author would recommend using a metal tip to improve the quality of the signal at high frequency.

The impact force values for Experiment 1 and Experiment 2 are displayed in Figure 118. Another difference between Experiment 1 and Experiment 2 is that the hammer hit of the second experiment was voluntarily harder in term of force, to obtain more high amplitude data points. Also, for each test, the structure has been excited five times for Experiment 1 and eight times for Experiment 2, once again to obtain more high amplitude data points.

The accelerometer used was uniaxial, with a direction parallel to the bolt axis. The acceleration and the force time-histories were recorded for 60 seconds with a sample rate of 10,000 samples per seconds.

The signal processing workflow described in Chapter 4 was used to “reverse filter” and “direct fit” each recording. The filter used was a Butterworth filter of order 3, used twice in a row, with a bandwidth of 6Hz, centred at the spectrum peak natural frequency. The fitting settings were: 5 periods fitted each time, with no overlapping. Also, the direct fitting procedure was stopped when the amplitude decreased to $1ms^{-2}$. The signal processing workflow was fast. The filtering step took 28s per mode and the fitting step took between 15s for the first mode to 0.3s for mode 12. The first mode took more time because more points were fitted, as the decay lasts longer and as there were more points per cycle, with the first mode compared to mode 12. This signal processing workflow was used to extract the instantaneous amplitude, the instantaneous natural frequency and the instantaneous damping ratio of the first 12 bending modes for each recording. Each recording contains the time history from one hammer hit.

6.1.3 Details of the tests carried out

The first experiment, Experiment 1, was conducted on a beam with two receding lap joints which were symmetrically placed and 16 joints with complete contacts. The author also wanted to maintain the symmetry of the position of the receding contact. The author assumed that having two receding contacts placed symmetrical, relative to the centre of the beam, would simplify the analysis of the results. This lead to the choice of an even number (18) of bolted lap joints. On reflection, this constraint of maintaining symmetry seems unnecessary and individual receding contact position could be investigated.

The results of Experiment 1 were promising. Therefore, the author decided to conduct a second experiment, Experiment 2, but this time with only one receding contact position at the time. Experiment 2 was intended to discover more detail of the effect of the individual receding contact joint positions.

However, the author made the mistake of remaking the surfaces of the components beams. The surfaces of the component beams had small scratches after Experiment 1. Therefore, the decision was made to remake the surfaces of the component beams. This decision seems to have led to an increase of damping ratio between the two experiments which will be discussed later. The resurfacing process made the two experiments incomparable. The author recommends no resurfacing of the surfaces to make tests comparable.

Please note that the surface roughness was not measured for Experiment 1. Therefore, the surface roughness is unknown for Experiment 1. Between Experiment 1 and Experiment 2, the two interfaces of the component beams were resurfaced to reach a smooth surface finish. Due to the orientation of the grinding tool, a surface finish of Ra = 0.3μm was achieved in the longitudinal direction, and a smoother surface finish of Ra = 0.08μm was measured in the orthogonal direction.

The average thickness of the component beams during Experiment 1 was 10.0mm, with a variation of +/-0.1mm, across the 19 component beams. The resurfacing removed some material from the component beams. The average thickness of the component beam during Experiment 2 was 9.7mm, with a variation of +/-0.1mm,

across the 19 component beams. The difference of thickness reduces the stiffness of the structure which was measured by smaller natural frequencies. This reduced stiffness will be described later.

Before Experiment 1 and Experiment 2, as displayed in Figure 119, each 19 component beams, 18 bolts and 36 washers were cleaned. A solvent was used to remove any trace of lubricant from the manufacturing process.

Figure 119 Cleaning and assembly step

As explained before in Subsection 6.1.1, the main objective was to investigate the effect of the position of receding contacts on a structure. To achieve that, shims need to be used to turn on or off the nonlinear behaviour of the bolted lap joint. Placing or removing washer size shims creates, respectively, complete contact or receding contact. The shims allow the testing of multiple positions of receding contacts within the same structure. The tests are comparable because all the tests were performed on the same structure. Indeed, the mass, the rigidity and the surface finished of the structure were the same across all tests.

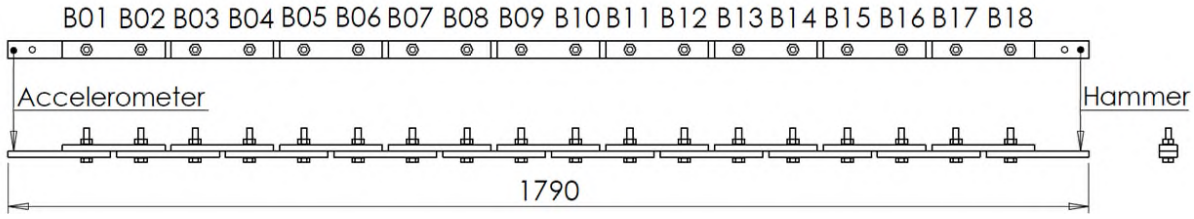

Figure 120 Top view and side view of the built-up beam with the bolt number position

To simplify the definition of each test, the bolt positions were named B01 to B18 as displayed in Figure 120. The tests with one receding contact were named BXX. For example, the test ‘B14’ stands for the test with a receding contact at the bolt position 14 and with complete contacts at all the other bolt positions. The tests with two receding contacts were named BXX&BYY. Tests with only complete contacts were named AllCompleteZ, with ‘Z’ depending on the experiment number. Also, a test with only receding contacts was named AllRecedingZ, with ‘Z’ depending on the experiment number.

If the experiment would be performed again, one ‘Allcomplete’ test would be performed between each test with receding contacts. This way the variation of the ‘Allcomplete’ test (with complete contact everywhere) would be more precisely measured. Also, the each test with a receding contact could be compared to the ‘Allcomplete’ tests performed just before or after.

All the tests conducted during Experiment 1 are listed in Table 13.

All the tests conducted during Experiment 2 are listed in Table 14.

Table 13 Tests of Experiment 1 with two receding contacts in chronological order

Bolt position	B01	B02	B03	B04	B05	B06	B07	B08	B09	B10	B11	B12	B13	B14	B15	B16	B17	B18
AllComplete1																		
B01&B18																		
B02&B17																		
B03&B16																		
B04&B15																		
B05&B14																		
B06&B13																		
B07&B12																		
B08&B11																		
B09&B10																		
AllReceding1																		
Legend:	*Complete contact*					*Receding contact*												

Table 14 Tests of Experiment 2 with one receding contact in chronological order

Bolt position	B01	B02	B03	B04	B05	B06	B07	B08	B09	B10	B11	B12	B13	B14	B15	B16	B17	B18
AllComplete2																		
B01																		
B02																		
B03																		
B04																		
B05																		
B06																		
B07																		
B08																		
B09																		
B10																		
B11																		
B12																		
B13																		
B14																		
B15																		
B16																		
B17																		
B18																		
AllComplete2Bis																		
Legend:	*Complete contact*					*Receding contact*												

6.1.4 Results for the test Allcomplete1, B08&B09 and AllReceding1

To verify the properties of the assembled beam, the FRF of the two extreme tests ‘AllReceding1’ and ‘AllComplete1’ and the intermediary test ‘B08&B09’ were plotted in Figure 121.

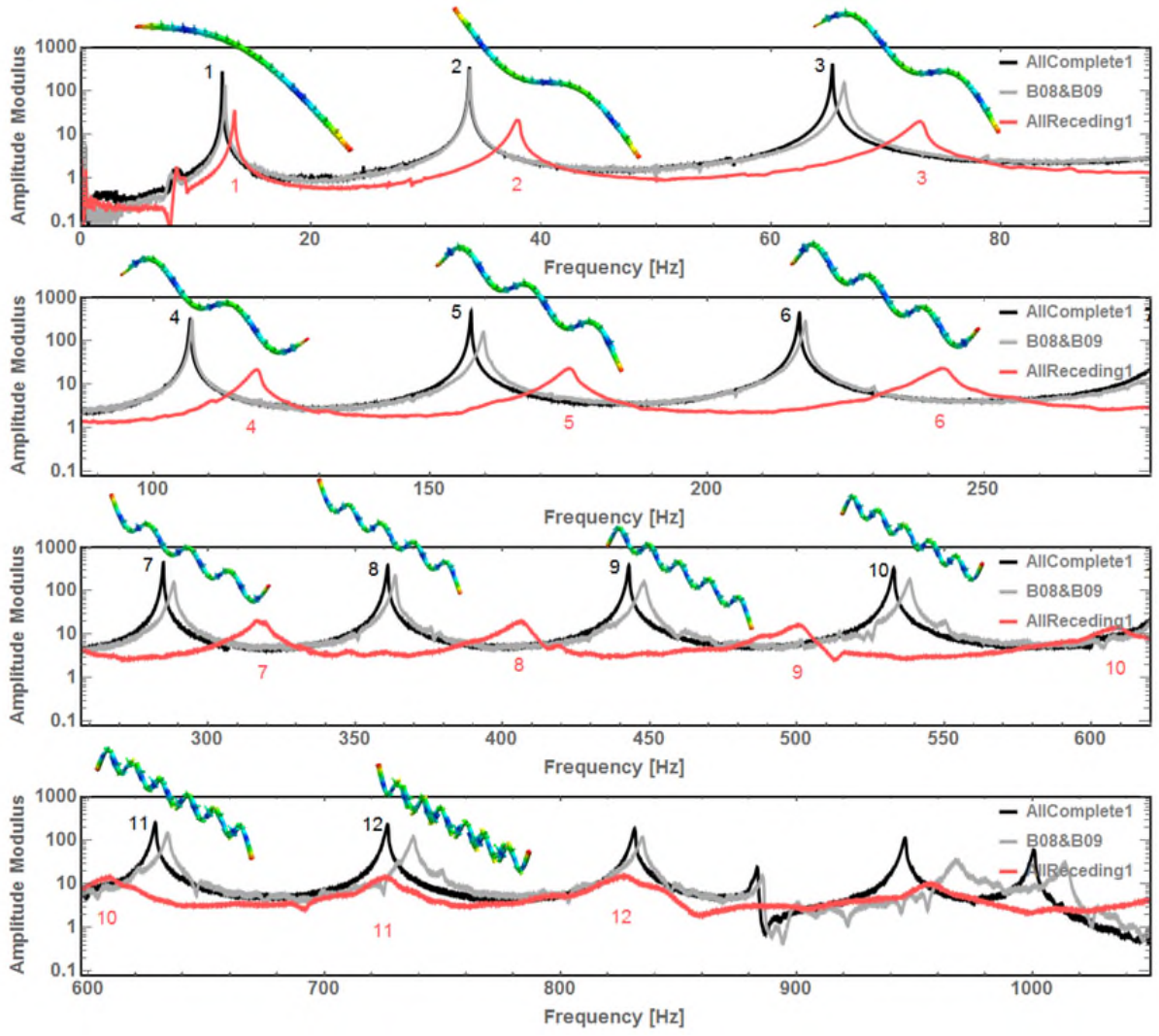

Figure 121 Frequency Response Functions (FRF) of the test AllComplete1 (complete contacts at all the bolted lap joints), B08&B09 (receding contacts at the Bolt position 8 and 9) and AllReceding1 (receding contacts at all the bolted lap joints).

The first 12 simulated bending mode shapes are also inserted in Figure 121, beside each resonance peak, to help the reader visualise the meaning of the peaks. These mode shapes were obtained from a finite element simulation described in Section 7.3. The mode number is also given next to each peak.

For the test ‘Allcomplete1’ with shims at every bolt location, all the peaks of Figure 121 are sharp and almost-symmetric, which is characteristic of small damping and linear resonance behaviour. Allcomplete1 behaves as expected like a single piece of material, even if composed of 19 components beam and 18 joints, probably because

there is almost no friction inside the joints due to the limited interface created by the shim restraining the contact patch.

Conversely, for the ‘AllReceding1’ test with no shim anywhere, the FRF curve has asymmetric peaks. Those asymmetric peaks are characteristic of nonlinear behaviour due to the change of the natural frequency during the decay. Also, the peaks are broad, which is characteristic of a highly damped structure. This data confirmed that the design for the receding contact chosen does have a dynamic nonlinear behaviour.

The ‘B08&B09’ test shows a behaviour situated between ‘AllReceding1’ and ‘Allcomplete1’. Also, modes two and four seem less damped than the other modes for the ‘B08&B09’ test.

The main point is that Figure 121 shows that the ‘AllComplete1’ test behaves linearly (with an almost constant natural frequency and an almost constant small damping ratio). The shims make the structure behave a homogeneous steel beam. The linear behaviour is remarkable because the built-up beam is composed of 18 bolted lap joints. Therefore, AllComplete1 could be used as a reference to compare with the test with one or two receding contacts.

In conclusion, placing washer size shims in the interface, to turn receding contacts into complete contacts, create a linear behaviour from a nonlinear lap joint. The result described in this section validates the method described the Subsection 6.1.1 at the beginning of this chapter.

6.1.5 Plotting of the experimental results

The result of this experiment was complex to display. Indeed 30 tests were performed, 12 modes studied and three parameters estimated. Those three parameters are the instantaneous envelope amplitude, the instantaneous natural frequency and the instantaneous damping ratio, which will be called amplitude, natural frequency and damping ratio for short. The classic way to display the results is to plot the damping and the frequency of multiple tests against the amplitude one mode at a time. However, this plotting method is complex to interpret, especially if the 30 tests are displayed at once.

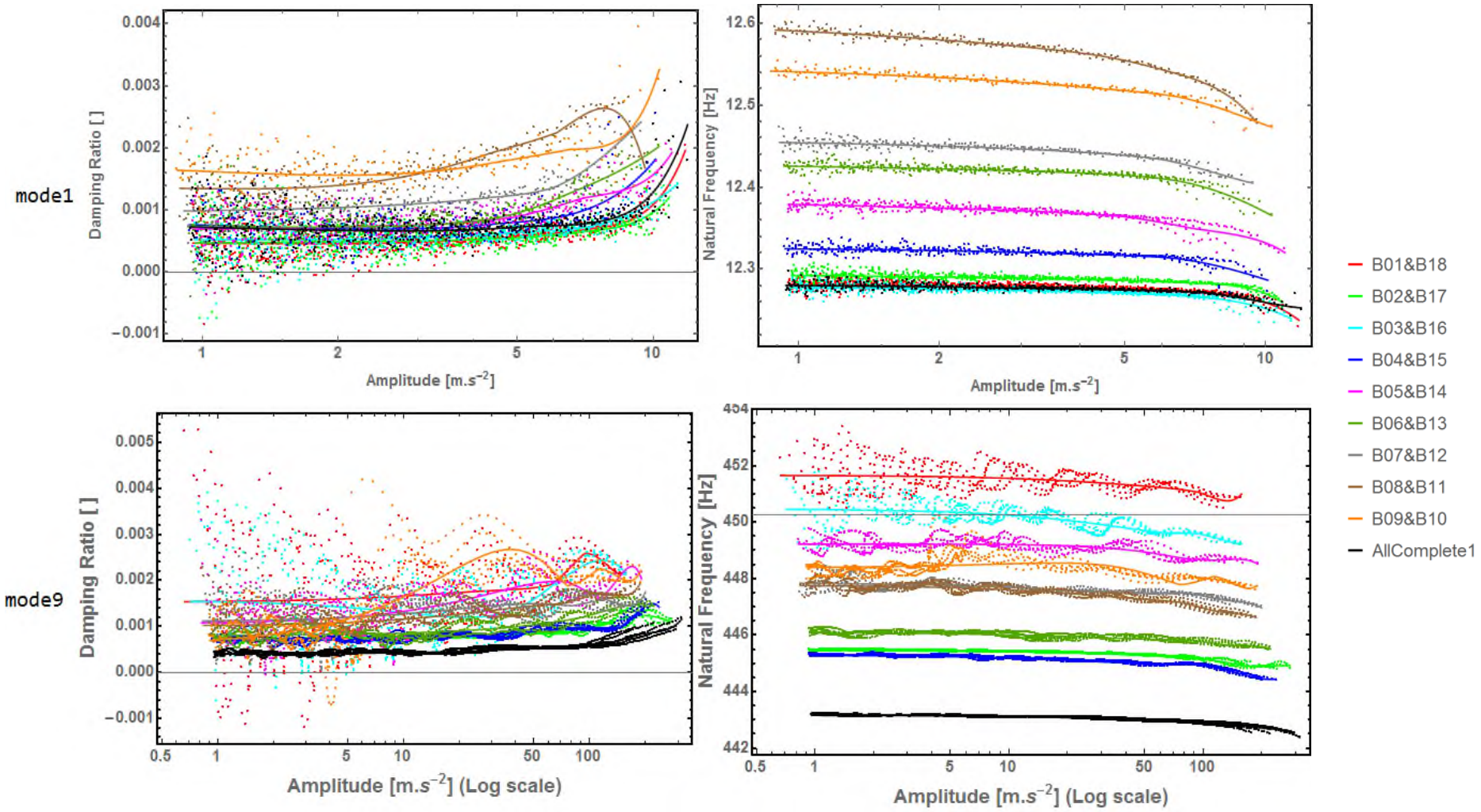

Figure 122 Damping ratio and Natural frequency as a function of the amplitude from Experiment 1 for modes 1 and 9

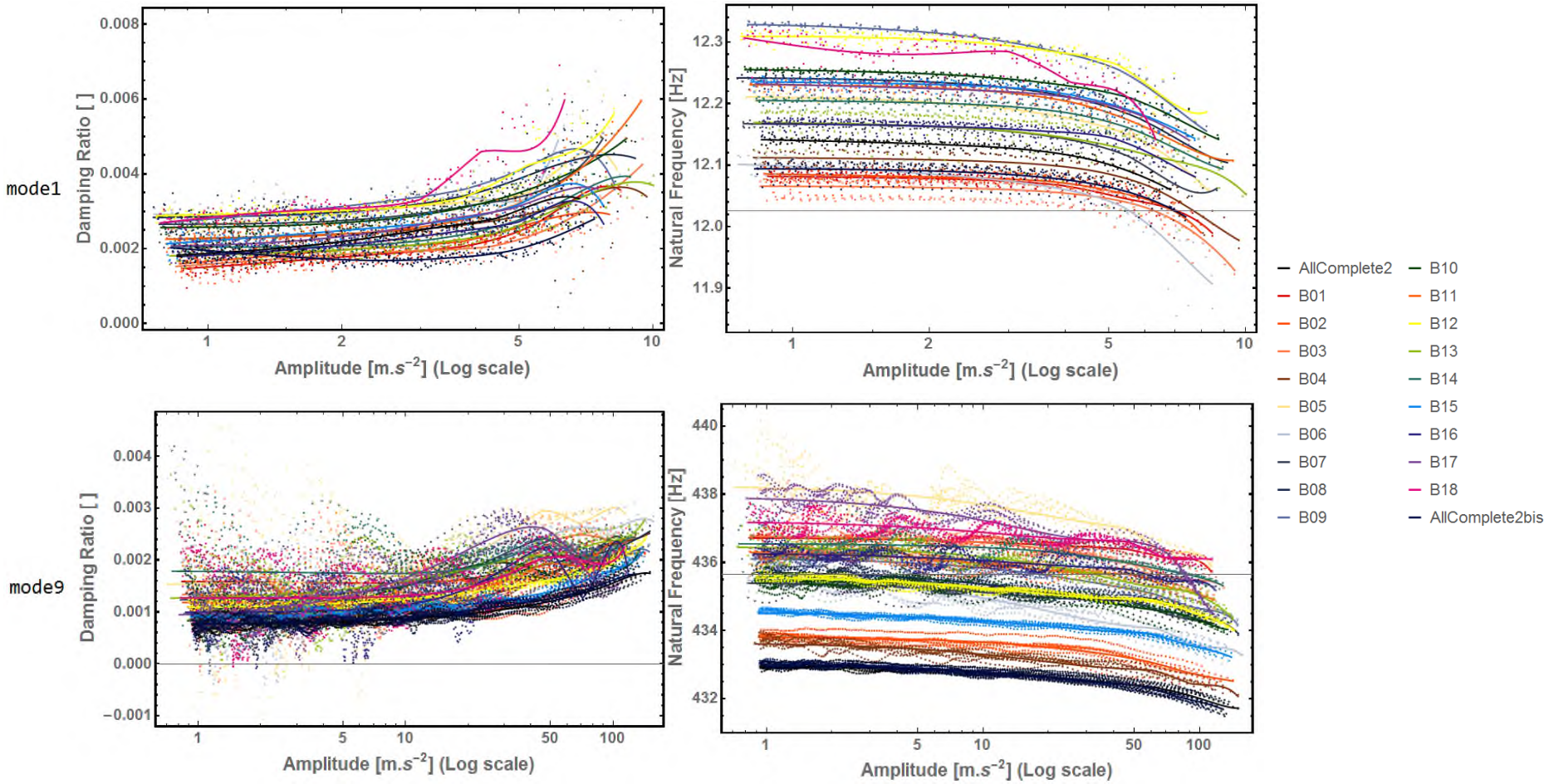

Figure 123 Damping ratio and Natural frequency as a function of the amplitude from Experiment 2 for modes 1 and 9

The results of the direct fitting methods are plotted in Figure 122 and Figure 123. Mode 1 and mode 9 are representatives of the two behaviours measured. The rest of the modes are displayed in 10.3Appendix A and Appendix B. In Figure 122 and Figure 123, the points generated by the direct fitting method are displayed. Trend lines of a 6th order polynomial were fitted to each data set. One data set is composed of the fitted data of five or eight hammer hits. In other words, one data set corresponds to one test described in Table 13 or in Table 14.

Firstly, the plots show that the natural frequency and the damping ratio are correlated to the amplitude. Also, the data shows that introducing receding contacts increases the damping ratio and the natural frequencies. The mode in which there is an increased damping ratio depends on the position of the receding contacts and the mode. The mode shapes, which give the displacement of each mode at each location, are useful for interpreting the data.

Also for multiple modes like mode 9 but not mode 1, the tests with high damping ratio and high natural frequency tend to have an oscillating value of damping ratio and natural frequency. This oscillating behaviour is frequently displayed in 10.3Appendix A and Appendix B. No explanation was found for these amplitude dependant oscillations except maybe mode interactions or signal processing artefacts. This oscillating behaviour could be interesting to investigate in future work.

From those observations, it seems necessary to rethink the method for displaying this information. As the parameter investigated was the position of the receding contacts, the position should be placed on the x-axis, and the measured parameters (damping ratio and natural frequency) should be on the Y-axis, with colour used to display amplitude.

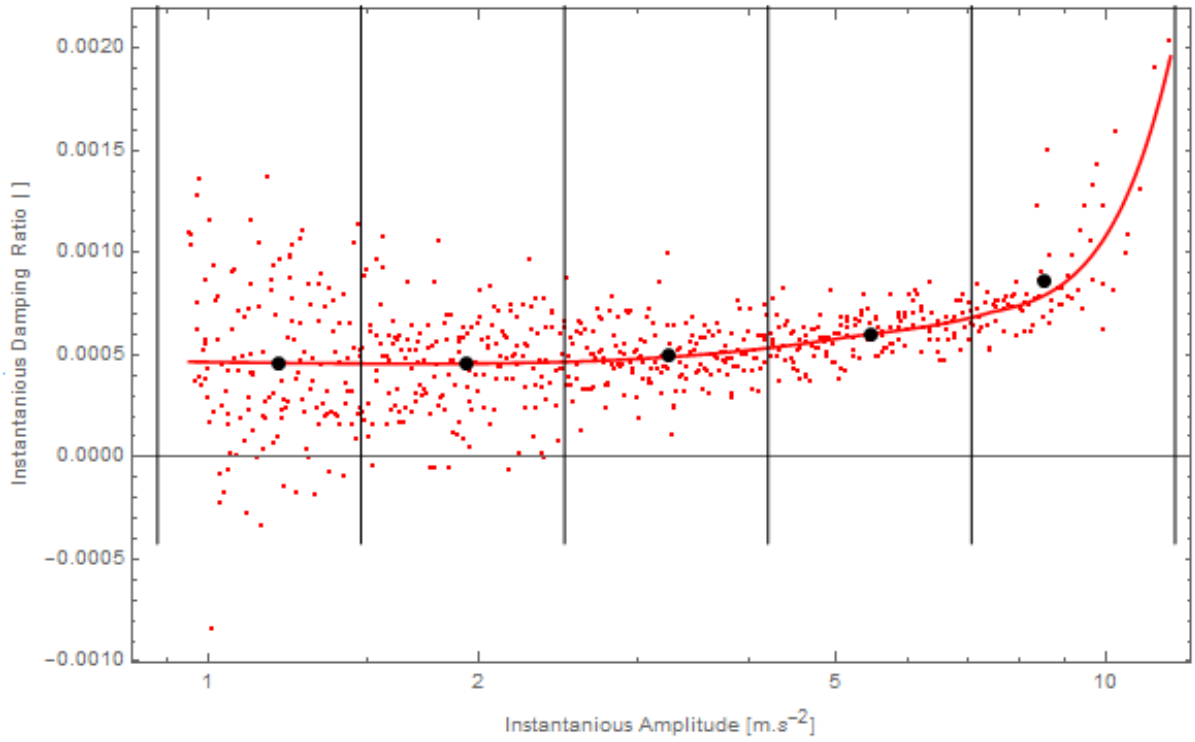

Figure 124 Generation of five average points, in black, depending on the amplitude intervals (black vertical lines), for one category (B01&B18) and mode 1. The average data point is the average of all the data points in the amplitude interval.

The solution selected is to average data within each set. The data points were averaged into five amplitude intervals. These intervals were defined based on the minimum and maximum amplitude measured across all the tests. These five amplitude intervals were calculated for each mode. These amplitude intervals are logarithmically equally spaced. Figure 124 illustrates the extraction of five average values corresponding to the five amplitude intervals of mode 1 from the B01&B18 test. The average values of damping ratio and natural frequencies were then used to create the following plots. As an example, Figure 125 shows the damping ratio and natural frequency as a function of the receding contact location.

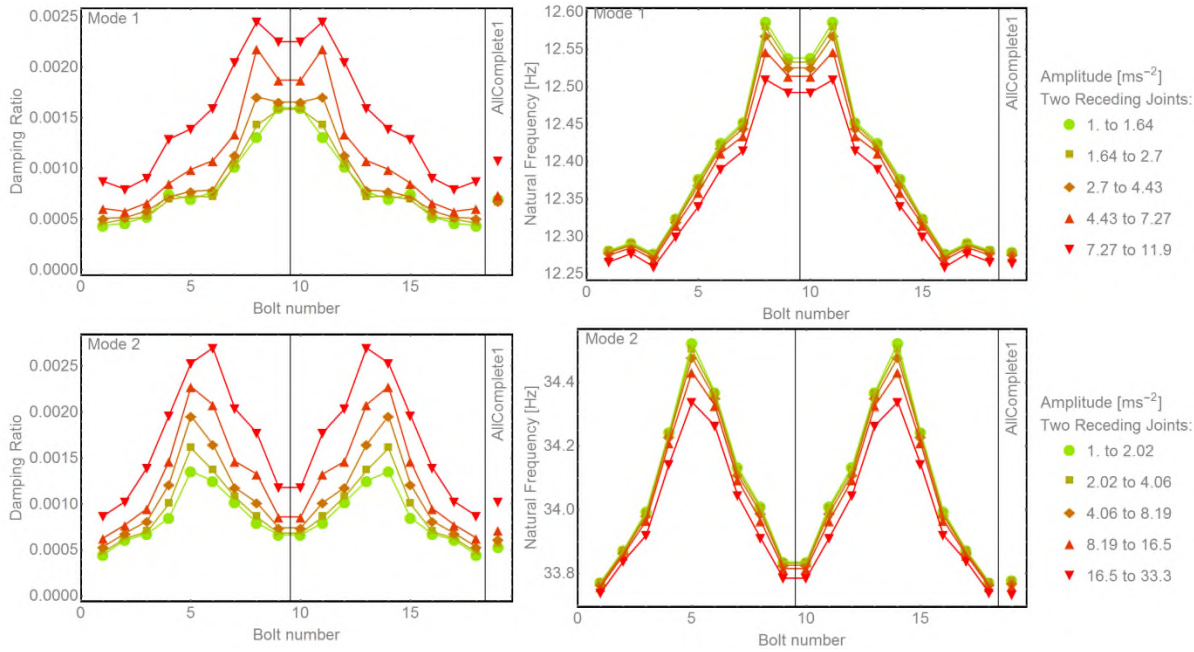

Figure 125 Damping ratio and natural frequency plotted as a function of two receding contact positions. The measured data points are joined by lines to help the readability. The colour represents the amplitude intervals which are mode dependent. On the right, the results of the AllComplete1 test are displayed.

In Figure 125, the x-axis represents the location where the shims were removed. The x-axis is in bolt-number-units. The relation between the bolt number unit and the location is

$$position\ in\ bolt\ number\ unit = \frac{\text{position in meter} - 0.13}{0.090} + 1 \qquad \textbf{(6-1)}$$

For the experiment with two receding contacts, because the shims were removed symmetrically on the beam, each set of five points were displayed twice to improve the readability. The axis of symmetry used to duplicate these points is the vertical grey line displayed in every plot.

As the measurement of the ratio between the tests with receding contacts and 'AllComplete' tests was the objective of this experiment, a ratio was calculated and displayed. The five averaged data points were respectively divided by the corresponding point from the AllCompleteX test in terms of amplitude. For the damping, the following equation was used:

$$Scaled\ damping\ ratio\ = \frac{damping\ ratio}{AllCompleteX\ damping\ ratio} = \frac{\zeta}{\zeta\ ref} \quad \textbf{(6-2)}$$

For the natural frequency the following equation was used:

$$Scaled\ natural\ frequency\ = \frac{natural\ frequency}{AllCompleteX\ natural\ frequency} \quad \textbf{(6-3)}$$

The scaled natural frequency, the scaled damping ratio are all dependant on the amplitude interval of the average point, for more details see Figure 124. For Experiment 1, the AllComplete1 was used to scaled the damping ratio and the natural frequency. For Experiment 1, the AllComplete2Bis was selected, instead of AllComplete2, because AllComplete2Bis had a lower damping ratio for the first mode as displayed in Figure 125.

Figure 126 shows the template plots for the scaled results.

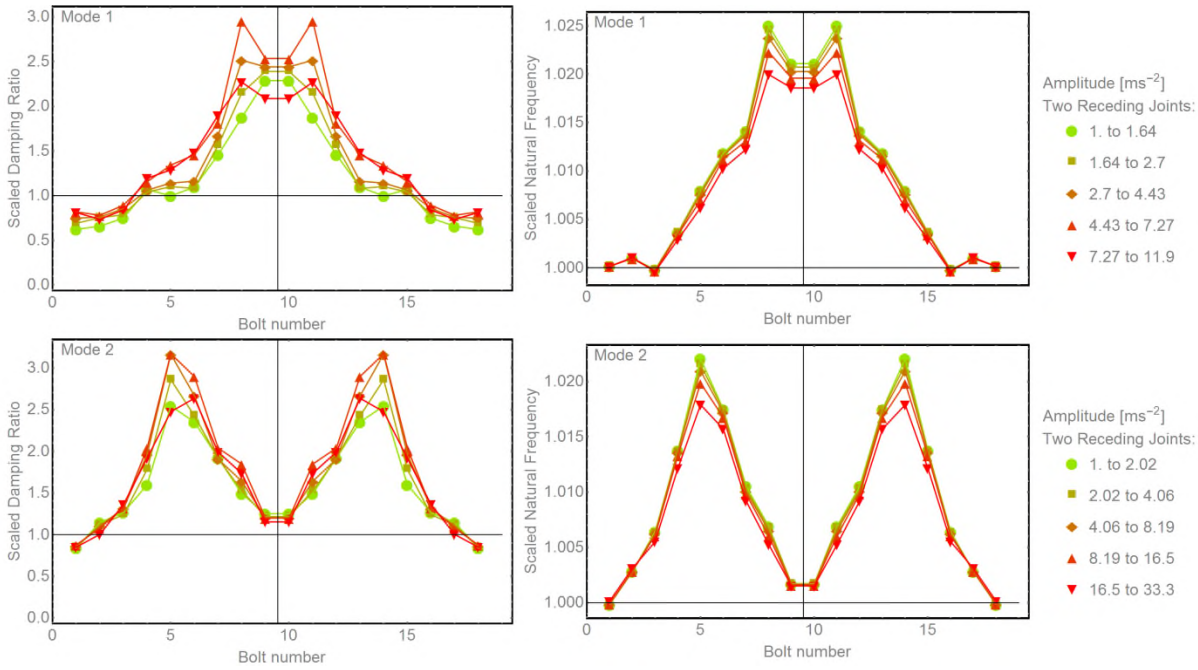

Figure 126 Scaled damping ratio and scaled natural frequency, depending on the position of two receding contacts, for mode 1 and 2. The measured data points are joined by lines to help the readability. The colour represents the amplitude intervals which are mode dependent.

The experiment results for Experiment 1, using the template of Figure 125 and Figure 126 for the 12 first bending modes, are plotted in:

- Section 6.2 for **two** receding joints in term of damping ratio and natural frequency
- Section 6.3 for **two** receding joints presented as **scaled** damping ratio and scaled natural frequency
- Section 6.4 for **one** receding joint in term of damping ratio and natural frequency
- Section 6.5 for **one** receding joint presented as **scaled** damping ratio and scaled natural frequency

The observations from the data sets are given at the end of each section. Then, this chapter's data sets are compared to models in chapter 7. The interpretation and discussion of the results are performed in Chapter 8.

6.2 Experimental result: two symmetrical receding contacts

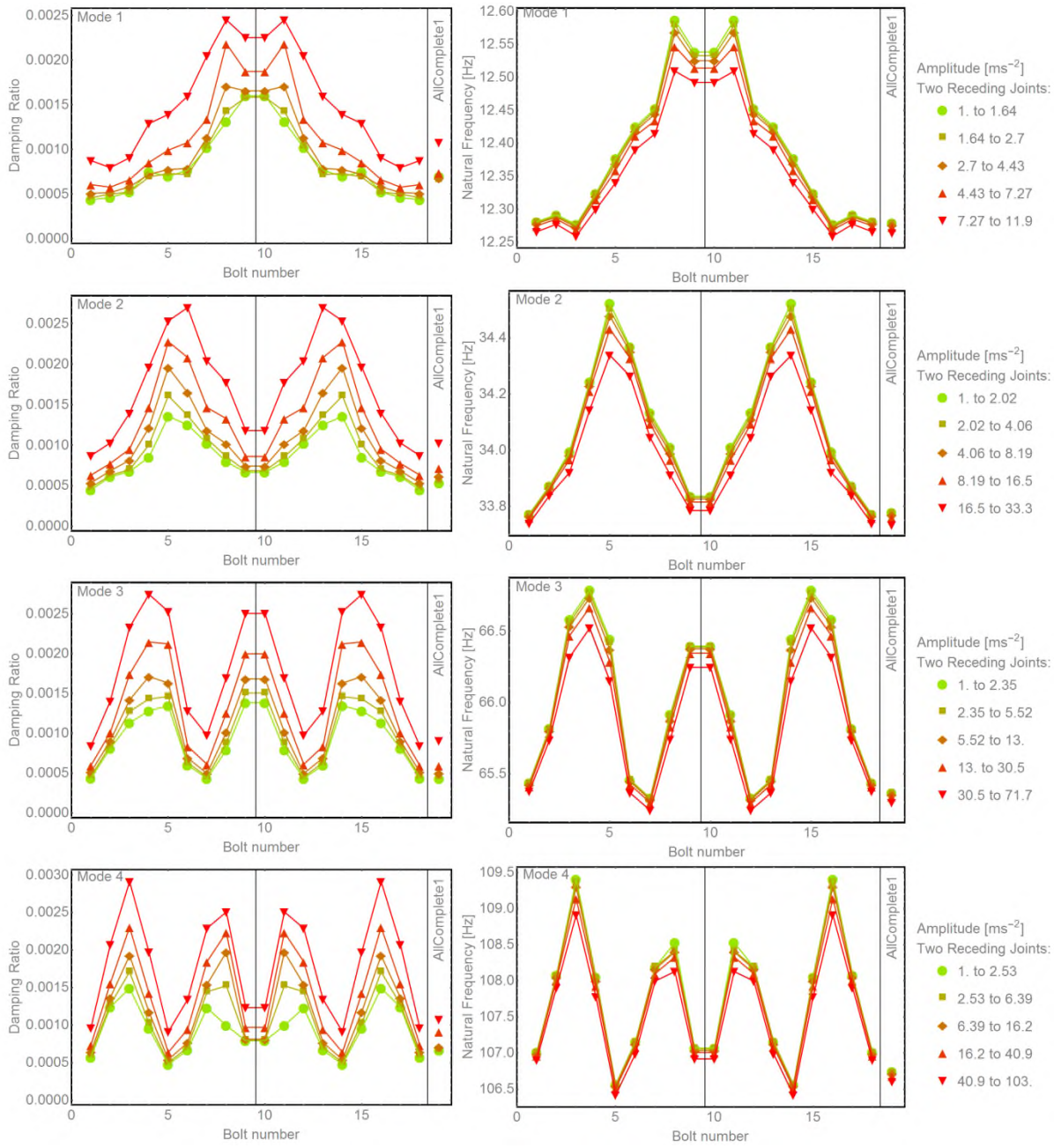

Figure 127 Damping ratio and natural frequency depending on the position of two symmetrical receding contacts for modes 1 to 4. This grid of plots follows the same template as Figure 125.

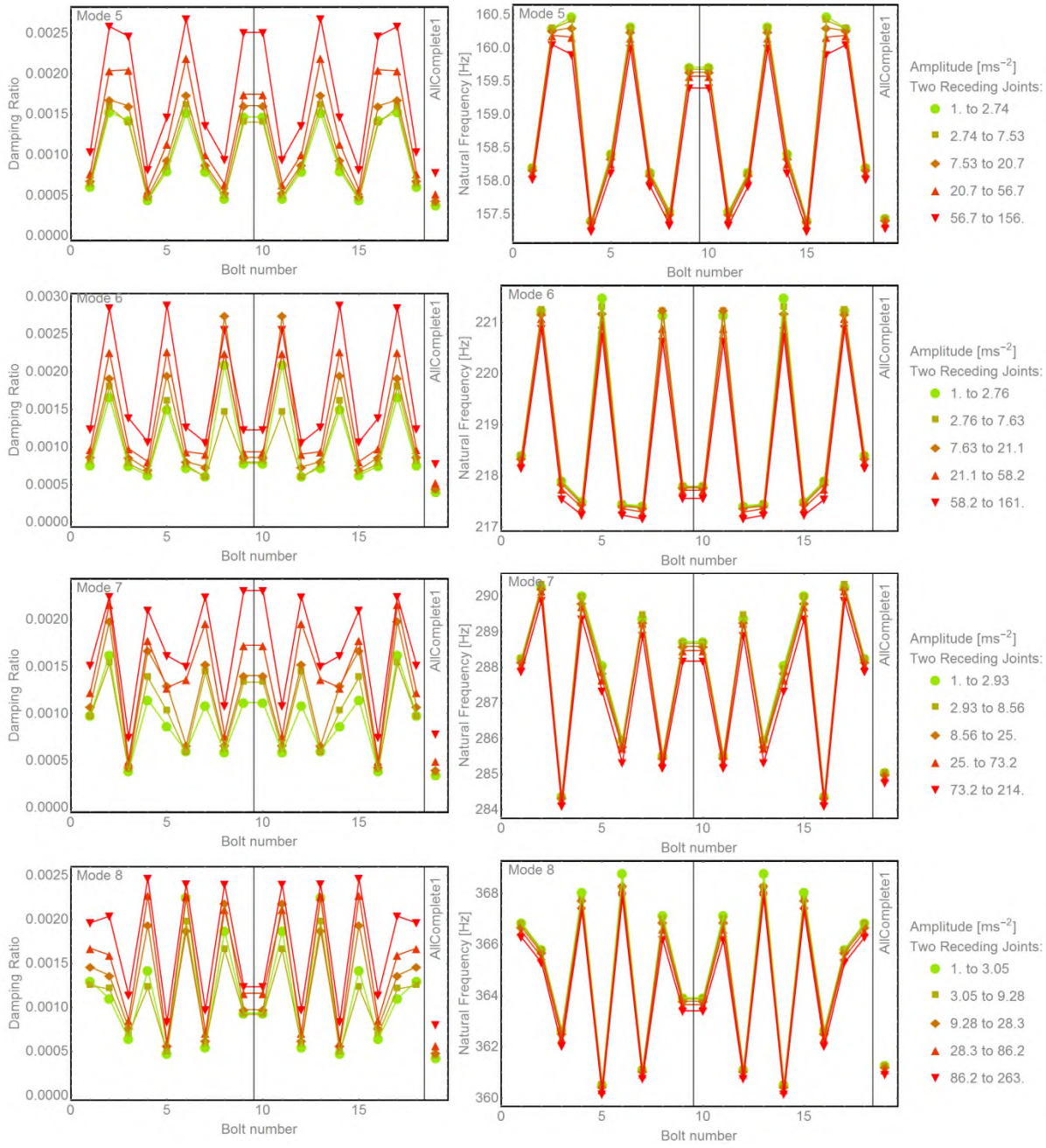

Figure 128 Damping ratio and natural frequency depending on the position of two symmetrical receding contacts for modes 5 to 8. This grid of plots follows the same template as Figure 125.

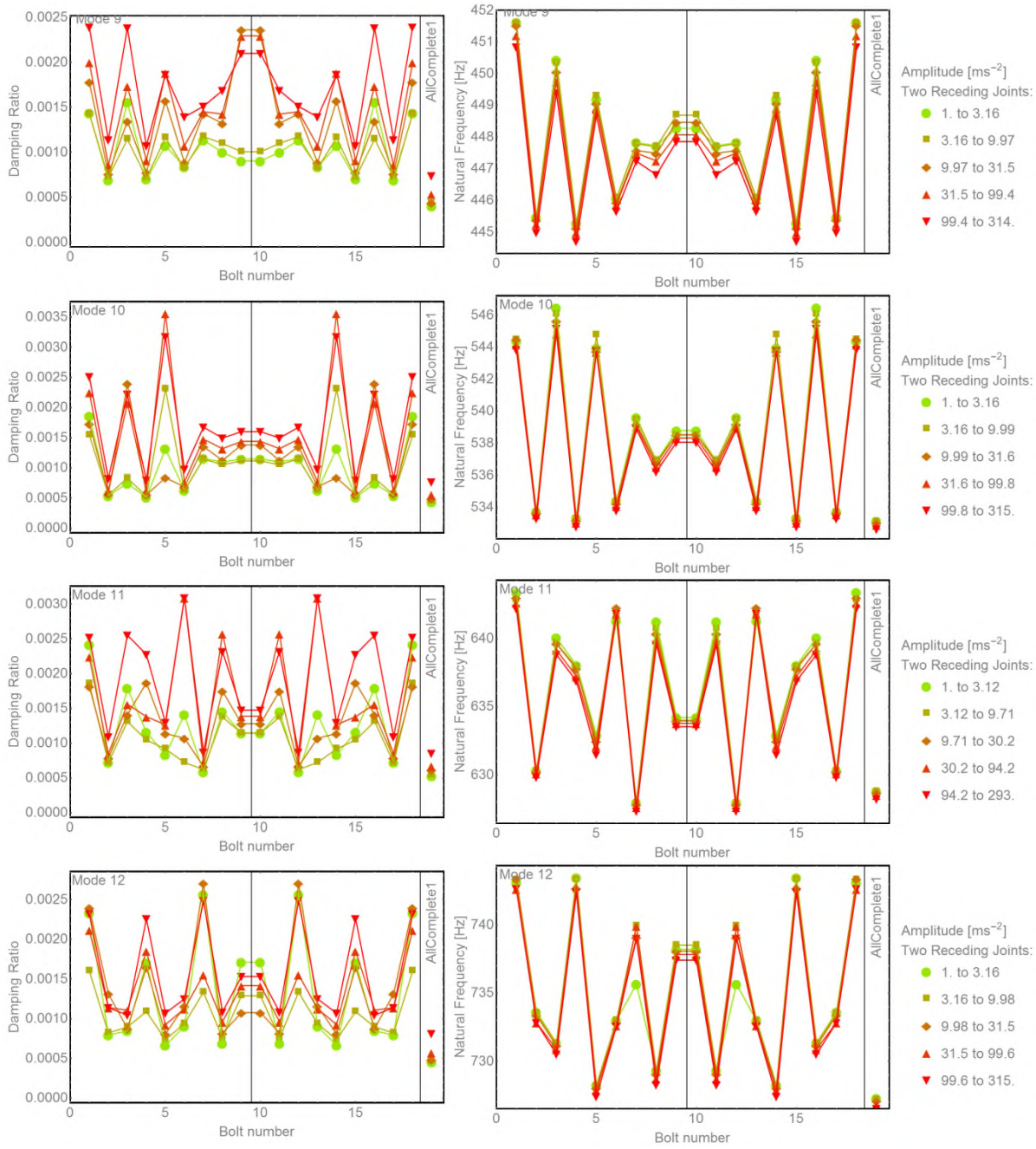

Figure 129 Damping ratio and natural frequency depending on the position of two symmetrical receding contacts for modes 9 to 12. This grid of plots follows the same template as Figure 125.

Here are the observations linked to the results displayed in Figure 127, Figure 128 and Figure 129.

First of all, an important reminder: the results of this section are perfectly symmetrical because of the way they are displayed, not because of a symmetrical

behaviour of the experiments. Indeed, the data of Figure 127, Figure 128 and Figure 129 are composed of a set of 9 tests with two receding contacts and one test with only complete contacts. Each test has two receding joints placed symmetrically in the beam. To match the display of the other experiment with receding contacts, each test is displayed two times in each plot using a line of symmetry.

The experimental results, for the two receding joints, show that when the amplitude decreases, see legends, the natural frequency increases (loosening effect) and the damping ratio decreases (nonlinear damping). The change of the natural frequency is correlated to the damping ratio in almost all tests and modes.

The data show a wave pattern. This wave pattern has as many waves as the mode number until mode eight. For the smallest values of the wave pattern, the value of the damping and frequency are similar between the AllComplete1 tests and the other tests. In other words, the AllComplete1 test has the smallest damping and frequency in most cases. Therefore, adding two receding contacts rigidifies the structure (an increase of the natural frequencies) and increases the dissipation of energy (higher damping ratio) compared to the AllComplete1 test with complete contacts everywhere.

The data points are sorted by amplitude for the first modes, but this order gradually disappears as the mode number increases. The damping changes increase and are noisier than the frequency changes, but this could be due to the scale of the plots.

This paragraph lists what is noticeable about the numerical values. The range of damping ratio, from 3×10^{-4} to 3×10^{-3}, is shared between modes. The maximum amplitude increases with the mode number, see the legend. For example the maximum measured amplitude of vibration of mode 1, 5 and 12 are respectively 11.9, 156 and 315 ms^{-2}. The difference between the natural frequency of the AllComplete1 test and the maximum frequency of the other tests increases with the mode number:

Max frequency – Ref frequency:

- Mode 1: 12.60 – 12.25 = 0.35Hz
- Mode 5: 160.5 – 157 = 3.5Hz

- Mode 12: 750 – 720 = 30Hz

Summary observations: two receding joints:

- The plots are symmetrical due to the way the data is displayed, not because of a measured physical phenomenon.
- There are amplitude dependent natural frequencies and amplitude dependent damping ratios
- The damping ratio and the natural frequency are correlated.
- Wave pattern: There are as many waves as the mode number
- The AllComplete1 test has the smallest damping ratio and natural frequency (for most cases)
- The two receding contacts rigidify the structure and increase the damping
- The data is noisier for the higher modes than the lower modes
- The range of values for the damping ratio is independent of the mode number
- However, the range of values for the frequency and amplitude are mode dependant.

6.3 Experimental result: scaled results for two symmetrical receding contacts

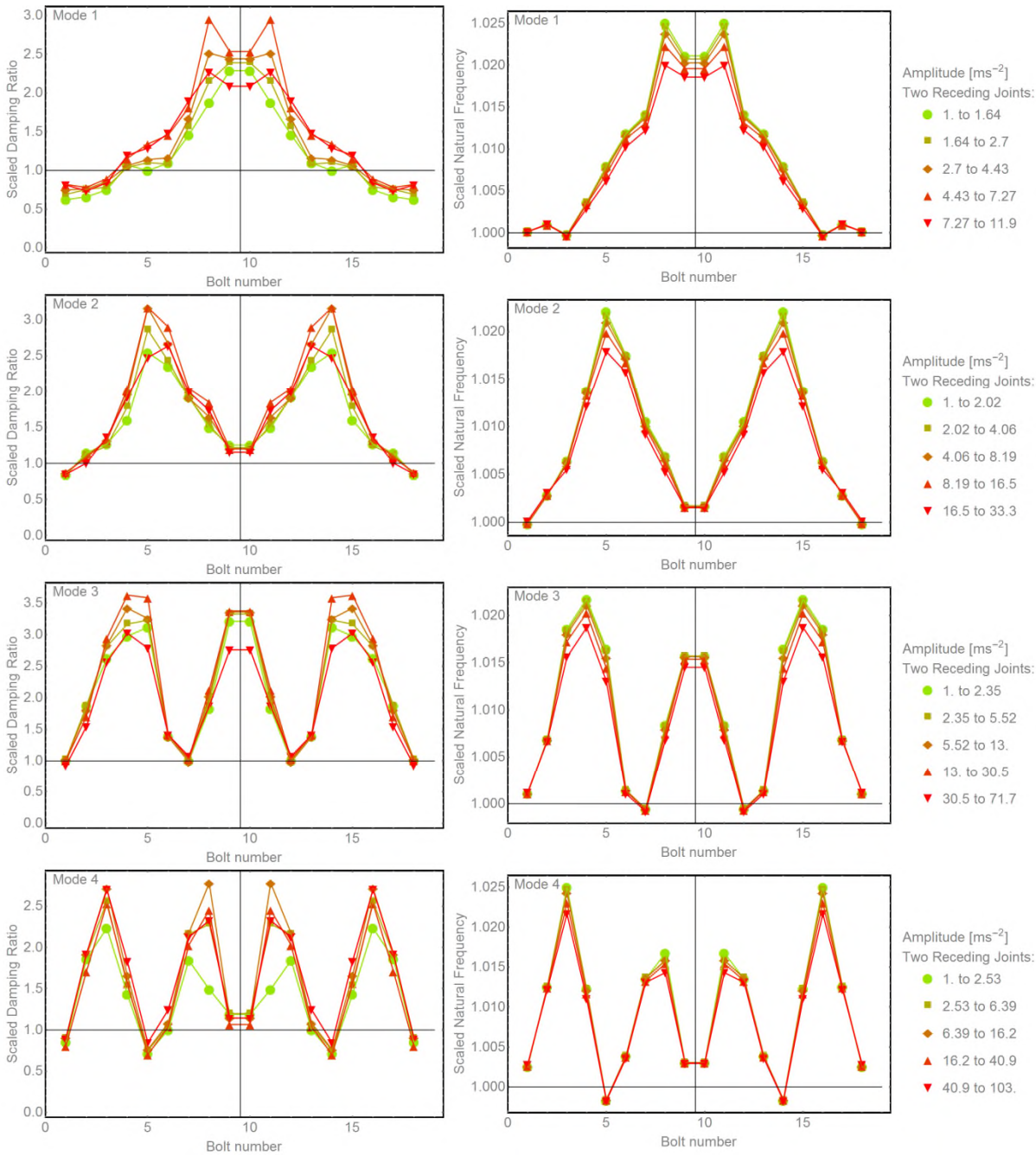

Figure 130 Scaled damping ratios and scaled natural frequencies depending on the position of two symmetrical receding contacts for modes 1 to 4. This grid of plots follows the same template as Figure 126.

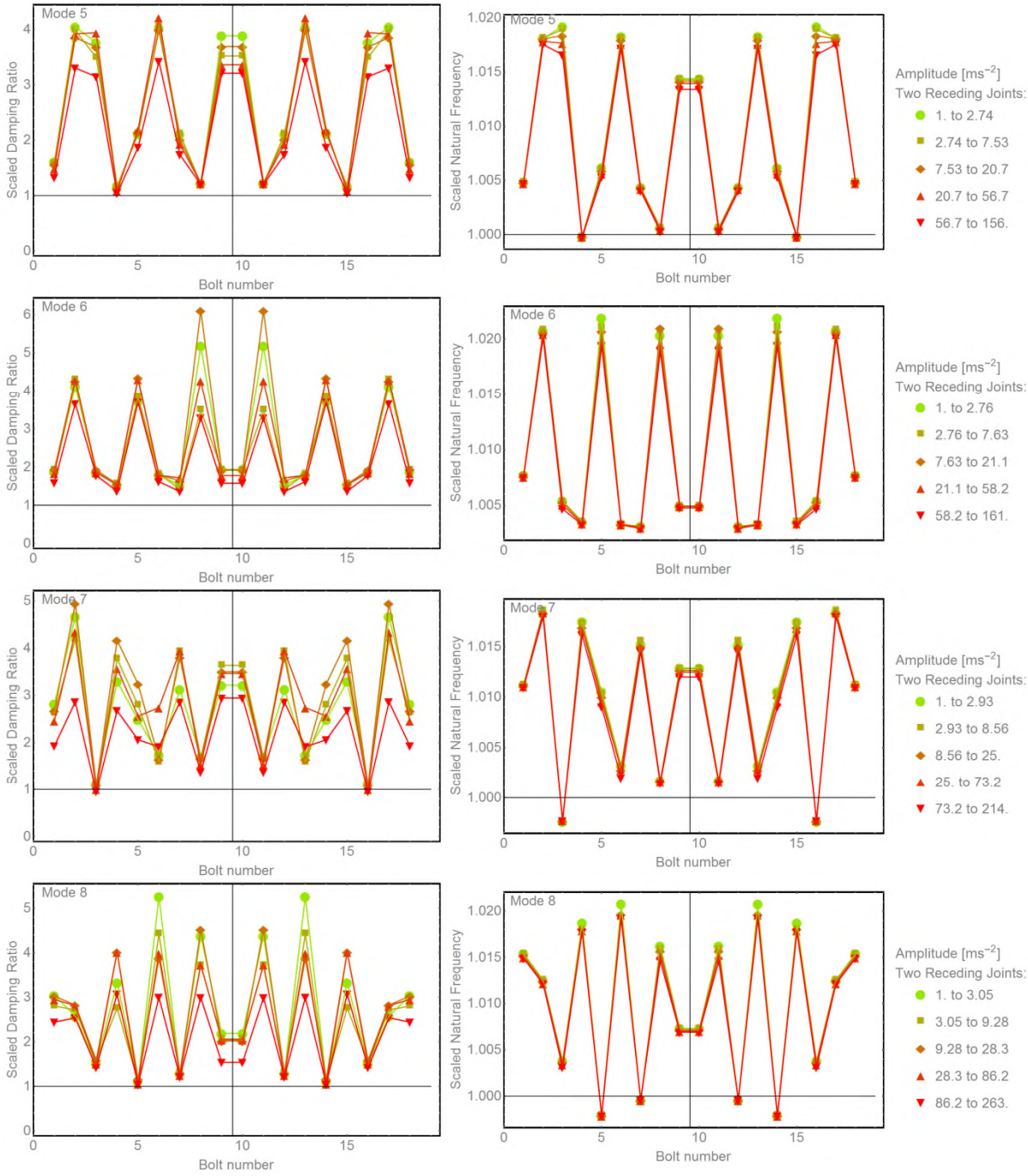

Figure 131 Scaled damping ratios and scaled natural frequencies depending on the position of two symmetrical receding contacts for mode 5 to 8. This grid of plots follows the same template as Figure 126.

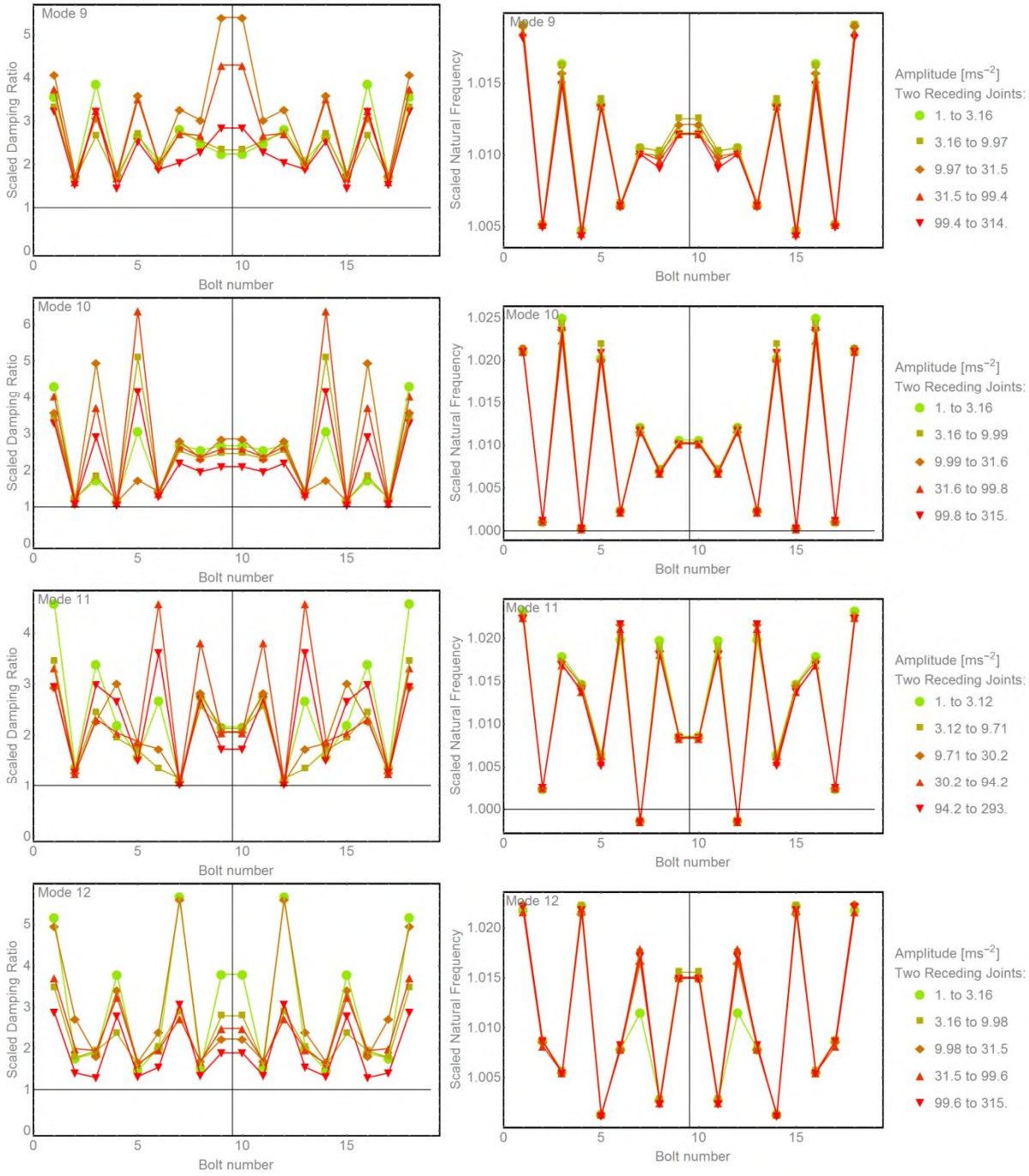

Figure 132 Scaled damping ratios and scaled natural frequencies depending on the position of two symmetrical receding contacts for mode 9 to 12. This grid of plots follows the same template as Figure 126.

Once again, as in the previous Section 6.2, Figure 130, Figure 131 and Figure 132 are perfectly symmetrical due to the way the data is displayed, not because of two separate measurements of behaviour. The tests of shims were symmetrical;

therefore the data points were symmetrically duplicated and each point is displayed twice.

Figure 130, Figure 131 and Figure 132 display the scaled damping ratio and scaled natural frequency. The scaled data corresponds to the ratio between the value measured for the AllComplete1 test and the tests with two receding contacts, for each amplitude range of value (see the legend).

The damping data points are grouped. In other words, the amplitude does not impact the scaled damping ratio. For this observation, it can be assumed that adding two receding contacts amplifies the weaker nonlinear damping behaviour linked to the amplitude of the AllComplete1 test. This amplification, created by adding two receding contacts follows a wave pattern as described in Section 6.2, for all modes less than 8. However, when the data is plotted with the scaled data, the frequency waves and the damping waves are very similar.

The range of scaled natural frequencies is the same for all modes with a value between 1 and 1.025. This observation means that the stiffening of the structure, observed in Section 6.2, is increasing the natural frequency by 2% for all modes, following the wave pattern. The range of scaled damping ratio is more erratic. The minimum value is at 0.8 (mode 1) but for the rest of the data set, the scaled damping ratio is greater than 1. The maximum value varies between mode: 3.4 (mode 4), 5 (mode 7) and even 6 (mode 6). Thus, the damping ratio has a more erratic behaviour than the natural frequency.

There are data points which do not follow the pattern described before, for example B08&B11 (receding contacts at the bolt number 8 and the bolt number 11) for mode 6. Though, the most intriguing ones are two exceptional behaviours of the first mode. First, the tests B08&B11 has a stronger damping and stiffening effect than B09&B10, which creates a “cat” silhouette different from the wave shape everywhere else. Also, for the first mode, the damping seems to decrease for the three tests at the extremities: B01&B18, B02&B17 and B03&B16. That could be due to the variability between assemblies which for that test increases the damping ratio of the AllComplete1 test and lower the damping ratio of the other cases. Because of those data points, two AllComplete tests were performed as references for the one

receding joint experiment (Experiement2), one at the beginning and one at the end. Those two tests, AllComplete2 and AllComplete2Bis, allow a comparison between before and after the multiple disassembly and reassembly necessary to perform this experiment.

Summary observation: Two receding joints scaled data:

- Once again, the data is symmetrical due to the way it is plotted.
- The scaled data is the tests with two receding contacts divided by the AllComplete1 test
- The scaled damping ratio seems independent of the amplitude. Therefore, adding a receding contact could amplify the nonlinear behaviour of the AllComplete1 test
- Wave patterns exist for both damping and frequency
- The range of scaled natural frequencies is between 100% and 102% whereas the scaled damping ratio is erratically recorded between 0.8 and 6.
- Two noticeable variations exist from the wave pattern for mode 1.

6.4 Experimental result: Damping and frequency for one receding contact

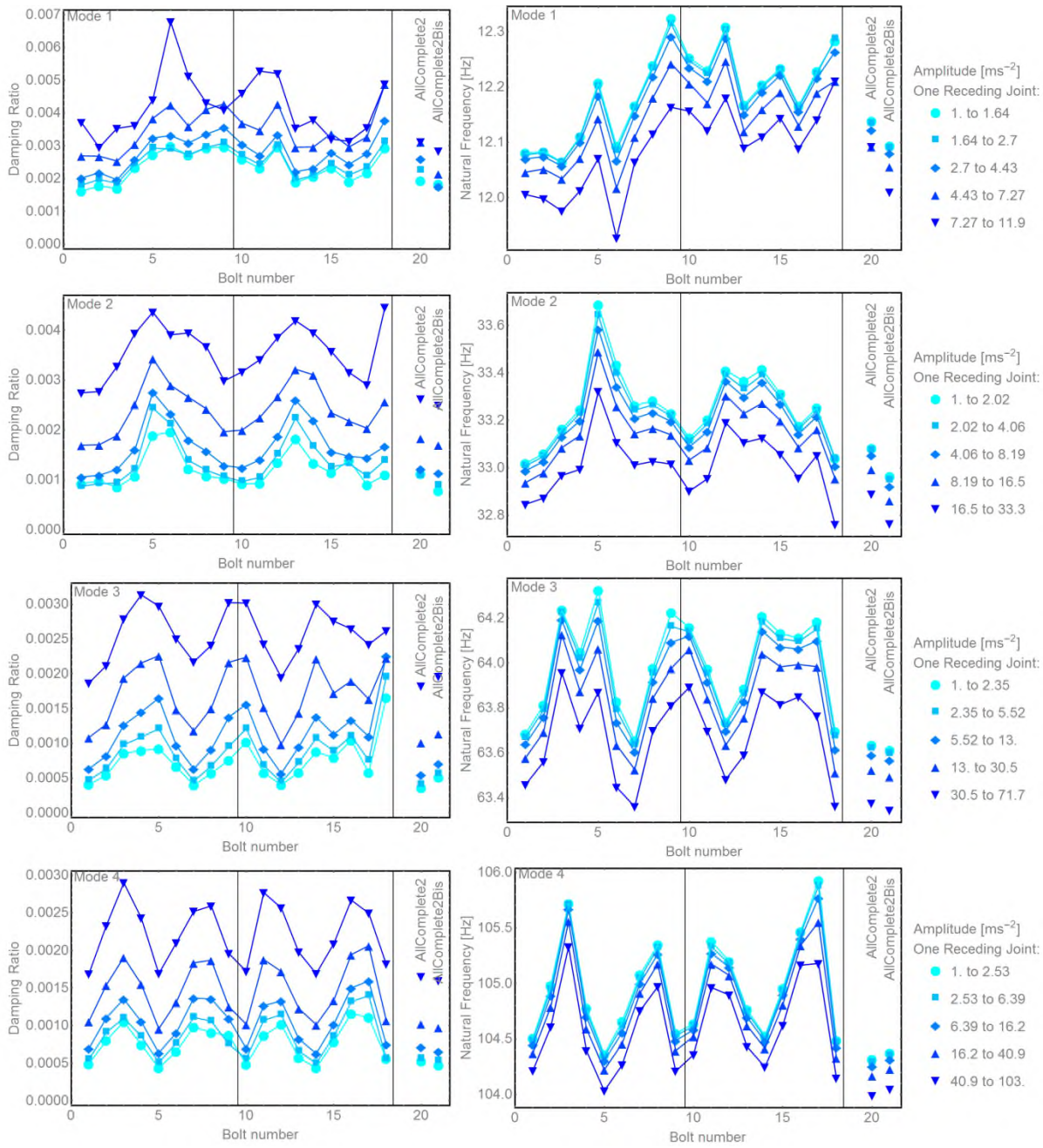

Figure 133 Damping ratios and natural frequencies depending on the position of two symmetrical receding contacts for modes 1 to 4. This grid of plots follows the same template as Figure 125.

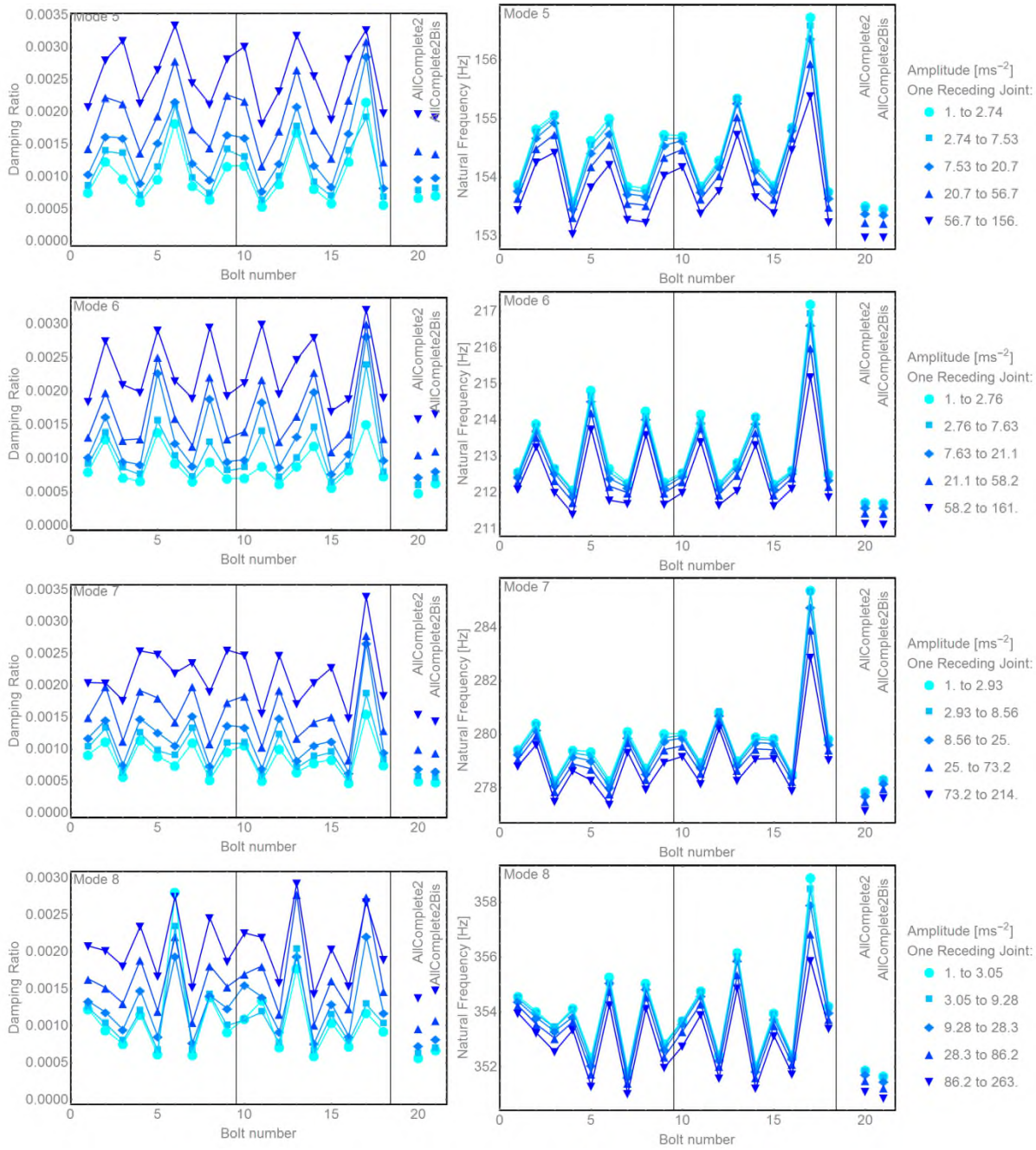

Figure 134 Damping ratios and natural frequencies depending on the position of two symmetrical receding contacts for modes 5 to 8. This grid of plots follows the same template as Figure 125.

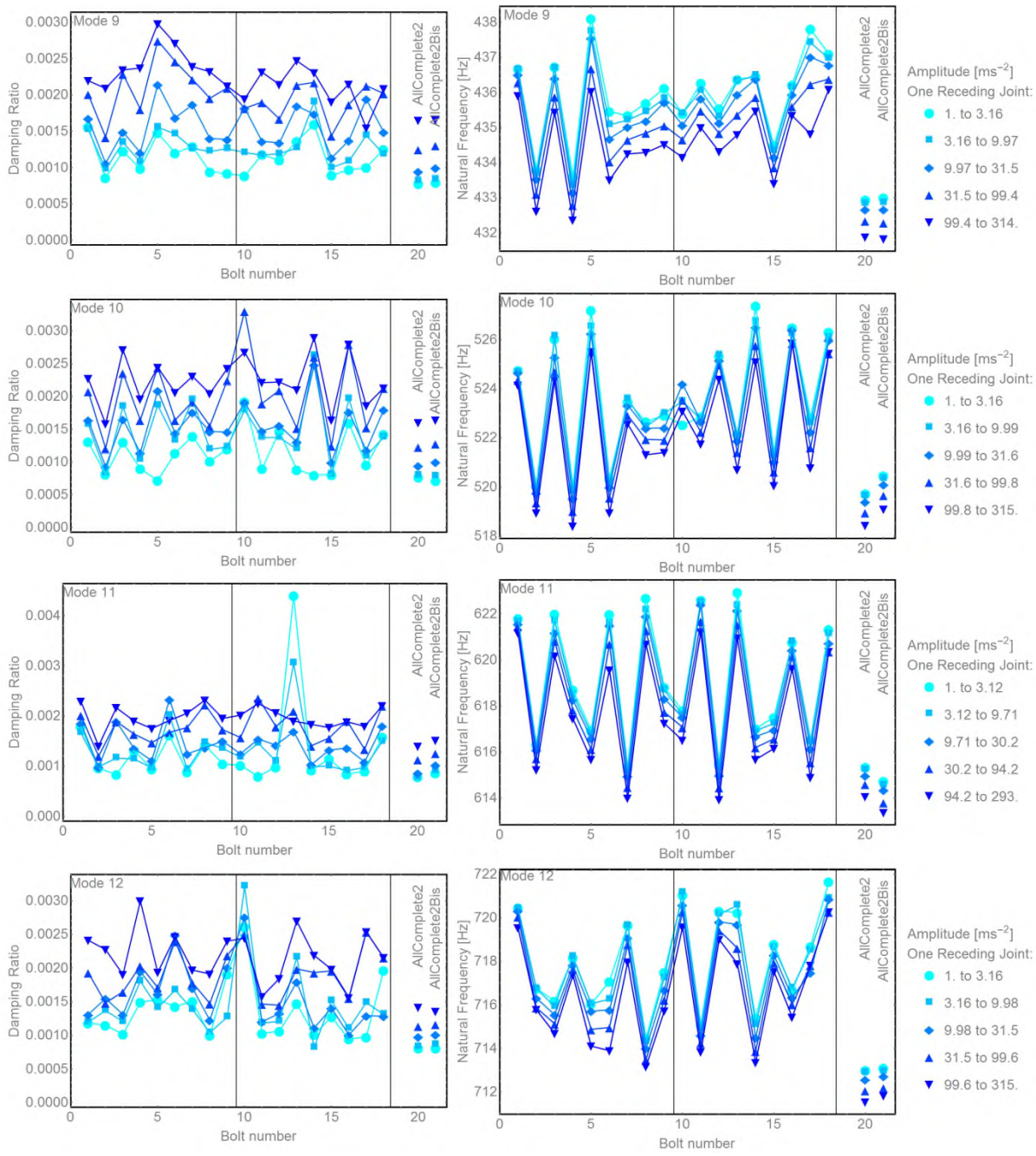

Figure 135 Damping ratios and natural frequencies depending on the position of two symmetrical receding contacts for modes 9 to 12. This grid of plots follows the same template as Figure 125.

For all modes and all tests, the beam seems to have the same nonlinear behaviour: the damping decreases and simultaneously the natural frequency increases when the amplitude decays. This nonlinear behaviour was already measured on the sandwich beam. The only exception is B06, and B13 at mode 8 where the damping is stronger at low amplitude compared to high amplitude.

For all the modes and almost all cases, the two ‘AllComplete’ tests have the lowest damping ratio and lowest natural frequencies. Removing one shim, to transform a complete contact into a receding contact, amplifies the nonlinear behaviour described in the previous paragraph. This amplification seems correlated to the receding contact location and the number of the mode.

A wave pattern can be observed which resembles the mode shapes of a free-free beam.

There is a small difference between the two ‘AllComplete’ tests. This shows that the experiment has an inherent variability between assemblies, but the effect of a receding contact seems more significant. As written previously, the two AllComplete’ tests were performed before and after all of the tests with one receding contact. The test AllComplete2Bis was used to scale the data.

Test B17 has an exceptionally large damping and a higher frequency for all the modes higher than 4. Test B18 has large damping ratio for mode 1 to 3.

Summary of observations for the damping and frequency: one receding joint:

- Consistent nonlinear behaviour: the damping and frequency increases when the amplitude decays
- The two ‘AllComplete’ tests have a smaller damping ratio and smaller natural frequencies compared to the other tests
- The tests with one receding contact have in most cases a more intense nonlinear behaviour than the ‘AllComplete’ tests only with complete contacts everywhere
- Exceptional behaviour is recorded for B17 and B18 at specific modes and amplitude levels

6.5 Experimental result: scaled results for one receding contact

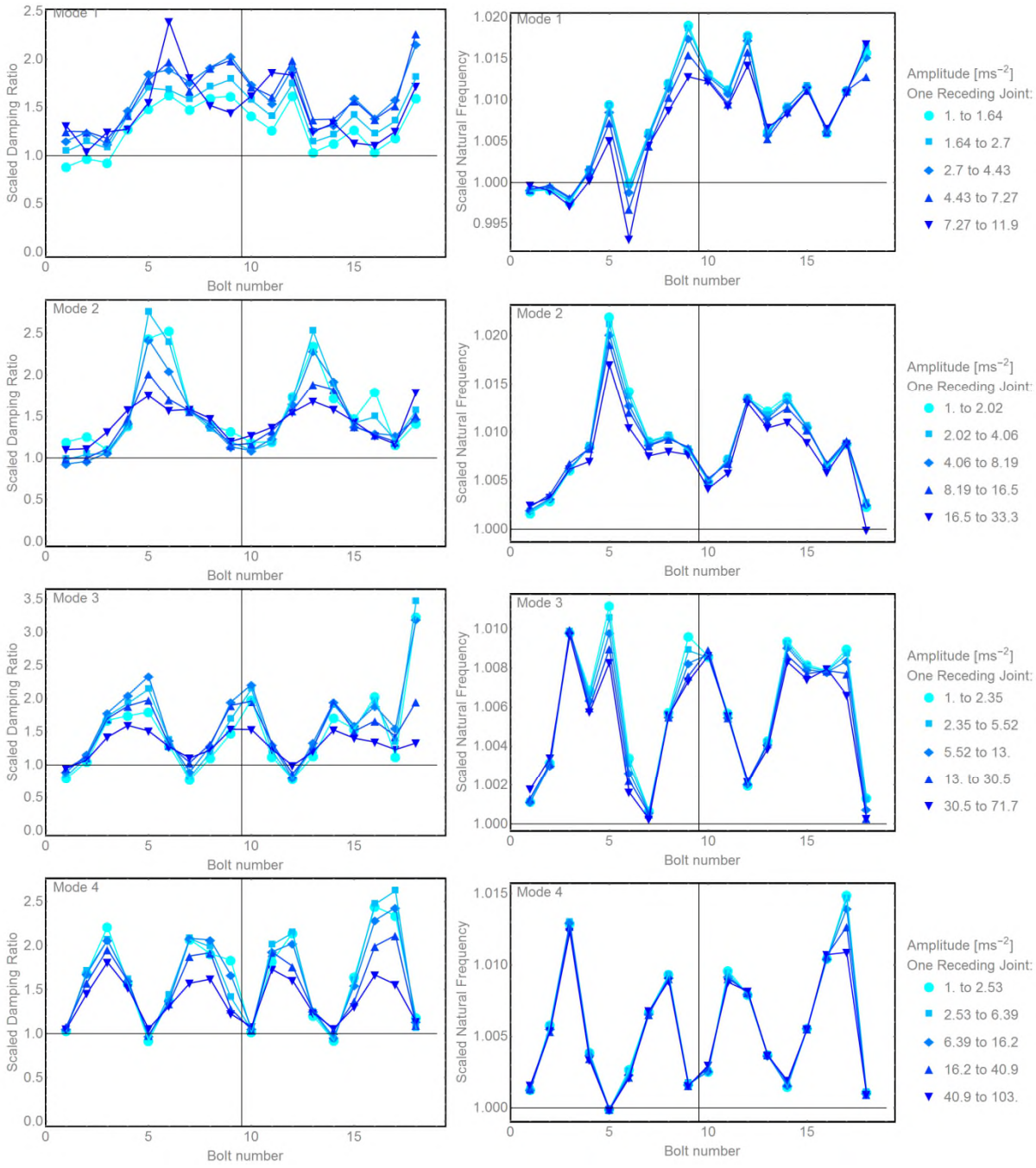

Figure 136 Scaled damping ratios and scaled natural frequencies depending on the position of a single receding contact for modes 1 to 4. This grid of plots follows the same template as Figure 126.

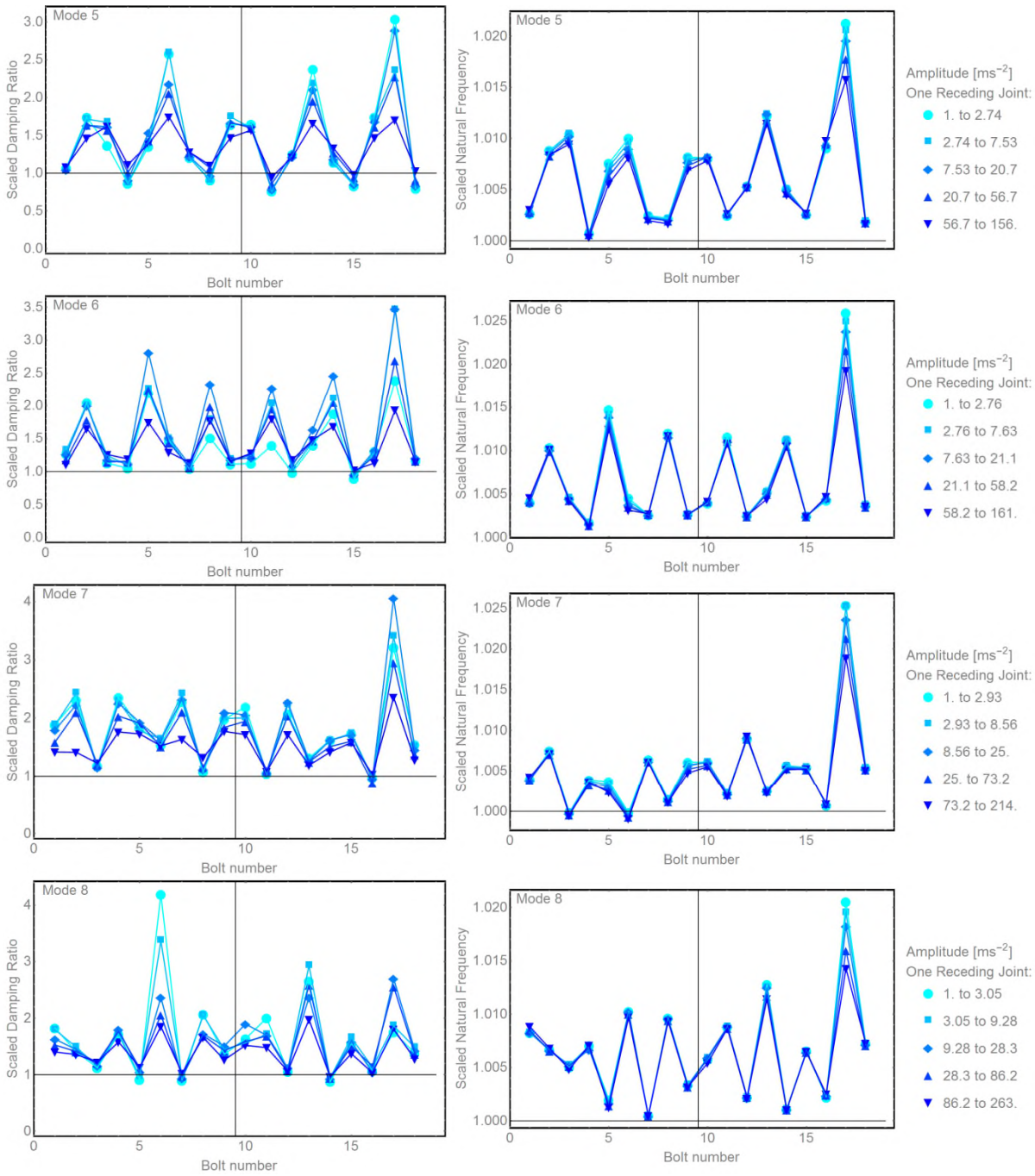

Figure 137 Scaled damping ratios and scaled natural frequencies depending on the position of a single receding contact for modes 5 to 8. This grid of plots follows the same template as Figure 126.

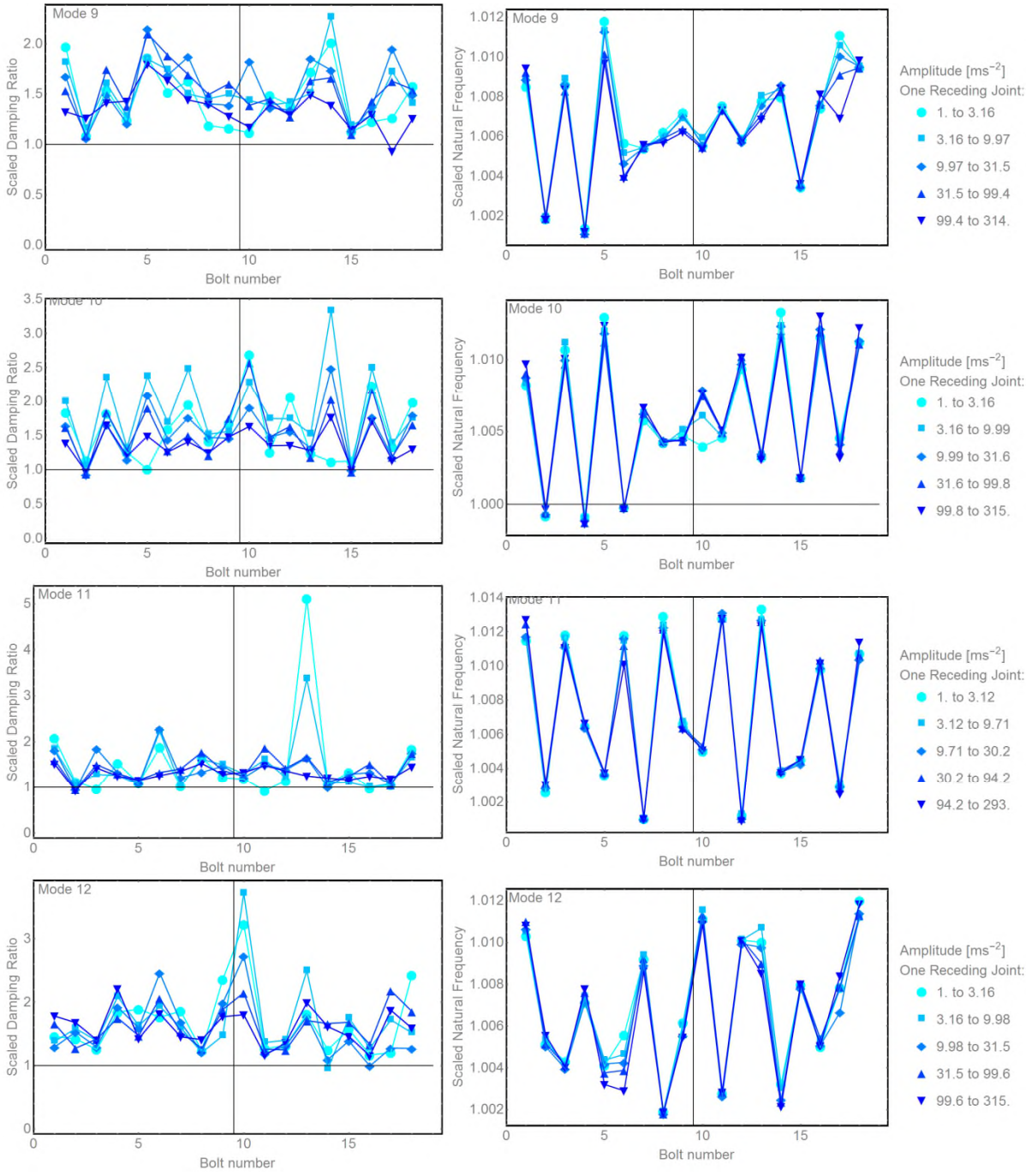

Figure 138 Scaled damping ratios and scaled natural frequencies depending on the position of a single receding contact for mode 9 to 12. This grid of plots follows the same template as Figure 126.

The amplitude does not seem to influence the scaled data, in most cases. Indeed, the scaled data stays globally the same for all the five amplitude intervals.

There is a clear similarity of behaviour between the scaled damping ratios and the scaled natural frequencies for each mode.

The points create a pattern of a semi-sinusoidal or a half wave shape, with the same number of half wave shapes as the mode number. This is less readable at a higher mode, due to there being a smaller number of bolts compared to the mode number (example 18 bolt locations for mode number 12), in short, spatial aliasing.

The range of scaled damping ratio is between 1 and 2 and exceptionally at 3 or 0.8, whatever the mode. The scaled natural frequency varies between 100% and 101%, with exceptional cases at 102% and 99.5%.

Scaled data stays surprisingly within the same range of values in most modes. This range of value is between 1 and 2.5 for the damping. For the scaled natural frequencies the range of values is between 1 and 1.0125 (B17 excluded). Therefore, the damping ratios change 125 times more than the natural frequencies or around two orders of magnitude more. Calculation: (2.5-1) / (1.0125-1) = 125.

The previous observations have multiple exceptions. The damping, for the modes higher than mode 8, does not seem to follow the consistency of the frequency. The strongest deviation is observed for B17 and B18. Please note that the hammer hits were performed next to B18. Also B05, B06, B13 has some erratic values, for example, the damping of mode eight. Note that the suspensions were placed between to B05, B06 and between B13 and B14. Finally, the scaled damping ratios and the scaled natural frequencies (but less frequently) seems correlated to the amplitude especially for B17 at multiple modes.

Summary observation for the scaled data: one receding joint:

- The scaled data seems independent of the amplitude
- The data follows a wave pattern
- There are the same number of waves as the mode number
- The scaled damping has value between one and three with multiple exceptions
- The scaled natural frequency follows the same trend as the damping but with around two orders of magnitude smaller change in value.

- Erratic behaviour for modes higher than 8.
- Exceptional behaviour for B05, B06, B13 closed to the position of the suspension
- Also, exceptional behaviour for B17 and B18 at specific modes or amplitude levels. B17 and B18 are the two positions closest to the hammer impact location.

6.6 Synthesis of the experimental results of Chapter 6

Table 15 Summary of the experimental results of the joint position experiment

Experiment name	Experiment 1				Experiment 2			
Number of receding contact	Two receding contacts placed symmetrically compared to the center of the beam				One receding contact			
Tests names	AllComplete1, B01&B18, B02&B17, B03&B16, B04&B15, B05&B14, B06&B13, B07&B12, B08&B11, B09&B10, AllReceding1				AllComplete2, B01, B02, B03, B04, B05, B06, B07, B08, B09, B11, B12, B13, B14, B15, B16, B17, B18, AllComplete2Bis			
Y-axis of the plots	Damping Ratio	Natural Frequency [Hz]	Scaled Damping Ratio	Scaled Natural Frequency	Damping Ratio	Natural Frequency [Hz]	Scaled Damping Ratio	Scaled Natural Frequency
Behaviour when the amplitude decrease	Decrease	Increase	Constant	Constant	Decrease	Increase	Constant	Constant
Wave pattern	Amplitude dependent	Amplitude dependent	Yes	Yes	Amplitude dependent	Amplitude dependent	Yes	Yes
Range of values for the Y axis	0.0005 to 0.0035	12.25 Hz to 750 Hz	0.8 to 6	0.999 to 1.025	0.0004 to 0.007	11.95 Hz to 722 Hz	0.95 to 5	0.991 to 1.025
Exceptional tests	B08&B11	B08&B11	B01&B18, B02&B17, B03&B16, B08&B11	B08&B11	B06, B13, B17, B18	B17	B05, B06, B13, B17, B18	B17
Noisy modes	9, 10, 11 and 12		9, 10, 11 and 12		9, 10, 11 and 12	1, 2, 3	8, 9, 10, 11 and 12	1, 2, 3

Table 15 was created to synthesise the experimental results of the joint position experiment. To understand Table 15, five observations, linked to the five last rows of Table 15, are given in the five following paragraphs. After that, three observations are provided this time based on the three columns divisions of Table 15. There is some redundancy between the row observations and the column observations.

First row, this experiment follows the same amplitude dependent nonlinear behaviour as the one measured in Chapter 3: When the amplitude of vibration decreases, the instantaneous damping ratio decrease and the instantaneous natural frequency increases.

Second row, a wave pattern can be observed across all the experimental data for modes less than mode 9. In another words, the transformation between a complete contact and a receding contact show an amplification of the nonlinear behaviour of a joint following a wave pattern. This wave pattern exhibits as many waves as the mode number. Moreover, the two amplitude dependant phenomenon, described before, are amplified following the wave pattern.

Third row, the range of value of the damping ratio, and the range of value of scaled data either for the damping ratio or the natural frequency are remarkably limited across the 12 modes investigated.

Forth row, some tests seem to indicate that the position of the suspension or the location of the hammer hits could have an impact on the nonlinear behaviour of a receding contact.

Fifth row, modes larger than 8 have a noisy behaviour. Also the first three modes, for the tests with one receding contact, are not following the trend of the other modes.

First column division between Experiment 1 and Experiment 2, the trend of the tests with two receding contacts are similar to the results with one receding contact. However, the detailed results are not directly comparable.

Second column division between scaled and unscaled data, the notion of scaled data helps the interpretation of the experimental results. The notion of scaled data was introduced in Section 6.1.5. The scaled damping ratio or the scaled natural

frequency is calculated by dividing the data with one or two receding contacts by the corresponding data with a complete contact. Using scaled data shows a display of the experimental results in clusters. When scaled, the natural frequencies have the same range of values across all modes, which is remarkable. Furthermore, with the scaled data the correlation between the damping ratio and the natural frequency is clear.

Third column divisions between damping ratio and natural frequency, there are two clear correlations between the measured damping ratio and the measured natural frequency. Primarily, when the amplitude decreases, the natural frequency increases, simultaneously the damping ratio decreases. Secondly, both the damping ratio and the natural frequency have the same wave pattern, linked to the position of the joint. Also, the results linked to the damping ratio have more chaotic behaviour than the results with the natural frequency. Indeed, the damping ratio results have more exceptional tests and noisy modes than the natural frequency results.

6.7 Conclusion of Chapter 6

The joint location experiments identified a correlated between the position of a joint in a built-up structure and its nonlinear dynamic behaviour.

The position of the joints was investigated by changing the position of a receding contact. Washer size shims were introduced in the interface to change the receding contacts of multiple lap joints into complete contacts. By placing washer size shims at all location except one, in a beam with 18 identical bolted lap joints, the location of the joint could be changed in a comparable way. By comparing the tests with complete contact everywhere with the tests with receding contacts, the effect of the position of a joint on the dynamic behaviour was investigated.

An amplitude dependent behaviour was measured for the damping ratio and the natural frequency. The damping ratio decreased when the amplitude decreased. Simultaneously, the natural frequency increased when the amplitude decreased. The intensity of the amplitude dependent behaviour changes depending of the position of the joints. This change of intensity follows a wave pattern, with as many waves as the mode number.

Two separate experiments, named Experiment 1 and Experiment 2, were conducted. In Experiment 1, the positions of two symmetrically placed receding contacts were investigated. Experiment 2 investigated the effect of the position of one receding contact. The component beams, were resurfaced between the two experiments. This resurfacing changed the rigidity and the mass of each component beam. This resurfacing also changes the surface finish thus the dissipation of energy in each joint. Therefore, the value of damping ratio and natural frequency of the two experiments are not directly comparable, so two different names were used. However, the scaled data is comparable

7 SIMULATIONS

This chapter describes two simulations which help to understand the results of the joint position experiment better. The first simulation, presented in Section 7.1, is a unidimensional beam model. In Section 7.2, this unidimensional beam model was used to fit the experimental results of the previous chapter. The second simulation, described in Section 7.3, is a finite element analysis of the structure tested experimentally. A synthesis of all the results, experimental and the two models, linked to the joint position experiment is then presented in Section 7.4, Section 7.5 and Section 7.6. Finally, Section 7.8 concludes the joint position experiment.

7.1 Comparison between beam theory and experimental data

Now that the experimental results have been plotted, it is possible to compare the experimental result with the classic beam theory. Bishop and Johnson (1960) explain how to calculate the theoretical displacement (or mode shape) for each mode for a free-free beam. The shear force is obtained by derivation of the displacement function with respect to the position, as described in the literature review chapter in Subsection 2.1.4 Static Beam theory. Moreover, the bending moment is the derivative of the shear force.

This beam theory model gives an analytical equation for the displacement, shear force and bending moment at any place in a beam. However, this model supposes that the beam has a uniformed cross-section which is approximately the case for the joint position experiment.

The results of the comparison between the experimental results and the beam theory are plotted in Figure 139. The beam theory curves are unscaled; therefore they do not need a Y-axis.

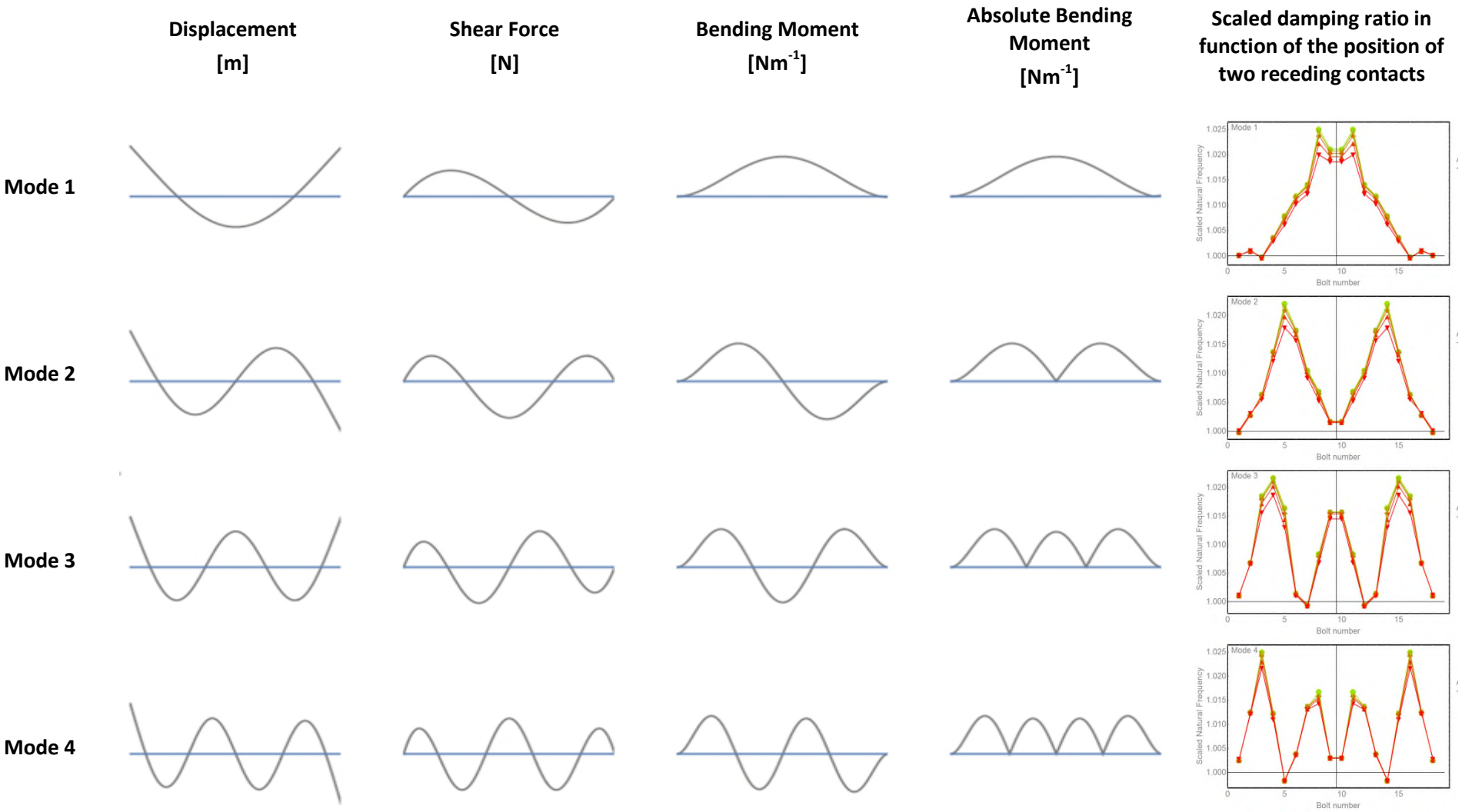

Figure 139 Comparison between beam theory (columns one to four) and the experimental result (fifth column, source: Figure 130).

It is clear, from Figure 139, that the scaled damping ratio is correlated to the absolute bending moment, as defined in the beam theory model, and not the shear force or the mode shape.

The interpretation of this correlation between bending moment and scaled damping ratio is given in Chapter 8 Discussion.

7.2 Fitting of the experimental data set using the absolute bending moment

Table 16 Nomenclature for Subsection 7.2 and 10.3Appendix C in the order of definition

Variable	Definition	Unit
x_b	Position on the beam	$[m]$
$B(\lambda, x_b)$	unscaled-absolute-bending-moment function	$[Nm]$
λ	Solutions of Equation (7-2)	$[m^{-1}]$
l	Length of the beam	$[m]$
M	First fitting variable for data display using the damping ratio or the natural frequency	$[no\ unit]$ $or\ [Hz]$
N	Second fitting variable for data display using the damping ratio or the natural frequency	$[no\ unit]$ $or\ [Hz]$
P	Third fitting variable used to scale the absolute bending moment model based on the scaled data set	$[no\ unit]$
$FitScalDampTwo$	Fitted variable P from the data set of the scaled damping ratio with two receding contact	$[no\ unit]$
$FitScalDampOne$	Fitted variable P from the data set of the scaled damping ratio with one receding contact	$[no\ unit]$
$FitScalFreqTwo$	Fitted variable P from the data set of the scaled natural frequency with two receding contact	$[no\ unit]$
$FitScalFreqOne$	Fitted variable P from the data set of the scaled natural frequency with one receding contact	$[no\ unit]$

From the equation for the bending moment given by Bishop and Johnson (1960), the unscaled-absolute-bending-moment function can be defined as:

$$B(\lambda, x_b) \coloneqq \tag{7-1}$$

$$\left|\cosh(\lambda x_b) - \cos(\lambda x_b) - \frac{\cosh(\lambda l) + \cos(\lambda l)}{\sinh(\lambda l) - \sin(\lambda l)}\left(\sinh(\lambda x_b) - \sin(\lambda x_b)\right)\right|$$

$$with\ \{\lambda, x_b\} \in \mathbb{R}^2$$

$$and\ l = 1.79m\ or\ 19.4444\ bolt - number - unit$$

(). The variable x is the position on the beam. The variable l corresponds to the length of the beam investigated. The variable λ is defined as the real solution of the equation:

$$\mathrm{Cos}[x]\mathrm{Cosh}[x] - 1 = 0 \tag{7-2}$$

Table 17 Calculated value of λ for the 12 first bending modes

Mode Number	λ
1	0.243259238
2	0.403879095
3	0.565488403
4	0.727054225
5	0.888621925
6	1.050189544
7	1.211757166
8	1.373324789
9	1.534892411
10	1.696460033
11	1.858027655
12	2.019595277

The model defined in Equation (7-3) was used to fit the experimental value of damping ratio and natural frequency. The real variable C and D were fitted using all the experimental values with one receding contact or two receding contacts. The 'AllComplete' tests were not included in the fitting.

$$M * B(\lambda, x) + N \quad with\ M * N \in \mathbb{R}^2 \tag{7-3}$$

The model defined in Equation (7-4) was used to fit the scaled damping ratio and the scaled natural frequency. This time only the variable P was fitted using

all the scaled data of each test. It was assumed that the scaled data was equal to one at both extremities of the beam.

$$P * B(\lambda, x) + 1 \; with \; P \in \mathbb{R} \quad \textbf{(7-4)}$$

All the fitting results are displayed with the experimental data in the synthesis plots in Section 7.5 and Section 7.6. Also, the exact values found for the fitted variables ‘M’ and ‘N’ are in 10.3Appendix C. Furthermore, the exact values found for the fitted variable ‘E’ are in 10.3Appendix C.

7.3 Finite element model analysis

A Finite Element Method (FEM) analysis was conducted to simulate the natural frequencies of the beam. This simulation digitally mirrors the procedure described in Chapter 6.

This frequency analysis simulates the mode shapes and the natural frequencies. The uses of mode shapes help to visualise the behaviour of the structure at each mode, whereas the natural frequencies can easily be compared with the values measured experimentally.

A more advanced nonlinear analysis could have achieved an estimation of the damping ratio of each mode. A nonlinear simulation was not conducted for the following two reasons: Firstly, no successful nonlinear simulation of the damping of joint was found in the literature and, secondly, the author had a limited time to learn how to use the complex software necessary to perform a nonlinear analysis. The author estimated that two years were necessary to achieve some results with a nonlinear analysis. Also, a nonlinear analysis would have necessitated the need for an expensive software licence. On the other hand, a simple linear frequency analysis using SOLIDWORKS (Dassault Systemes) was achievable in the time frame, the license was already in place, and the author had already performed this type of analysis in the past. Also, SOLIDWORKS is used by numerous designers of structures; therefore if a method worked on that software, it would be directly useful for the target audience of this work.

Table 18 Parameters used in the FEM analysis

	Mass density	Elastic modulus	Simulated volume
Small beam	7500 kgm^{-3}	1.80 E 11 Nm^{-2}	4.93657e-05 m^3
Nut	6900 kgm^{-3}	1.95 E 11 Nm^{-2}	1.41107e-06 m^3
Bolt	6600 kgm^{-3}	1.95 E 11 Nm^{-2}	5.41051e-06 m^3
Shim	8400 kgm^{-3}	1.95 E 11 Nm^{-2}	2.35619e-08 m^3
Washer	6000 kgm^{-3}	1.95 E 11 Nm^{-2}	2.98824e-07 m^3

The frequency analysis uses as input the geometry, the mass density and the elastic modulus. The geometry of all the components is defined in Section 6.1.2. The only difference is the use of a shim of 0.1mm instead of 0.05mm in real life. This adjustment was necessary because the computer used for the simulation could not perform the simulation with a mesh precision of 0.05mm. The values used for the mass density and the elastic modulus are displayed in Table 18. The mass density was deduced from the weight of the part and the simulated volume. An elastic modulus (also called Young's modulus) of 1.8 $\times 10^{11}$ Nm^{-2} (180MPa) for the small beams was used. This value of 180MPa was found by matching the first simulated natural frequency and the first measured natural frequency of one small beam, using a trial-and-error procedure. The default elastic modulus of steel given by SOLIDWORKS was used for the other components.

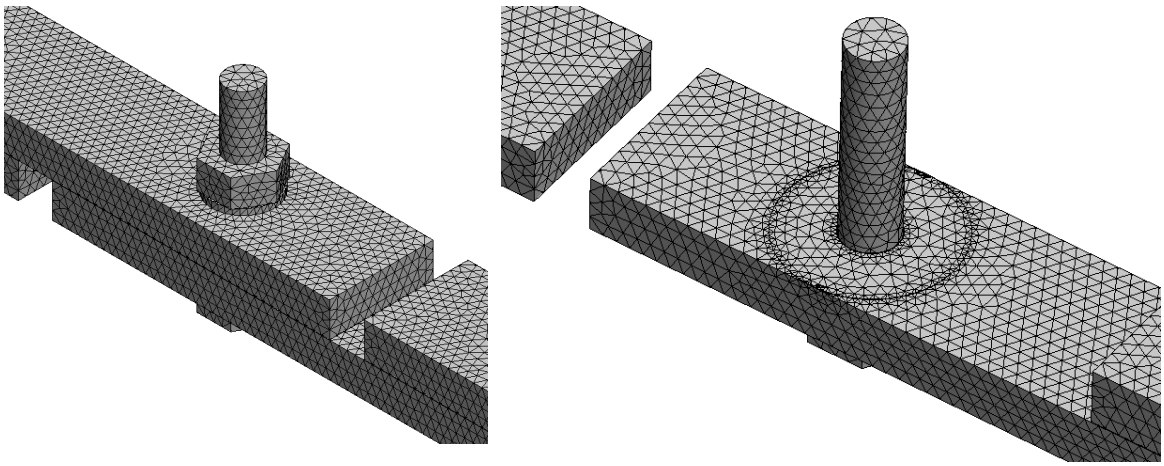

Figure 140 Two close-ups of the 3.6 million D.O.F. mesh used. One beam was removed, to show the mesh at the interface in a receding contact for the image on the right.

Table 19 List of the tests simulated

Complete contacts everywhere	Two receding contacts	One receding contact
FE_AllComplete1	B01&B18, B02&B17, B03&B16, B04&B15, B05&B14, B06&B13, B07&B12, B08&B11, B09&B10	B01, B02, B03, B04, B05, B06, B07, B08, B09, B11, B12, B13, B14, B15, B16, B17, B18

In total, 28 tests of shims were simulated as listed in Table 19. One SOLIDWORKS assembly file was created and duplicated 28 times to simplify the execution of the 28 FEM simulation. This assembly file was composed of all the components as described in Subsections 6.1.2. All the components were bound together using the “global contact” setting.

A special method was used to create either a complete contact or a receding contact at the interface. At the interface of every lap joint, two shims of 20mm or 30mm of diameter by 0.1mm thickness were placed at the same position. The value of 30 mm for the diameter of the receding contact was estimated from a pressure film test which measured the constraint across the interface. To create a complete contact, the 20 mm diameter shim stayed in place and the 30 mm diameter shim was removed from the simulation, see Figure 141 (1). Conversely, if a receding contact was needed the 30 mm diameter shims remained, and the 20 mm diameter shim was deleted, see Figure 141 (2). This method avoids the human error associated with the manual, repetitive disassembly and reassembly of each joint in the software.

However, this method increased the thickness at the joint by 0.1mm for receding contacts compared to the real structure where no shims were used. This increase in thickness of 0.1mm is thought to have a negligible effect.

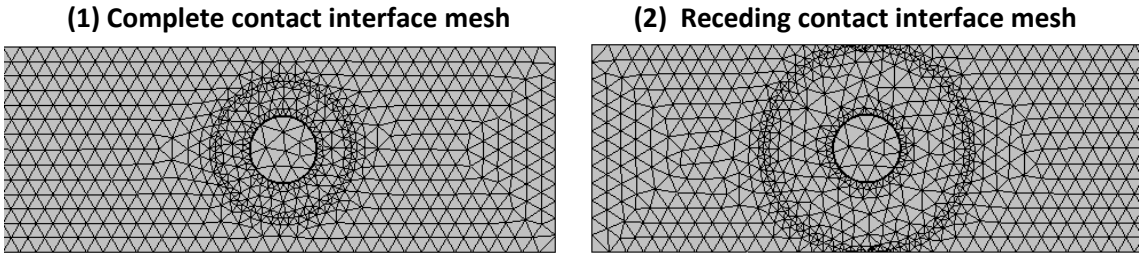

Figure 141 The two meshes used at the interface of a lap joint to simulated a complete contact and a receding contact. A 0.1 mm thick shim of 20mm (1) or 30mm (2) diameter was used to change the lap joint interface mesh.

As explained before, numerical shims of 0.1 mm of thickness were used instead of 0.05mm thick of the physical experiment because the computer used could not run a mesh with a 0.05mm precision. Therefore, the thickness of the shim was doubled as a compromise.

The natural frequencies were simulated. The same post-treatment of the frequencies were carried out following the post processing of the experimental data. The natural frequency of each tests with receding contact were divided by the simulated natural frequency of the FE_Allcomplete1 case. The name "FE_Allcomplete1" is a contraction of "Finite Element analysis with all the joint positions with complete contacts linked to Experiement1". Each mode shape of each test was visually categorised to isolate only the bending mode. The mode shapes simulated are very closed to the beam theory, as shown in Table 20, which confirmed that the current experimental structure could be modeled as a beam.

Table 20 The 12 first simulated bending mode shapes from the Ref FEM test. The colour blue, green, yellow and red represents respectively no, small, medium and large displacement compared to a neutral position.

Mode number	Simulated Mode shape	Mode number	Simulated Mode shape
1	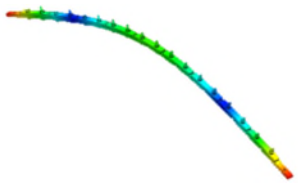	7	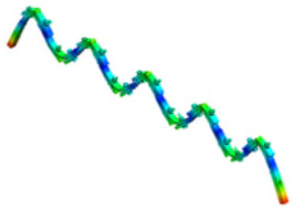
2	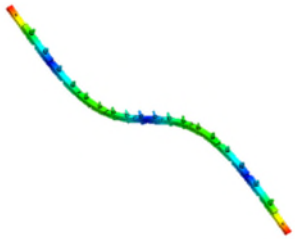	8	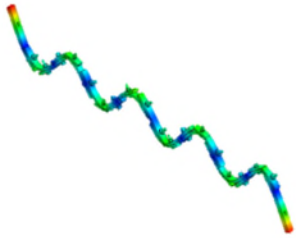
3	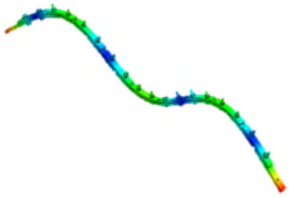	9	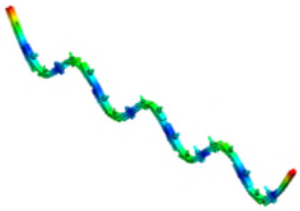
4	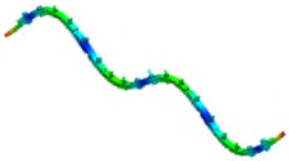	10	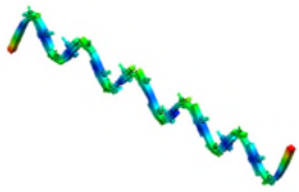
5	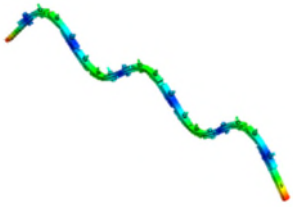	11	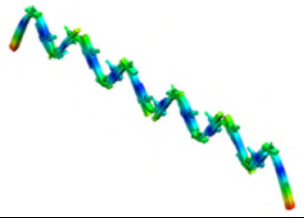
6	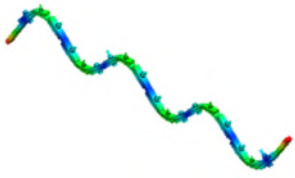	12	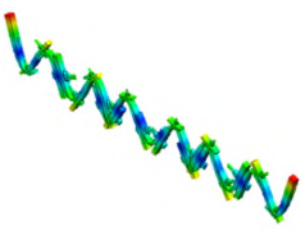

Another interesting observation, true for all the simulated mode shapes, is the way the small beams interpenetrate or get separated at the antinode of the mode shapes, but not at the extremities or the nodes. An example of the way the small beams interpenetrate or get separated is shown in Figure 164.

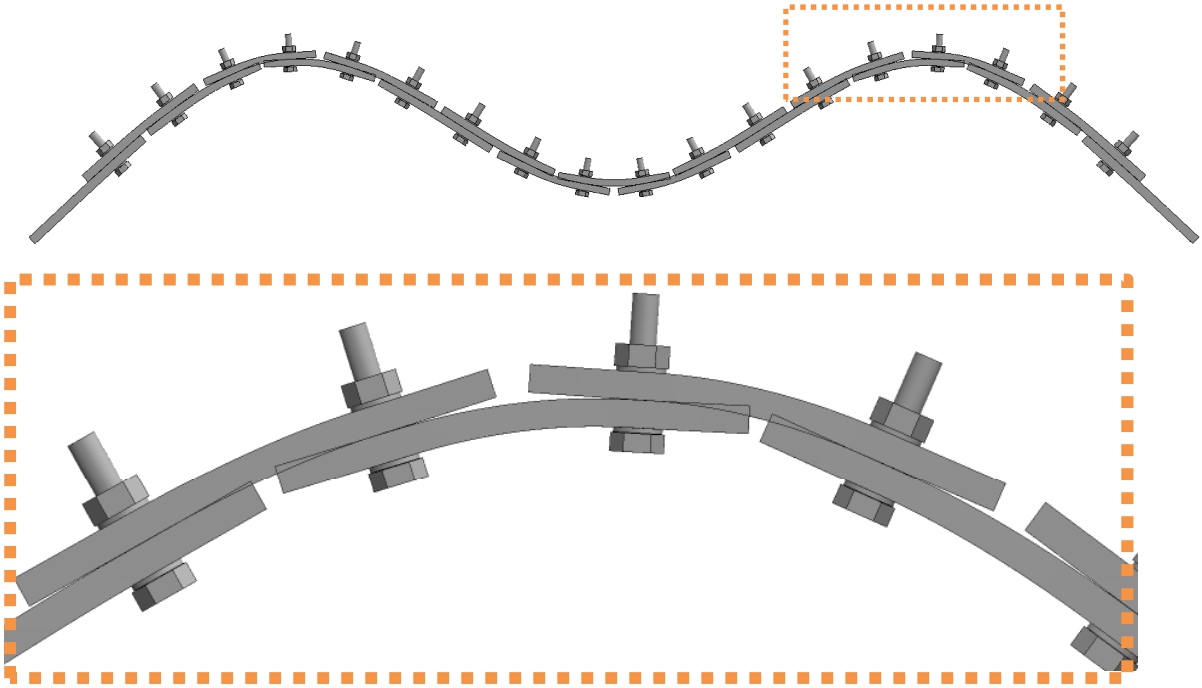

Figure 142 Two views of the mode shape of the third bending mode of the Ref FEM test. It is noticeable that the joints at the anti-node of the mode shape have their interface which open and close up. At the opposite, the interface at the nodes and the interface at the extremities seem to stay still.

The results for the natural frequencies from the FEM analysis are plotted in Section 7.4, Section 7.5 and Section 7.6 with the experimental data and absolute bending moment model fitted. The simulated resulted are described in those sections in comparison with the other data sets. The raw values of simulated natural frequency are also given in Table 21 and Table 22.

Table 21 FEM analysis result for two receding joint (natural frequency in Hz)

Mode #	1	2	3	4	5	6	7	8	9	10	11	12
B01&B18	12.044	33.661	65.369	106.94	158.08	218.48	287.80	365.62	451.50	543.50	641.84	742.37
B02&B17	12.108	33.733	65.652	107.81	159.85	220.90	289.64	364.89	446.27	534.19	630.98	733.91
B03&B16	12.272	33.861	66.120	108.50	159.59	218.27	285.22	362.31	449.42	542.57	638.14	732.11
B04&B15	12.411	33.990	66.370	107.79	157.66	217.81	288.79	366.20	446.47	534.12	636.14	741.29
B05&B14	12.120	34.102	66.055	106.82	158.39	220.36	287.21	361.22	449.33	541.98	632.40	730.90
B06&B13	12.519	34.154	65.495	107.17	159.79	218.05	286.05	366.69	447.04	535.15	640.25	734.01
B07&B12	12.509	33.726	65.336	108.15	158.39	217.92	289.43	361.62	448.70	540.50	630.28	740.11
B08&B11	12.198	33.754	65.705	107.95	157.64	220.39	285.47	365.63	447.36	536.93	638.97	729.61
B09&B10	12.585	33.687	66.158	106.93	159.44	217.96	288.23	363.28	448.48	538.39	634.69	737.40
Ref FEM	12.094	33.599	65.339	106.74	157.50	217.13	285.11	361.00	444.27	533.61	629.73	728.36

Table 22 FEM analysis result for one receding joint (natural frequency in Hz)

Mode #	1	2	3	4	5	6	7	8	9	10	11	12
B01	12.245	33.686	65.321	106.82	157.78	217.79	286.42	363.26	447.79	538.46	635.65	735.25
B02	12.432	33.677	65.449	107.24	158.62	218.95	287.31	362.86	445.14	533.70	630.09	730.79
B03	12.528	33.746	65.714	107.64	158.58	217.75	285.22	361.70	446.86	538.16	634.10	730.36
B04	12.357	33.852	65.824	107.27	157.57	217.45	286.90	363.60	445.35	533.80	632.72	734.64
B05	12.561	33.933	65.654	106.76	157.93	218.72	286.17	361.07	446.68	537.82	631.02	729.48
B06	12.306	33.926	65.424	106.94	158.63	217.59	285.55	363.79	445.66	534.31	634.77	731.25
B07	12.331	33.833	65.323	107.44	157.95	217.50	287.27	361.28	446.34	537.15	629.90	733.92
B08	12.270	33.785	65.487	107.34	157.56	218.74	285.27	363.19	445.85	535.12	634.47	728.86
B09	12.519	33.681	65.730	106.83	158.43	217.55	286.57	362.17	446.20	536.13	631.92	733.15
B10	12.231	33.622	65.736	106.84	158.43	217.55	286.57	362.17	446.19	536.12	631.92	733.14
B11	12.574	33.729	65.479	107.34	157.56	218.74	285.28	363.20	445.86	535.13	634.48	728.87
B12	12.425	33.832	65.317	107.44	157.95	217.50	287.27	361.28	446.34	537.14	629.91	733.92
B13	12.389	33.914	65.395	106.95	158.64	217.59	285.55	363.79	445.67	534.32	634.78	731.26
B14	12.258	33.916	65.687	106.76	157.93	218.72	286.17	361.08	446.68	537.80	631.02	729.47
B15	12.334	33.851	65.833	107.26	157.57	217.45	286.90	363.60	445.36	533.80	632.72	734.65
B16	12.217	33.765	65.728	107.61	158.55	217.70	285.15	361.62	446.75	538.01	633.94	730.16
B17	12.244	33.709	65.471	107.27	158.65	218.99	287.37	362.94	445.23	533.83	630.25	730.98
B18	12.203	33.687	65.330	106.83	157.78	217.79	286.43	363.26	447.80	538.47	635.67	735.26
Ref FEM	12.094	33.599	65.339	106.74	157.50	217.13	285.11	361.00	444.27	533.61	629.73	728.36

The simulated value of natural frequencies displayed in Table 21 and Table 22 are interesting because they are quickly calculated. Indeed, a six-year-old high-standard laptop computer took less than an hour to calculate the natural frequencies of one test with a mesh of three millions degree of freedoms with SOLIDWORKS 2018. The computer's processor used was an Intel Core i7-4810MQ CPU at 2.80 GHz, 4 cores, 8 Threads helped by 16GB of RAM. In addition a software macro for the FEM analysis described here seems relatively easy to program.

More importantly, the natural frequencies displayed in Table 21 and Table 22, if realistic, quantifies the impact of a change of joint design on the dynamic nonlinear behaviour of lap joints. The simulated natural frequencies correspond to multiple positions and multiple modes. The data set of the simulated natural frequencies displayed in Table 21 and Table 22 is extremely valuable for an engineer, as this data set could allow prediction of the impact of a structure design upgrade.

In conclusion, a FEM analysis was conducted. The mode shapes and natural frequencies of all the tests of the joint position experiments were simulated. The type of contact, either complete contact or receding contact, was simulated by changing the diameter of a shim placed in the interface. The simulated mode shapes confirmed that the structure investigated in the joint position experiment could be modelled as a beam. More importantly, the simulated values of natural frequency, if realistic, have the potential to predict the dynamic nonlinear behaviour linked to lap joints.

7.4 Synthesis of results: template of the plots

Figure 143 and Figure 144 are the templates for the plots used in Section 7.5 and Section 7.6 respectively. These two templates limit the size of the caption below each figure of Section 7.5 and Section 7.6.

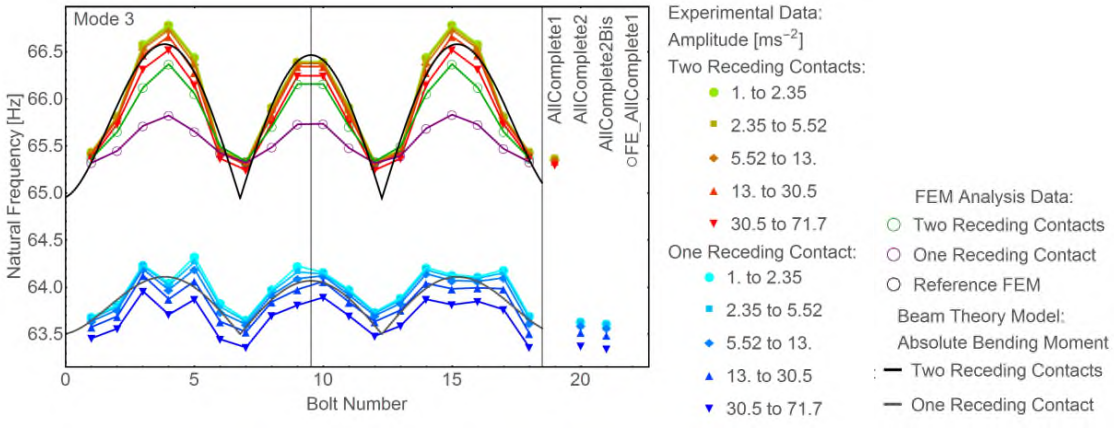

Figure 143 Template for the synthesis diagram of the experimental, fitted and simulated results for the natural frequencies and the damping ratio plots.

Figure 143 displays the natural frequency as a function of the position of one and two receding contacts for mode 3. The points are the experimentally measured values already presented in Chapter 6. On the right-hand side, the four ‘AllComplete’ tests are outlined. The circles correspond to the simulated results, see Section 7.3 for details. The experimental and simulated data sets are joined by lines to help the readability. The curved lines are the fitted absolute bending moment model, as explain in Section 7.2. The colour featured in the legend specifies the number of receding joints and the amplitude intervals. Once again, the data sets with two receding joints, either experimental or simulated, are displayed twice with a central symmetry represented by the vertical grey line.

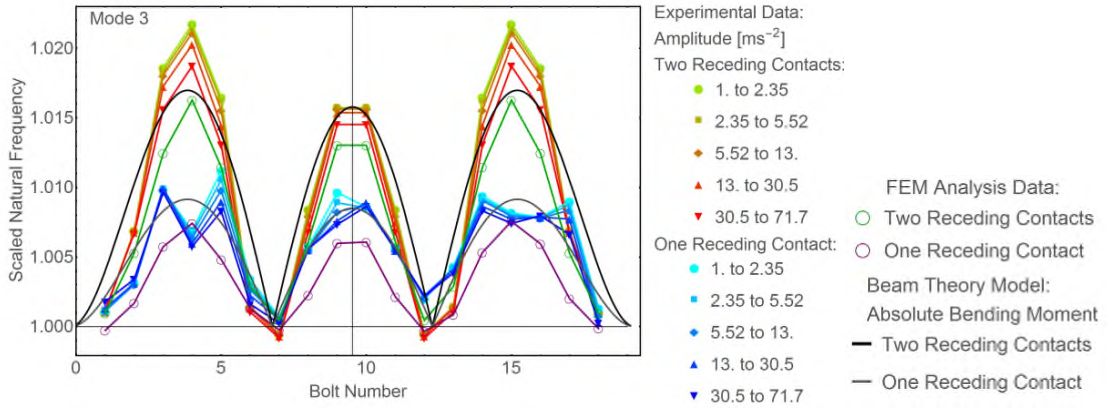

Figure 144 Template of the synthesis diagram for the experimental, fitted and simulated scaled data sets.

Figure 144 displays the scaled natural frequency as a function of the position of one and two receding contacts for mode 3. The scaled damping ratio and scaled natural frequency are defined in equations (6-2) and (6-3). The points represent the experimentally measured values already presented in Chapter 6. The curved lines are the fitted absolute bending moment model as explained in Section 7.2. The circles correspond to the simulated results, see Section 7.3 for details. The experimental and simulated data sets are joined by lines to help the readability. The colour signifies the number of receding joints and the amplitude intervals as detailed in the legend. Again, the data sets with two receding joints,

either experimental or simulated, are displayed twice with a central symmetry represented by the vertical grey line.

7.5 Synthesis of results: damping ratio and natural frequency

Figure 145, Figure 146, Figure 147, Figure 148, Figure 149 and Figure 150 present a synthesis of the results of the joint location experiments. These figures display all the experimental results, all the simulated results and the fitted model. The left column of plots represents the damping ratio. The right column of plots is the natural frequency. Each row is one bending mode, see the top left corner of each plot for the mode number. The 12 first bending modes are analysed. Two modes are displayed in each figure.

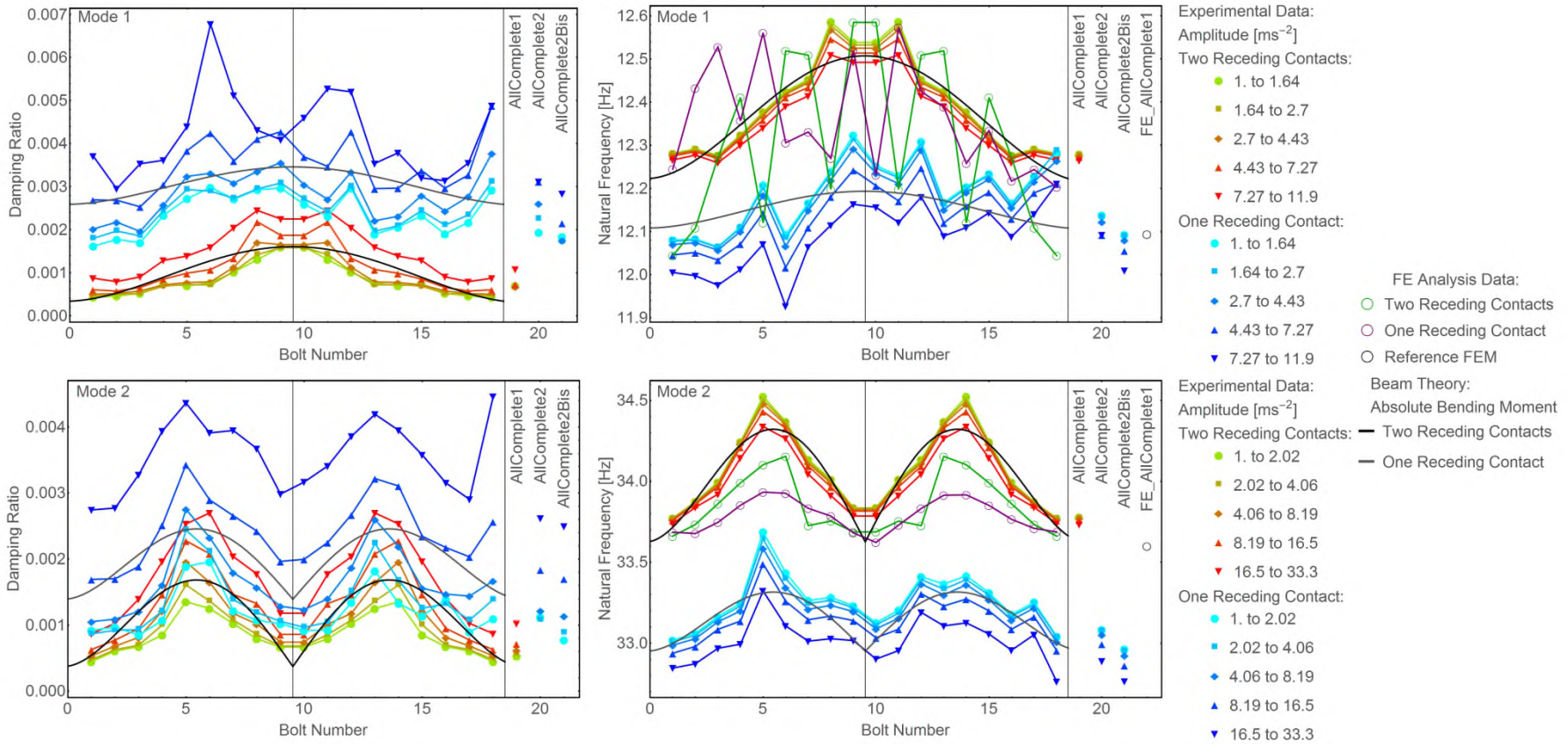

Figure 145 Synthesis of results: Damping ratios and natural frequencies for modes 1 and 2. This grid of plots follows the template in Figure 143.

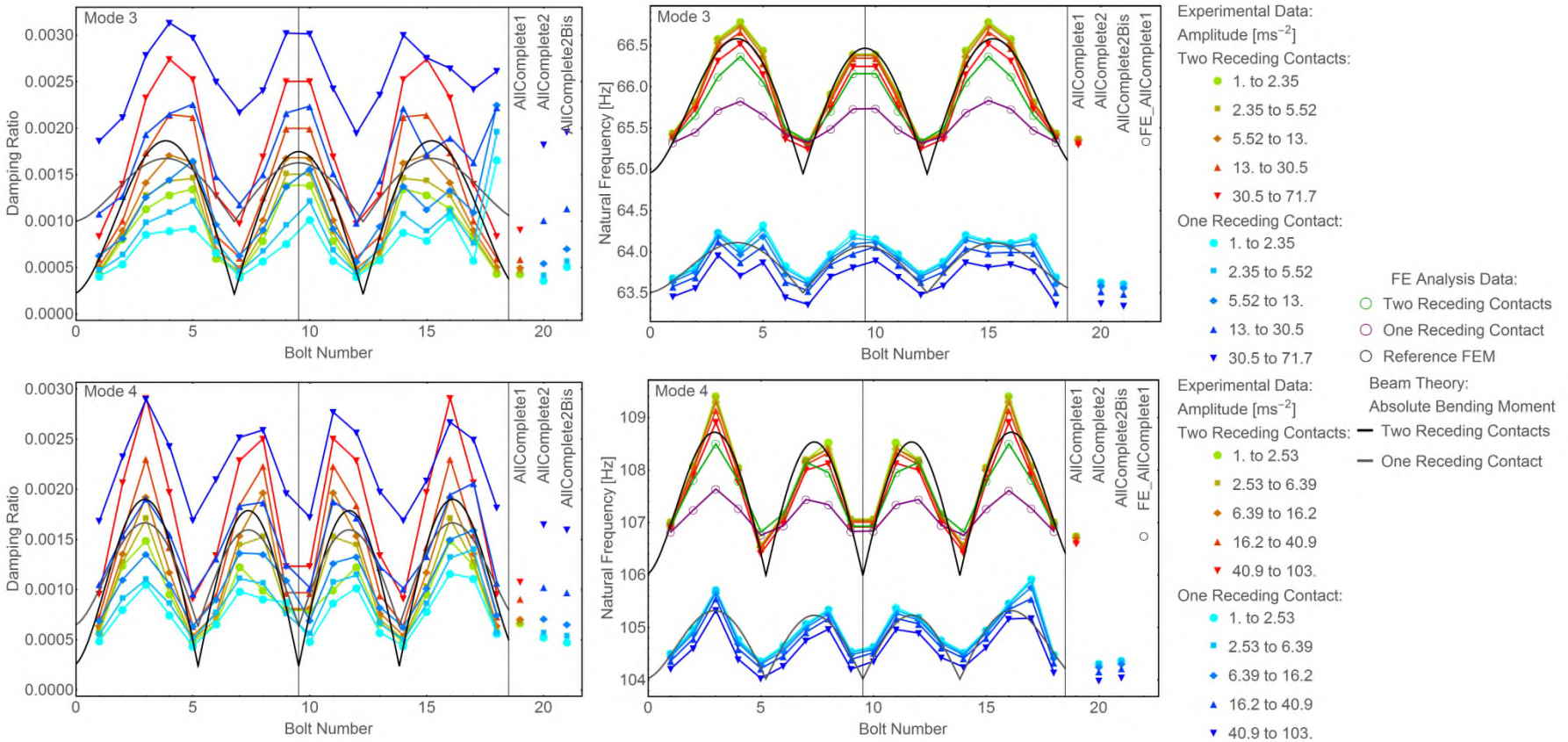

Figure 146 Synthesis of results: Damping ratios and natural frequencies for modes 3 and 4. This grid of plots follows the template in Figure 143.

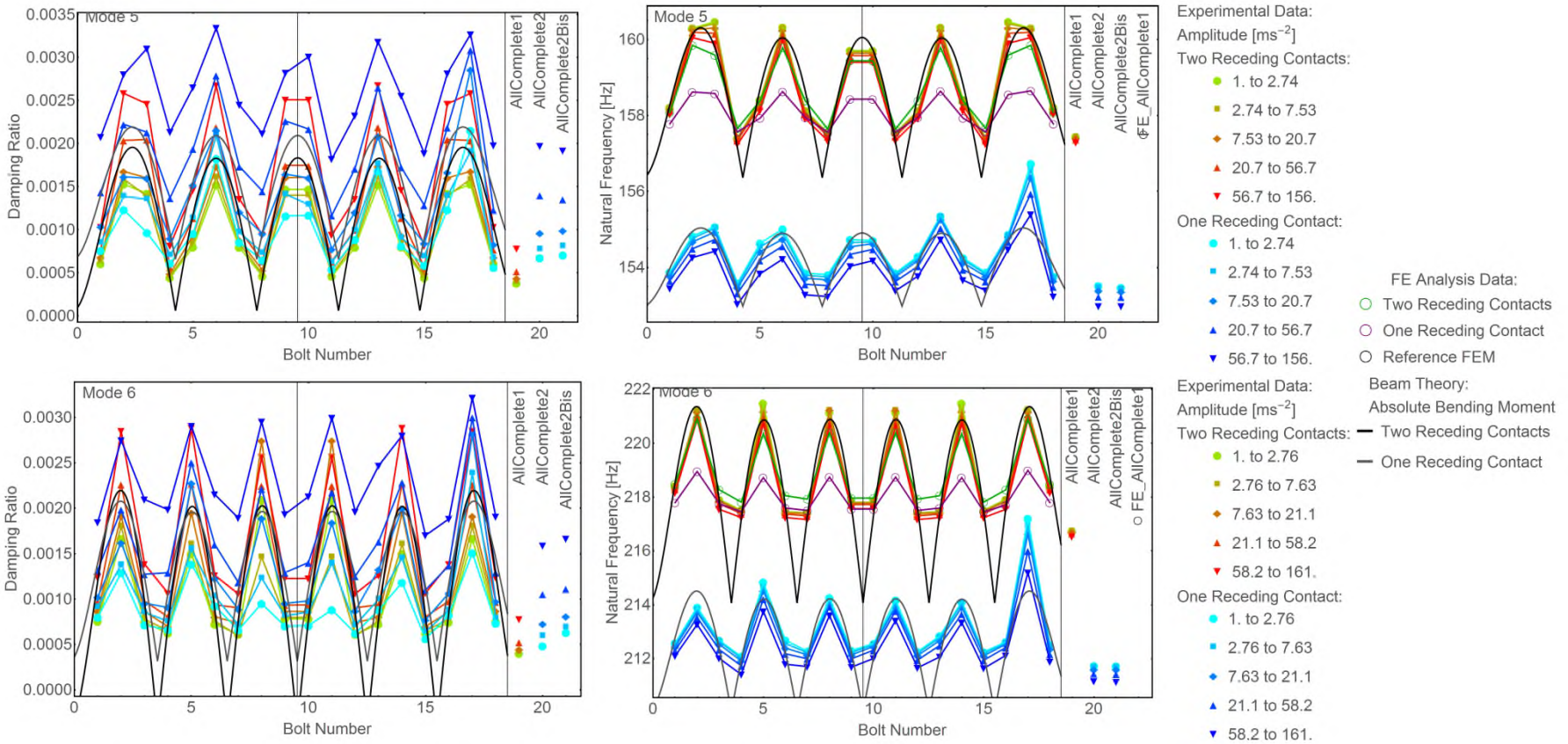

Figure 147 Synthesis of results: Damping ratio and natural frequency for modes 5 and 6. This grid of plots follows the Figure 143 template.

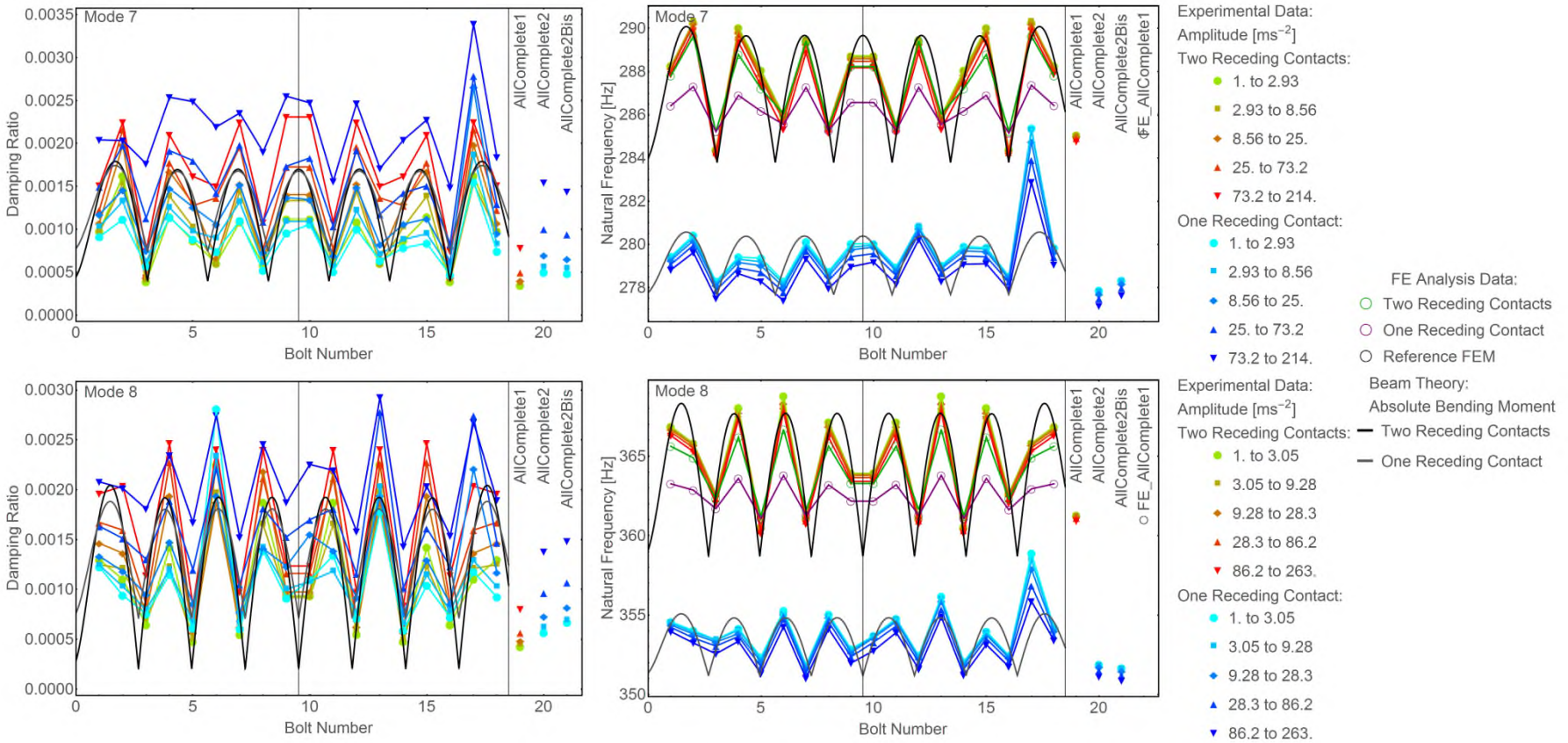

Figure 148 Synthesis of results: Damping ratio and natural frequency for modes 7 and 8. This grid of plots follows the Figure 143 template.

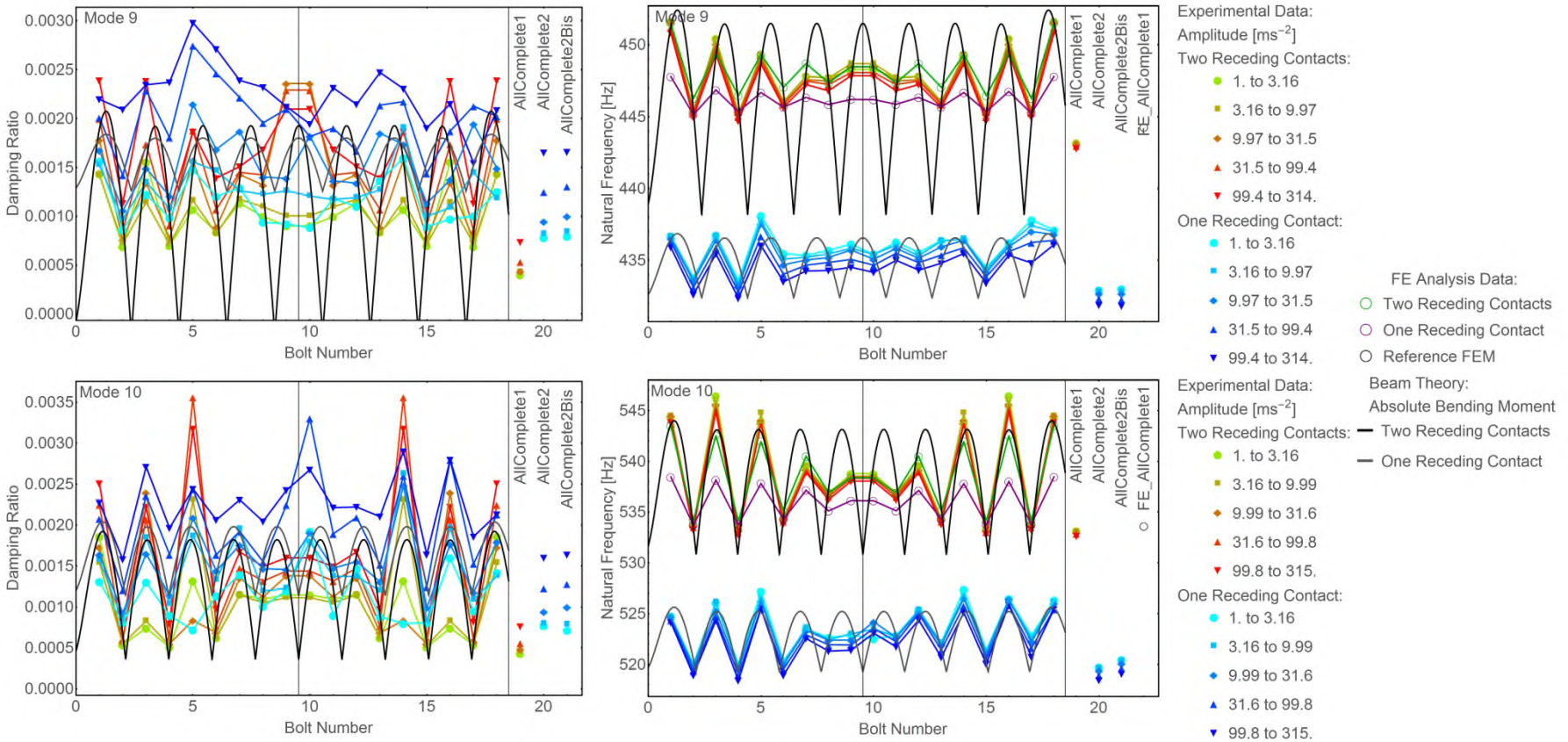

Figure 149 Synthesis of results: Damping ratio and natural frequency for modes 9 and 10. This grid of plots follows the Figure 143 template.

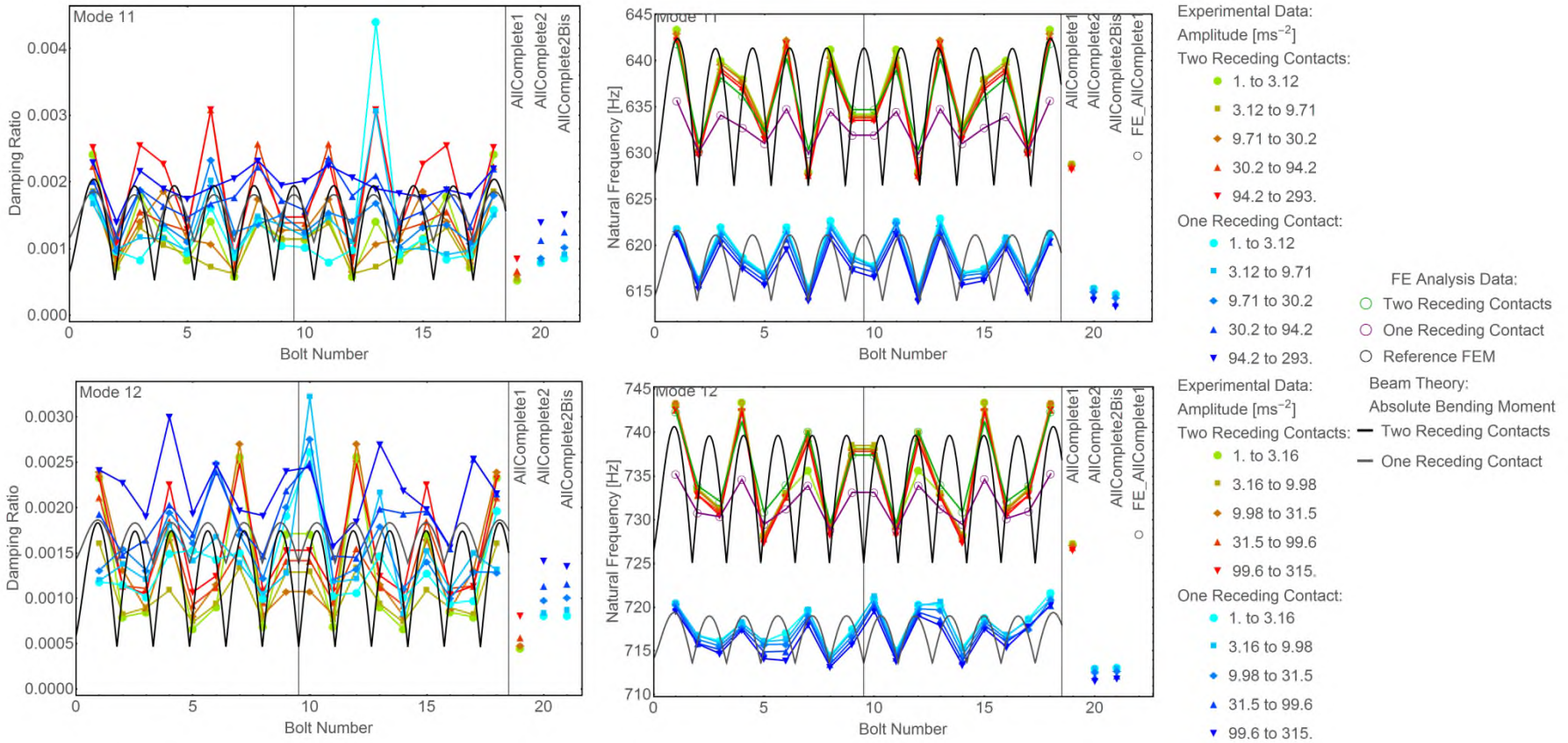

Figure 150 Synthesis of results: Damping ratios and natural frequencies for modes 11 and 12. This grid of plots follows the template in Figure 143.

Here are the observations which can be made on the results plotted in Figure 145, Figure 146, Figure 147, Figure 148, Figure 149 and Figure 150:

Observation across all modes:

- The simulated natural frequencies of the FEM analysis follow the wave pattern of the experimental values, except for mode one which is analysed separately:
    - For the two receding contacts the simulated values match almost perfectly every single experimental point with an error of less than 1%.
    - The results of one receding contact follow the same trend but with a consistent offset.
        - The offset can be explained as being due to the resurfacing. Indeed, the change of thickness was not implemented in the simulation. If the thickness of the beam was correctly changed, the simulated natural frequencies should also be accurate.
- AllComplete1 is different compared to AllComplete2 and AllComplete2Bis, whereas all AllComplete tests are only composed of complete contacts:
    - The values of damping ratio for AllComplete1 are smaller than the ones of AllComplete2 and AllComplete2Bis
    - The values of natural frequency for AllComplete1 are higher than the ones of AllComplete2 and AllComplete2Bis
    - The resurfacing between AllComplete1 and AllComplete2 and AllComplete2Bis could explain the two previous points:
        - The reduced thickness after the resurfacing of the small beams reduced the rigidity, therefore the overall natural frequency shifted.
        - The resurfacing probably improved the surface finish, therefore higher damping ratio values could be measured.

- The experimental damping ratios with one or two receding contacts are very similar. Once again, the resurfacing could be an influence.
- The measured damping ratio for each amplitude colour has the same wave pattern as the absolute bending moment model from the beam theory. However, the range of values of measured damping ratio is so important that fitting all measured data points of each mode at once does not make sense.

Observation for mode 1:

- For mode 1 only, the experimental damping ratios with two receding contacts are close to four times the experimental damping ratio values with one receding contact.
- The damping ratio and the natural frequencies from the experiments are chaotic for mode 1 and do not follow the same trend as the other modes.
- The simulated natural frequencies are as extraordinary as the experimental results:
    - The most disturbing observation is that the output of the FEM analysis with one receding contact does not show a central symmetry, whereas the input meshes had a perfect central symmetry. Strangely, two mirror meshes have two different values of simulated natural frequencies for this first mode only.
    - Surprisingly, one test with two receding contacts, B01&B18, has a smaller simulated natural frequency than AllComplete1 with complete contacts everywhere
    - The FEM natural frequencies are noisy for mode 1 and do not follow the same wave trend as the other modes
    - No explanation was found for these observations except numerical errors.

Observation for modes 9 to 12:

- For the natural frequency, the fitted model and the FEM results indicate that the experimental results are still following the wave pattern

- The experimental values of damping ratio are too noisy to allow any definite conclusion to be reached.

Focusing on the damping ratio, the main difference between the experimental data set with one or two receding contacts is the difference between AllComplete1 and AllComplete2 and AllComplete2Bis. The AllComplete tests are composed only of complete contacts, so, because there should be no friction, all three AllComplete tests should have a very small identical damping ratio. However, AllComplete1 has a smaller value of damping ratio than AllComplete2 and AllComplete2Bis for all the modes. Chronologically, the small beam was reused from another experiment. Then, AllComplete1 was performed just before the test with two receding contacts. After that, the beam was resurfaced and AllComplete2 and AllComplete2Bis were performed respectively before and after the tests with one receding contact. Therefore, the surface quality of AllComplete2 and AllComplete2Bis was guaranteed, whereas AllComplete1 may have some scratches on the surface of the small beams.

Due to the way the scaled data is calculated, all the experimental data points for two receding contacts, presented in Section 7.6, are only dependant on the AllComplete1 test. This dependency on the test AllComplete1 weakens all interpretations of the data set using the scaled data. The experimental results with two receding contacts presented in Section 7.6 should be considered with caution because these results are scaled. The scaled data is calculated using a reference, AllComplete1, which is not double checked. If this experiment were repeated, a repeatability test on the AllComplete tests would be performed, before and after each test with a receding contact. The variability of the ‘AllComplete’ test would be interesting to measure. Also, it would be possible to scale the data using the data of the ‘Allcomplete’ test performed just before the test with a receding contact.

7.6 Synthesis of results: scaled data

Figure 151 Figure 152 Figure 153 Figure 154 Figure 155 and Figure 156 present the same data set as in 7.5 but this time using the scaled damping ratio and the scaled natural frequency. These figures display all the experimental results, all the simulated results and the fitted model. The scaled data was defined in Section 6.1.5. As a reminder, the scaled data is calculated as follows: the damping ratio or natural frequency value of each amplitude interval of each test with a receding contact was divided by the corresponding AllComplete test value. The left column of plots represents the scaled damping ratio. The right column of plots is the scaled natural frequency. As explained before, AllComplete1 and AllComplete2Bis were used to scale the data of respectively Experiment 1 with two receding contacts and Experiment 2 with one receding contact. All the FEM results used only one AllComplete test, FE_AllComplete1.

Each row corresponds to one bending mode. The mode number is given in the top left corner of each plot. The 12 first bending modes were analysed.

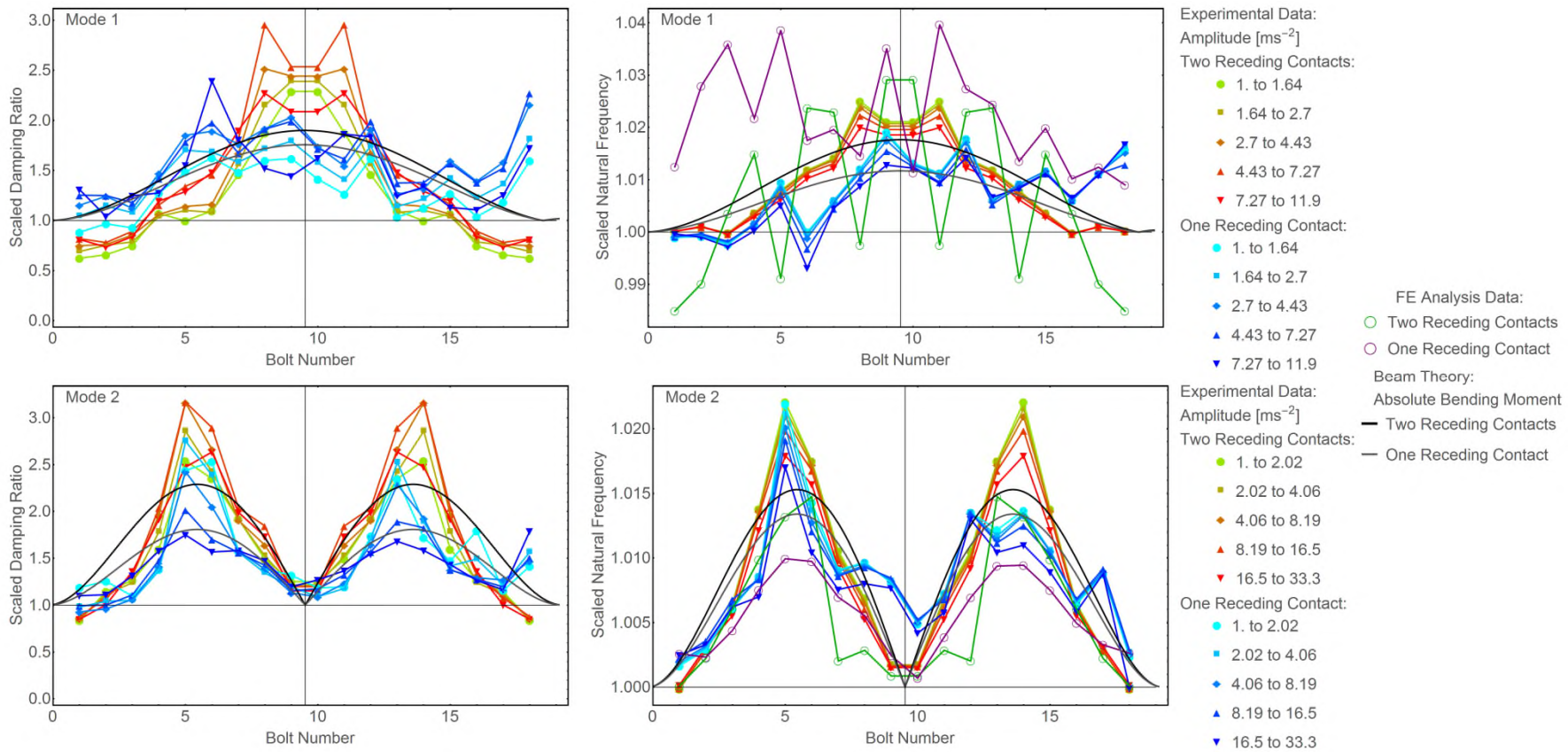

Figure 151 Synthesis of the scaled data for modes 1 and 2. This grid of plots follows the template in Figure 144.

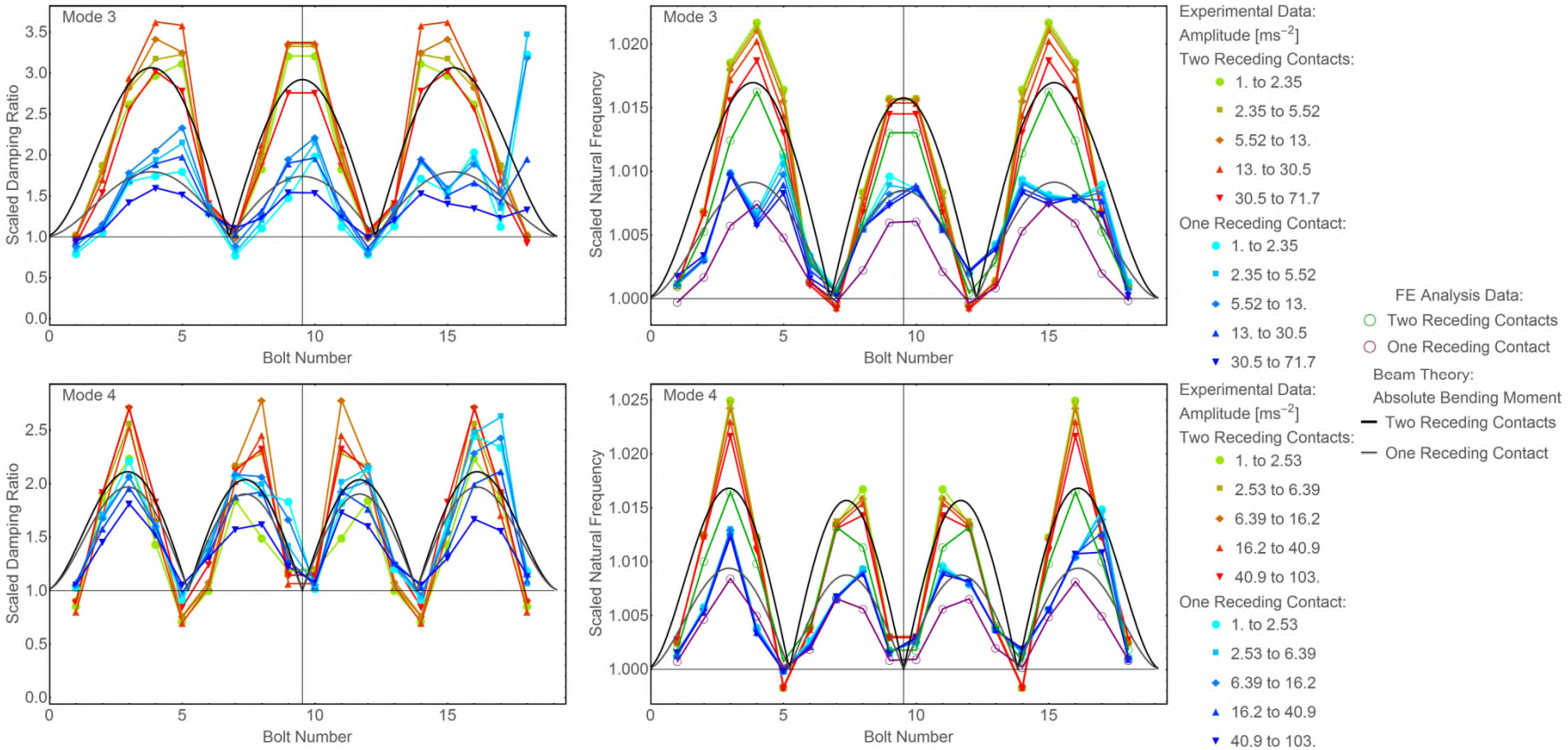

Figure 152 Synthesis of the scaled data for modes 3 and 4. This grid of plots follows the template in Figure 144.

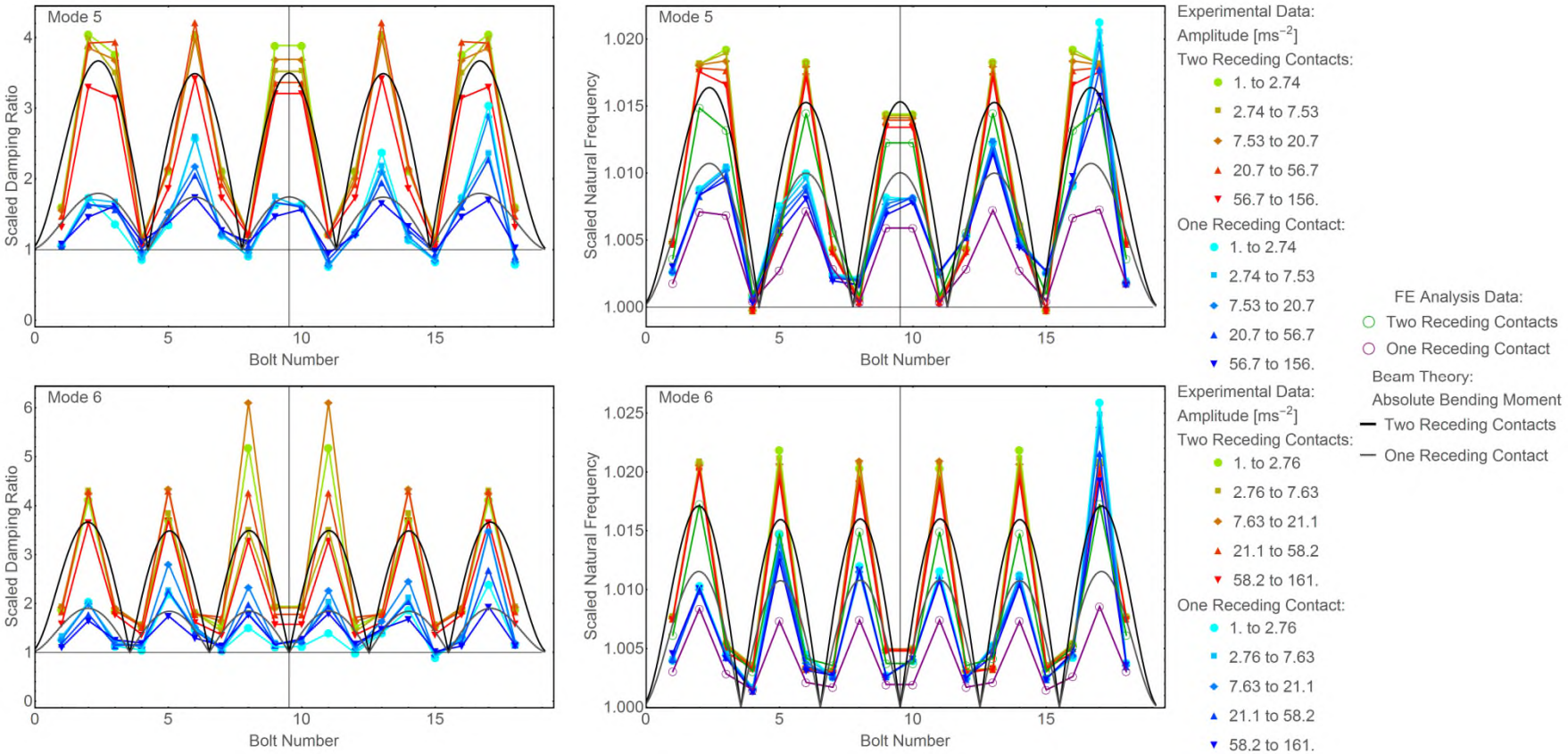

Figure 153 Synthesis of the scaled data for modes 5 and 6. This grid of plots follows the template in Figure 144.

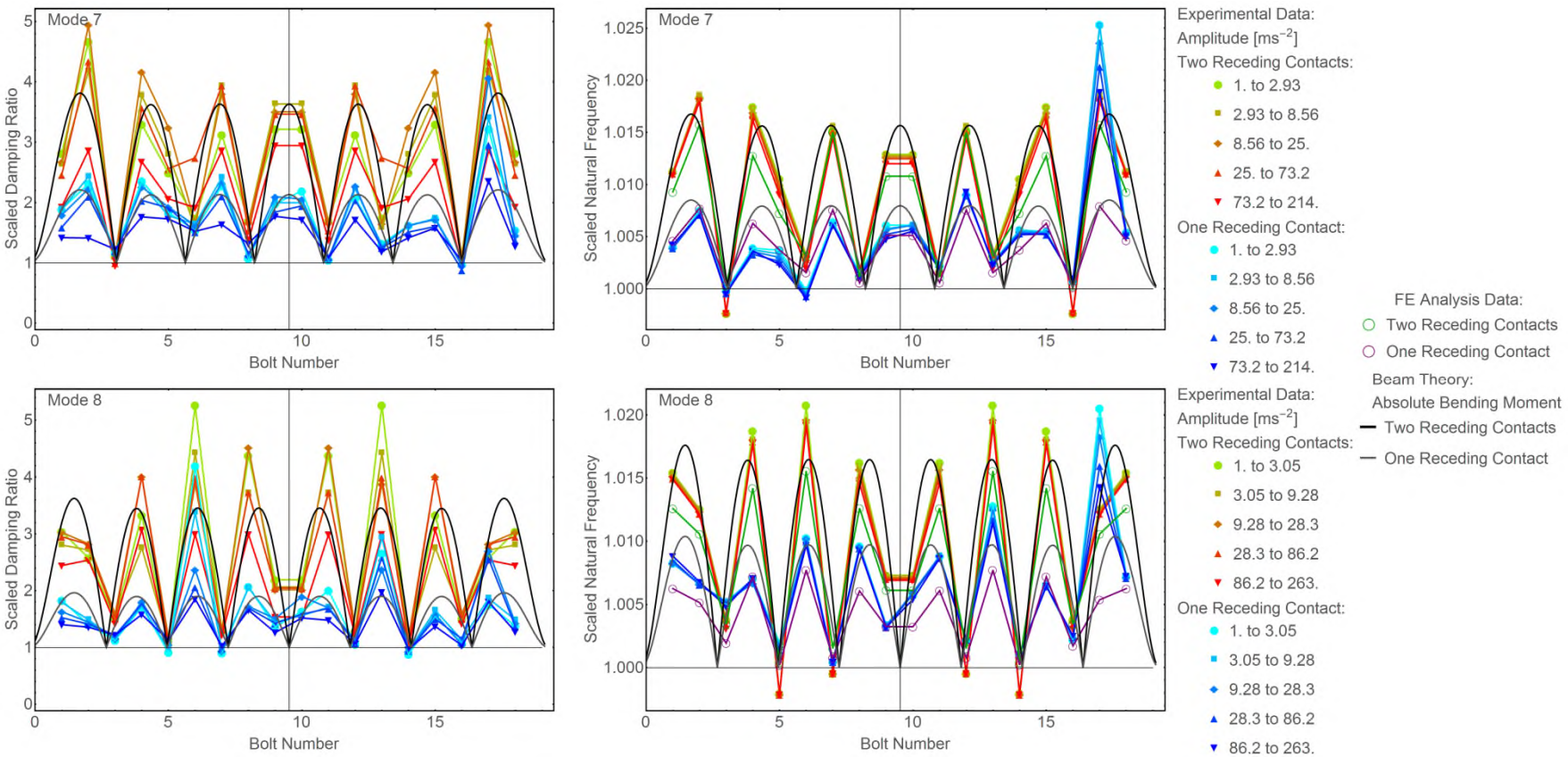

Figure 154 Synthesis of the scaled data for modes 7 and 8. This grid of plots follows the template in Figure 144.

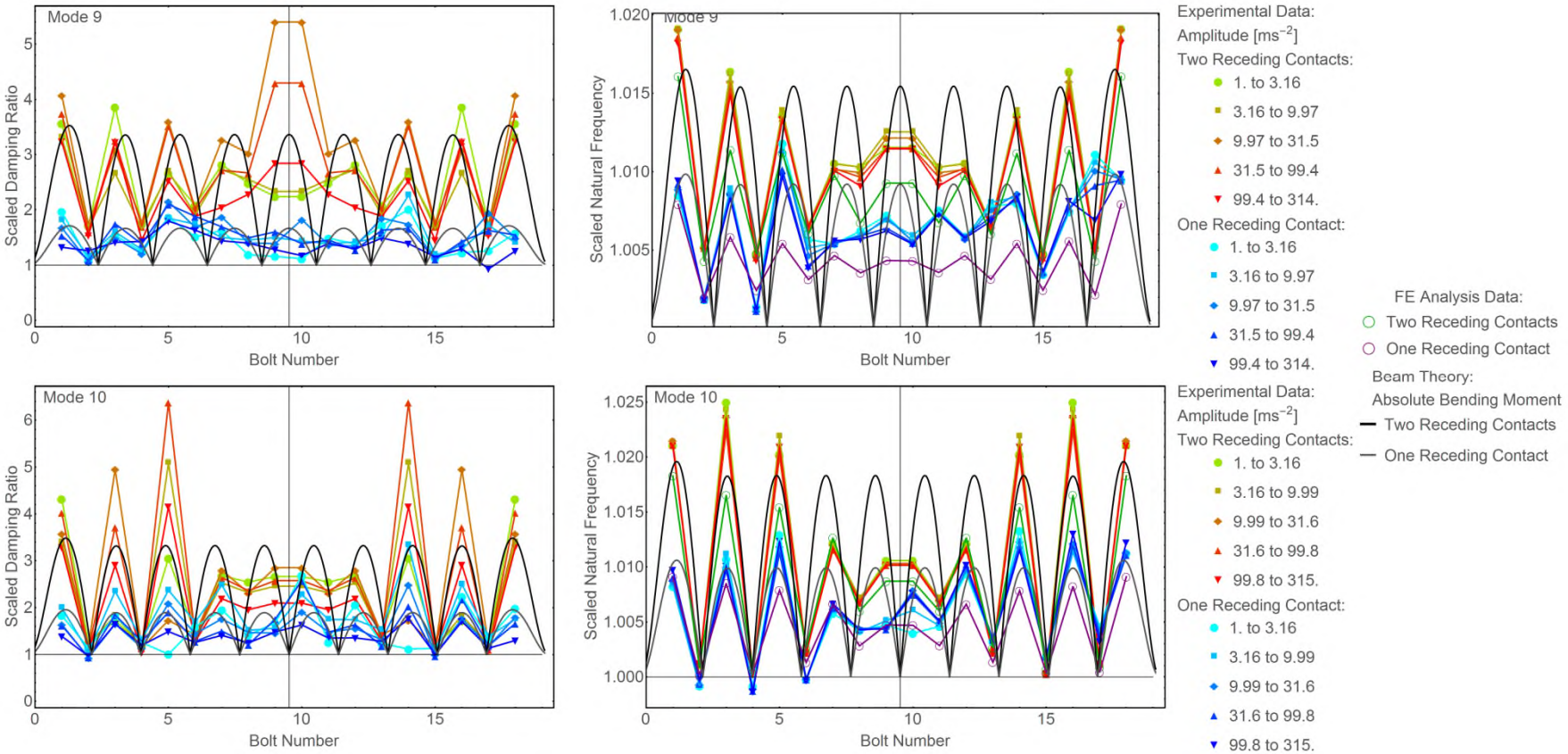

Figure 155 Synthesis of the scaled data for modes 9 and 10. This grid of plots follows the template in Figure 144.

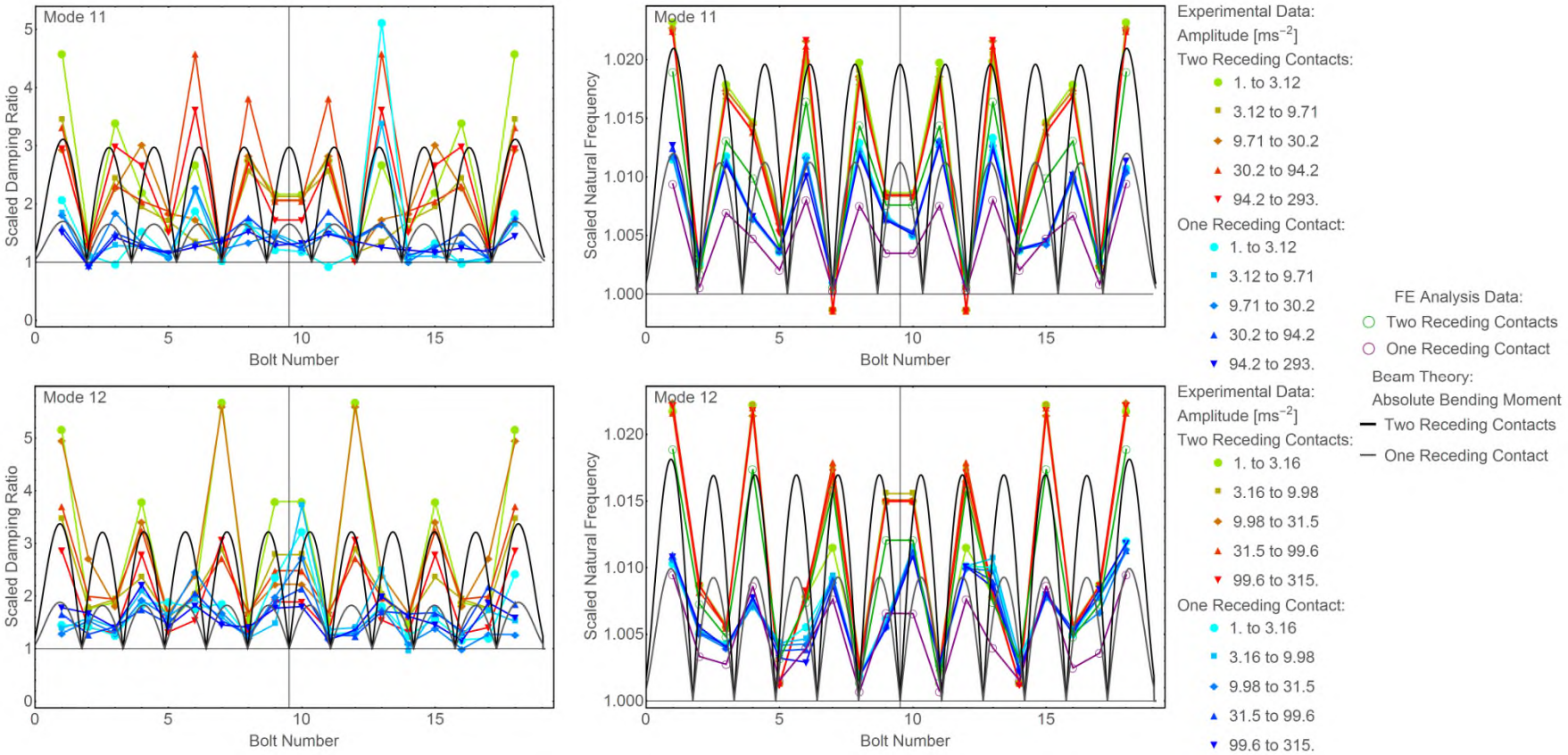

Figure 156 Synthesis of the scaled data for modes 11 and 12. This grid of plots follows the template in Figure 144.

Observation across all modes:

- All the experimental and simulated scaled data are correlated to the absolute bending moment, except mode 1 (see after).
    - The scaled simulated natural frequencies from the FEM analysis follow perfectly the shape of the absolute bending model. This is true either for one or two receding contacts.
    - The majority of the scaled experimental data follows the fitted absolute bending model
- The scaled data with two receding contacts are around double or triple the scaled data with one receding contact

Observation for mode 1:

- The scaled data is chaotic for mode 1 and does not follow the same trend as the other modes. This observation is true for the experimental results and also for the simulated results.

Observation for mode 9 to 12:

- For the scaled natural frequencies, the fitted model and the FEM results indicate that the experimental results are still following the wave pattern of the fitted model for modes 9 to 12
- The scaled damping ratios are too noisy to allow any definite conclusion to be reached.

7.7 Prediction of the dynamic nonlinear behaviour of a lap joint

The results of Section 7.6 show that a simple finite element simulation could simulate the scaled natural frequency accurately. The simulated results were achieved just by changing the diameter of a numerical shim placed between the components of a lap joint. A change in diameter was used to simulate the physical change of the contact patch between a complete contact and a receding contact. This change of diameter causes the modification of the mesh at the interface of a joint as shown in Figure 157. In conclusion, just by changing the mesh of a linear finite element model (FEM) simulation, an accurate simulation of the scaled natural frequency was obtained.

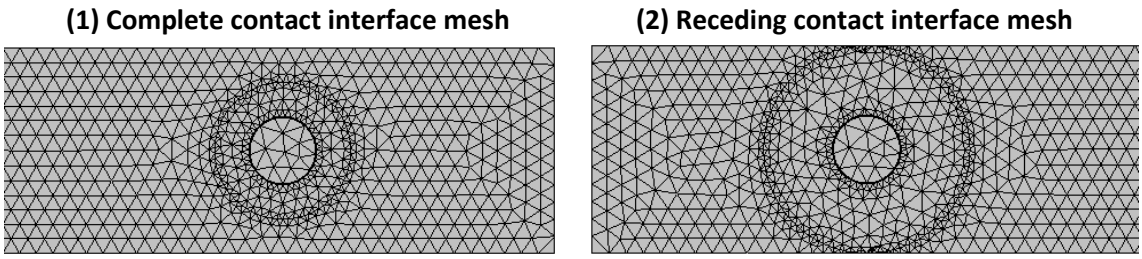

Figure 157 Duplication of Figure 141 already displayed in Section 7.3. The two meshes used at the interface of a lap joint to simulate a complete contact and receding contact. A 0.1 mm thick shim of 20mm diameter (1) or 30mm diameter (2) was used to change the lap joint interface mesh. Only the central disc bound the two main components of the joint together. The numerical shim creates a gap in the rest of the interface.

Those results open the door to a procedure which could predict the dynamic nonlinear behaviour of a lap joint. This procedure needs three inputs: the geometry, the mass and the modulus of elasticity of each component. The geometry of each component should be measured precisely as a small variation between the model and the manufactured item could reduce the precision of the simulation. Also, the mass can be simulated, but a measurement of each component would improve the precision of the FEM results. The modulus of elasticity is more difficult to measure. Using values from the literature could create a large offset of the natural frequencies. However, a precise and realistic value of the modulus of elasticity can be obtained by selecting the modulus of elasticity so that the FEM analysis matches the simulated natural frequencies and the measured natural frequencies for each component alone. By definition, there is no joint in a component, thus, no dynamic nonlinear behaviour should be measured. Therefore, measuring the natural frequencies of a component is one of the simplest tasks of an experimental modal analysis. A trial-and-error procedure on the value of modulus of elasticity in simulation should make the simulated and the measured natural frequencies match. Thus, a precise and realistic value of modulus of elasticity can be estimated.

7.7.1 Prediction based on mode shapes

An estimation of the dynamic nonlinear behaviour of a lap joint is achievable just by studying the simulated mode shapes. Indeed there is a correlation between the

components separation and interpenetration in the mode shape, and the amplitude dependant damping ratio and natural frequencies which were measured as shown in Figure 158. This estimation will not work if the mesh glues the components together at the interface of the joint investigated, thus, blocking any visible separation and interpenetration of the components. Therefore, an accurate estimation of the size of the contact patch at the interface is needed to estimate the dynamic nonlinear behaviour of a lap joint by studying mode shapes.

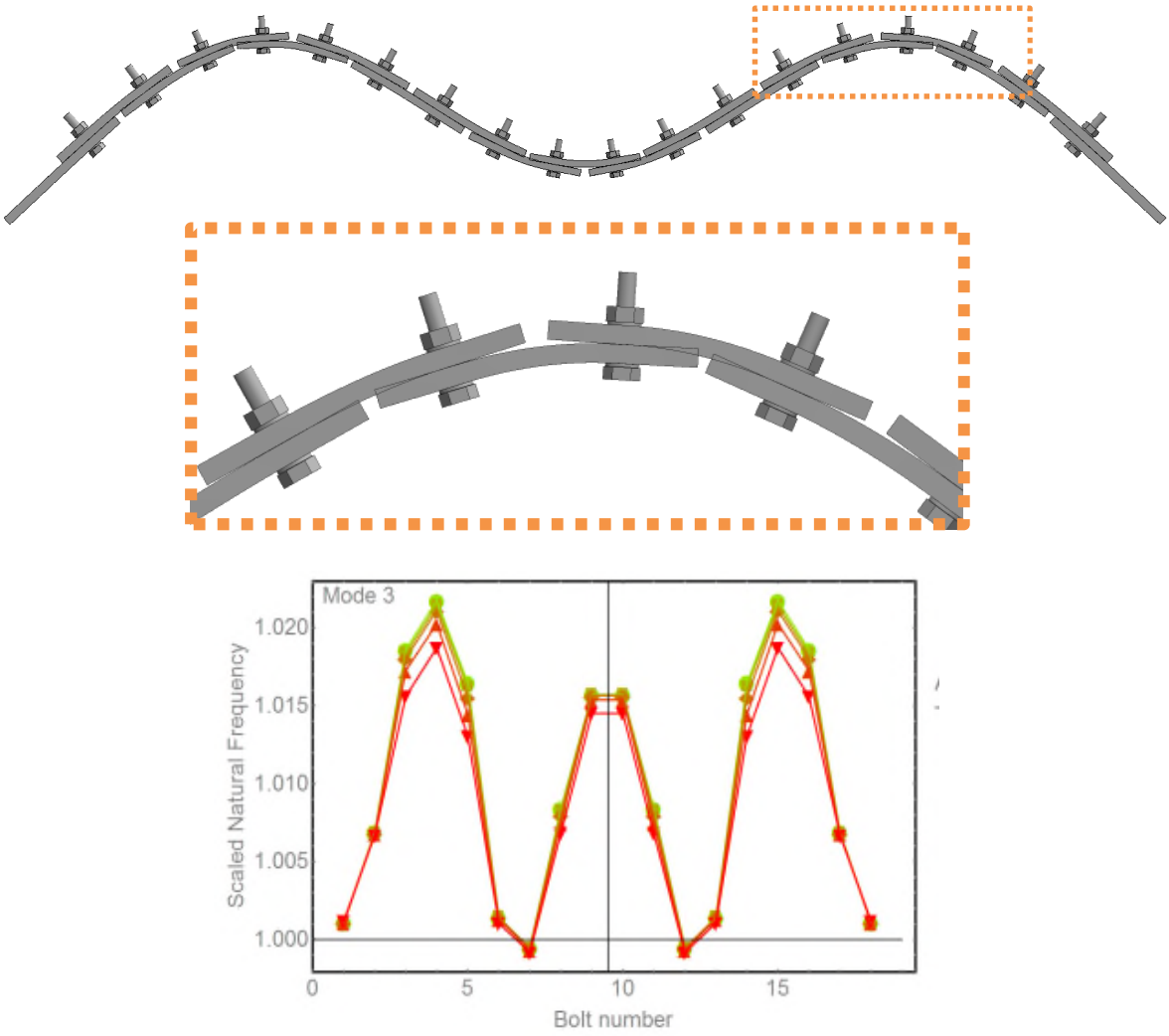

Figure 158 Top row, example of a mode shape. Middle row, zoom of the anti-node of the top row mode shape. The components separate and interpenetrate at the antinodes of the mode shape. Bottom row, plot of the scaled natural frequency as a function of the position of two receding contacts (source: Section 6.3). In the plot, the higher the scaled damping ratio, the higher the nonlinear dynamic behaviour of the lap joint at that bolt position if there is a receding contact. There is a correlation

between the components interpenetrating and the nonlinear dynamic behaviour of a joint.

7.7.2 Simulation of a contact patch

One of the major difficulties, when this procedure is used, is to know the exact size of the contact patch in a receding contact. The algorithm described in Figure 159 was developed to estimate the size of the contact patch.

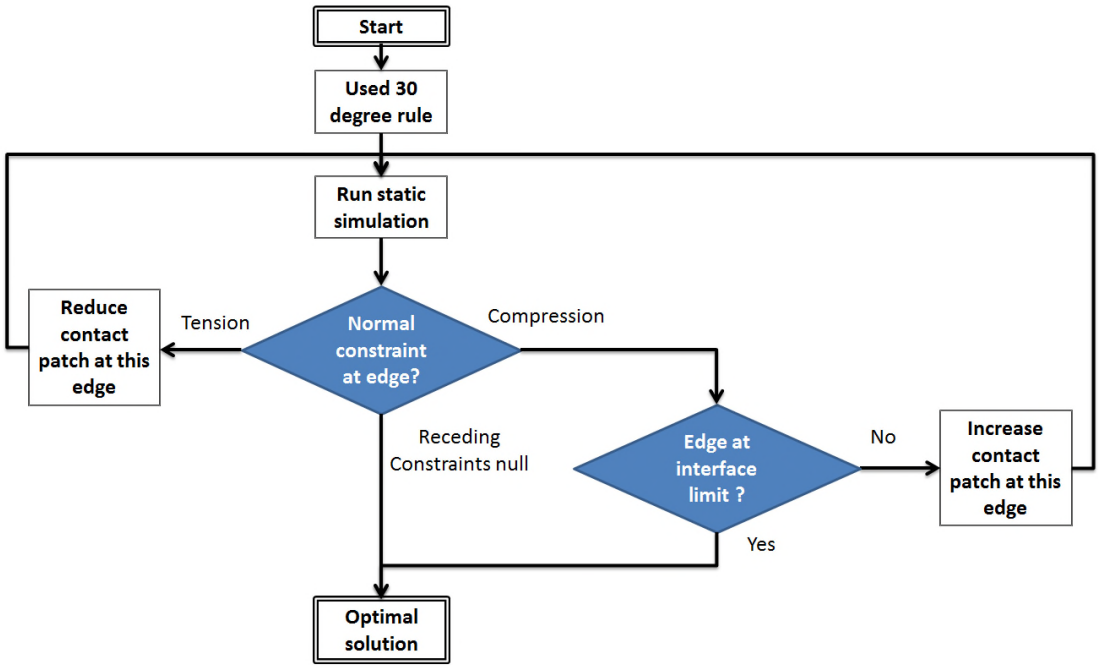

Figure 159 Procedure to obtained the best possible simulated contact patch

Also, a static analysis can predict the amplitude dependant nonlinear behaviour of a lap joint. Indeed, the algorithm of Figure 159 can also be used with a quasi-static analysis which includes a simulated static bending moment. This simulated static bending moment should match the bending moment of the experimental vibration. Therefore, the shape of the contact patch could be estimated for multiple bending moment values. The always stuck region and rolling region could be estimated for multiple values of static bending moment. Therefore, the natural frequency and the damping ratio could be estimated for multiple levels of amplitude. In conclusion, a prediction of the nonlinear behaviour of a lap joint could be achieved. Preliminary investigations using the method described in this paragraph generated promising results with exaggerated static bending moment values. However, the simulated

contact patch did not change with realistic value of bending moment. These inconclusive results were not included in this thesis.

7.7.3 Example of applications

Using this simulation procedure allows the ranking of different interface designs of one joint on the entire mode simulated. The natural frequencies need to be scaled by one test to allow all the modes to be displayed at once. The change in natural frequency reveals which mode is the most affected by the modification of the design of a joint. This could be useful, for example, when the amount the weight of a joint needs to be reduced, to reduce to fuel consumption of a car or an aircraft.

Another way to use this procedure is to compare the impact of the position of a joint on the natural frequency of one mode. This could be useful to choose the location of a damper when the vibration of one mode is problematic.

A prediction of the scaled damping ratio, between different tests of a structure, could probably be achieved using the procedure described before. Indeed the joint position experiment and the sandwich beam experiment show that there is a clear correlation between the nonlinear damping ratio and the change of natural frequency.

7.8 Conclusion of the joint location experiments

This section concludes the joint position experiments which were presented in Chapter 6 and Chapter 7.

The influence of the position of a receding contact was investigated on a structure with 18 possible locations for the receding contact. Instead of investigating the position of a joint, the position of one or two receding contacts was investigated and compared to a test with complete contacts everywhere. The experimental tests were performed in a controlled environment to limit any exterior factor except the complete contacts or receding contacts. The change between a complete and a receding contact was performed by placing or removing washer size shims in the polished interface of the bolted lap joints. Multiple tests with either zero, one or two receding contacts were tested by exciting the structure with a hammer and recording the vibration with an accelerometer. The instantaneous damping ratio, natural frequency

and amplitude were extracted from the signal, processing and plotted as a function of the position of the receding contacts. The notion of scaled data was introduced. This scaled data emphasises the change between a complete contact and a receding contact in a lap joint.

The values of damping ratio and natural frequency, displayed in Section 7.5, show that the experiments have an amplitude dependant nonlinear behaviour, as detailed in Table 23, with a receding contact when submitted to a bending moment at the position of the lap joint. However, a linear behaviour (weakly dependant on the amplitude) was measured with a complete contact whatever the position.

Table 23 The amplitude dependant nonlinear behaviour of a receding or complete contact in a lap joint. This table summaries the results of Chapter 7

Type of contact	**Receding contact (behaviour scaled by the amount of bending moment)**		**Complete contact**	
Measured value	**Damping Ratio**	**Natural Frequency**	**Damping Ratio**	**Natural Frequency**
Trend when the amplitude decrease	Decrease (amplitude dependant damping ratio)	Increase (amplitude dependant natural frequency)	Almost constant	Almost constant

The measured scaled damping ratios and scaled natural frequencies are correlated with the absolute bending moment as defined by beam theory and not the shear force. More precisely, the change between a complete contact and a receding contact is greatest at the antinode of the bending moment. Conversely, at the node of the bending moment, a smaller change was measured with scaled data close to a value of one.

A linear finite element model (FEM) analysis was performed. This simulation used two different meshes at the interface of the lap joints to simulate either a complete contact or a receding contact. The simulated natural frequencies are realistic, as they are extremely closed to the measured natural frequencies. These FEM analyses corroborate the comparison between the absolute bending moment model

and the experimental results. The FEM analysis presented in this chapter opens the door to a predictive procedure for the nonlinear behaviour of lap joints submitted to vibration. This procedure could predict the behaviour of a joint only by changing the mesh of a linear FEM analysis.

All the implications of the results presented in this chapter are discussed in the next chapter, Chapter 8 Discussion.

8 DISCUSSION

In the first section, Section 8.1, a new interpretation is proposed of the results presented in Chapter 3, Chapter 6 and Chapter 7. In the second section, Section 8.2, the impact of the literature is described. The third section, Section 8.3, lists the different contribution of this thesis.

8.1 Interpretation of the results

8.1.1 Summary of the main results

In summary, the main result of Chapter 3, Chapter 6 and Chapter 7 is the detection of an “unexplained mechanism”. This unexplained mechanism exists in a receding contact submitted to a bending moment, but not in a complete contact. This unexplained mechanism transforms the bending moment causing an increased dissipation of the vibration energy and results in a reduction of rigidity at the joint. In other words, this unexplained mechanism is the cause of two amplitude dependent nonlinear behaviours of a lap joint with a receding contact: The decreasing of damping ratio and the increase of natural frequency, when the amplitude decreases during the decay of vibration as summarised in Table 24. Moreover, this unexplained mechanism does not exist inside a complete contact. Indeed, there is only minor amplitude dependent nonlinear behaviour measured in a structure composed only of complete contact joints, see AllComplete tests in Subsection 7.5. Therefore, from the result shown in Table 24, we can conclude that there is a presence of an unexplained mechanism in receding contacts, but not in complete contacts.

Table 24 The two measured amplitude dependent nonlinear behaviours of a receding or complete contact in a lap joint. This table was already presented in the conclusion of Chapter 7.

Type of contact	**Receding contact (behaviour scaled by the amount of bending moment)**		**Complete contact**	
Measured value	**Damping Ratio**	**Natural Frequency**	**Damping Ratio**	**Natural Frequency**
Trend when the amplitude decrease	Decrease (amplitude dependant damping ratio)	Increase (amplitude dependant natural frequency)	Almost constant	Almost constant

The following hypothesis will be used in this section: the two bolts lap joint of chapter 3 has the same behaviour as the one bolt lap joint of Chapter 6, even if they have a different geometry. Therefore, the results of chapter 5 will be extrapolated to interpret the results of the lap joint investigated in chapter 6 and 7.

This hypothesis could be wrong. A validation could be done by performing the shim size experiment described in Section 5.4 on the lap joint of chapter 6 with one bolt. And in reverse, the joint position experiment, described in Subsection 6.1.1, could be performed on the two bolts lap joints of the sandwich beam. If the two reverse experiments reach the same results as the original ones, than this hypothesis could be validated. Those two reverse experiments are part of the future work.

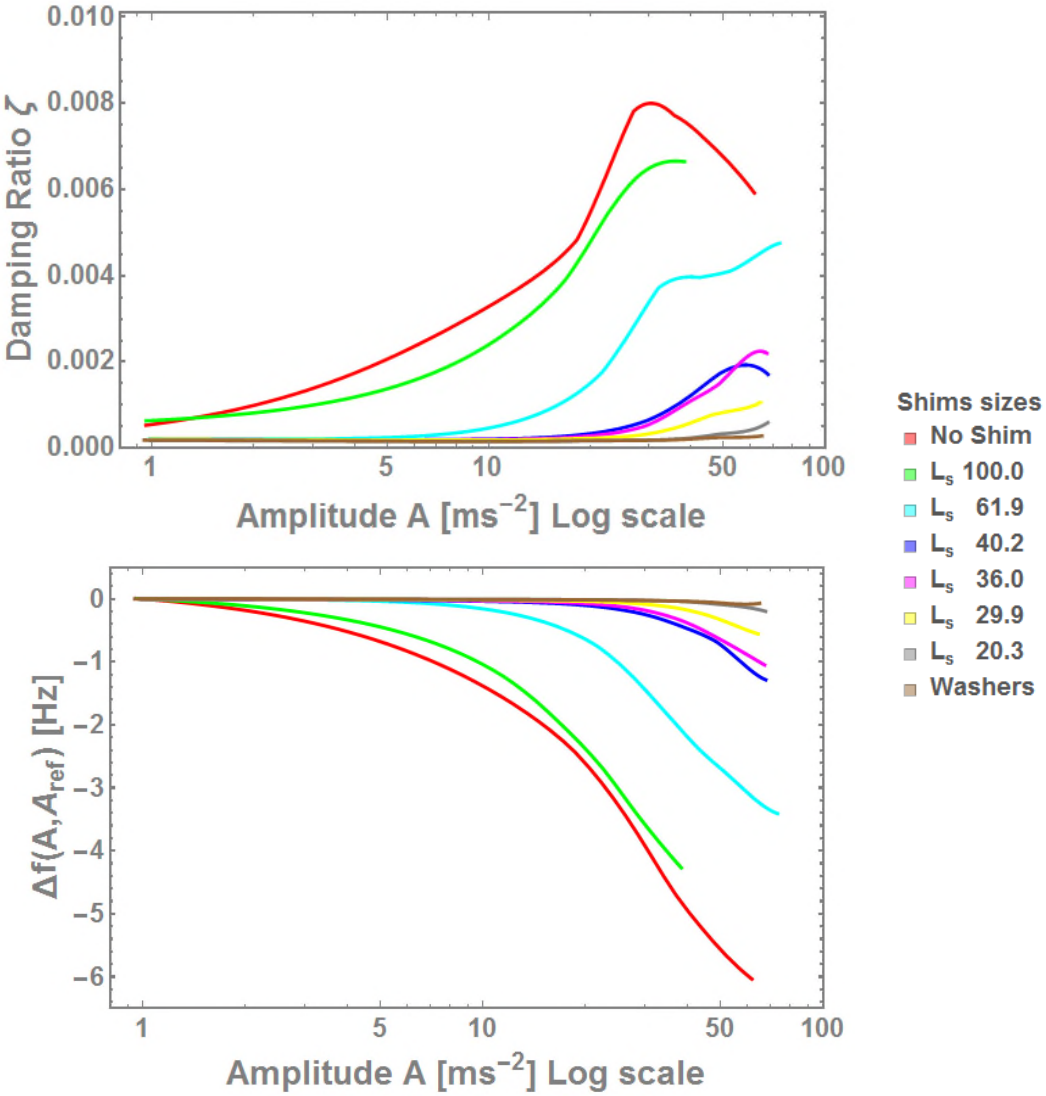

Figure 160 Trend lines of the damping ratio and the change in natural frequency (Δf) [Hz] against amplitude for multiple shim sizes. For more detail see Section 5.4.

The results of Figure 160 show that when placing shim of different size in the interface, a behaviour in between a complete contacts and a receding contacts is measured. More specifically, the behaviour is simply dependant on amplitude. The in-between interface size acts as a receding contact if the amplitude of vibration is higher than a “locked-up limit”. This locked-up limit is dependent on the length of the shim. When the amplitude is below the locked-up limit, the interface is locked-up and the joint does not dissipate energy, which was is characteristic of a complete contact. If the amplitude is higher than the locked-up limit than there is an amplitude dependent frequency and damping ratio, characteristic of a receding contact. For

example, this locked up limit is 5ms^{-2} for a 60mm shim, whereas the locked-up limit of the 20.3 mm shim is at 50ms^{-2}.

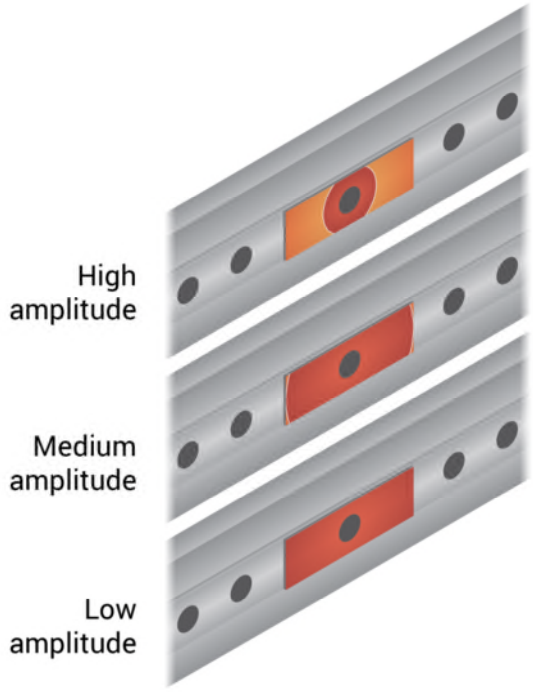

Figure 161. Illustration of the bound region in red and slip region in orange depending on the amplitude for a 60 mm long shim. High amplitude = 50 ms^{-2}. Medium amplitude = 5 ms^{-2}. Low amplitude = 1 ms^{-2}.

This locked-up limit was interpreted in the Discussion Section 5.7 as follows: There is a “bound region” where there is no relative displacement at the interface. This bound region would grow from the centre of the bolt axis when the amplitude decreases. When the bound region reaches the limit of the interface, than the interface is locked, as illustrated in Figure 102. Due to the vibration a “slip region” dissipates energy at the joint interface due to micro-friction. Taking into consideration the results of chapter 6 and 7, a novel interpretation is proposed in this section, Section 8.1.

The impact of the position of the joint was investigated by changing receding contacts into complete contacts. To quantify the change of the two amplitude dependant behaviours when a complete contact is turned into a receding contact, the data sets were scaled. The scaled data quantifies the change between the

AllComplete tests, with complete contacts everywhere, and a test with one or two receding contacts. The definition of the scaled data is repeated here:

$$Scaled\ Damping\ Ratio\ = \frac{damping\ ratio}{AllComplete\ damping\ ratio} \quad \textbf{(8-1)}$$

$$Scaled\ Natural\ Frequency\ = \frac{natural\ frequency}{AllComplete\ natural\ frequency} \quad \textbf{(8-2)}$$

The magnitude of the two amplitude dependant behaviours is correlated to the value of the absolute bending moment depending on the position of the joint. As shown in Figure 162, which is a sample of the Section 7.6 plots, there is a clear correlation between the scaled data and the absolute bending moment. Thus, this unknown mechanism should be the cause of a scaled natural frequency between 100% and 102%, and a scaled damping ratio between 100% and 600%, as a function of the value of the absolute bending moment at the joint location. The two scaled data are greater than 100%, this means that the switch between a complete contact and a receding contact stiffens the structure and increases the damping. Moreover, this increase of stiffness and damping is correlated to the absolute bending moment applied to a joint. The amount of bending moment is linked to the position of the lap joint.

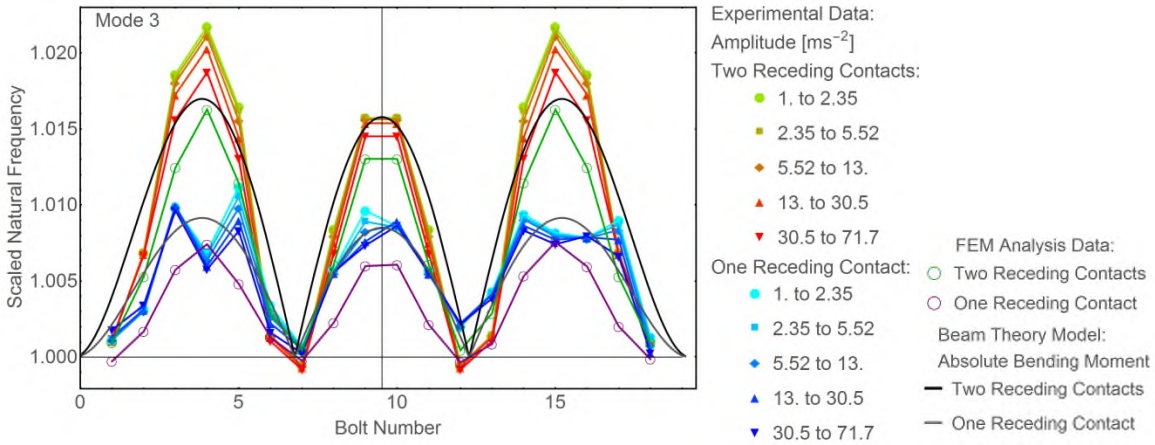

Figure 162 Synthesis diagram of the experimental, fitted and simulated results plotted for mode 3, already displayed in Section 7.6. The scaled natural frequency is defined in the equations (6-2) and (6-3). The scaled natural frequency is displayed as a function of the position of one and two receding contacts. The points represent the experimentally measured values previously presented in Chapter 6. The curved lines

are the fitted absolute bending moment as explained in Section 7.2. The green and purple circles correspond to the simulated natural frequencies, see Section 7.3 for details. The experimental and simulated data set are joined by lines to help the readability. The colour signifies the number of receding joints or the amplitude of the vibration as detailed in the legend. The data sets with two receding joints, either experimental or simulated, are displayed twice following a central symmetry represented by the vertical grey line.

Figure 163 is the evidence that shear force plays a minor role in the nonlinear behaviour of the lap joint. The interpretation is that the shear force loading could create a nonlinear behaviour, as shown in the literature review Subsection 2.3.2, but the shear force has a weaker effect than the bending moment loading. Consequently, the bending moment is considered to be the main cause of the amplitude dependant behaviour in a lap joint, not shear force.

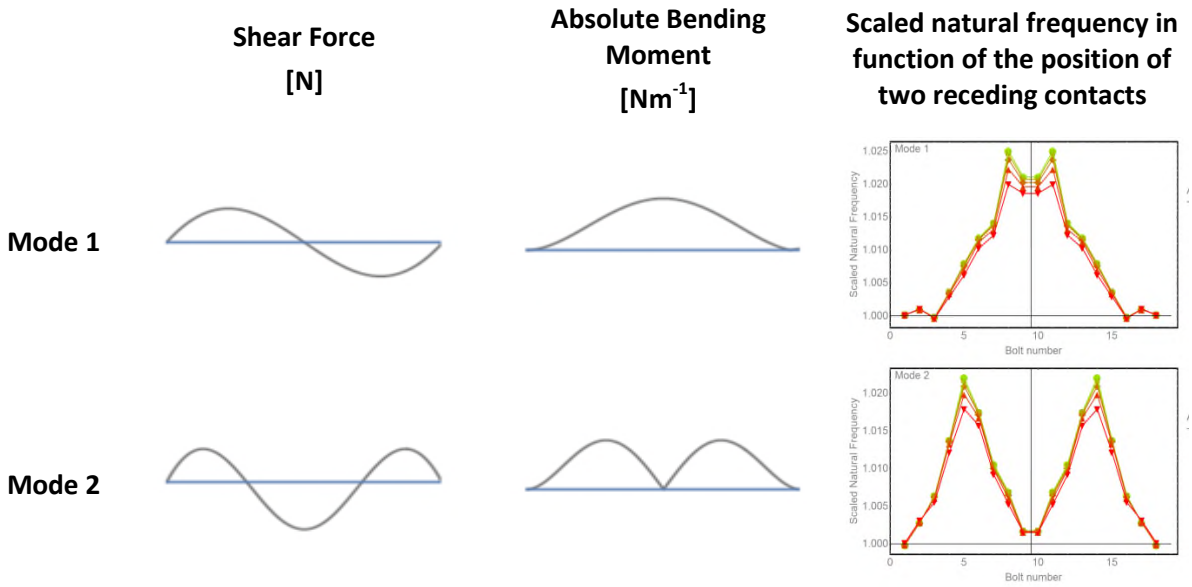

Figure 163 Comparison between the shear force, the absolute bending moment from the beam theory, columns one and two, and the experimental results, third column. This figure is an extract of Figure 139 displayed in Section 7.1.

One of the clues, which help to find an explanation, is the simulated mode shape from the finite element model analysis. In the simulated mode shapes, the interfaces of the lap joints are opened-up and interpenetrated, but only at the antinode of the bending moment, as in the mode shape displayed in Figure 164.

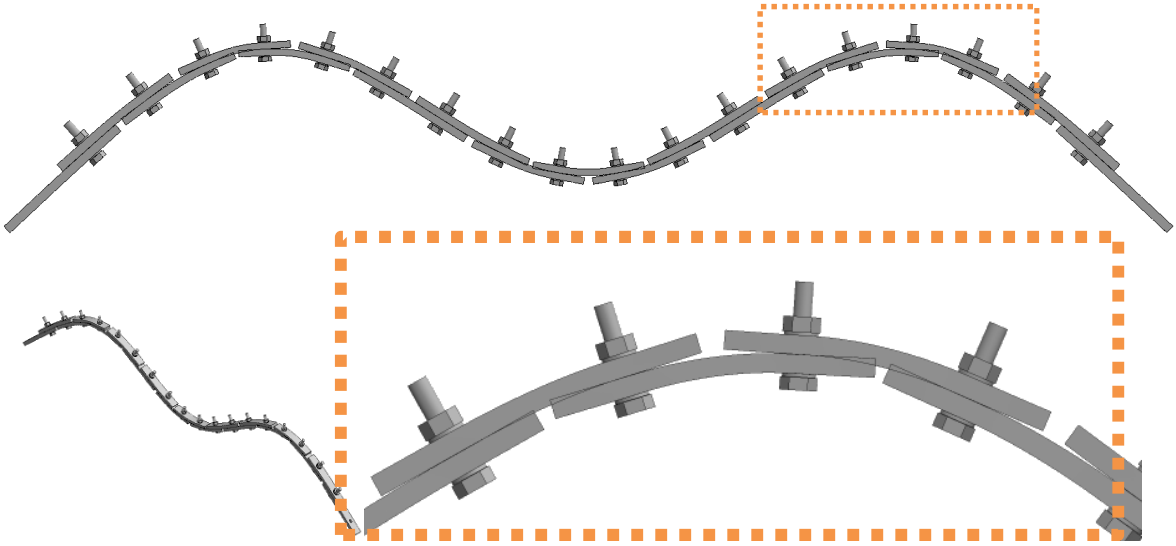

Figure 164 Three views of the mode shape of the third bending mode of the FE_AllComplete1 test. It is noticeable that the joints at the anti-node have an interface which opens and closes up. Conversely, the interface at the nodes and the interface at the extremities remain still.

As shown in Table 25, the bending moment in a beam is similar to the mode shape, except at the extremities. Indeed the extremities are nodes for the bending moment and are antinodes for the mode shapes. Moreover, in Figure 164, only the interface at the antinode of the bending moment open and close up.

Table 25 Comparison between the mode shape and the bending moment for the third bending mode

	Mode shape	Bending Moment
Mode 3	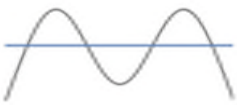	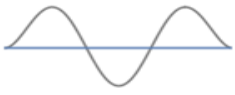

8.1.2 Rolling contact

From an initial consideration of all the evidence, the notion of “local deformation” of the lap joint interface was the first explanation found for the “unknown mechanism” described before. This hypothetical local deformation creates a shear force locally due to the Poisson effect. The Poisson effect is the fact that a material when compressed vertically, extends horizontally. Then, the Poisson effect would create

tangential displacements, thus microfriction, and damping. However, this “local deformation” was hard to imagine, visualise or even relate to other physical effects. Consequently, the notion of relative tangential displacement was excluded from the interpretation.

Afterwards, the focus was turned to the notion of the contact patch, so the key question was: “how does the bending moment change the contact patch?” The solution found for the “unknown mechanism” was the notion of a “rolling” contact patch.

A visualisation of a rolling contact patch is a sphere on a plane. Both the sphere and the plane are infinitely rigid. The center of gravity of this sphere is in the lower part of the sphere. The contact between the sphere and the plane does not need to slip to model the phenomenon. When the sphere is pushed into an unstable position, it rolls and creates an oscillation movement as shown in Figure 165.

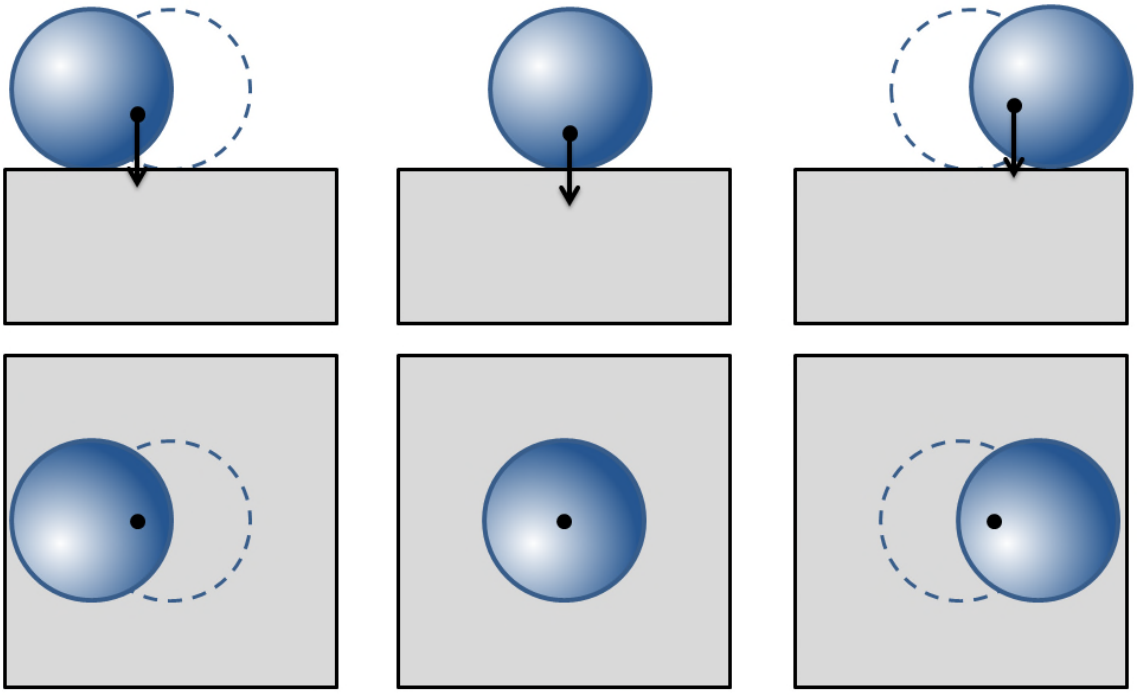

Figure 165 Oscillation movement of a rolling sphere on a flat half-space. The top row displays the side views and the bottom row displays the top view. Three positions of the movement are displayed: The extreme left position, the neutral position and the extreme right position. The sphere cannot slide along the plane. The black point is the center of gravity. The black arrow represents the gravitational force. The dashed line

circle represents the sphere at an equilibrium position. The sphere oscillates after a first bending moment excitation.

The contact between the two components of a lap joint is close to the contact of a sphere on a flat half-space when there is a receding contact. As the steel components are elastic: the contact patch looks like a line in 2D, as shown in Figure 167. The gravitational force corresponds to the bolt force which pushes the two surfaces against each other. The sphere shape corresponds to the shape of each component after the receding effect of bolt tension has occurred, similar to the shape of the component with a receding contact in Figure 166. The two concepts of receding contact and complete contact are at the foundation of all the results of this thesis.

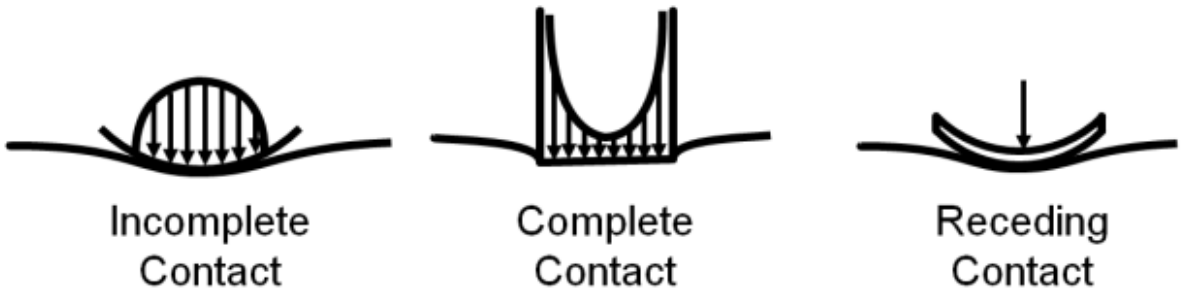

Figure 166 The three types of contact identified by Hills, Nowell, and Sackfield (1993, p40)

The oscillating rolling motion is started by the bending moment, in both cases for either a lap joint or the sphere. The oscillation rolling motion, in the case of the sphere model, is created by a transfer between kinetic energy and gravitational potential energy. The oscillation rolling motion, in the case of the bolted lap joint, is created by an alternative transfer of energy between the kinetic energy and the elastic strain energy in either the components or in the bolt.

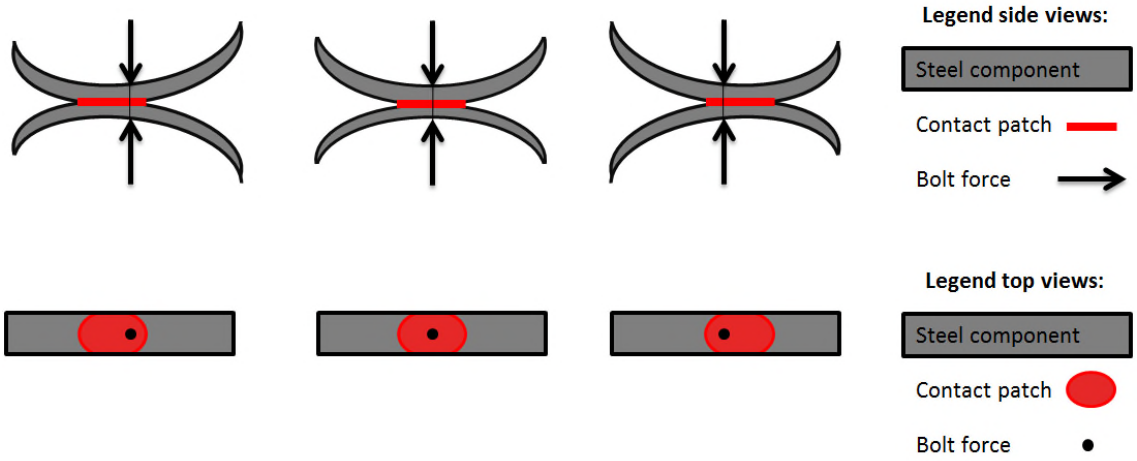

Figure 167 Rolling effect of two components of a bolted lap joint. The components are represented with an exaggerated deformation due to the receding effect. The central position is the neutral case when there is no bending moment. The two side positions are the position of the two components after being submitted to a bending moment. The contact patch evolves due to the bending moment and the receding effect creating a rolling effect.

8.1.3 Interface Limit

There is a fundamental difference between the interface and the actual contact patch in a bolted lap joint. As a reminder, the interface is defined in this thesis as the area where two components may enter into contact. Whereas the contact patch is the actual surface in contact at the interface of a joint. Therefore, if the geometry of the component changes, then, the interface changes also, and the contact patch may change also. To emphasis the impact of the components geometry on the interface, the **interface limit** will be displayed as a bold black line in the following figures of this section. Three different interfaces limits are given as examples in Figure 168.

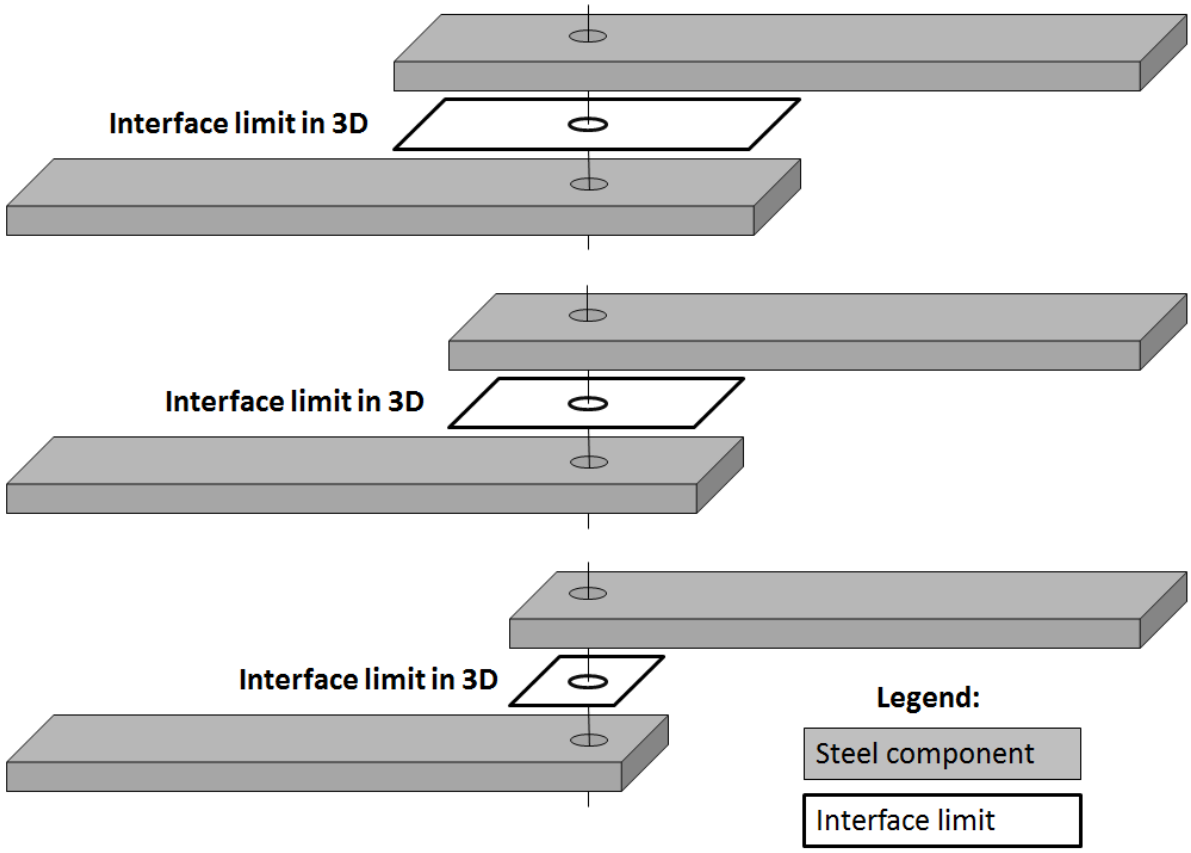

Figure 168 Interface limit for three different geometries of component.

The receding effect tends to create a gap away from the bolt location. Figure 169 is an illustration of this receding effect inside a lap joint. By definition, the contact patch is always inside the interface limit. The contact patch may change due to a modification of the interface limit. Due to the receding effect, the contact patch is often smaller than the interface. The contact patch of the receding contact, as tested in the joint position experiment, is similar to the contact patch of the rolling sphere given in Figure 165. The different views presented in Figure 169 will be reused in the following figures in this section.

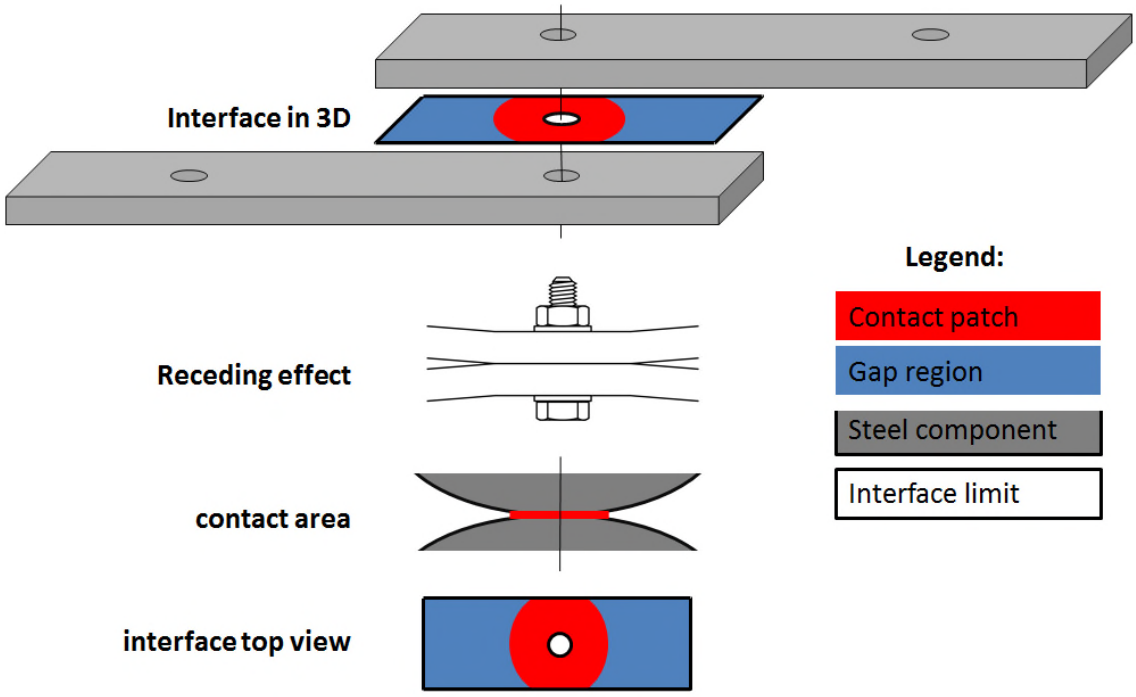

Figure 169 Impact of the receding effect on the contact patch in a neutral test (without vibration excitation). The contact patch is smaller than the interface. Where the is no contact in the interface, a gap region in blue is displayed. The interface is defined as all the surfaces where contact could happen. In contrast, the contact patch is where the contact happens at a specific time.

8.1.4 Failure of the shear force friction model

It was thought that the shear force was the cause of the nonlinear behaviour in a bolted lap joint. It is proposed in Figure 170 that friction in lap joint is due to shear force. If the receding joint is submitted to a pure shear force as defined in beam theory, we obtain Figure 170. The effect of the cyclic shear force creates a compression and traction excitation. The resulting motion is transverse sliding of the two-components against each other.

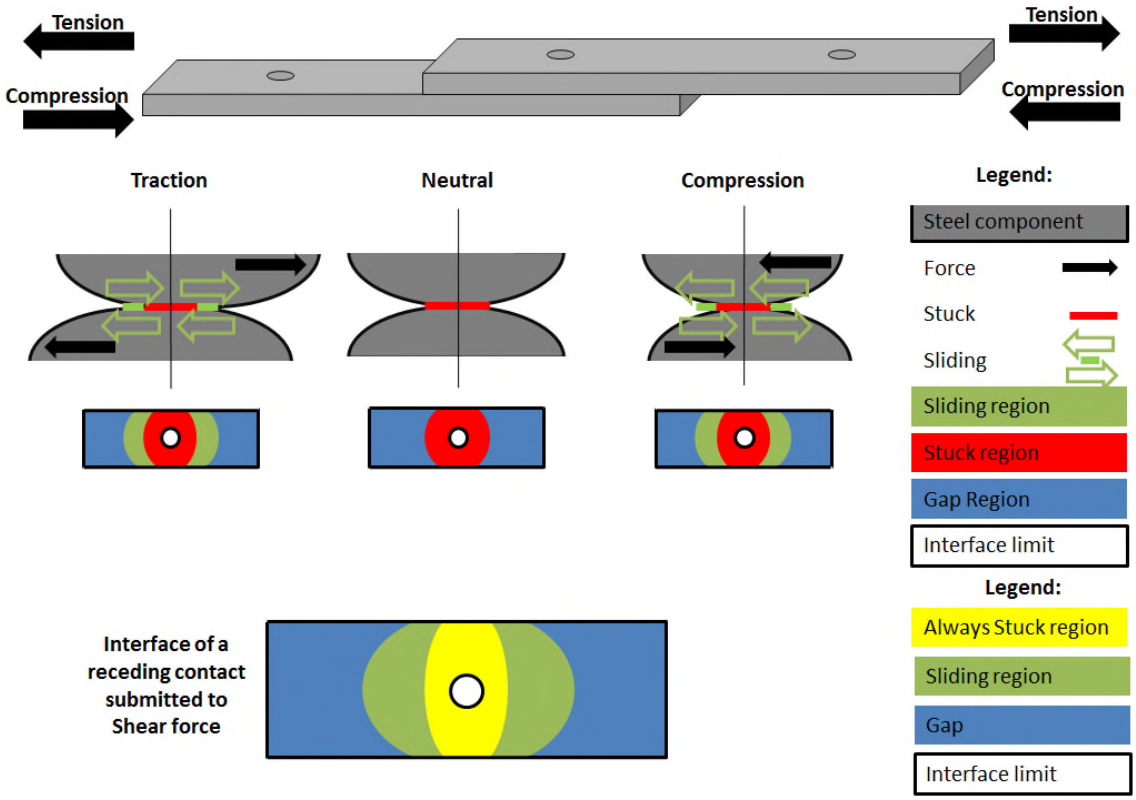

Figure 170 The interpretation of the origin of damping due to shear force in a lap joint. Top row: Example of pure shear force cyclic excitation as defined in the beam theory. Second row: side view of where sliding happens due to the shear force. Bottom row: top view of the interface in the three extreme cases of the pure shear excitation cycle (tension, neutral and compression).

This interpretation is close to the interpretation given by Kess, Rosnow, and Sidle (2002) displayed in Figure 25.

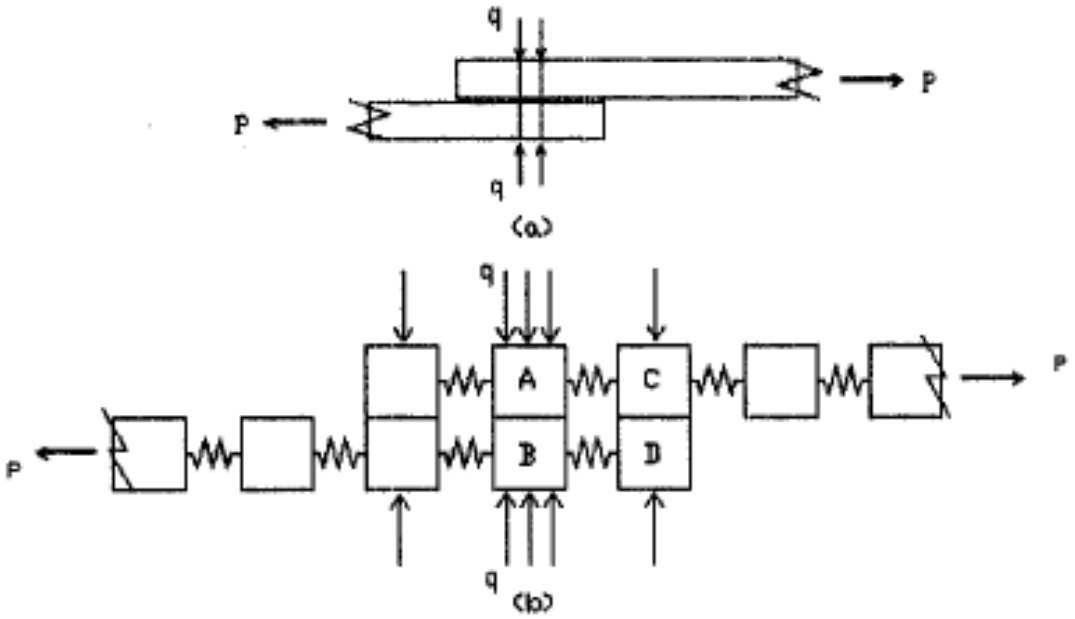

Figure 171 Spatially discretized model of lap joint by Kess, Rosnow, and Sidle (2002).

However, the joint position experiment shows that the bending moment is the only loading method correlated to the nonlinear behaviour of a lap joint. Therefore Figure 170 is wrong for the bending mode of this specific design of lap joint. Alternatively, this interpretation using slip may work for alternating compression and tension with longitudinal excitation. However in this thesis, the subject studied is the bending modes, not the compression mode. The data collected indicates that the alternating bending moment is the main loading mechanism for bending modes, not shear force. Thus, a new interpretation is needed for cyclic bending moment excitation.

8.1.5 Dynamic contact patch

Figure 172 is an interpretation of how a cyclic bending moment excitation affects a receding contact. The cyclic bending moment B excites the lap joint. Figure 172 illustrates the three deformed shapes that the lap joint will undertake during a cycle of bending moment excitation. The two extreme deformed shapes are named B and -B. Between these two extremes, the lap joint returns to a neutral deformed shape. This neutral deformed shape of the lap joint is due to the receding effect under the static loading of the bolt..

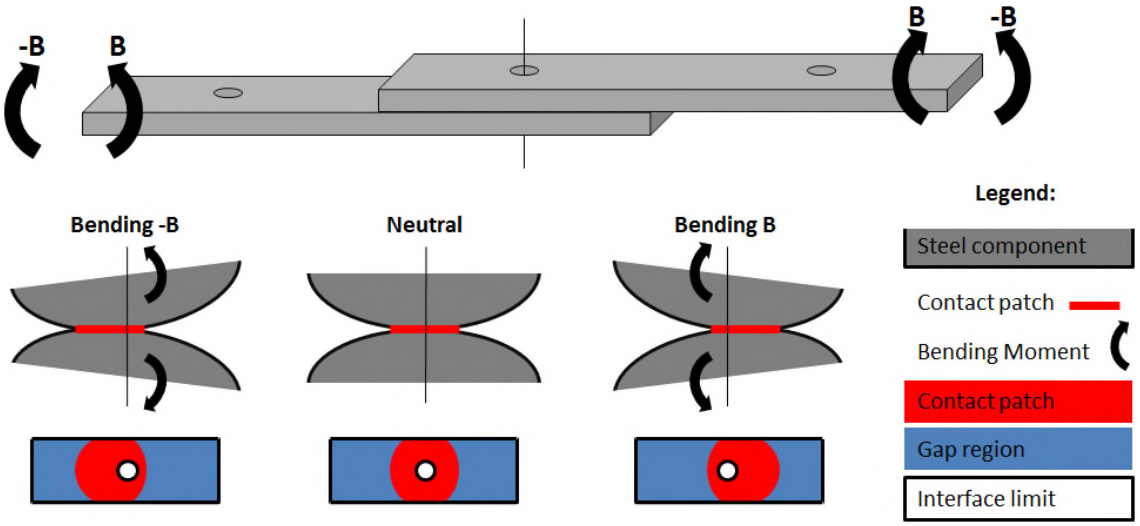

Figure 172 Interpretation of the origin of damping due to a bending moment in a lap joint. Top row: pure bending moment cyclic excitation as defined in beam theory. Second row: side view of the contact patch change due to the rolling effect of the bending moment B and -B. Bottom row: top view of the interface with the contact patch limit changed due to the bending moment.

The rolling contact patch illustration in Figure 172 describes the best interpretation found to explain the nonlinear behaviour of a lap joint submitted to vibration. The two extreme contact patch surfaces are used in the next subsection, Section 8.1.6, to quantify the rolling effect.

This changing contact patch, due to the bending, can be called a dynamic contact patch. This dynamic contact patch is dependent on the amount of bending at the joint location. This dynamic contact patch can be restricted by a small interface limit.

8.1.6 Always Stuck, Rolling and Gap Region

From Figure 172, three new abstract concepts were created: the “always stuck region”, “rolling region” and the “gap region”. The definitions of the always stuck region, rolling region and the gap region are given in Figure 173.

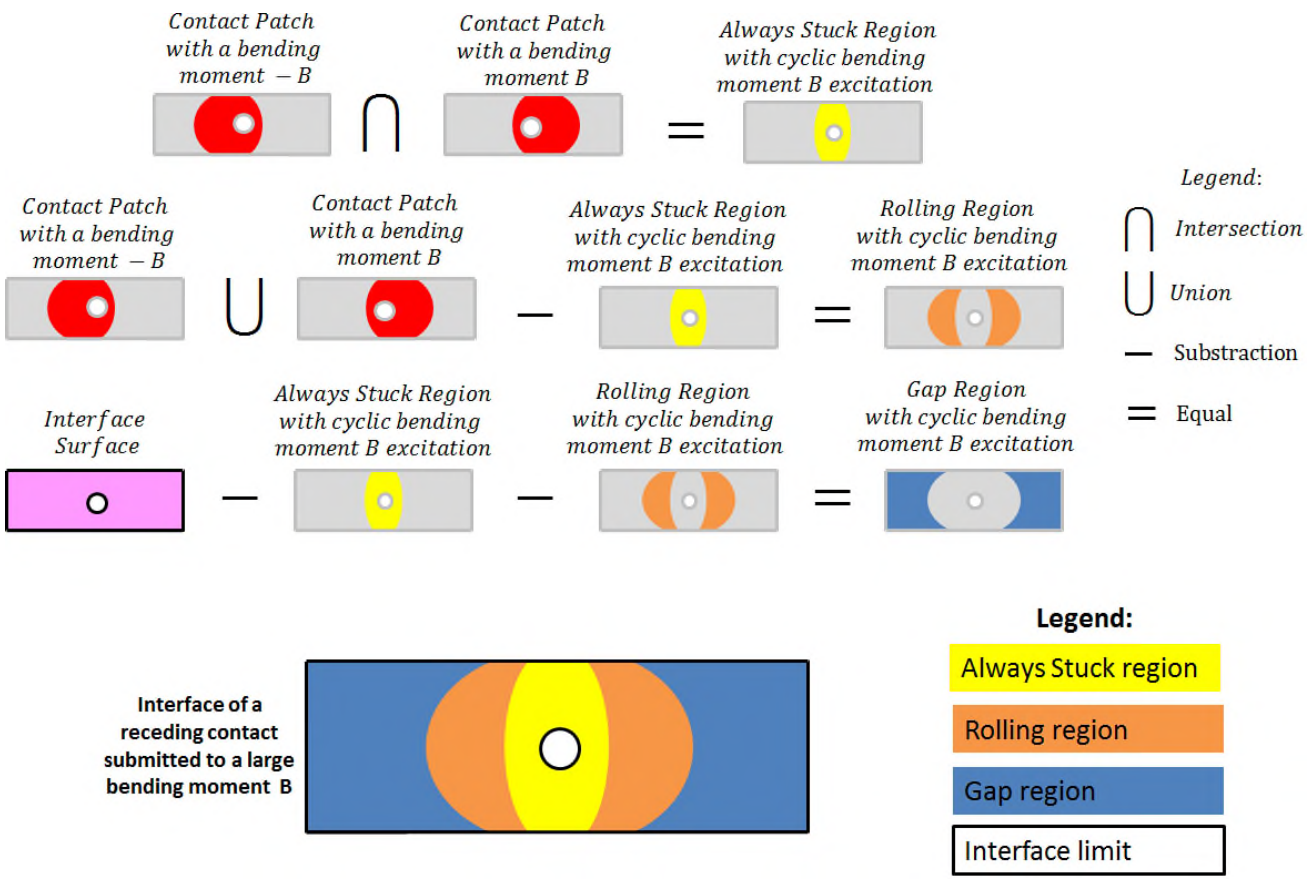

Figure 173 Definition of the always stuck region, the rolling region and the gap region and the top view of the interface with the three types of region. The always stuck region is where the contact patch is maintained during a cycle. The rolling region is where the contact patch changes and the gap region is where no contact happens during the whole cycle of vibration. The interface surface is the sum of all the surfaces where a contact patch could exist.

The dynamic contact patch allows the definition of two different regions with opposite behaviour: The “always stuck” region and the “rolling region”. The region in the interface where there is no contact during the cycle of vibration is called the “gap region”. The word “region” is used here to designate a surface area. The always stuck region is the area of the contact patches which stay in contact during the whole cycle of bending moment excitation. The rolling region is where the contact patch “rolls” due to the bending moment, as in the sphere on the plane described in Figure 165. The rolling region delimits the area where the contact patch evolves due to the bending moment.

8.1.7 Correlation with experimental results

The concepts of “always stuck region” and “rolling region” were designed to be correlated to respectively the measured natural frequency and the damping ratio. Indeed, the size of the always stuck region is correlated to the measured natural frequency. Also, the size of the rolling region is correlated to the measured damping ratio.

In this thesis, only the size of the always stuck and rolling regions will be used to quantify the rolling effect. The sizes of these regions were considered adequate enough to perform an interpretation of the experimental results. Indeed, finding an interpretation of the results is the goal of this discussion chapter. A more elaborated and mathematical model, which quantifies the rolling effect, the bending moment and the amplitude, could be created in the future.

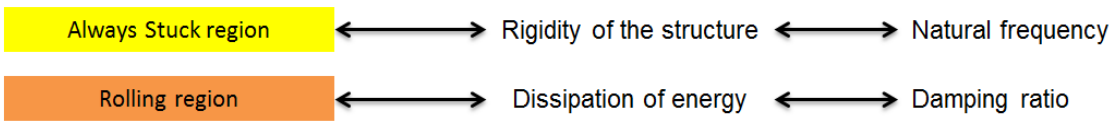

Figure 174 First row, the relation between the always stuck region and the natural frequency. Second row, the relation between the rolling region and the damping ratio.

The size of the always stuck region is correlated to the rigidity of the structure and the natural frequency as shown in Figure 174. If the size of the always stuck region changes, automatically the value of the natural frequency should follow. If the size of the always stuck region increases, the natural frequency increases also. On the other hand, if the size of the always stuck region decreases, the natural frequency decreases also.

The size of the rolling region is correlated with the damping ratio measured as shown in Figure 174. If the size of the rolling region increases, the damping ratio should increases. Conversely, if the size of the rolling region decreases, the damping ratio decreases also.

The effect of the amplitude of vibration can be easily explained from this interpretation. The value of the amplitude of the vibration is directly related to the value of the bending moment which excites the lap joint. Put differently, the bigger the amplitude of vibration, the bigger the bending moment. Thus, the bigger the bending moment, the bigger the rolling region and inversely the smaller the always stuck region, in term of surface size, as shown in Figure 175.

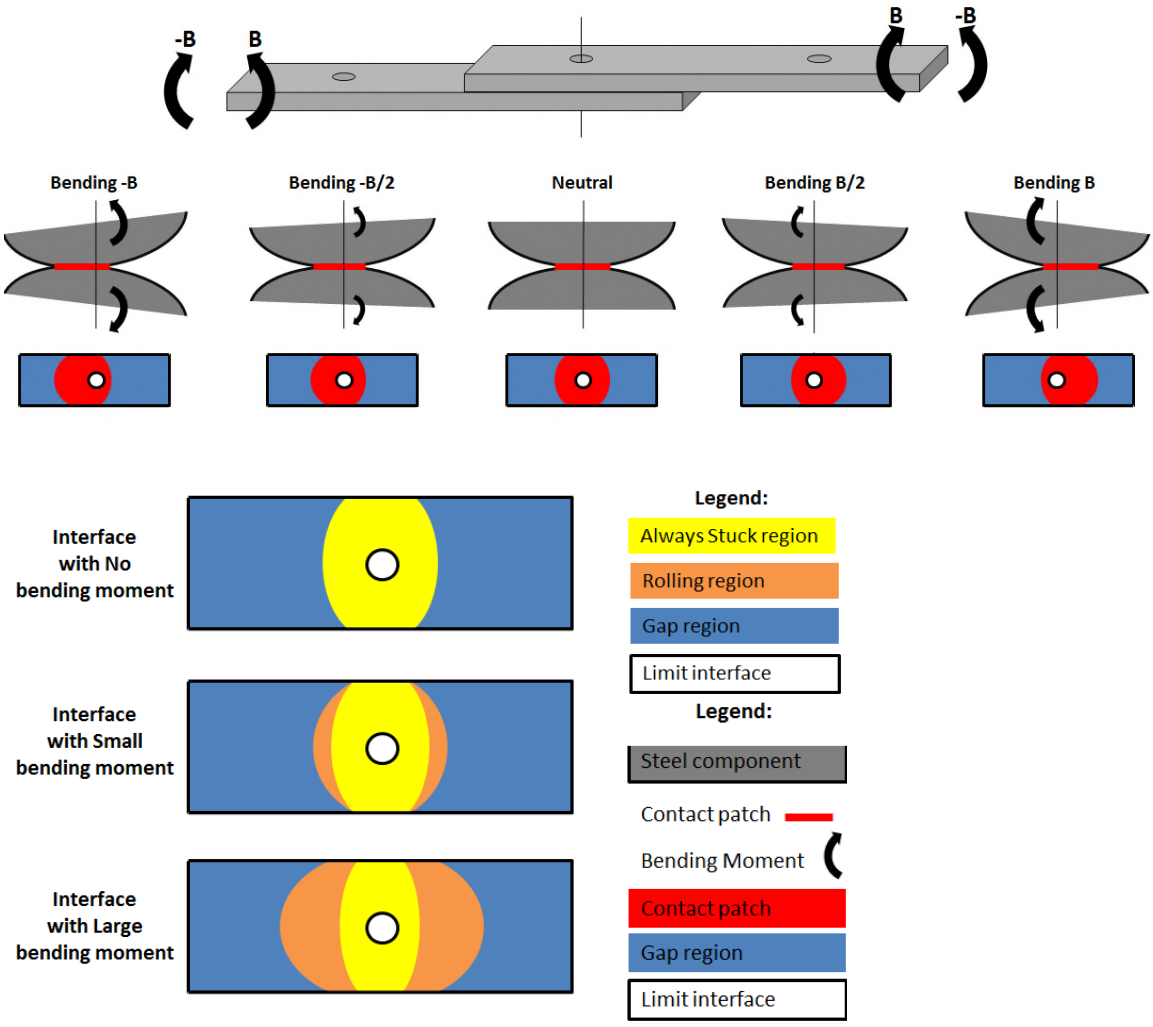

Figure 175 Interpretation of the influence of the amplitude on the nonlinear behaviour of a bolted lap joint. This diagram explains why the bending moment in a lap joint creates an amplitude dependant damping ratio and natural frequency. The top row is an example of pure bending moment cyclic excitation as defined in beam theory. The second row details the impact of the amplitude of bending moment on the change of the contact patch. The third row describes the impact of the amplitude of the bending moment on the always stuck region and the rolling region. The fourth row is the relationship between the size of the

always stuck region and the rolling region and respectively the natural frequency and the damping ratio.

Figure 175 explains why there is a loosening effect in a lap joint: when the amplitude of vibration decreases, the always stuck region increases as shown in Figure 175; thus, the natural frequency increases. Also, Figure 175 explains the nonlinear damping of a lap joint: when the amplitude of vibration decreases, the rolling region decreases as shown in Figure 175; thus, the damping ratio decreases. In conclusion, the damping ratio and the natural frequency inside a lap joint with a receding contact are amplitude dependent because the size of the always stuck region and the rolling region is connected to the bending moment, which is connected to the amplitude of vibration.

Adding a shim between the two components of a lap joint reduces the size of the interface and automatically the size of the contact patch as shown in Figure 176. Note that, the concept of interface is defined in this thesis as the surfaces which may enter in contact, whereas the contact patch is the surfaces which are in contact at a particular instant.

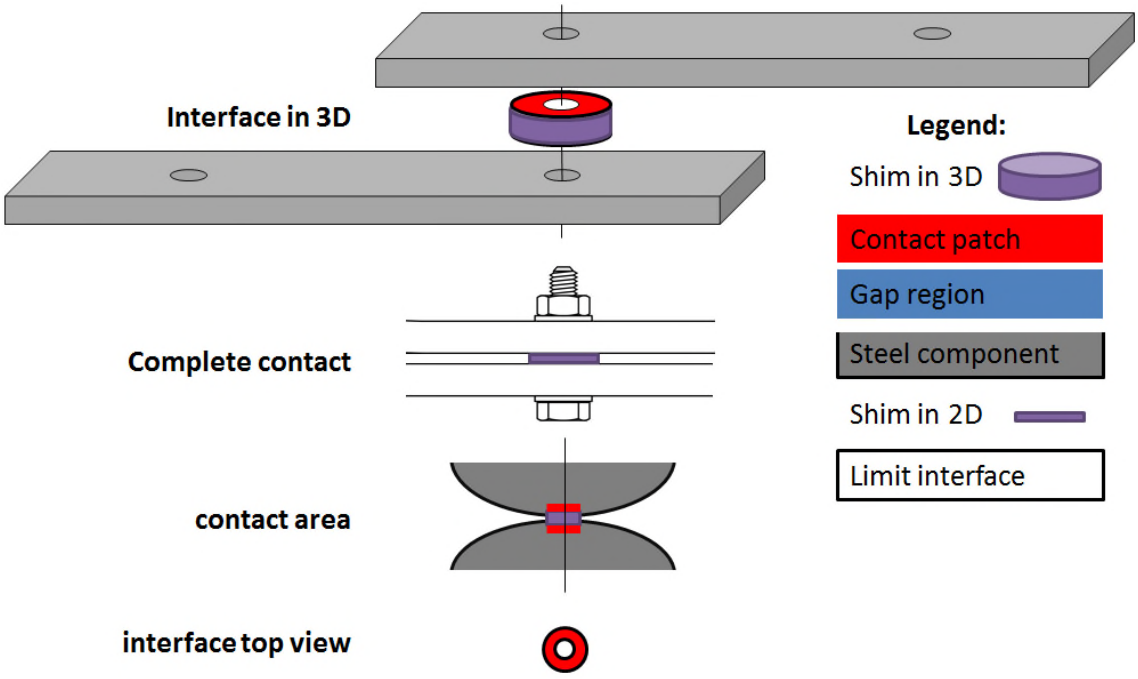

Figure 176 Illustration of the effect of a washer sized shim on the interface and the contact patch of a bolted lap joint. There is no gap region with a complete contact.

With the same interpretation, the fact that the scaled natural frequency is greater than 1, in most of the experimental results, can be explained. When there is no vibration, the contact patch of the complete contact is smaller than the contact patch of the receding contact as displayed in Figure 177. The always stuck region of the complete contact is small, so the natural frequency is small. Therefore, the always stuck region of the receding contact is larger, so the natural frequency with a receding contact is larger. The scaled natural frequency is the ratio between the natural frequency with a receding contact and the natural frequency with a complete contact. In conclusion, the scaled natural frequency is greater than 100% in most experimental cases because the always stuck region of the receding contact is bigger than the always stuck region of the complete contact.

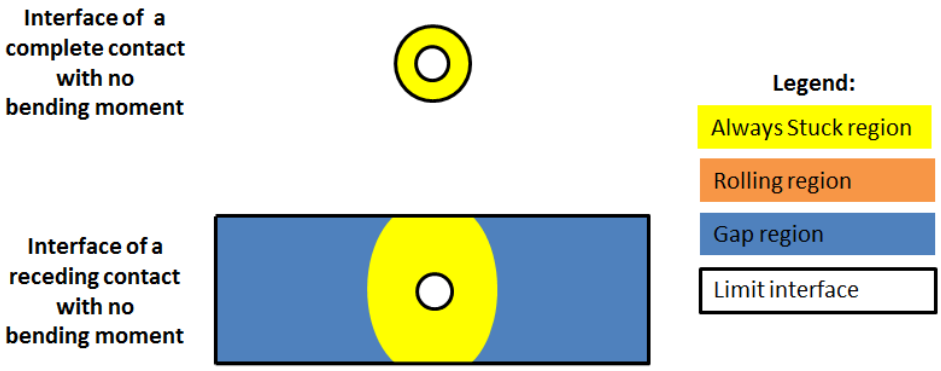

Figure 177 Static contact patch of a complete contact, with a washer size shim, and of a receding contact, without a shim.

The complete contact generates no joint damping or a very small amount of damping because the contact patch of a complete contact does not evolve due to the bending moment as shown in Figure 178.

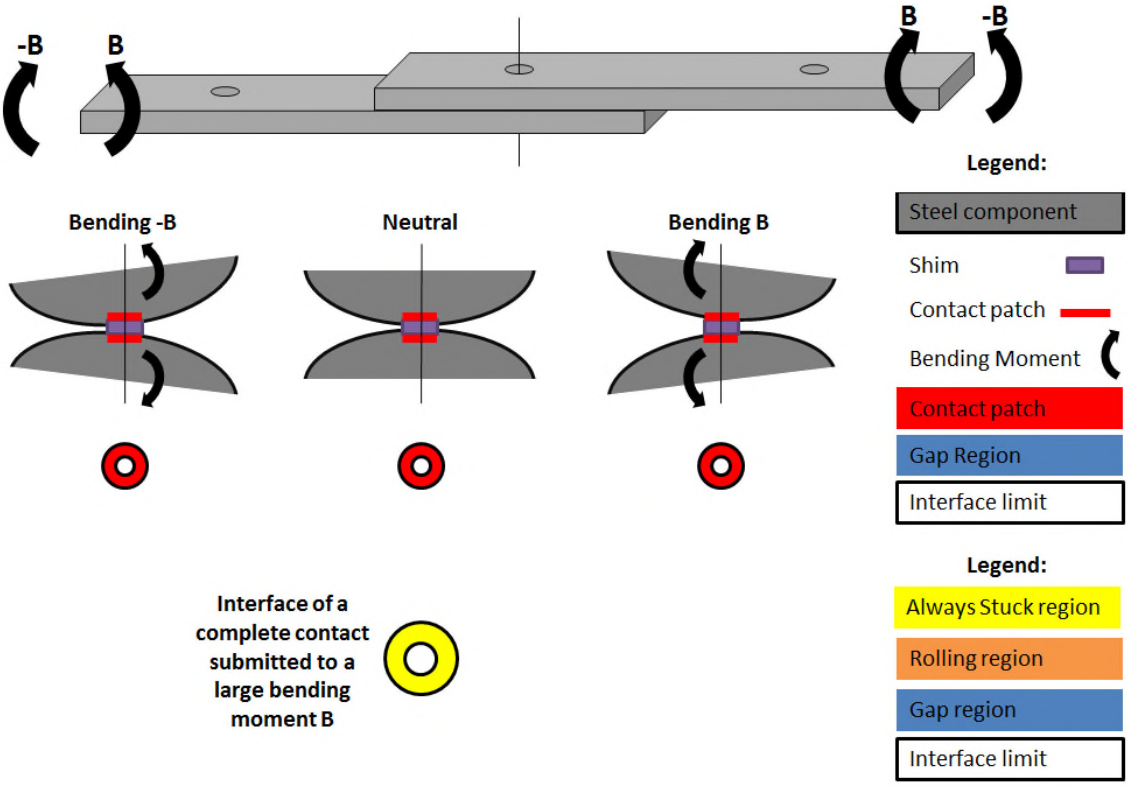

Figure 178 Interpretation of the absence of damping due to a bending moment in a lap joint with a washer sized shim. Top row: Example of a pure bending moment cyclic excitation as defined in beam theory. Second row: side view of the contact patch which stays the same whatever the bending moment. Bottom

row: top view of the interface which stays the same for the cycle of bending. The always stuck region is where the contact is maintained during the vibration cycle. The rolling region is where the contact patch changes and the gap region is where no contact happens during the cycle of vibration. With a washer sized shim, there is no rolling region, so no joint damping.

Finally, why, in the joint position experiment, is the measured scaled damping ratio greater than 100%? Indeed, the damping ratio increases when a complete contact is turned into a receding contact. Following the same reasoning, this increase of damping ratio is interpreted as an increase in the size of the rolling region, as shown in Figure 179. When the rolling region increases in size, the damping ratio increases as well. The scaled damping ratio is defined as the ratio between the damping ratio of a receding contact divided by the damping ratio of a complete contact. This scaled damping ratio has to be greater than 100% because the rolling region of a receding contact is bigger than the rolling region of a complete contact.

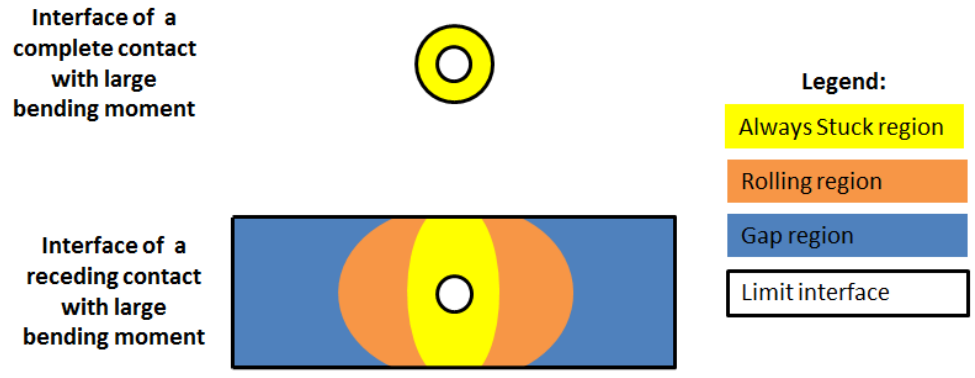

Figure 179 Behaviour at the interface of a lap joint for a complete contact and a receding contact

8.1.8 Speculation on the origin of rolling damping

This section presents certain speculations on the source of friction in bolted lap joints when submitted to a bending moment. These speculations are not corroborated by measurement.

The shear force is the foundation of most friction models including the Coulomb friction model. In the Coulomb model, if the shear force is greater than the normal force multiplied by a coefficient of friction, then there is a relative tangential displacement.

The main problem with the Coulomb model is the hypothesis that there is actual sliding in the interface. Indeed, the surfaces of both main components are forced to be in contact due to the bolts. Moreover, the surfaces should then be interlocked by many micro asperities of both surfaces' roughness, as in Figure 180. Those micro asperities would make any sliding between the two components difficult, even with no normal constraint to hold them together. So no transversal sliding in the contact patch seems possible. On the other hand, the micro-asperities do not block any normal displacement, as displayed in Figure 180. A normal displacement at the interface could, for example, be an alternative opening and closing of the edge of the contact patch.

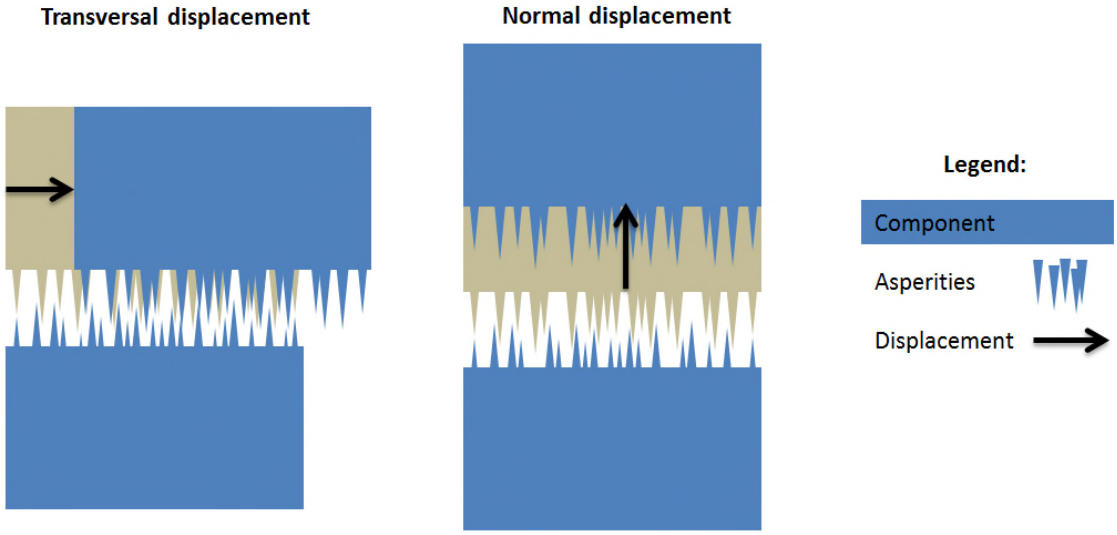

Figure 180 Juxtaposition of the transversal displacement and the normal displacement of two components with exaggerated roughness asperities

The interpretation presented in Section 8.1 was that the bending moment force created a rolling effect and not a shear force. Therefore, the Coulomb model was not used in the interpretation.

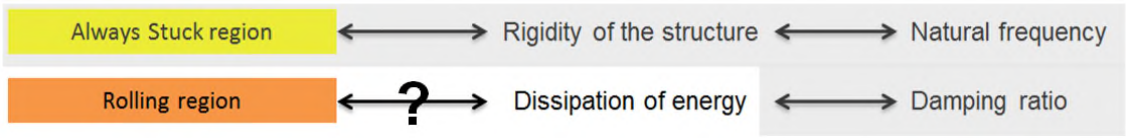

Figure 181 Why is the rolling region correlated to the dissipation of energy?

The question “Why is the rolling region correlated to the dissipation of energy?”as illustrated in Figure 181, is still unanswered. Intuitively, the origin of the damping could be due to the creation of micro-connections and the rupture of those micro-connections between the roughness asperities as illustrated in Figure 182. In the rolling region, two surfaces of the components enter in contact and get separated. As explained before, it is thought that a relative tangential displacement seems not to happen in the rolling region, only normal displacement. The mechanism of dissipation of energy would look like Velcro which closed and opened at each cycle of vibration. There is no evidence on which to base this explanation of micro-connection. More work and evidence are needed to validate or refute this micro-connection type of joint damping.

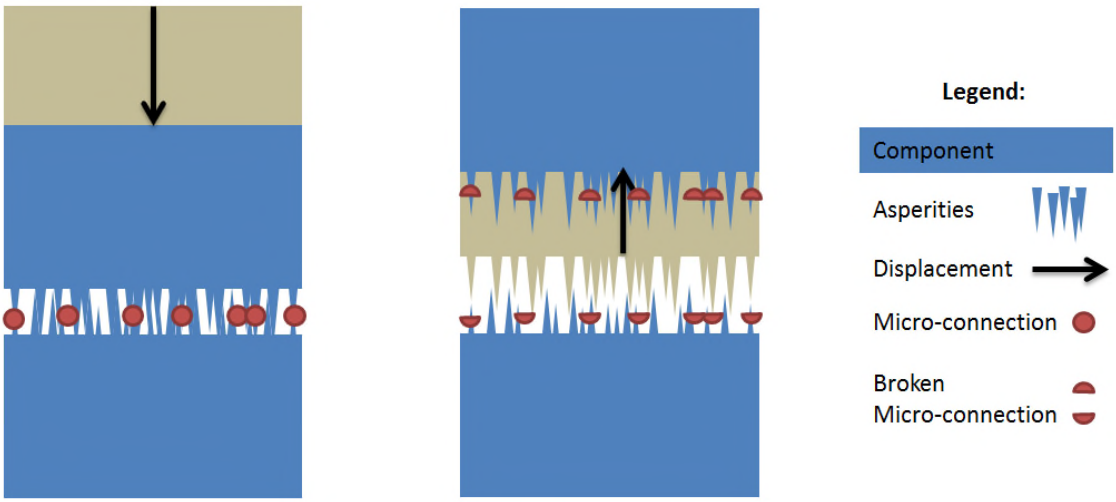

Figure 182 Interpretation of the way the rolling effect dissipates the vibration energy in a bolted lap joint. The two surfaces in contact create an alternative normal displacement at a microscopic level. The asperities create micro-connections when they enter in contact. The micro-connections are broken when the two surfaces separate.

8.1.9 Synthesis of the interpretation

Figure 183 is a synthesis of the interpretation proposed in this section. By answering the two following questions a prediction of the behaviour at a bolted lap joint can be made. First does the joint have a complete contact or a receding contact? If there is a receding contact, is the joint submitted to a cyclic bending moment excitation? If so then a large amplitude dependant damping ratio is expected, and a large amplitude dependant shift of natural frequency is expected. If there is no bending moment excitation or the joint has a complete contact in the first place, then the joint damping should be low and not amplitude dependant, also the joint rigidity should not be amplitude dependant.

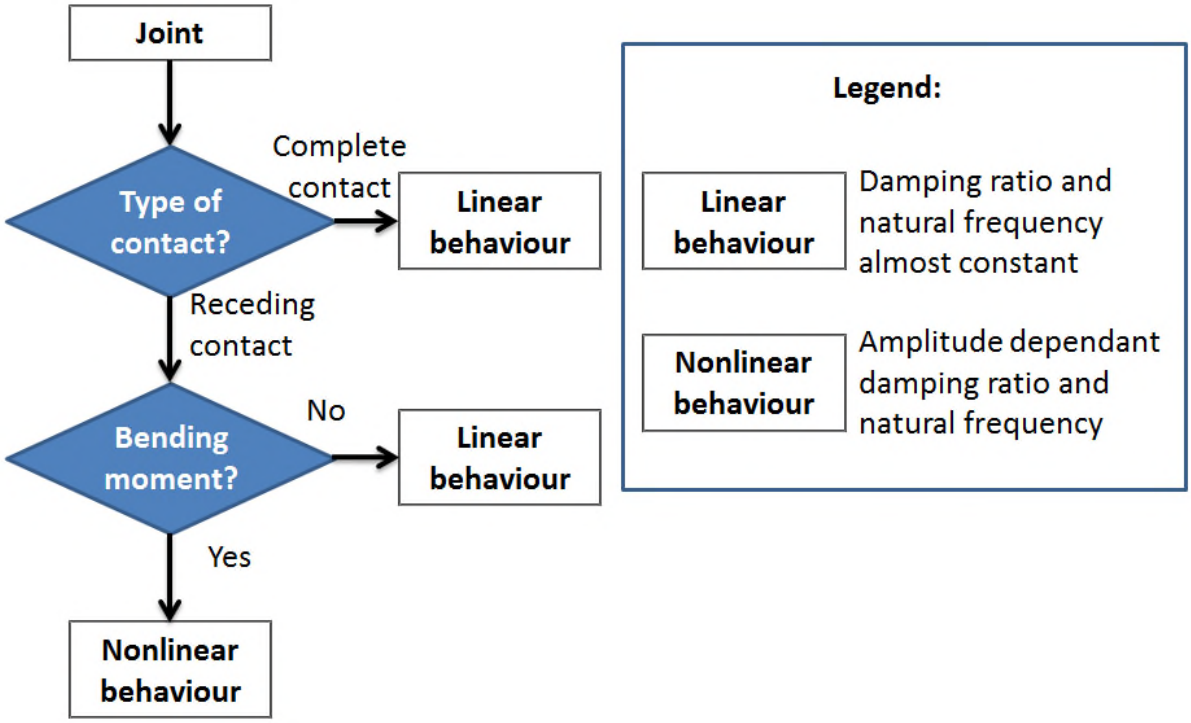

Figure 183 Two questions to predict the dynamic behaviour of a joint

This prediction method proposed in Figure 183 can be wrong for many reasons and should be used with caution. The prediction may be wrong, for example, if the bolted lap joint design is different (more than one bolt), if the mode in question is not a bending mode, if the material is not steel, if the surfaces are

not smooth, if the amplitude of vibration is extremely weak or extremely strong, If the bolt torque is too low.

The interpretation of the results of the sandwich beam experiment is very similar to the one proposed for the joint position experiment. An explanation, for the amplitude dependent nonlinear behaviour of lap joints, was proposed in the discussion Section 5.7. This explanation was based on the shim length experimental results. It is based on the change of three different regions. This interpretation is very close to the one proposed in this section, except that the sliding region was renamed the rolling region. The similarity was possible because of the two interpretation top views for the shear force and the bending moment. The similarity is very noticeable when comparing the top view on the last row of Figure 170 and the last row of Figure 172. Those two top views are displayed again in Figure 184. Therefore, the conclusion of the sandwich beam experiment and the joint position experiment are almost identical. The main difference is that the main source of the nonlinear behaviour is not sliding but rolling.

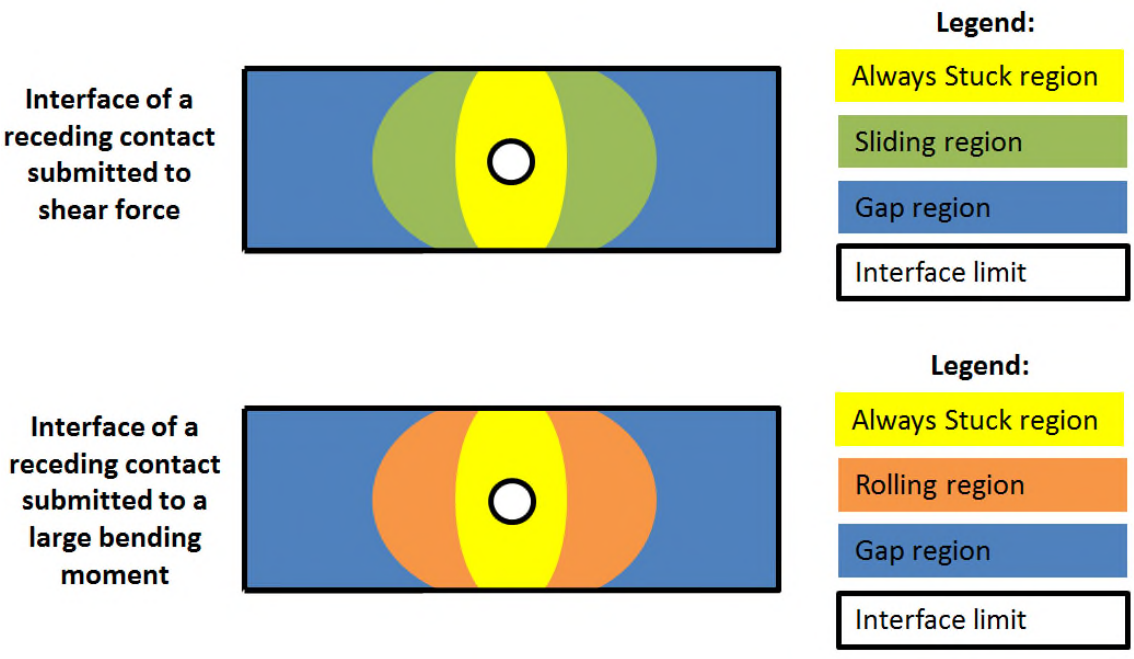

Figure 184 Interpretation of the different behaviour at the interface of a bolted lap joint using sliding (top row) and rolling (bottom row).

In conclusion, the explanation, given in this document, of the origin of nonlinear behaviour in a bolted joint is that the two components of a lap joint roll like a sphere on a plane, due to the combination of the receding effect and a bending moment. The receding effect reduces the size of the contact patch and the rolling effect changes the contact patch. This modification of contact patch creates damping and changes the rigidity of the structure. The joint damping and the joint rigidity are nonlinear because they depend on the amplitude of vibration. This amplitude of vibration is linked to the bending moment. However in a complete contact, regardless of the amplitude, the contact patch does not change. Therefore, in a complete contact, there is no change of contact patch, so no rolling, no change of rigidity and no nonlinear damping. This interpretation conclusion is synthesised in Table 26.

Table 26 Summary of the interpretation of the nonlinear behaviour of bolted lap joint

Type of contact	**Receding contact (behaviour scaled by the amount of bending moment)**		**Complete contact**	
Measured value	**Natural Frequency**	**Damping Ratio**	**Natural Frequency**	**Damping Ratio**
Trend when the amplitude decrease	Increase (amplitude dependant natural frequency)	Decrease (amplitude dependant damping ratio)	Almost constant	Almost constant
Interpretation of the trend when the amplitude decrease	The always stuck region increases when the bending moment decrease	The rolling region decreases when the bending moment decrease	The always stuck region stays almost the same	The rolling region stays almost the same

8.2 Impact on the literature

The interpretation, proposed in 8.1, shines a new light on the behaviour of the Brake-Reuss Beams. The nominal Brake and Reuss Beams (BRB) with a

bolted lap joint is shown in Figure 185. Smith, Brake, and Reuß (2015) did not point out that the odd numbered bending modes of the BRB (mode one, three and five) have a stronger nonlinear behaviour than the even bending mode (mode two and four). The BRB has a receding contact patch at the centre of the beam which is comparable to the test B08&B09 of the joint position experiment investigated in Chapter 6 and 7. The two structures have almost the same geometry of lap joint. The bolt position 8 and 9 (B08 and B09) are displayed in Figure 186. Therefore, the conclusion of the joint position experiment could be extended to the BRB. Thus, the difference between the odd or even bending moment modes can be explained as follows: The BRB lap joint is submitted to a larger bending moment excitation for the odd bending mode compared to the even bending mode.

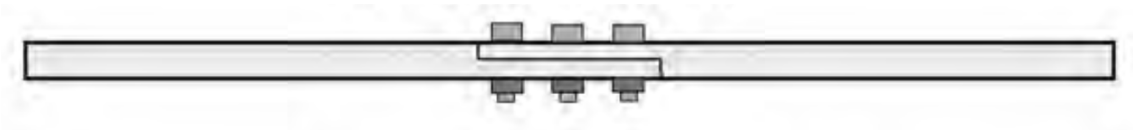

Figure 185 Nominal Brake and Reuss Beam (BRB). Source : Cooper et al. (2017)

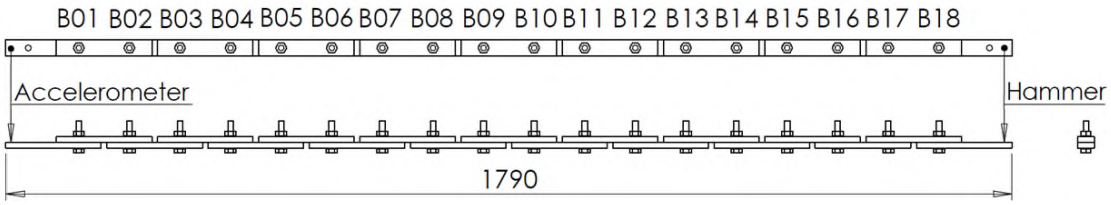

Figure 186 Built-up beam with 18 bolted lap joint investigated in Chapter 6.

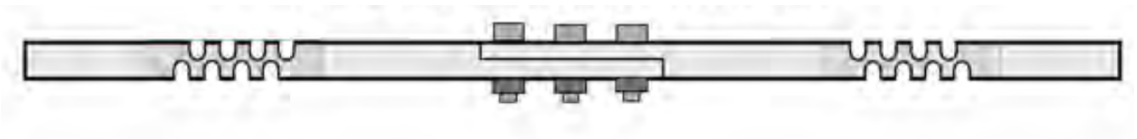

Figure 187 Stiffness Modified Beam (SBRB). Source : Cooper et al. (2017)

Also, a new interpretation of the results can be drawn from the paper by Cooper et al. (2017). This paper investigates the impact of the modification of the structure far from the lap joint of the BRB, also called the “far-field effect”. In that paper, the Stiffness Modified Beam (SBRB) produces less damping than the

classic BRB. The SBRB is displayed in Figure 187. Using the results of the joint position experiment, the explanation is that the joint of the SBRB generates less damping because the structure bends at the spring location, and does not bend at the lap joint location. By extension, the far-field effect could be explained by the modification of the amount of bending moment at the joint location, caused by modification of the structure geometry far from the joint. In short, when the mode shapes change, the excitation of the joints changes also.

8.3 Contributions sorted by objectives

The contributions of this thesis are listed in this subsection. The contributions are organised by reference to the objectives given in Section 2.7.

Objective 1: Identify the dominant parameters which affect the nonlinear behaviour of bolted lap joints

The dominant parameters which affect the nonlinear behaviour of a bolted lap joint, measured and tested in this thesis, in order of importance are:

1. The interface limit of the lap joint has a direct impact on the type contact (receding contact, complete contact or in-between) (Section 8.1)
2. The cyclic bending moment loading at the position of a joint is correlated to the nonlinear behaviour of a lap joint. (Section 8.1)
3. The nonlinear behaviour depends on the amplitude of vibration. (Section 5.7)
4. Some measurements show that the joints close to the hammer hits have a superior nonlinear damping and loosening effect, compare to a joint located father from the hammer hits. (Section 6.4)
5. Lubrication with grease increases the damping of a receding contact compared to a dry contact. However oil does not increase the damping. (Section 5.8)
6. More work is needed to understand the effect of the roughness of the surfaces in contact. The roughness may have change the damping and rigidity of structures. It seems that smoother surfaces could lead to an

increased damping ratio and an increase of the change of natural frequency due to amplitude. (Section 7.5)

7. The suspension (length, strings material and position) have a minor but measurable impact on the dynamic of a monolithic beam. More work is needed to measure the impact of the experimental set-up on the nonlinear dynamic behaviour of bolted lap joint. (Chapter 3)

Objective 2: Investigate the damping and stiffness properties of bolted lap joints

8. An experiment using shims of different sizes within a joint shows that the size of the contact patch grows as the amplitude of vibration decays. (Subsection 5.2.3)
9. By using shims to transform multiple receding contacts into complete contacts, revealed that the damping of lap joints with one bolt is correlated to the bending moment. (Section 7.1)
10. An interpretation of the origin of the damping and stiffness properties of bolted lap joints was suggested for joints with two bolts (Section 5.7) and with one bolt. (Section 8.1). For two bolt joints, slip is assumed to happen in a region far from the bolts axis, whereas, for a one bolt joint, the rolling should be dominant. More work is necessary. (Section 10.1)
11. The always stuck region shrinks, due to a cyclic bending moment, linked to the amplitude of vibration, which is correlated to a reduction of the stiffness of the joint, which is measured by a decrease of the natural frequencies. (Section 8.1)
12. The size of the rolling region increases, due to a cyclic bending moment linked to the amplitude of vibration, and is correlated to an increase of the energy dissipated, which is measured by an increased damping ratio. (Section 8.1)

Objective 3: Reduce the uncertainty linked to the dynamics of joints

13. Section 8.1 proposes an interpretation which links together almost all the measured behaviour based on the size and the behaviour of the contact patch in the joint interface. (Section 8.1)
14. Section 7.7 proposes a finite element procedure which quantifies the impact of a design change on the natural frequencies of a structure. (Section 7.7)

Objective 4: Improve the experimental method and signal processing workflow applicable to nonlinear dynamic structures

15. The experimental method and signal processing workflow developed in this thesis used suspended structures with one accelerometer and impact excitation to investigate joints. The reverse filtering and direct fitting signal-processing methods enable instantaneous natural frequencies and damping ratios to be plotted as a function of amplitude. (Chapter 3)
16. The use of shims of different sizes, to change the lap joint contact patch and interface, allow for a comparison between a receding contact, a complete contact and variants in-between these two extremes. (Chapter 6)
17. The use of a beam with multiple lap joints enabled the investigation of the position of one or multiple receding contacts in a structure, hence the impact of the position of a joint. (Subsection 6.1.1)
18. The use of simulated shims in a finite element model modal analysis enables the importance of individual joints to be determined. (Section 7.3)

9 CONCLUSION

The main objective of this thesis was to investigate the nonlinear dynamic behaviour of joints. An experimental approach was used to reach this objective. Two novel experiments were performed to measure and quantify the effect of the size of a joint interface and the importance of individual interfaces in a structure with many joints. Both revealed novel results. Also, an accurate finite element simulation of an interface predicted the nonlinear frequency behaviour of bolted lap joints.

The shim sizes experiment, presented in Chapter 3, shows that the size of the contact patches associated with the geometry of the interface is a dominant parameter of the nonlinear dynamic behaviour of bolted lap joint. In this thesis, the use of shims within a joint has provided insights into the nonlinear behaviour at the interface of joints. This leads to the categorisation of contacts which make a joint between two components: a complete contact prevents all slip or rolling in the joint, whereas a receding contact has a changing contact patch which creates frictional nonlinear behaviour. A complete contact has large stress at the edge of its contact patch, whereas a receding contact has minimal stress at the edge of the contact patch.

The joint location experiments, in chapter 6, identified a correlated between the position of a joint in a built-up structure and its nonlinear dynamic behaviour. An amplitude dependent behaviour was measured for the damping ratio and the natural frequency. This amplitude dependent behaviour change depending on the position of the joints following a wave pattern, with as many waves at the mode number. The position of a receding contact was investigated using a novel experimental method. Washer size shims were introduced in the interface to change a receding contact into a complete contact. By placing shims at all location except one, in a beam with 18 identical bolted lap joints, the effect of the position of a joint on the dynamic behaviour was investigated. The measured effect of the joint location was correlated to the amount of bending moment for most of the 12 first bending modes analysed. The amplitude

dependent nonlinear behaviour, for a lap joint with one bolt, is the strongest at the antinode of the bending moment.

In Chapter 7, a simulation of the Chapter 6 experiment predicted the measured change of natural frequency due to the placement of shims at a joint location. The mesh at the interface of the joint was restricted to simulate the effect of a washer sized shim. Also, the mode shape behaviour at the joint was correlated to the effect of the shim in the interface. This simulation is a positive step in the prediction of nonlinear dynamic behaviour of a joint.

In Chapter 8 the results were discussed. The results were interpreted as a probable causality between the joint loading and the change of contact patch in the joints. If the loading at the joint location changes the contact patch, then a nonlinear dynamic behaviour is expected. However, if the contact patch is restricted by a washer sized shim and the contact patch does not change, then the natural frequency and the damping ratio is not dependent of the amplitude of vibration. If the contact patch changes due the bending moment, then the joint has a nonlinear dynamic behaviour. Therefore, the accurate prediction of the dynamic contact patch seems the key to any successful simulation the nonlinear dynamic behaviour of bolted lap joints.

The literature on the nonlinear dynamic behaviour of bolted lap joints was reviewed. The main conclusion was that there is a lack of a predictive model which likely arises due to a lack of knowledge of the inner physics at the interface of joints. It was for this reason that an experimental approach was chosen.

To analyse the experimental signals, a new signal processing workflow was implemented (Chapter 4). The workflow extracts the instantaneous natural frequency, damping ratio and amplitude from the measured time history due to impact excitation. A reverse filtering method avoids filter ringing by reversing the time history, performing bandpass filtering, and then reversing again. In a second step, five-cycle-section of the filtered time history is fitted using a customized vibration decay model.

10 FUTURE WORK

Section 10.1 provides possible experimental layouts which are variations of the shim experiments presented in this thesis. Section 10.2 describes how the current signal processing work flow can still be improved. Finally, Section 10.3 suggests future work on a predictive model of the nonlinear dynamic behaviour of joints.

10.1 Experimental future work

One major piece of evidence which is missing in this thesis is a shim size experiment, as presented in Section 5.4, performed on a lap joint with one bolt. Indeed, the shim size experiment performed in Section 5.4 was on the sandwich beam. The sandwich beam has a very specific geometry with a long interface and with two bolts. The results with a two bolt joint in Chapter 5 were extrapolated to interpret the results of a one bolt joint investigated in Chapter 6 and Chapter 7. The mode shape of the two structures investigated are noticeably different in Figure 188 and Figure 189 This extrapolation from a two bolt joint to interpret a one bolt joint could be wrong. If more time was allocated, the first experiment would be a shim size experiment as described in Chapter 5 on a one bolt lap joint as investigated in Chapter 6.

Figure 188 First bending mode of the sandwich beam with two bolts from a finite element model analysis. See chapter 3 for more details.

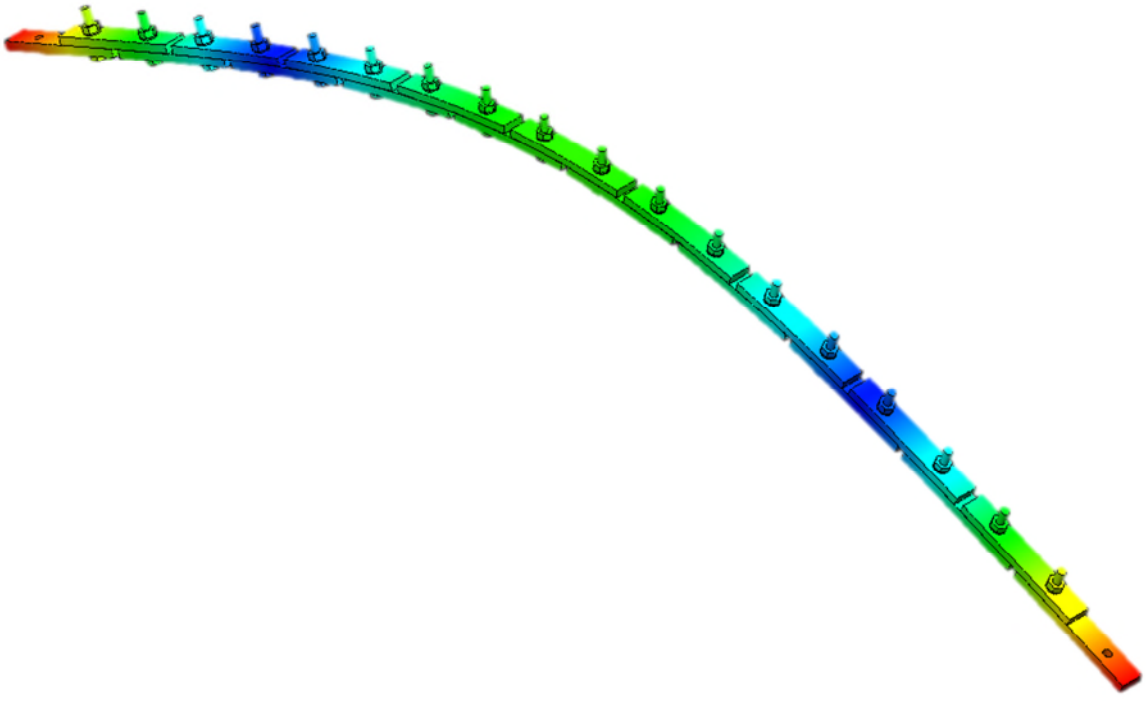

Figure 189 First bending mode of the 18 bolted lap joint structure investigated in chapter 6 and Chapter 7

Also, preliminary results show that the number of bolts could have a major impact on the behaviour of bolted lap joints, but more work is needed to reach a conclusion. An unfinished investigation, due to a lack of time, on the impact of the position of the two bolts in the sandwich beam show intriguing results. Seven symmetrical positions of bolts were tested on the sandwich beams and the position with the highest measured damping ratio was at the node of the first bending mode, where the bolts are located in Figure 188. Note that, the cyclic shear force excitation of a beam is the greatest at the node of the first bending mode. Therefore, they may be a correlation between the shear force and the bolt position in a joint with two bolts. The results of the joint position investigation with two bolts are in contradiction with the results of the joint position experiment with one bolt. Consequently, they may be two categories of joints: joint with two bolts and the joints with one bolt. The joint with two bolts could have a nonlinear dynamic behaviour correlated to the shear force in the joint, whereas the joint with one bolt could have a nonlinear dynamic behaviour correlated to the bending moment. More work is needed to verify if the preliminary results, of the impact of the position of two bolts, are valid.

The nonlinear dynamic behaviour of joints seems to be correlated to the surface roughness. The surface roughness at the interface of joints could be investigated using multiple shims with different surface roughness, materials or manufacturing techniques.

The investigation on the impact of the thickness of the shim was limited, and more information could be obtained by changing the thickness of the shims. Indeed, only 100mm long shims of different thickness were tested. However, when a very slim washer-size-shim is placed in a bolted lap joint, then contact may happen away from the shim, thus more friction, and more nonlinear dynamic behaviour. More work is needed to know how slim a washer-size-shim can be before a nonlinear dynamic behaviour is measured in a joint.

A new experimental layout could help study the precise effect of bending on a bolted lap joint The solution found is inspired by the Gaul and Lenz's (1997)

experimental layout, and by the improved design proposed by Süß, Janeba, and Willner (2017), see Figure 190.

Figure 190 Original Lenz and Gaul (1995) resonator (left); Süß, Janeba, and Willner (2017) improved design (right)

Figure 191 Difference between shear and bending loading as proposed in subsection 2.3.1.

However, Instead of applying a shear loading to the bolted joint, a bending excitation will be applied to the bolted lap joint. The two types of loading are defined in Figure 191. However, this bending loading seems hard to create, therefore the focus was oriented on recreated a similar change of the contact patch due to an opening and closing effect generated by the bending moment.

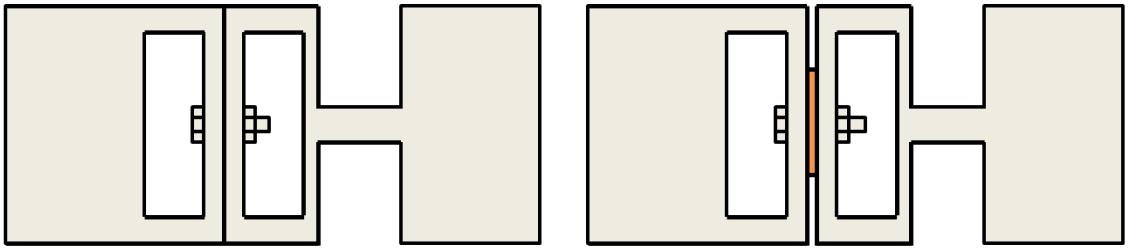

Figure 192 Proposed experimental layout. The orange part is a shim placed between the two components to modify the size of the interface limit of the joint, which will affect the contact patch size.

The best solution proposed only applies a cyclic axial loading as shown in the bolted lap joint in Figure 192. It should allow a detail investigation of the opening and closing in a bolted lap joint. It has double symmetries which simplify the mode shapes and the calculation of the force applied. Besides, shims of different shape could be placed between the two components to customise the contact patch. One advantage, as it is based on Gaul's resonator layout, is that the force and the displacement of the bolted lap joint can be directly measured (something difficult with a beam experiment). To obtain the force and displacement each component needs to be modelled as a spring or a mass as in Figure 193. The resonance of the spring-mass on the right of the figure will be used to excite the joint spring. This experiment design was not modelled, manufactured or tested.

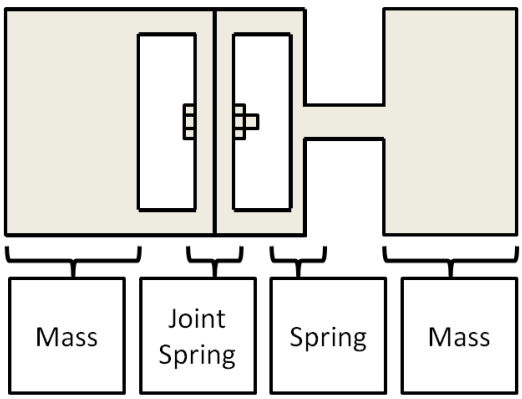

Figure 193 Mass and spring model of the proposed experiment

Further experiments could be carried out using shims to investigate other parameters like the impact of the width of the contact patch. Shims of different width as shown in Figure 194, could point out if the damping of a bolted joint is correlated to the size of the contact patch surface. Indeed, the damping could be correlated or not with the width of the contact patch. It is possible that the damping is correlated to the surface where friction acts. The implication of such results should clarify the way friction acts in a bolted joint, which should help the prediction of joint behaviour.

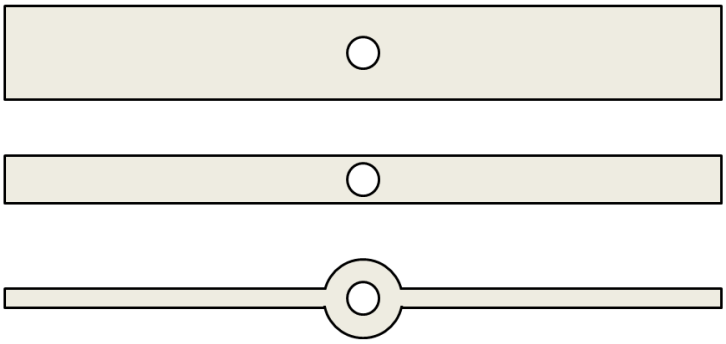

Figure 194 Proposed shim-width-experiment: Top view of three shims of the same length but with 3 different widths

Another promising shim experiment would use concave shims, as proposed in Figure 195. This concave shim should in theory increase the frictional damping compared to a simple flat receding contact. Also, convex shims should be interesting to investigate.

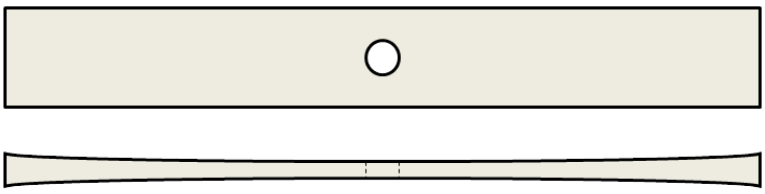

Figure 195 Top and side view of a hypothetic double concave shim which should have more damping than a simple receding contact.

The main idea comes from the observation that damping increase as the size of the shims increases until a certain limit. This limit is probably due to opening

due to the receding contact, or gap between the two components of the lap joints as shown in Figure 196 Receding contact.

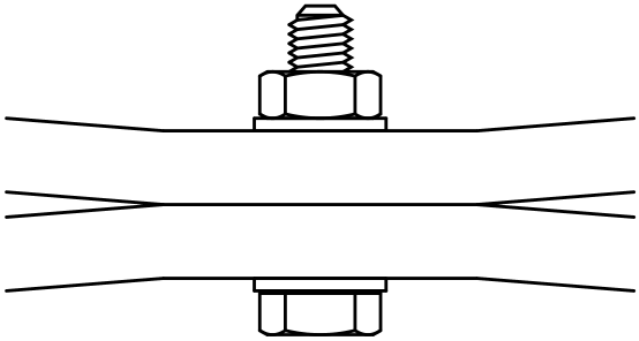

Figure 196 Receding contact

The interface of a receding contact is stuck in the centre due to the bolt force; the receding effect opens up the interface; finally the vibration make the two surfaces roll against each other as shown in the top of Figure 197. The double concaves shim would fill most of the gap created by the receding effect, therefore force a contact far away from the bolt, as shown in the bottom of Figure 197. The curvature should allow the contact patch to evolve further than a simple receding contact. As the rolling region is larger, the damping ratio measured should be higher. Furthermore, a single concave surface should be as effective. However, if a concave shim is “too concave” the always stuck region could cover the whole interface; therefore a complete contact would be created. No preliminary tests were carried out to investigate the idea of a concave shim.

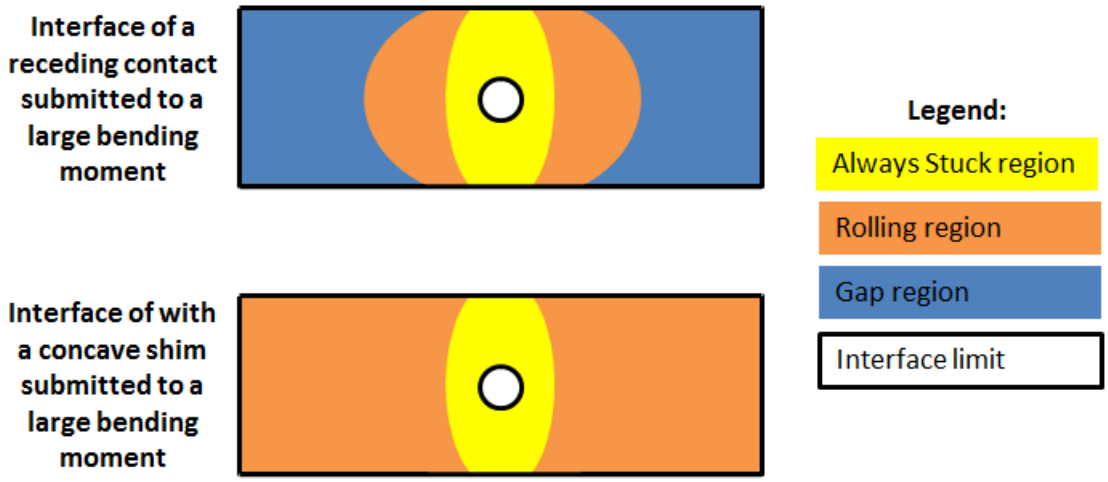

Figure 197 top row, top view of the expected behaviour at the interface of a receding contact in a lap joint. Bottom row, expected behaviour at the interface with a concave shim. See Figure 195 for an illustration of a concave shim. The expected behaviour is an average over multiple cycles when the joint is submitted to a bending moment due to vibration. As the rolling region is bigger, more damping is expected with the concave shim.

Also, a very simple question which has never been investigated concerns the additional effect of joint damping. How does the damping contribution of each joint add up? Figure 198 is an illustration of this question. Once again, shims could be used to answer this question. One of the major results of this thesis is that a washer size shim could be used to shut down the frictional damping of a lap joint. This new technology could be used to single out the damping contribution of one, two or ‘n’ joints. Preliminary results indicate that the damping of two joints is more than one joint, but less than the sum of the individual joint damping. More investigations are necessary to have a better understanding of the way joint damping adds up.

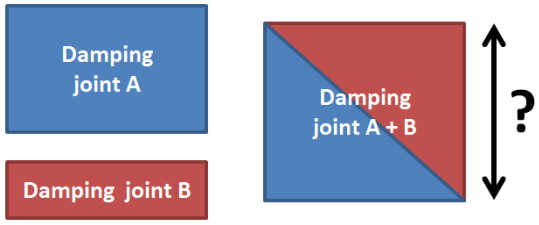

Figure 198 Research question: How does the damping of two joints add-up?

10.2 Future work on signal processing

There is room for improvement in the current workflow. The reverse filtering method could be improved by removing the side effects which are the phase shift or the amplitude reduction. Also, the current direct fitting method could also be extended to fit two or more modes at the same time. Fitting multiple modes simultaneously would simplify the filtering of modes which have almost the same natural frequency. Modal filtering could be another option to deal with two modes with almost the same natural frequency. Cylindrical structures are for example out of reach of the current workflow. All the structures investigated in this document were designed to have well spaced natural frequencies. Therefore, no preliminary work was done on the idea of fitting multiple modes simultaneously.

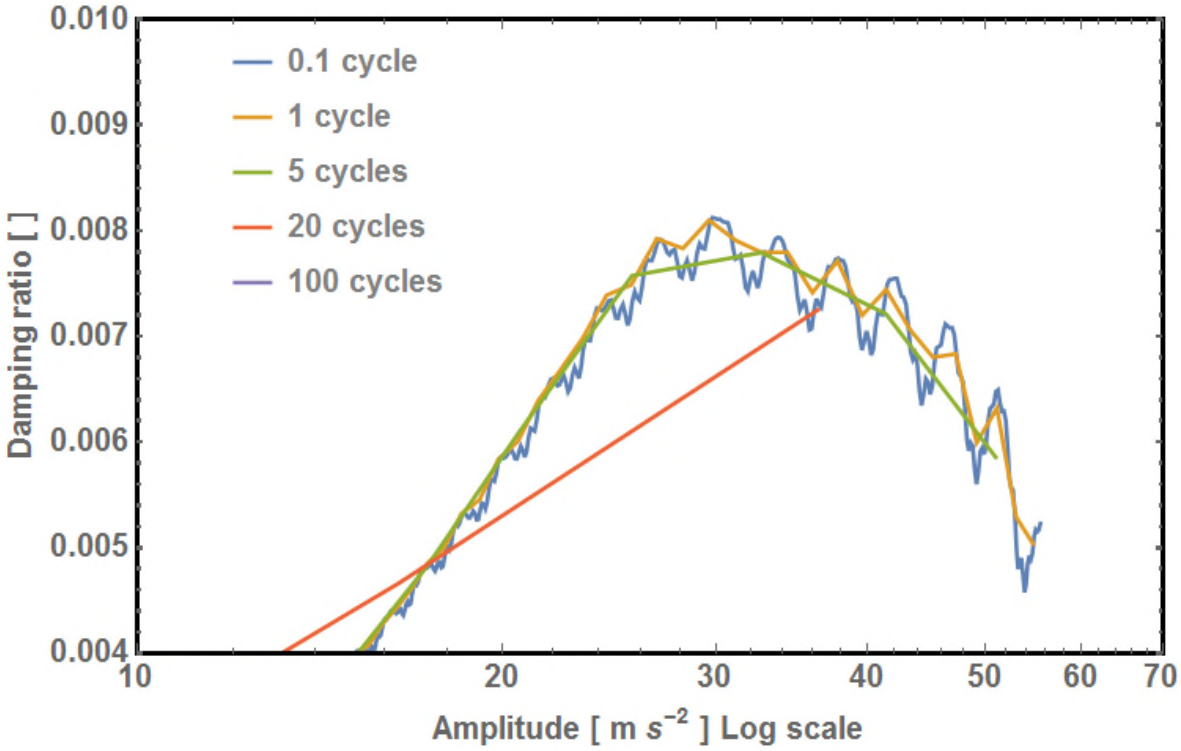

Figure 199 Result of the direct fitting method with different numbers of cycles. See Section 4.3 for more details.

All the fitted data points, presented in this document, are the result of fitting three or five cycles at once. The direct fitting method could be used with an input signal which is less than a cycle. For example, the input time history could be cut into samples of 0.1 cycle and each sample fitted. The results would give more points than if the input time history is cut in samples of five cycles as shown in Figure 199.

If a part cycle investigation was possible, the results could point out precisely when friction happens during a cycle of vibration. The current workflow cannot investigate a signal with a resolution smaller than a cycle in the time domain. Indeed, the direct fitting method needs an input signal with several cycles to create good results. Preliminary tests show that if the input signal is smaller than three cycles, the fitting results have an oscillatory behaviour even with theorical theoretical sinusoidal exponential decay time histories. Even if the direct fitting method would work, the reverse filter method currently removes all

harmonics, if they exist. A new filtering method which includes the harmonics, if they exist, could be useful to study phenomena shorter than a cycle. The current excitation method is also problematic for a part cycle investigation. The hammer hit naturally excites multiple modes at once; therefore a filtering step is necessary. To avoid the filtering step, a sin-stop excitation could be used instead. A sin-stop excitation consists of single harmonic excitation with a detachable shaker. In conclusion, the current experiment set-up and the signal processing workflow would necessities multiple improvements to be used for a part cycle investigation.

10.3 Future work on model

The focus of modelling of joints should be oriented for the creation of predictive models for the designers of joints. Indeed, it seems counterproductive to design joints without taking into consideration the nonlinear dynamic behaviour of a joint, only to perform later an extensive modal analysis on a prototype, when there is a limited possibility of modifying the design of the joints. The literature review concluded that most of the models reviewed were “fitted model”, as illustrated in Figure 200, made for the engineer in charge of prototype testing, not for the designers of joints. If the research focus was more oriented in predicting the nonlinear dynamic behaviour of joints for the designer of joints, fewer problems should show up during the prototype testing, and more importantly, less failure due to joints should occur during the life cycle of products. More work is necessary to identify what are the needs in models at each step of the design of joints and if any joints are necessary in the first place.

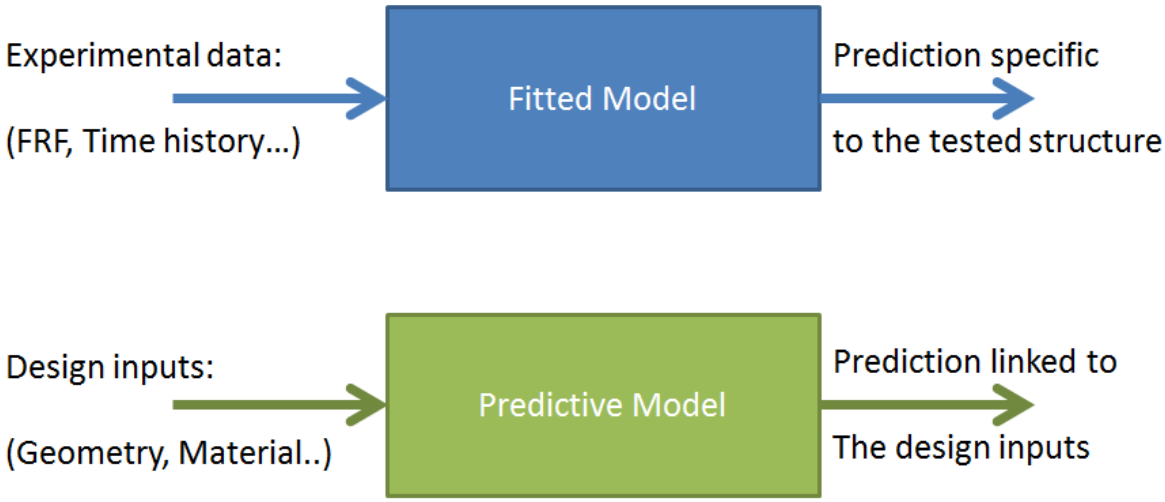

Figure 200 illustration of the difference between a fitted model and a predictive model in term of input and output of the two types of model.

After a consolidation of the experimental results of this thesis, the possibility of a predictive model of the nonlinear dynamic behaviour of joints would have been considered, if enough time was available. This predictive model should take into consideration the size of the interface and the location of the interface as they are correlated to the nonlinear behaviour of a joint. As the user of this predictive model will be the designer of joints, this model should only use inputs which are controllable by a designer of joints. The design inputs identified in the literature review were: geometry, material, type of fastener, torque, excitation type, excitation (type, location and amplitude), lubrication, surface roughness and life cycle of the product. The output of this predictive model should be, ideally, the precise effect of each interface in a joint to any type of vibration, at any time of the product life cycle. At first, the predictive model should just give the right order of magnitude for the dissipation of energy and the nonlinear stiffness due to a joint. This model could be a fitted model, but ideally, this model should need the least amount of experimental data to perform a prediction and be a true predictive model, as experiments are expensive and time-consuming. More work is necessary to identify what are the details of such a predictive model of the nonlinear dynamic behaviour of joints.

This thesis gives a foundation which could be used to create a predictive model based on the concept of complete and receding contacts and in-between cases. The correlation between complete and receding contacts and the nonlinear dynamic behaviour, exposed in Chapter 5, is a first step in the predictive model for the nonlinear behaviour of contact patches in joint. Receding contacts have an amplitude dependent behaviour whereas complete contacts have a behaviour independent of the amplitude. The difference between a complete contact and a receding contact is only based on the normal stress at the boundary of the contact patch. If the normal stress is equal to zero at the boundary of the contact patch there is a receding contact, if there is compression at the boundary of the contact, then there is a complete contact. The normal constraint in a joint can be simulated, based only on the geometry, using a static simulation. Therefore a prediction of the type of static contact in a joint can be made, allowing a prediction of the nonlinear dynamic behaviour. Thus a designer of joints, if he knows the joint geometry, can predict the behaviour of a joint. Preliminary results on the prediction of the normal stress at the interface of joints show promising results. In conclusion, a first rough predictive model of the nonlinear dynamic behaviour of joints aimed for the designer of joints seems possible in the near future.

A more elaborated predictive model based of the loading at the joint location for one mode seems also possible with more work. The amplitude dependent change of the always-stuck-region due to the vibration loading may be simulated with current finite element analysis software. If the behaviour in each region of the joint interface could be predicted for each mode, then a detailed prediction should be achieved. Other parameters (like the surface roughness, the lubricant or the material) should also be investigated and integrated in a predictive model. A simulation of joints could be at first manually performed, but an automatic digital procedure seems also achievable. Therefore, a fully automatic prediction of the nonlinear dynamic behaviour of joints, with a large range of design inputs, and a detail output for each mode and each region of joint interface, may exist one day.

In the long term future, the creation of a taxonomy of joint geometries with their associated nonlinear dynamic behaviour seems an achievable objective. This thesis investigated two joint geometries: the sandwich beam with two bolts and the lap joint with one bolt, both only in bending. Other loadings of these two joint geometries may have a different behaviour, for example in a torsional mode. Furthermore, other joint geometries may have a completely different dynamic behaviour. More work should improve the understanding of the physics behind the vibration of all joints geometries.

REFERENCES

Ahmadian, Hamid, and Hassan Jalali. 2007. “Identification of Bolted Lap Joints Parameters in Assembled Structures.” *Mechanical Systems and Signal Processing* 21 (2): 1041–50. doi:https://doi.org/10.1016/j.ymssp.2005.08.015.

Allen, Matthew S., and Randall L. Mayes. 2010. “Estimating the Degree of Nonlinearity in Transient Responses with Zeroed Early-Time Fast Fourier Transforms.” *Mechanical Systems and Signal Processing* 24 (7). Elsevier: 2049–64. doi:10.1016/j.ymssp.2010.02.012.

Berger, Ej. 2002. “Friction Modeling for Dynamic System Simulation.” *Applied Mechanics Reviews* 55 (6): 535. doi:10.1115/1.1501080.

Bickford, John H. 2007. *Introduction to the Design and Behavior of Bolted Joints Non-Gasketed Joints*.

Bishop, R.E.D., and D.C. Johnson. 1960. *The Mechanics of Vibration*. Edited by Cambridge University Press. Cambridge.

Brake, Assistant ProfessorMatthew R. 2019. “Assistant Professor at Rice University, Texas, USA.” https://mech.rice.edu/users/brake - Address: 226 Mechanical Engr. Bldg. 713-348-6142 Email: brake@rice.edu.

Brake, M. R. W., J. G. Stark, S. A. Smith, D. P. T. Lancereau, T. W. Jerome, and T. Dossogne. 2017. “In Situ Measurements of Contact Pressure for Jointed Interfaces During Dynamic Loading Experiments.” In *Dynamics of Coupled Structures, Volume 4*, 133–41. Springer, Cham. doi:https://doi.org/10.1007/978-3-319-54930-9_13.

Brake, Matthew R., Pascal Reuss, Daniel J. Segalman, and Lothar Gaul. 2014. “Measurements and Modeling of Variability and Repeatability of Jointed Structures with Frictional Interfaces.” Vol. 1. SAND2013-9251C.

Brake, Matthew R W. 2017. *The Mechanics of Jointed Structures*. Edited by

Springer. Springer Nature. doi:10.1007/978-3-319-56818-8.

Budynas, R. G., and J. K. Nisbett. 2015. *Shigley's Mechanical Design*.

"Call for Applications for the 2016 Sandia National Laboratories Nonlinear Mechanics and Dynamics (NOMAD) Research Institute." 2016, 85000.

Catalfamo, S, S A Smith, F Morlock, M R W Brake, P Reuß, C W Schwingshackl, and W D Zhu. 2016. "Effects of Experimental Methods on the Measurements of a Nonlinear Structure (Presentation)." *SEM IMAC XXXIV Held January 25-28, 2016 in Orlando, FL.* doi:10.1007/978-3-319-29763-7_48.

Cooper, S B, M Rosatello, K Johnson, M S Allen, A A Ferri, and B R Pacini. 2017. "Effect of Far-Field Structure on Joint Properties."

Dassault Systemes. n.d. "SOLIDWORKS® 3D Mechanical CAD and/or Simulation Software - Version: 2018-2019 Student Edition."

Dossogne, T, T W Jerome, D P T Lancereau, and S A Smith. 2017. "Experimental Assessment of The Influence of Interface Geometries on Structural Response." In *35th IMAC, A Conference and Exposition on Structural Dynamics, 2017*. Garden Grove, California.

Esteban, Jaime, and Craig A. Rogers. 2000. "Energy Dissipation through Joints: Theory and Experiments." *Computers and Structures* 75 (4): 347–59. doi:10.1016/S0045-7949(99)00096-6.

Ewins, D J. 2000. *Modal Testing. Theory, Practice and Application.* Mechanical Engineering Research Studies: 10. Hertfordshire, UK Research Studies Press Ltd c2000.

———. 2016. "Exciting Vibrations: The Role of Testing in an Era of Supercomputers and Uncertainties." *Meccanica: An International Journal of Theoretical and Applied Mechanics AIMETA*. Springer Netherlands. doi:10.1007/s11012-016-0576-y.

Feeny, BF, and JW Liang. 1996. “A Decrement Method for the Simultaneous Estimation of Coulomb and Viscous Friction.” *Journal of Sound and Vibration* 2 (0): 2–9.

Gaul, L., and J. Lenz. 1997. “Nonlinear Dynamics of Structures Assembled by Bolted Joints.” *Acta Mechanica* 125: 169–81. doi:10.1007/BF01177306.

Goyder, H G D, D P T Lancereau, P. Ind, and D. Brown. 2016. “Friction and Damping Associated with Bolted Joints : Results and Signal Processing.” In *Proceedings of ISMA 2016 - International Conference on Noise and Vibration Engineering and USD2016 - International Conference on Uncertainty in Structural Dynamics*, 755–69. https://extranet.cranfield.ac.uk/,DanaInfo=www.scopus.com+.

Goyder, Hugh. 2015a. “Damping Due to Joints in Built-Up Structures.”

———. 2015b. “Signal Processing Methods For Determining The Properties Of Bolted Joints.” In *Proceedings of the ASME 2015 International Design Engineering Technical Conferences & Computers and Information in Engineering Conference IDETC/CIE 2015*, 1–9.

Goyder, Hugh G D. 2017. “Private Conversation with Doc Goyder.”

Goyder, Hugh, and Philip Ind. 2013. “Detc2015-46843 Damping in a Composite Beam With a Jointed Interface,” 1–8.

Goyder, Hugh, Philip Ind, and Daniel Brown. 2013. “Measurement of Damping Due to Bolted Joints.” In *Proceedings of the ASME 2013 International Design Engineering Technical Conferences and Computers and Information in Engineering Conference IDETC/CIE 2013*. August 4-7, 2013, Portland, Oregon, USA: ASME.

Goyder, and Lancereau. 2017. “Methods for the Measurement Of Non-Linear Damping and Frequency in Built-Up Structures.” In *ASME 2017 International Design Engineering Technical Conferences and Computers and Information in Engineering Conference, Volume 8: 29th Conference on*

Mechanical Vibration and Noise, edited by American Society of Mechanical Engineers, 1–10. Cleveland, Ohio, USA. doi:10.1115/DETC2017-67007.

Gregory, Danny L., and Brian R. Resor. 2009a. “Chapter 2: Introduction to Experimental Program.” In *Handbook on Dynamics of Jointed Structures*, 44–54.

Gregory, Danny L, and Brian R Resor. 2009b. “Chapter 4 The Big Mass Device and Related Experiments.” In *Handbook on Dynamics of Jointed Structures*, 69–134.

Groper, Meshulam. 1985. “Microslip and Macroslip in Bolted Joints.” *Experimental Mechanics* 25 (2): 171–74. doi:10.1007/BF02328808.

Hartwigsen, C. J., Y. Song, D. M. McFarland, L. A. Bergman, and A. F. Vakakis. 2004. “Experimental Study of Non-Linear Effects in a Typical Shear Lap Joint Configuration.” *Journal of Sound and Vibration* 277 (1–2): 327–51. doi:10.1016/j.jsv.2003.09.018.

Heinstein, M. W., and D. J. Segalman. 2002. “Bending Effects in the Frictional Energy Dissipation in Lap Joints National Laboratories.” http://prod.sandia.gov/techlib/access-control.cgi/2002/020083.pdf.

Hills, D. A., R. Ramesh, R. M.N. Fleury, and K. Parel. 2017. “A Unified Approach for Representing Fretting and Damage at the Edges of Incomplete and Receding Contacts.” *Tribology International* 108. Elsevier: 16–22. doi:10.1016/j.triboint.2016.08.026.

Hills, D.A., D. Nowell, and A. Sackfield. 1993. “Essential Solid Mechanics.” *Mechanics of Elastic Contacts* i: 3–42. doi:10.1016/B978-0-7506-0540-3.50004-0.

Jewell, Emily A, Matthew S Allen, and Robert Lacayo. 2017. “Predicting Damping of a Cantilever Beam with a Bolted Joint Using Quasi-Static Modal Analysis.” In *Proceedings of the ASME 2017 International Design Engineering Technical Conferences and Computers and Information in*

Engineering Conference IDETC/CIE 2017, 1–10.

Kess, Harold R, Nathan J Rosnow, and Brian C Sidle. 2002. “Effects of Bearing Surfaces on Lap Joint Energy Dissipation.” In *The 20th International Modal Analysis Conference*. Los Angeles, CA, February 4-7, 2002. http://permalink.lanl.gov/object/tr?what=info:lanl-repo/lareport/LA-UR-01-5685.

Kuether, Robert J, and Matthew R W Brake. 2014. “Dynamics of Civil Structures, Volume 4” 4: 253–63. doi:10.1007/978-3-319-04546-7.

———. 2016. “Instantaneous Frequency and Damping from Transient Ring-Down Data.” *International Modal Analysis Conference (IMAC)*. doi:10.1007/978-3-319-29763-7_24.

Lancereau, Damien P T, Hugh G D Goyder, Philip Ind, and Daniel Brown. 2017. “Some Dynamic Properties of Contact Patches in Bolted Joints.” In *Volume 8: 29th Conference on Mechanical Vibration and Noise*. Cleveland. doi:10.1115/DETC2017-67008.

Lazan, B. J. 1968. *Damping of Materials and Members in Structural Mechanics*. Edited by Pergamon Press. London.

Maia, Nuno Manuel Mendes, and Julio Martins Montalvao e Silva. 1997. *Theoretical and Experimental Modal Analysis*. *Mechanical Engineering Research Studies*. Taunton, Somerset, England: Research Studies Press.

Mains, Michael. 2015. “Presentation Sides: Modal Parameter Estimation.” In *33rd A Conference and Exposition on Structural Dynamics · IMAC 2015*. Orlando, Florida, USA. https://www.vibetech.com/event/imac-xxxiv/.

Maloney, Christopher W, and Daniel M Peairs. 2000. “Characterization of Damping in Bolted Lap Joints.” In . Vol. 636. Orlando, FL.

Mayes, Randall L, Benjamin R Pacini, and Daniel R Roettgen. 2014. “A Modal Model to Simulate Typical Structural Dynamic Nonlinearity.” In *34th International Modal Analysis Conference, Paper #121*. Orlando, FL.

Meyer, Janette J., and Douglas E. Adams. 2015. “Theoretical and Experimental Evidence for Using Impact Modulation to Assess Bolted Joints.” *Nonlinear Dynamics* 81 (1–2). Springer Netherlands: 103–17. doi:10.1007/s11071-015-1976-6.

Organisation Internationale de Normalisation ISO 7089:2000. 2000. “(En) Plain Washers — Normal Series — Product Grade A.” www.iso.org.

Ouyang, H., M. J. Oldfield, and J. E. Mottershead. 2006. “Experimental and Theoretical Studies of a Bolted Joint Excited by a Torsional Dynamic Load.” *International Journal of Mechanical Sciences* 48 (12): 1447–55. doi:10.1016/j.ijmecsci.2006.07.015.

Peyret, Nicolas, Jean Luc Dion, and Gael Chevallier. 2016. “A Framework for Backbone Experimental Tracking: Piezoelectric Actuators, Stop-Sine Signal and Kalman Filtering.” *Mechanical Systems and Signal Processing* 78. Elsevier: 28–42. doi:10.1016/j.ymssp.2015.09.020.

Schwingshackl, C W. 2017. “Identification Reassembly Uncertainties for a Basic Lap Joint.” In , 35th IMAC, A Conference and Exposition on Structur. Garden Grove, California.

Segalman, D J. 2010. “A Modal Approach to Modeling Spatially Distributed Vibration Energy Dissipation.” https://www.osti.gov/biblio/993326.

Segalman, Daniel J. 2001. “An Initial Overview of Iwan Modeling for Mechanical Joints Acknowledgments.” *Control*, no. March: 3–8.

———. 2009. “Chapter 1 Introduction.” In *Handbook on Dynamics of Jointed Structures*, 27–44.

Segalman, Daniel J, and Danny L Gregory. 2009. “Chapter 19 Future Work,” 467–87.

Segalman, Daniel J, Danny L Gregory, Michael J Starr, Brian R Resor, Michael D Jew, James P Lauffer, and Nicoli M Ames. 2009. *Handbook on Dynamics of Jointed Structures*. doi:10.2172/1028891.

Smith, S, M R W Brake, and P Reuß. 2015. “The Effects of Boundary Conditions , Measurement Techniques , and Excitation Type on Measurements of the Properties of Mechanical Joints.”

Song, Y., C.J. Hartwigsen, D.M. McFarland, A.F. Vakakis, and L.A. Bergman. 2004. “Simulation of Dynamics of Beam Structures with Bolted Joints Using Adjusted Iwan Beam Elements.” *Journal of Sound and Vibration* 273 (1–2): 249–76. doi:10.1016/S0022-460X(03)00499-1.

Sracic, Michael W., Matthew S. Allen, and Hartono Sumali. 2012. “Identifying the Modal Properties of Nonlinear Structures Using Measured Free Response Time Histories from a Scanning Laser Doppler Vibrometer.” In *Topics in Nonlinear Dynamics, Volume 3, Proceedings of the 30th IMAC, A Conference on Structural Dynamics, 2012*, edited by D. Adams, G. Kerschen, and A. Carrella, 269–86. Springer New York. doi:10.1007/978-1-4614-2416-1_22.

Süß, Dominik, Anton Janeba, and Kai Willner. 2017. “The Mechanics of Jointed Structures, Chapter 6 - The Gaul Resonator: Experiments for the Isolated Investigation of a Bolted Lap Joint.” In , edited by Springer Nature, Springer. doi:10.1007/978-3-319-56818-8.

Vakis, A.I., V.A. Yastrebov, J. Scheibert, C. Minfray, L. Nicola, D. Dini, A. Almqvist, et al. 2018. “Modeling and Simulation in Tribology across Scales: An Overview.” *Tribology International* 125 (May). Elsevier Ltd: 169–99. doi:10.1016/j.triboint.2018.02.005.

APPENDICES

Appendix A Results for Experiement1 (see Section 6.1.5)

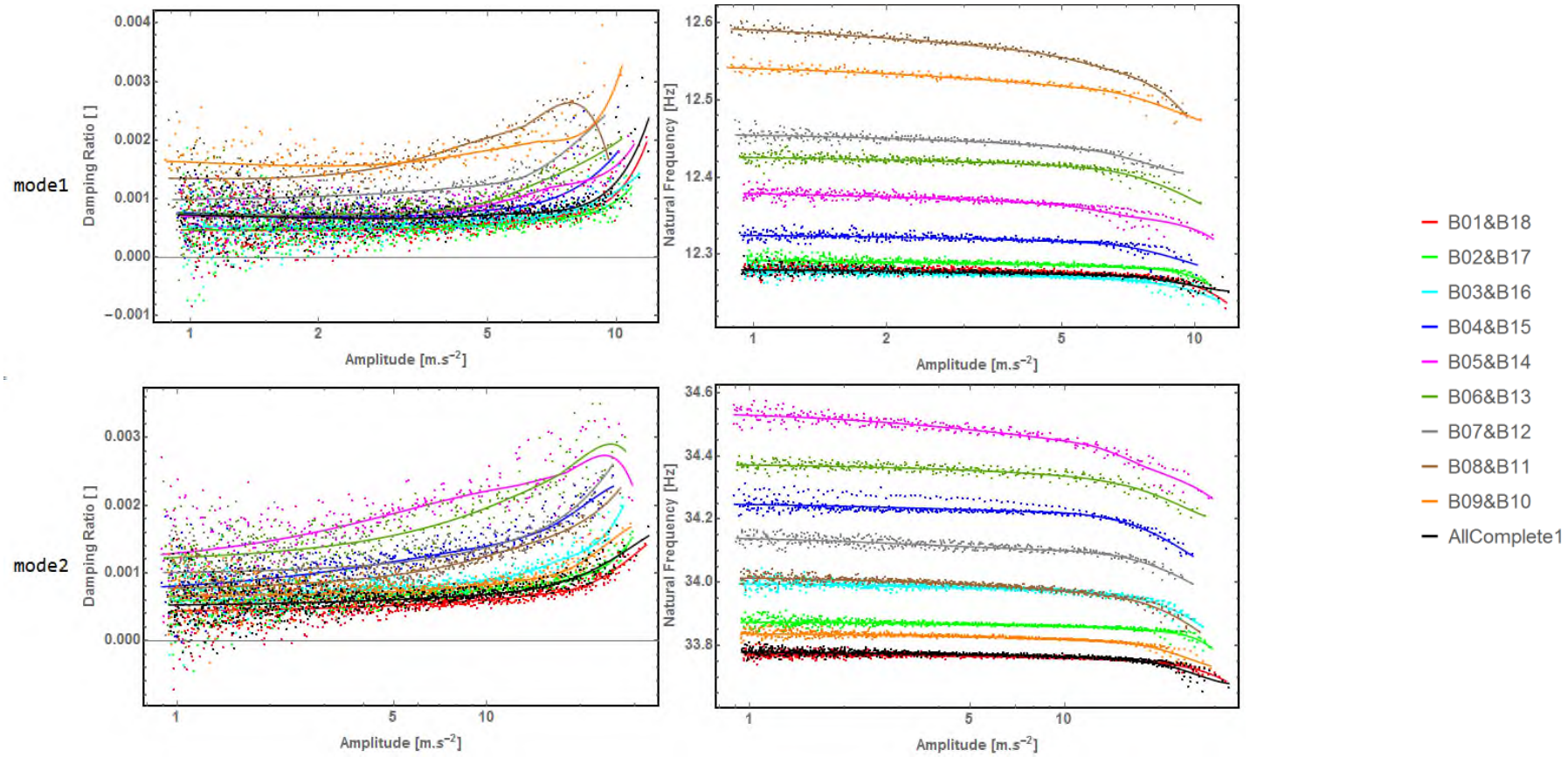

Figure 201 Damping ratios and natural frequencies as a function of amplitude from Experiment 1 for modes 1 and 2

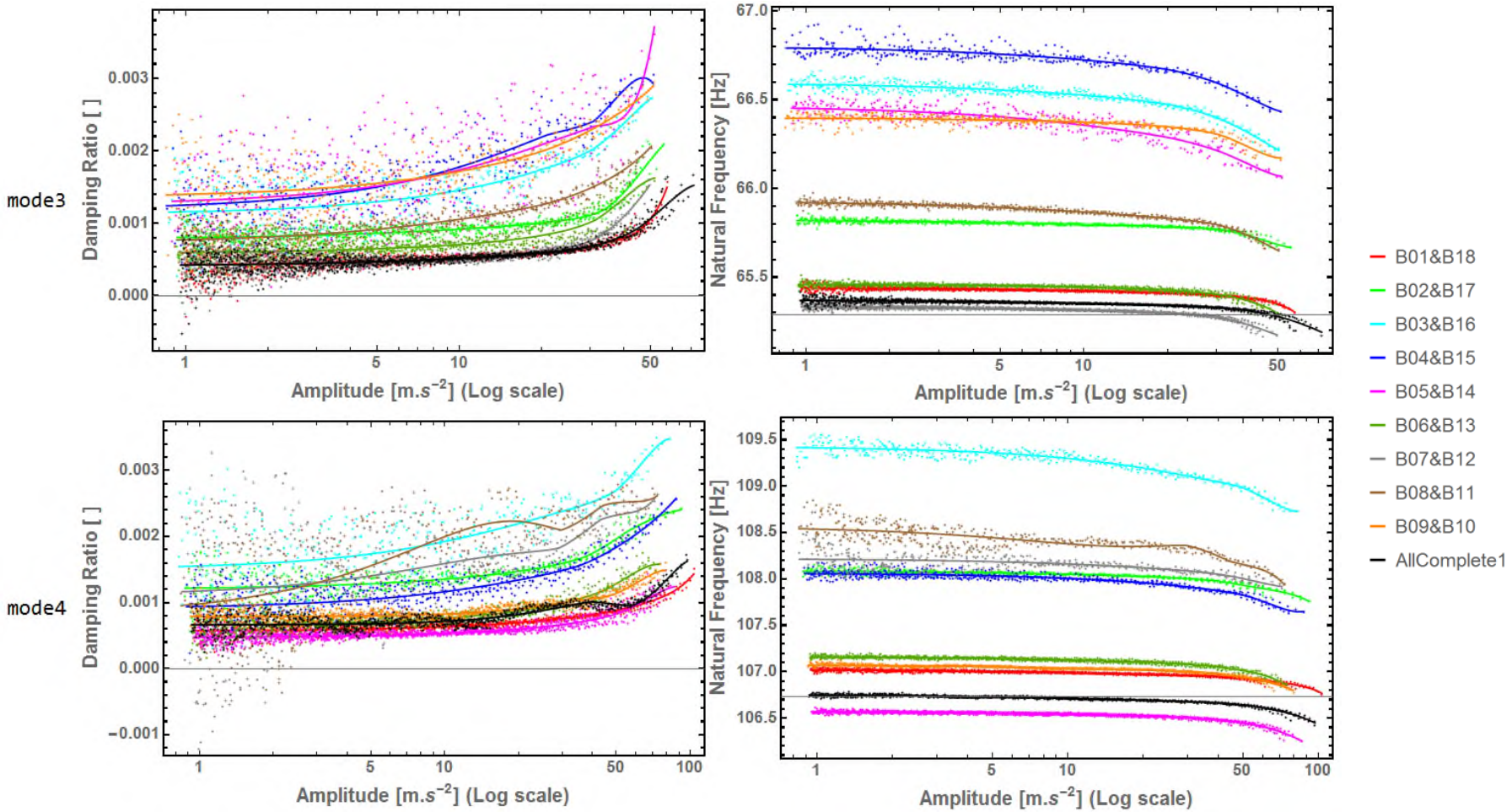

Figure 202 Damping ratios and natural frequencies as a function of amplitude from Experiment 1 for modes 3 and 4

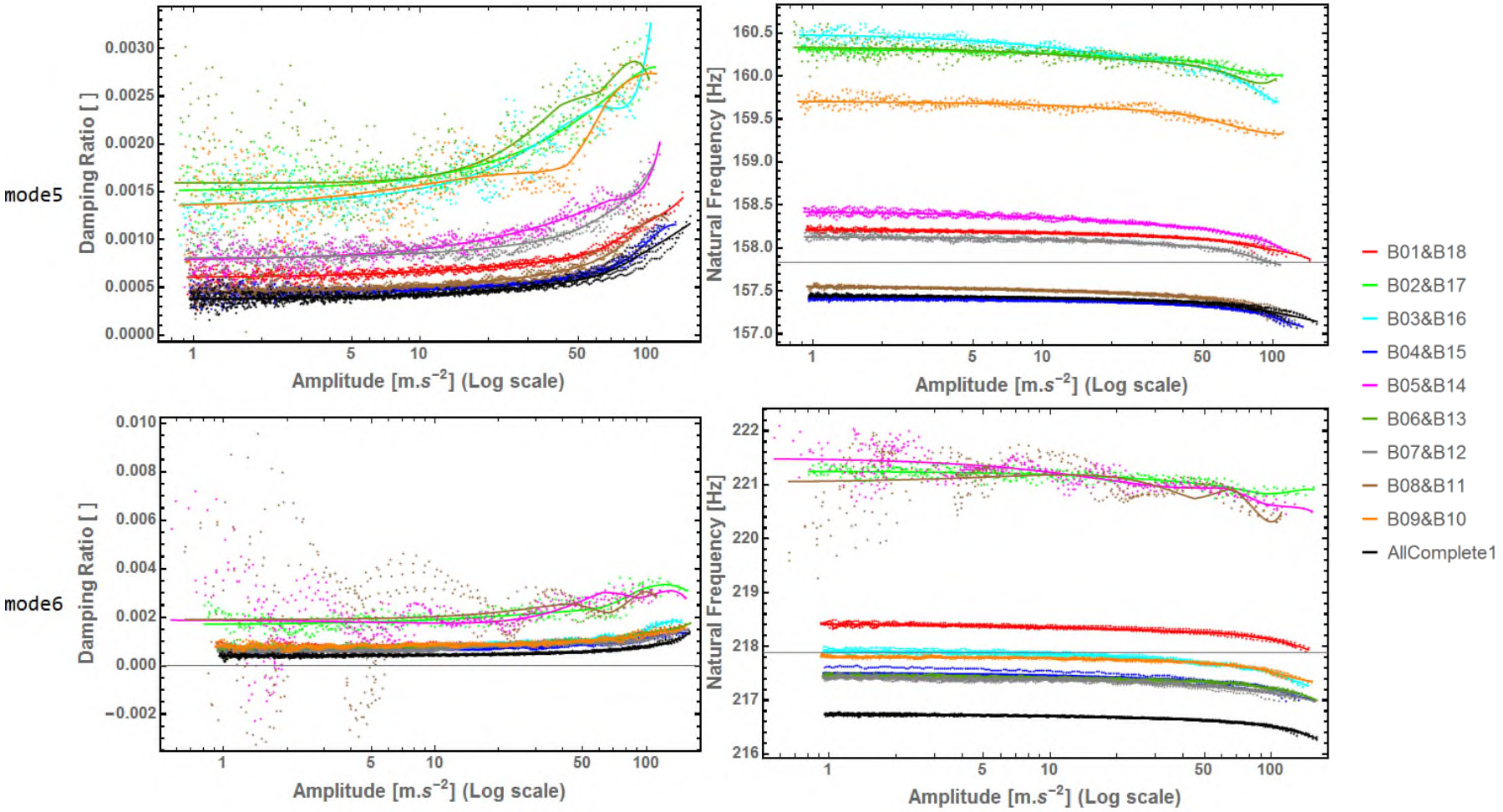

Figure 203 Damping ratios and natural frequencies as a function of amplitude from Experiment 1 for modes 5 and 6

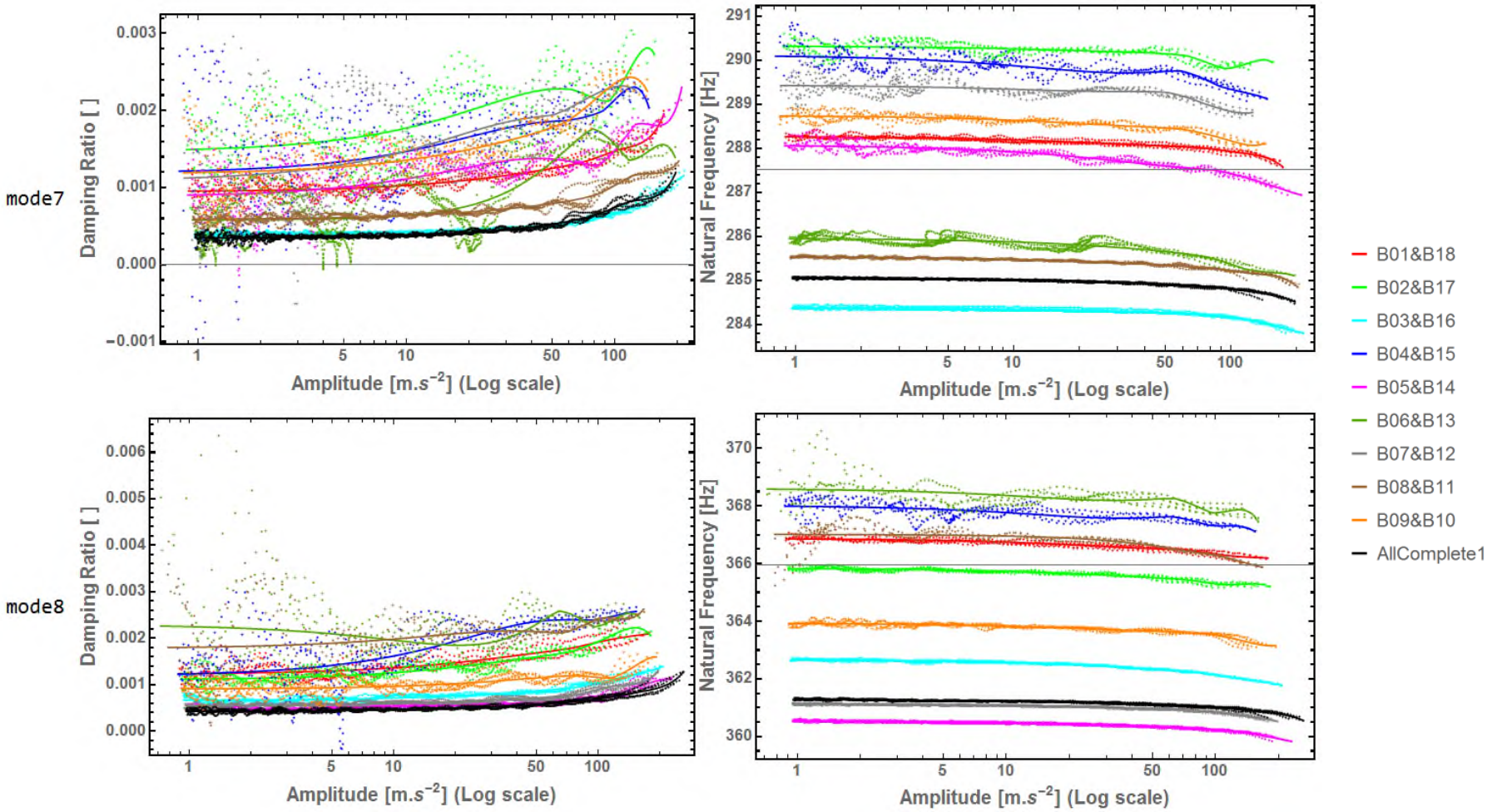

Figure 204 Damping ratios and Natural frequencies as a function of amplitude from Experiment 1 for modes 7 and 8

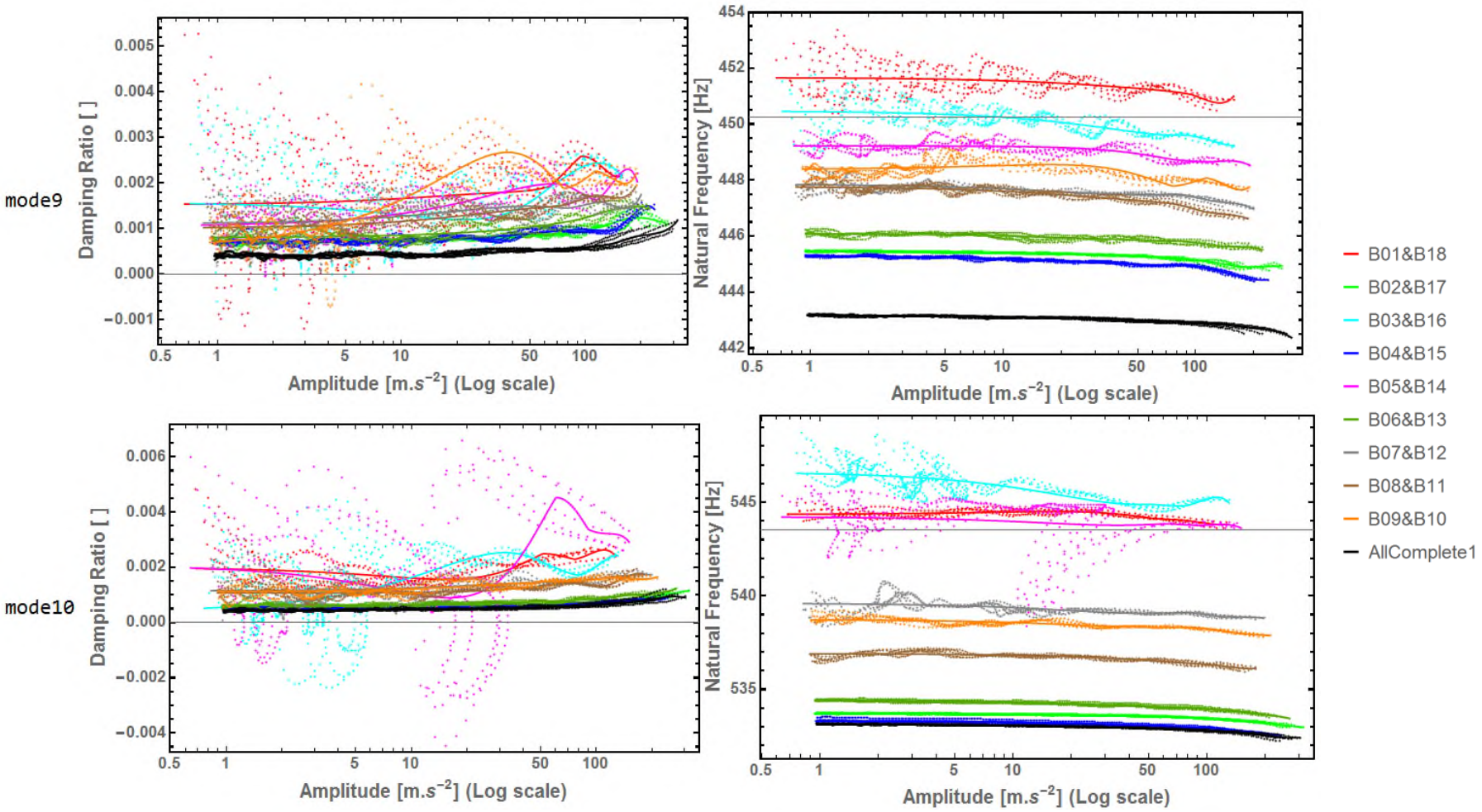

Figure 205 Damping ratios and natural frequencies as a function of amplitude from Experiment 1 for modes 9 and 10

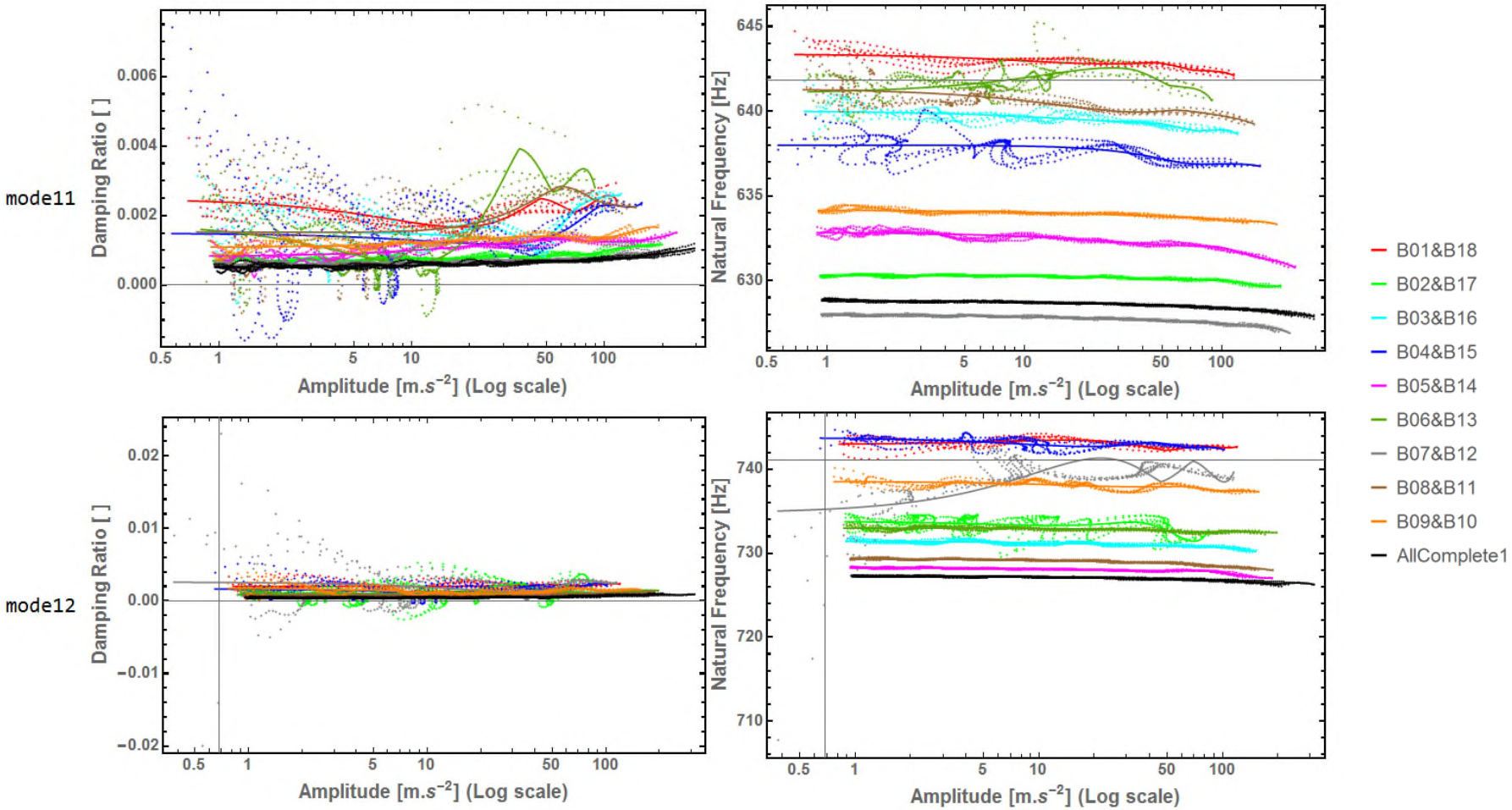

Figure 206 Damping ratios and natural frequencies as a function of amplitude from Experiment 1 for modes 11 and 12

Appendix B Result for Experiement2 (see Section 6.1.5)

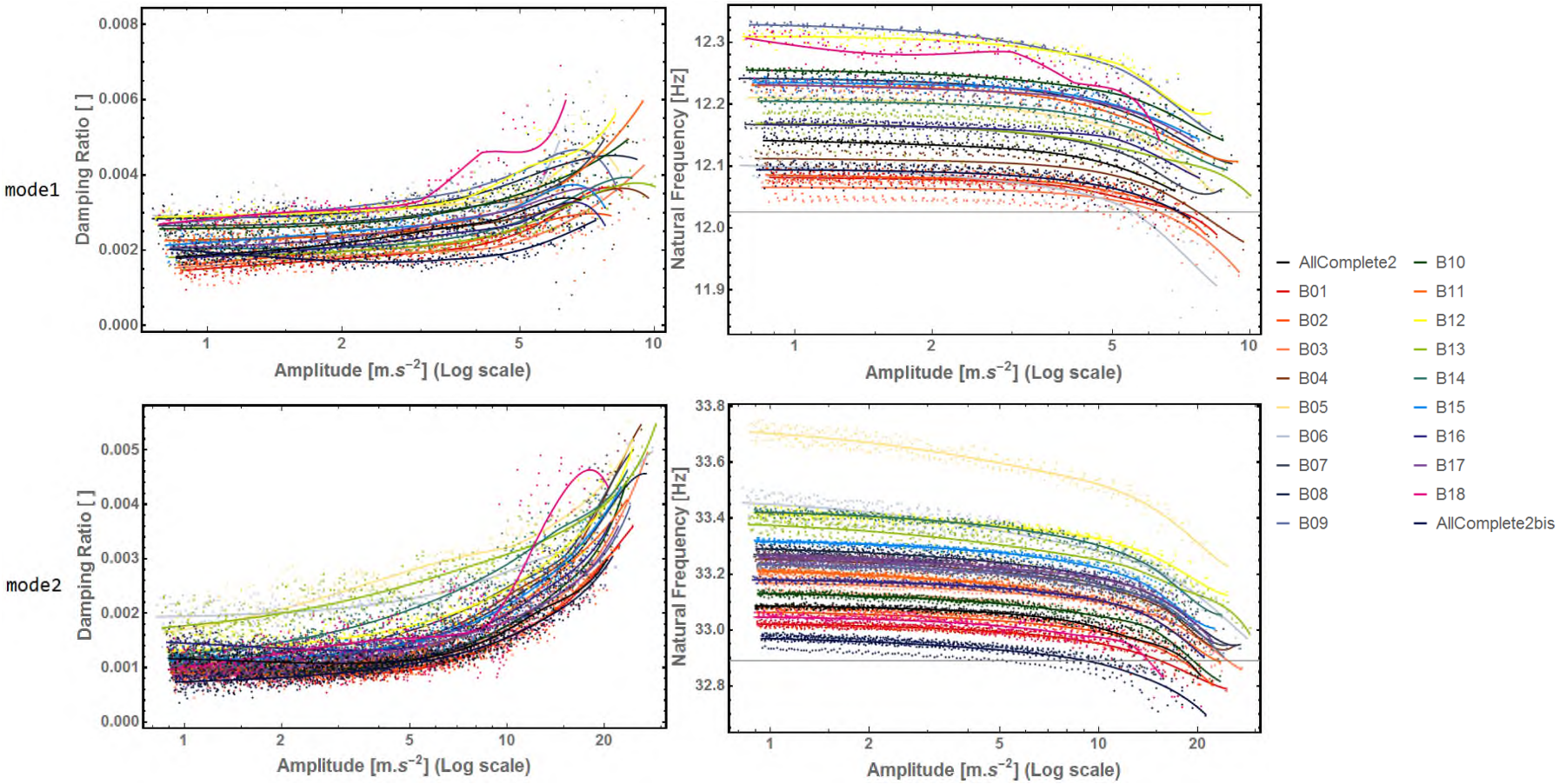

Figure 207 Damping ratios and natural frequencies as a function of amplitude from Experiment 2 for mode 1 and mode 2

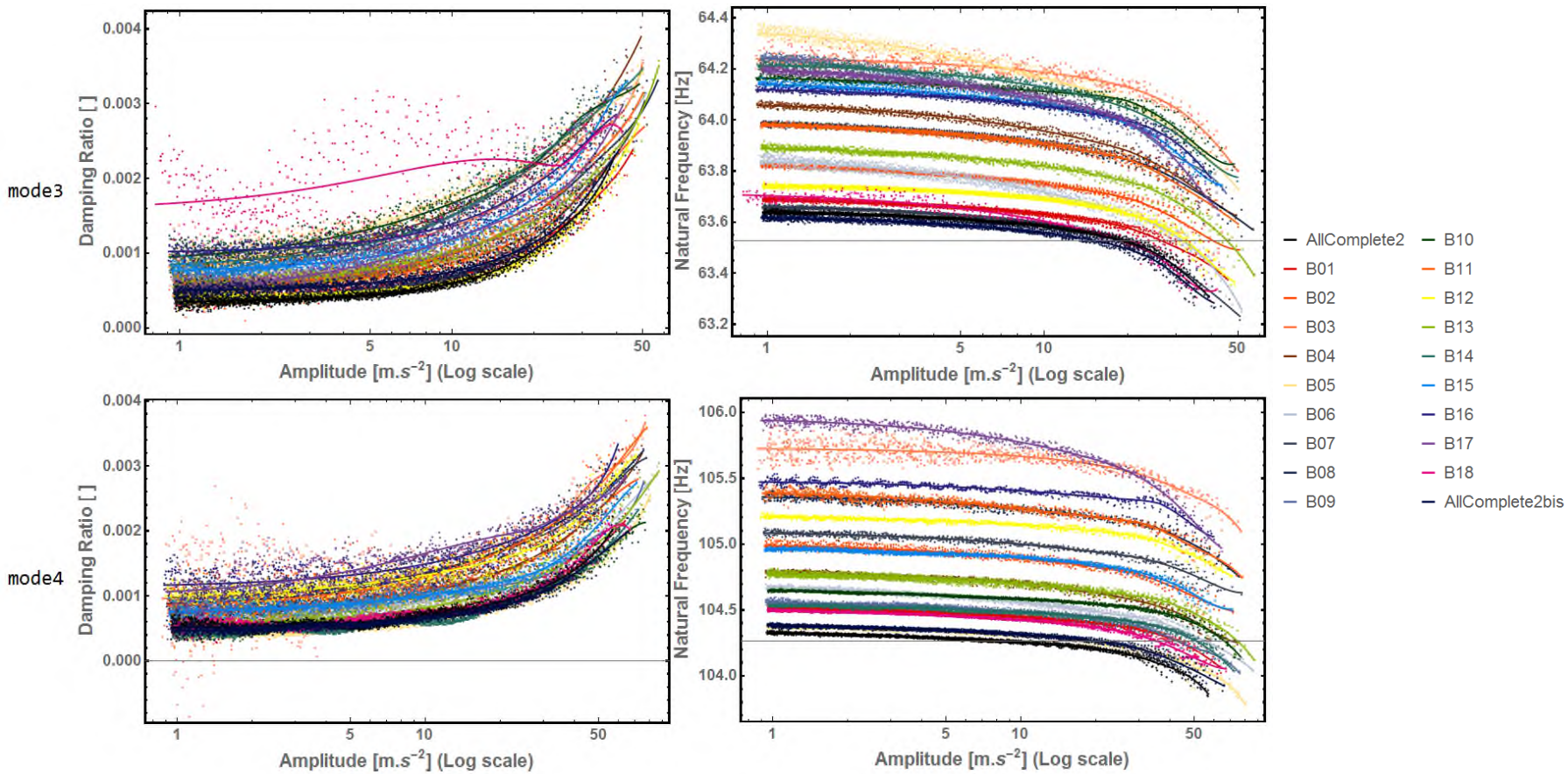

Figure 208 Damping ratios and natural frequencies as a function of the amplitude from Experiment 2 for mode 4 and mode 5

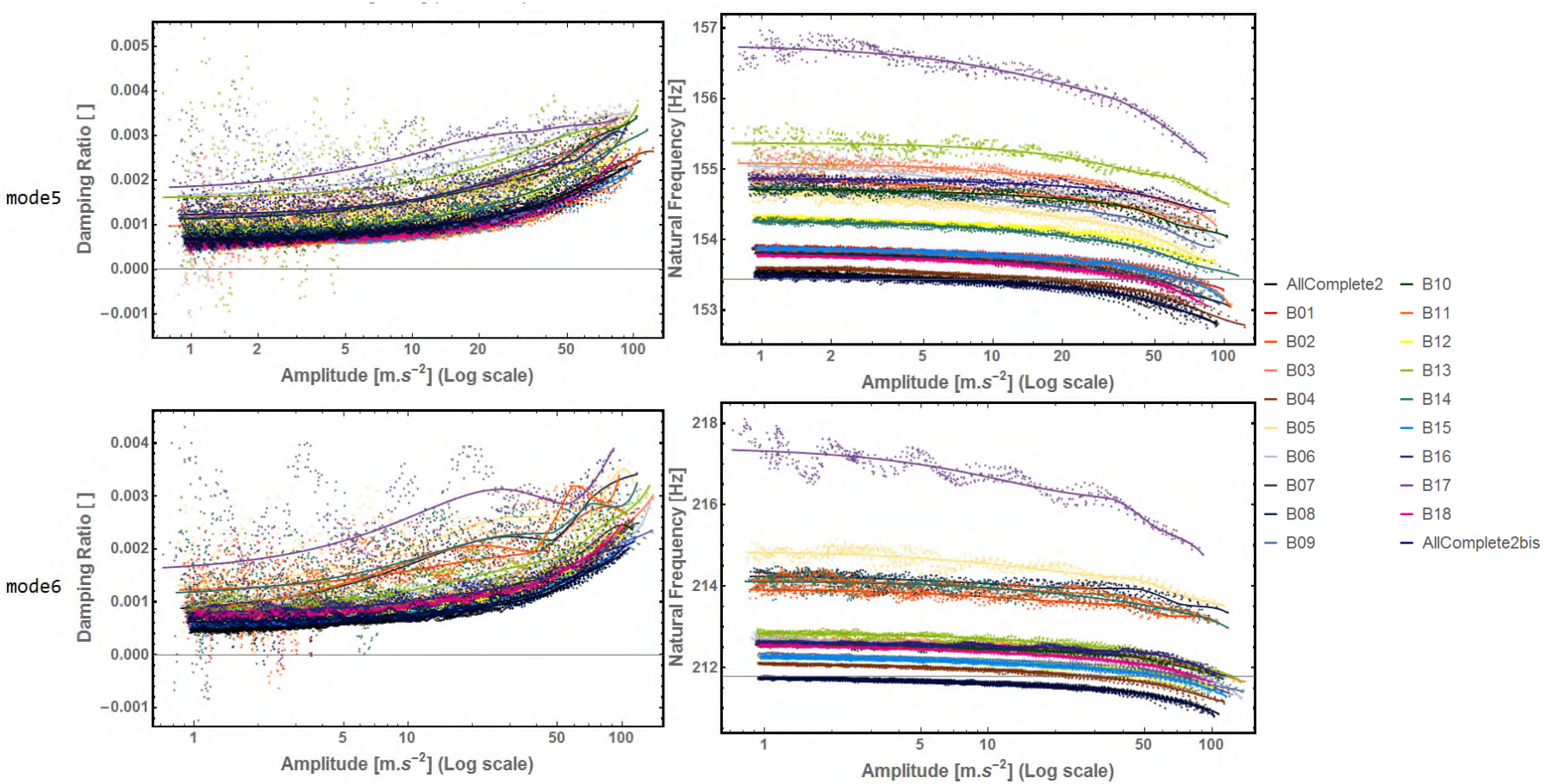

Figure 209 Damping ratios and natural frequencies as a function of amplitude from Experiment 2 for mode 5 and mode 6

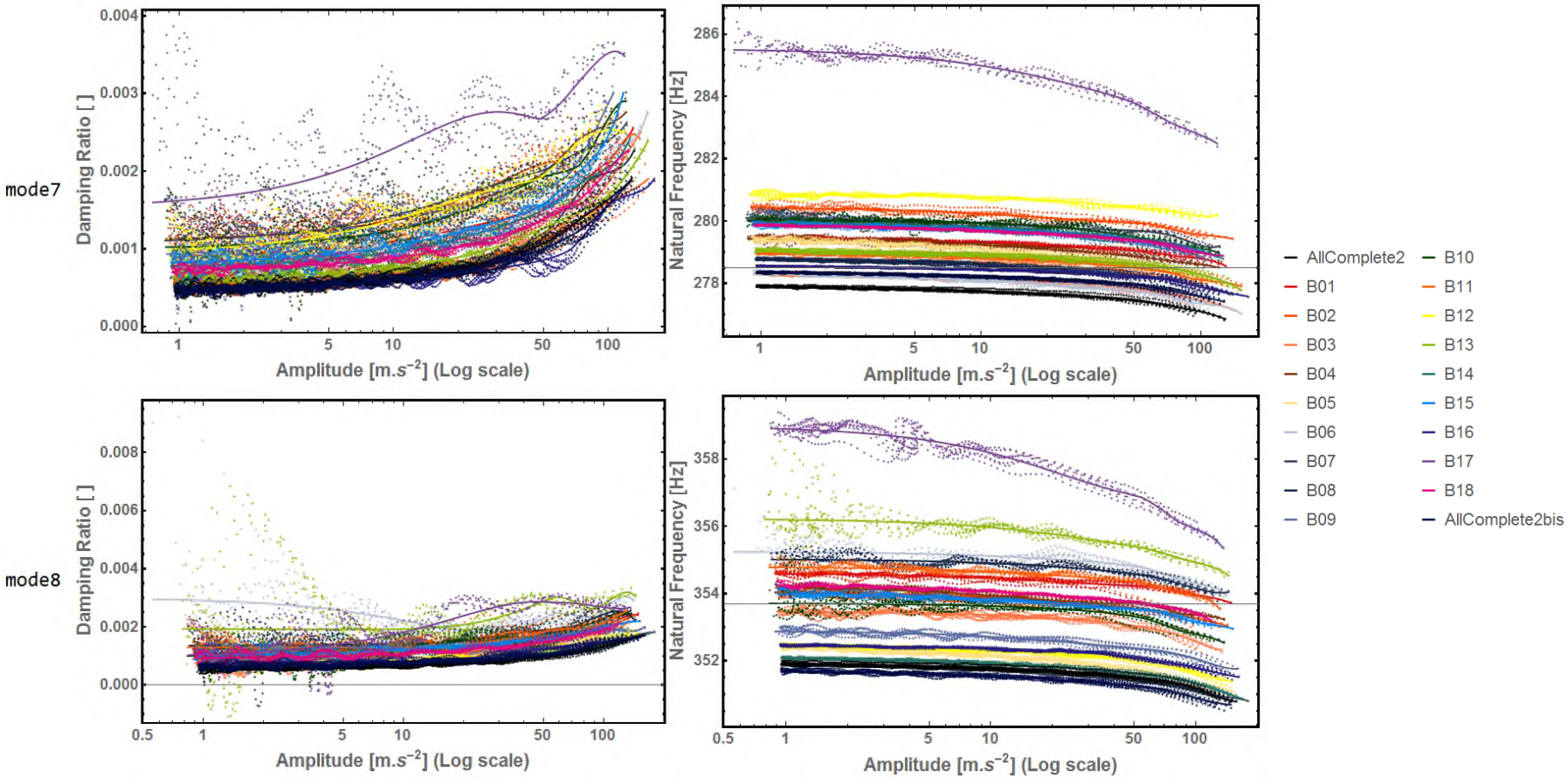

Figure 210 Damping ratios and natural frequencies as a function of amplitude from Experiment 2 for mode 7 and mode 8

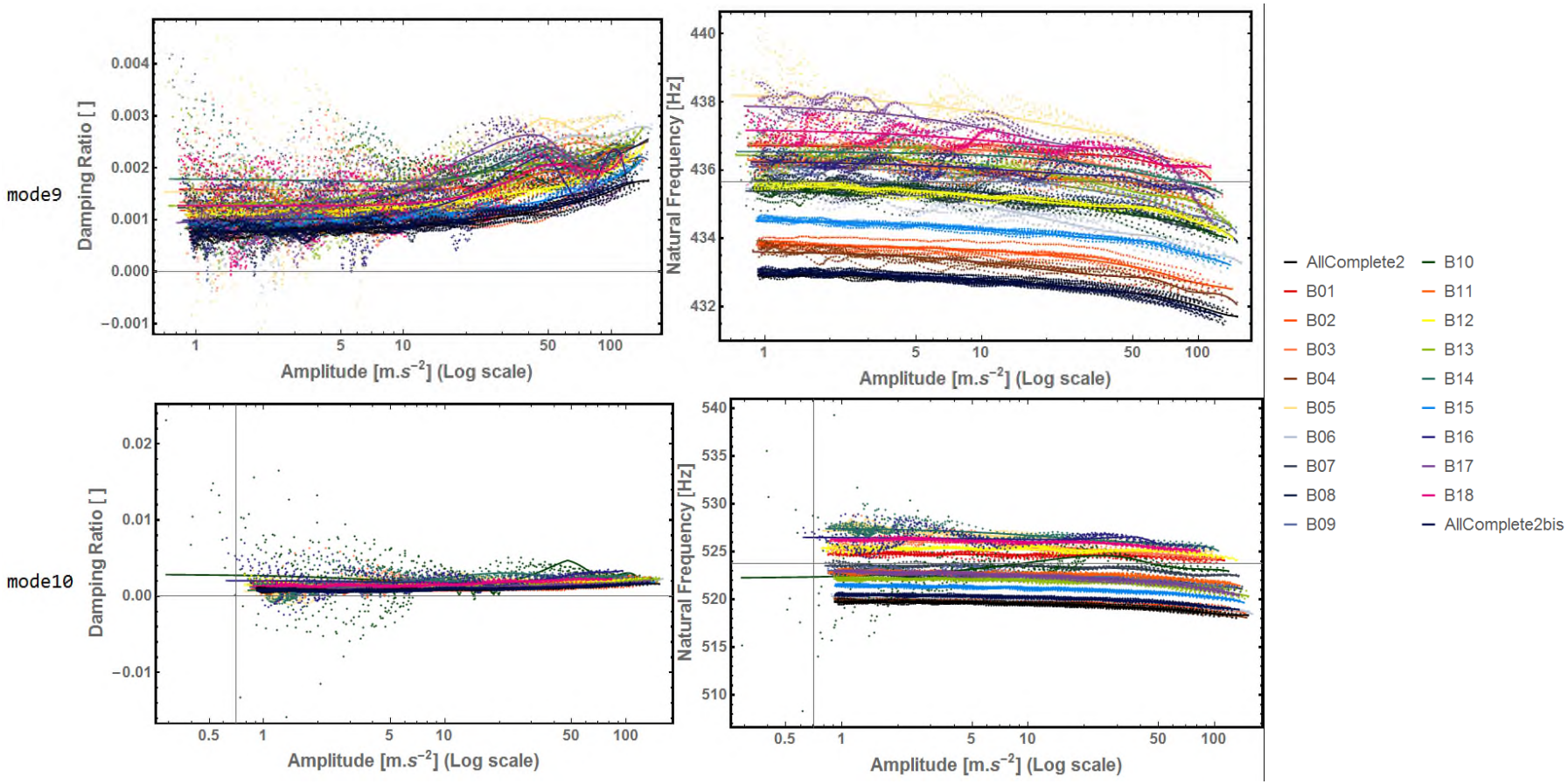

Figure 211 Damping ratios and natural frequencies as a function of amplitude from Experiment 2 for mode 9 and mode 10

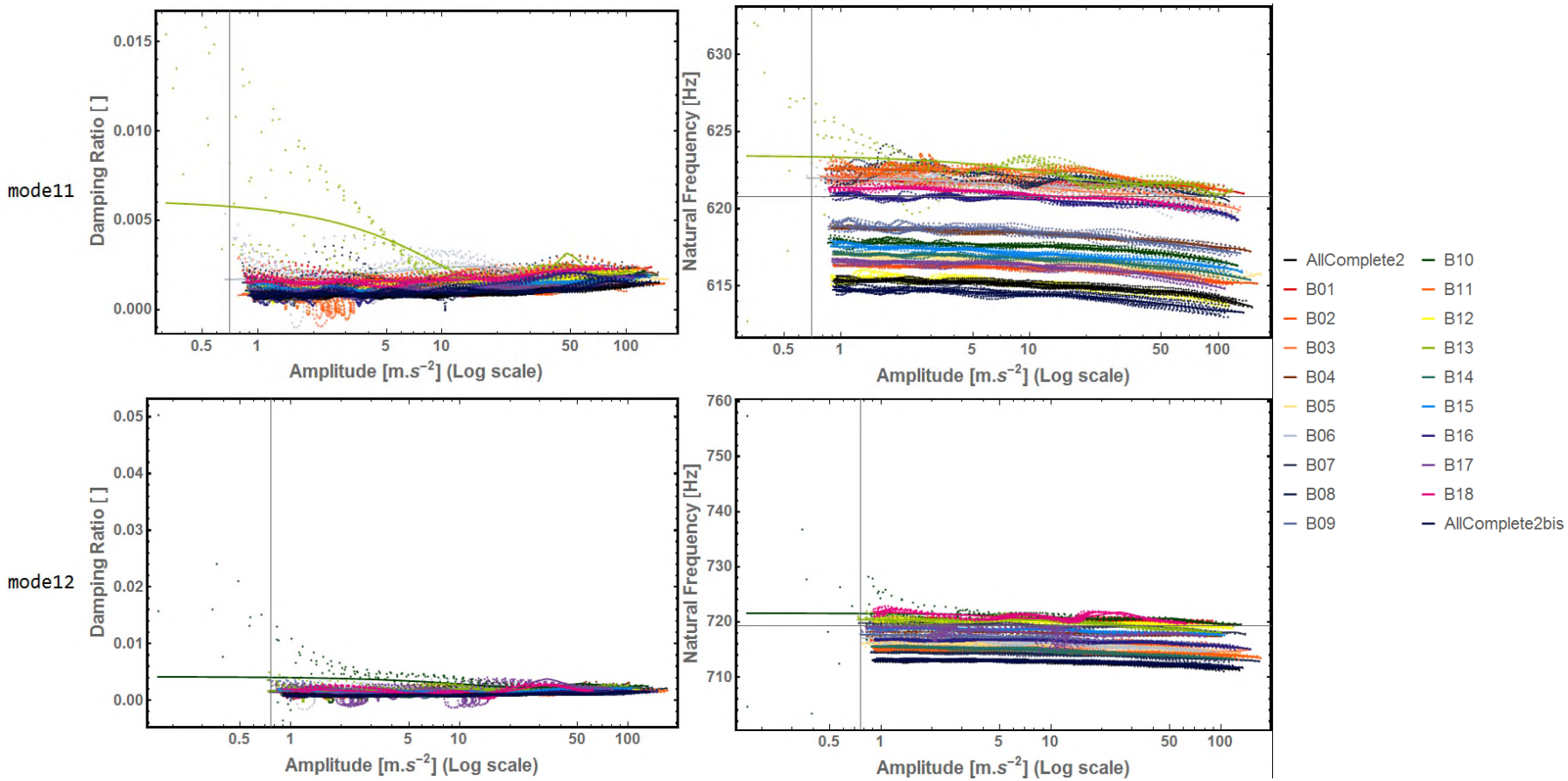

Figure 212 Damping ratios and natural frequencies as a function of amplitude from Experiment 2 for mode 11 and mode 12

Appendix C Fitting Result Joint Position

Table 27 Results from fitting in Chapter 7 of experimental data using Equation (7-3). See Section 7.2 for more details

	Damping Ratio [no unit]				Natural Frequency [Hz]			
	Two Receding Contacts		One Receding Contact		Two Receding Contacts		One Receding Contact	
Fitted Variables	**M**	**N**	**M**	**N**	**M**	**N**	**M**	**N**
Mode 1	0.000799234	0.000339893	0.000548631	0.002589750	0.179516	12.2228	0.0538707	12.1082
Mode 2	0.000868233	0.000373530	0.000705742	0.001392080	0.461010	33.6253	0.242041	32.9502
Mode 3	0.001092150	0.000212677	0.000449874	0.000994131	1.08224	64.9442	0.402355	63.5021
Mode 4	0.001100460	0.000235921	0.000680105	0.000636631	1.80428	105.991	0.861811	104.0190
Mode 5	0.001255040	0.000060289	0.001016230	0.000657375	2.61146	156.361	1.36222	152.9800
Mode 6	0.001709720	-0.000390889	0.001165610	0.000314993	4.83092	214.052	2.96739	210.0170
Mode 7	0.000923615	0.000394561	0.000662844	0.000740635	4.16611	283.784	1.91676	277.6710
Mode 8	0.001218700	0.000200092	0.000775830	0.000709127	6.37214	358.681	2.57300	351.1880
Mode 9	0.001506580	-0.000204490	0.000384832	0.001256370	9.44561	438.133	2.96013	432.3760
Mode 10	0.001036050	0.000356348	0.000595990	0.001138740	8.73389	530.789	4.20993	519.2680
Mode 11	0.001000230	0.000527299	0.000501789	0.001098030	10.5616	626.422	5.05529	613.9540
Mode 12	0.000906400	0.000461893	0.000314053	0.001388810	10.3500	725.019	3.82903	713.5940
Average	0.001118034	0.000213927	0.000650128	0.001076389	5.04989	295.835	2.20281	290.3022

Table 28 Results from fitting in Chapter 7 of experimental scaled data using the Equation (7-4)

	Scaled Damping Ratio [no unit]		Scaled Natural Frequency [no unit]	
	Two receding contacts	**One receding contact**	**Two receding contacts**	**One receding contact**
Fitted Variable	**P**	**P**	**P**	**P**
Column name	**FitScalDampTwo**	**FitScalDampOne**	**FitScalFreqTwo**	**FitEvoFreqOne**
Mode 1	0.567169	0.477313	0.0111391	0.00738217
Mode 2	0.85449	0.535331	0.010132	0.00887405
Mode 3	1.36482	0.524282	0.011222	0.00604771
Mode 4	0.734406	0.639995	0.0111165	0.00620682
Mode 5	1.76448	0.526655	0.0108274	0.00708814
Mode 6	1.76062	0.595371	0.0113128	0.00763089
Mode 7	1.85973	0.799743	0.0110802	0.00562859
Mode 8	1.73503	0.637024	0.0116401	0.00686926
Mode 9	1.67111	0.471923	0.0109221	0.00651271
Mode 10	1.64242	0.631263	0.0129481	0.0070186
Mode 11	1.39517	0.462168	0.0138591	0.00793473
Mode 12	1.56926	0.583381	0.011996	0.00656342
Average	1.40989	0.573704	0.011516	0.00697975

Table 29 Ratios between the fitted parameters for two and one receding contacts for the damping ratio and the natural frequency (see Table 28 for variable name)

	Damping Ratio	Natural Frequency
Calculated value	**FitScalDampTwo/ FitScalDampOne [no unit]**	**FitScalFreqTwo/ FitScalFreqOne [no unit]**
Mode 1	1.18825	1.50892
Mode 2	1.59619	1.14176
Mode 3	2.60322	1.85558
Mode 4	1.14752	1.79101
Mode 5	3.35035	1.52754
Mode 6	2.95718	1.48250
Mode 7	2.32541	1.96856
Mode 8	2.72365	1.69452
Mode 9	3.54106	1.67704
Mode 10	2.60180	1.84483
Mode 11	3.01875	1.74664
Mode 12	2.68994	1.82771
Average	2.47861	1.67222

Table 30 Ratios between fitted parameters of damping ratio and natural frequency for either one receding contact or two receding contacts (see Table 28 for variable name)

Number of receding contact	Two receding contacts	One receding contact
Calculated value	FitScalDampTwo /FitScalFreqTwo [no unit]	FitScalDampOne /FitScalFreqOne [no unit]
Mode 1	50.92	64.66
Mode 2	84.34	60.33
Mode 3	121.62	86.69
Mode 4	66.06	103.11
Mode 5	162.96	74.30
Mode 6	155.63	78.02
Mode 7	167.84	142.09
Mode 8	149.06	92.74
Mode 9	153.00	72.46
Mode 10	126.85	89.94
Mode 11	100.67	58.25
Mode 12	130.82	88.88
Average	122.48	84.29